A COUPLED MICROMECHANICAL MODEL OF MOISTURE-INDUCED

DAMAGE IN ASPHALT MIXTURES: FORMULATION AND APPLICATIONS

A Dissertation

by

SILVIA CARO SPINEL

Submitted to the Office of Graduate Studies of
Texas A&M University
in partial fulfillment of the requirements for the degree of

DOCTOR OF PHILOSOPHY

December 2009

Major Subject: Civil Engineering

A COUPLED MICROMECHANICAL MODEL OF MOISTURE-INDUCED

DAMAGE IN ASPHALT MIXTURES: FORMULATION AND APPLICATIONS

A Dissertation

by

SILVIA CARO SPINEL

Submitted to the Office of Graduate Studies of
Texas A&M University
in partial fulfillment of the requirements for the degree of

DOCTOR OF PHILOSOPHY

Approved by:

Chair of Committee,	Eyad Masad
Committee Members,	Hamn-Ching Chen
	Dallas Little
	Robert L. Lytton
	Anastasia Muliana
	Athanasios Scarpas
Interim Department Head,	John Niedzwecki

December 2009

Major Subject: Civil Engineering

ABSTRACT

A Coupled Micromechanical Model of Moisture-Induced Damage in Asphalt Mixtures:
Formulation and Applications. (December 2009)
Silvia Caro Spinel, B.S., Universidad de Los Andes (Bogotá, Colombia); M.S., Universidad de
Los Andes (Bogotá, Colombia)
Chair of Advisory Committee: Dr. Eyad Masad

The deleterious effect of moisture on the structural integrity of asphalt mixtures has been recognized as one of the main causes of early deterioration of asphalt pavements. This phenomenon, usually referred to as *moisture damage*, is defined as the progressive loss of structural integrity of the mixture that is primarily caused by the presence of moisture in liquid or vapor state. Moisture damage is associated with the development of different physical, mechanical, and chemical processes occurring within the microstructure of the mixture at different intensities and rates. Although there have been important advancements in identifying and characterizing this phenomenon, there is still a lack of understanding of the damage mechanisms occurring at the microscopic level. This situation has motivated the research work reported in this dissertation.

The main objective of this dissertation is to formulate and apply a numerical micromechanical model of moisture-induced damage in asphalt mixtures. The model focuses on coupling the effects of moisture diffusion—one of the three main modes of moisture transport within asphalt mixtures—with the mechanical performance of the microstructure. Specifically, the model aims to account for the effect of moisture diffusion on the degradation of the viscoelastic bulk matrix of the mixture (i.e., cohesive degradation) and on the gradual deterioration of the adhesive bonds between the aggregates and the asphalt matrix (i.e., adhesive degradation).

The micromechanical model was applied to study the role of some physical and mechanical properties of the constitutive phases of the mixtures on the susceptibility of the mixture to moisture damage. The results from this analysis suggest that the diffusion coefficients of the asphalt matrix and aggregates, as well as the bond strength of the aggregate-matrix interface, have the most influence on the moisture susceptibility of the mixtures.

The micromechanical model was further used to investigate the influence of the void phase of asphalt mixtures on the generation of moisture-related deterioration processes. Two different probabilistic-based approaches were used to accomplish this objective. In the first approach, a volumetric distribution of air void sizes measured using X-Ray Computed Tomography in a dense-graded asphalt mixture was used to generate probable void structures in a microstructure of an asphalt mixture. In the second approach, a stochastic modeling technique based on random field theory was used to generate probable air void distributions of the mixture. In this second approach, the influence of the air void was accounted for by making the physical and mechanical properties of the asphalt matrix dependent on probable void distributions. Although both approaches take into consideration the characteristics of the air void phase on the mechanical response of the mixtures subjected to moist environments, the former explicitly introduces the air phase within the microstructure while the latter indirectly includes its effects by modifying the material properties of the bulk matrix. The results from these simulations demonstrated that the amount, variability and location of air voids are decisive in determining the moisture-dependent performance of asphalt mixtures.

The results from this dissertation provide new information on the kinetics of moisture damage mechanisms in asphalt mixtures. In particular, the results obtained from applying the micromechanical model permitted identification of the relative influence of the characteristics of the constitutive phases of a mixture on its moisture-related mechanical performance. This information can be used as part of design methodologies of asphalt mixtures, and/or as an input in life-cycle analysis models and maintenance programs of road infrastructure.

DEDICATION

To my husband Mauricio, my children Camila and Alejandro, my parents Jairo and Carolina,

and my sister Liliana, for their unconditional love, patience and support

ACKNOWLEDGMENTS

This work would not have been possible without the support of my fellow students and friends. I especially want to acknowledge Allex Eduardo Alvarez-Lugo and Edith Arámbula-Mercado for their invaluable friendship, their permanent encouragement, and for sharing with me so many unforgettable academic and personal experiences. I am confident we will continue

working together in the years to come. I am thankful to Jonathan Howson, with whom I worked closely and who made my stay in College Station more enjoyable. I am also grateful for the academic support and friendship provided by Kamilla Vasconcelos, Veronica Castelobranco and Enad Mahmoud.

My family also played an important role in the development of this project. I wish to thank my parents, Jairo Caro-Greiffenstein and Carolina Spinel-Gómez, and my sister, Liliana, for their permanent support. My husband, Mauricio Sánchez-Silva, deserves much more than my gratitude. He has been the source of my strength during difficult times, he has inspired me to never give up, he has celebrated with me my small victories, he has taken care of my children when I had to work, and he has been extremely generous and patient with me. Many people can be grateful to their partners for being a source of strong moral support during their graduate studies. Few people, however, can also be grateful to them for contributing to their research work. I belong to that select group of people. I appreciate that I have a wonderful husband who spent many hours discussing with me interesting and intriguing technical topics related to this research. The final product of this dissertation is highly influenced by his contributions.

TABLE OF CONTENTS

LIST OF FIGURES

FIGURE   Page

LIST OF TABLES

TABLE   Page

CHAPTER I
INTRODUCTION[*]

An asphalt mixture is a multi-phase material that results from combining aggregates (i.e., crushed rocks with different sizes and proportions) and asphalt binder. This material is used in the wearing course of flexible pavements and/or as part of base layers. Distresses in asphalt pavements are caused by the combined effects of dynamic traffic loading and environmental changes. Examples of pavement distresses include fatigue cracking, permanent deformation or rutting, patch deterioration, bleeding and raveling (i.e., physical separation of the asphalt binder and aggregate that can result, for example, in the dislodgement of aggregate particles from the surface), among others.

Moisture plays a special role in the degradation of asphalt mixtures since it is not only the main source of raveling but also a major contributor to the evolution of other distresses. In fact, the detrimental effect of moisture in asphalt mixtures, commonly called *moisture damage*, is one of the main causes of early rehabilitation of asphalt pavements. This is particularly important when considering that recent surveys (FHWA 2006) demonstrated that 90% of the roads with medium to high volumes of traffic in the United States have been built using asphalt mixtures materials. At the microscopic level, moisture affects the internal structure of asphalt mixtures in two different ways: 1) by reducing the quality of the cohesive resistance of the asphalt matrix (i.e., a composite comprised of the fine portion of the aggregates and asphalt binder), and 2) by reducing the quality of the adhesive bond between the aggregates and the asphalt matrix. These two phenomena occur within the asphalt mixture at different intensities and rates, depending on the volumetric proportions of the mixture, the material properties characterizing its constitutive phases, and the type and severity of the external loading and environmental conditions.

Moisture damage in asphalt mixtures is a complex phenomenon that involves chemical, physical, and mechanical processes. It can be defined as the progressive loss of

---

This dissertation follows the style of *Journal of Materials in Civil Engineering (ASCE)*.

[*]The initial part of this chapter contains published material from the technical paper: "A Coupled Micromechanical Model of Moisture-Induced Damage" by S. Caro, E. Masad, A. Bhasin and D. Little (in press), with permission granted by the *Journal of Materials in Civil Engineering* (*ASCE*).

functionality of the material caused by the presence of moisture in liquid and/or vapor state. The effects of the presence of water at the aggregate-binder interface have been studied since 1932 from a microscale perspective (Nicholson 1932; Thelen 1958). The first reported efforts to identify and characterize the most common distress in asphalt mixtures associated with moisture damage, called *stripping*, date from the 1960s and 1970s (Field and Phang 1967; Fromm 1974; Lottman 1978). However, it was only in the 1980s when this subject attracted the attention of highway agencies and the pavement industry nationwide.

The main approach to this phenomenon during the last 30 years has been from a macroscale perspective, with the disadvantage that little information has been gained on the *physico-mechanical-chemical* mechanisms occurring at the interior of the material. Consequently, the understanding of the combined mechanisms and causes associated with moisture damage remains unclear.

During the last decade, however, the concern to understand the phenomenon of moisture susceptibility at the microscale level has increased and new experiments and analytical models have been proposed. Some of the latest contributions in this area, described in detail in Chapter II, include:

- the determination of the effect of water on the ideal work of adhesion between aggregates and binder using principles of physical adhesion through surface free energy measurements (Bhasin 2006),

- a deeper understanding of the chemical phenomena associated with moisture damage (Bagampadde et al. 2005; Bagampadde et al. 2006; Huang et al. 2002; Huang et al. 2005; Petersen and Plancher 1998),

- the identification and modeling of damage processes occurring in asphalt mixtures (Arambula et al. 2007) and in the fine matrix of these materials (Caro et al. 2008b; Masad et al. 2006c) by means of a viscoelastic fracture model that includes the effects of moisture on the structural integrity of the materials,

- the experimental recognition and modeling of different moisture transport mechanisms at the interior of the material (e.g., permeability and capillary rise) by means of X-ray Computed Tomography (CT) and image processing techniques ,

- experimental measurements of moisture diffusion coefficients in asphalt mixtures (Arambula et al. 2009a; Kassem et al. 2006; Kringos et al. 2008b), and

- the mathematical modeling of the main physico-mechanical processes related to moisture damage (Graham 2009; Kringos et al. 2008a; Kringos et al. 2008c).

It is recognized that an important contribution to better understand and prevent moisture damage should focus on the last area (i.e., the mathematical modeling of the phenomena), where little work has been conducted. The existing numerical models of moisture damage have demonstrated to be important tools for gaining understanding of the moisture deterioration phenomenon in asphalt mixtures and have motivated new modeling approaches. This dissertation aims to provide new information on the kinetics of moisture damage in the microstructure of asphalt mixtures by means of a finite element micromechanical model that couples the effects of moisture diffusion with the mechanical performance of asphalt mixtures.

Objectives

The main objectives of this research are:

- Conduct a comprehensive and critical review of the causes, mechanisms, and methodologies to characterize and model moisture damage in asphalt mixtures;
- formulate a numerical micromechanical model of moisture-induced damage in asphalt mixtures. The model incorporates mass transport processes and fracture mechanics principles to evaluate the moisture degradation of the components of the mixture;
- conduct a parametric analysis to identify the role of some physical and mechanical properties of the constituents of the microstructure on the initiation and development of moisture-induced damage; and
- use probabilistic modeling approaches to study the influence of the air void phase on the mechanical performance of mixtures subjected to moisture diffusion processes.

Dissertation Outline

This document consists of six chapters. The present chapter (Chapter I) demonstrates the significance of the topic, describes the research objectives, and provides the general outline for the dissertation. Chapter II contains a comprehensive literature review on moisture damage. This chapter includes a description of the internal and external factors influencing moisture damage,

the mechanisms and distress manifestations related to this phenomenon, and the methodologies and procedures that have been developed for its characterization and modeling.

Chapter III focuses on the formulation of the coupled micromechanical model of moisture-induced damage. This chapter summarizes the moisture damage mechanisms that were considered in the model (i.e., modes of moisture transport, degradation and fracture processes within the microstructure, and variables and parameters required), as well as the numerical methodology followed for its numerical implementation. The last part of this chapter presents an example of the application of the model to a simplified microstructure of an asphalt mixture.

Chapter IV presents a parametric analysis of the contribution of the physical and mechanical material properties of an asphalt mixture's microstructure on the development of moisture-induced damage. The analysis was conducted by means of the coupled micromechanical model introduced in Chapter IV.

The micromechanical model was further used in Chapter V to study the influence of the variability and internal distribution of the air void structure on the moisture-related mechanical response of asphalt mixtures. The first part of this chapter describes the geometry of the microstructure model and the characteristics and properties of the different phases of the mixture. The second part describes two probabilistic-based modeling approaches used to treat the air void phase within the microstructure and discusses the results obtained from the simulations. The first modeling approach consisted of explicitly including the air void structure within the microstructure of the mixture, while the second consisted of using a stochastic modeling technique to consider the material properties of the asphalt matrix of the mixture to be dependent on the characteristics of the air void structure.

Finally, Chapter VI summarizes the main conclusions obtained from this dissertation and proposes some areas of future work.

CHAPTER II
COMPREHENSIVE REVIEW OF MOISTURE DAMAGE
IN ASPHALT MIXTURES*

This chapter provides a comprehensive critical review of the studies conducted during the last 50 years on moisture damage in asphalt mixtures. The review has two main focus areas: 1) damage mechanisms, modes of moisture transport and theories explaining the adhesive bond between aggregates and asphalt binder, and 2) methodologies to assess, characterize and model moisture damage. The first part of this chapter provides a historic review of the identification of moisture as an important cause of deterioration in asphalt mixtures. Next, the different modes of moisture transport within the microstructure of asphalt mixtures are explained, as well as the relationships between these modes and the characteristics of the internal void structure of the mixtures. Afterwards, different theories explaining the adhesion generated between aggregates and asphalt binder are summarized, followed by a description of the effects of moisture on degrading the adhesion bond quality. The following section explains most of the experimental and analytical approaches that have been developed to characterize the susceptibility of asphalt mixtures to moisture damage. Finally, the last section reviews recent efforts to develop mathematical models of this phenomenon.

Objectives

The objectives of this chapter are:

- critically discuss modes of moisture transport in asphalt mixtures and their influence on moisture damage,

- describe the processes occurring at the aggregate-binder interface and the theories that explain the nature and resistance of this adhesive bond,

---

- present and discuss experimental methods and analytical approaches to assess moisture damage, and

- summarize existing mathematical and numerical models to computationally simulate moisture damage.

It is noteworthy to mention that although an important research area in moisture damage has focused on remediation practices to minimize moisture damage (Emery and Seddik 1997; Liu and Kennedy 1991; Wasiuddin et al. 2007; Williams and Miknis 1998), this topic was considered to be outside the scope of this review.

Identification of the Effects of Moisture on Asphalt Mixtures

The effects of the presence of water at the aggregate-binder interface have been studied since 1932 at a microscale perspective (Nicholson 1932; Thelen 1958). The first reported efforts to identify and characterize stripping in asphalt mixtures in the field date from the 1960s and 1970s (Field and Phang 1967; Fromm 1974; Lottman 1978). However, it was in the 1980s when this subject attracted the attention of highway agencies and the pavement industry nationwide (Taylor and Khosla 1983). Moisture damage contributes significantly to the premature deterioration of asphalt pavements, which, in total, leads to an annual extra vehicle operating cost estimated at more than $54 billion (Copeland 2005). Approximately 87 % of transportation agencies in the United States try to mitigate this problem by specifying moisture susceptibility tests and minimum standards, and 82 % of the agencies recommend the use of antistripping additives to prevent damage caused by this phenomenon (Hicks et al. 2003). In addition, exclusive attention to this topic in various national and international conferences testifies to its importance, e.g., Symposium on Evaluation and Prevention of Water Damage to Asphalt Pavement Materials, sponsored by the American Society of Testing and Materials (ASTM) in 1984 (Ruth 1984); Symposia on Moisture Damage, held in Laramie, Wyoming, in 2002; National Seminar on Moisture Damage Sensitivity, conducted in San Diego, California, in 2003; and International Workshops on Moisture Damage in Asphalt Mixtures, hosted by Delft University of Technology in 2005 and by Texas A&M University in 2007.

Research conducted on moisture damage can be grouped into:

- identification of damage mechanisms (parameters and distress manifestations),

- development and improvement of tests for control and prevention, and

- development of analytical methods to characterize and predict susceptibility of asphalt mixtures to moisture damage.

Most of the work reported in the literature between 1980 and 1995 is related to the first two topics. A significant achievement during this period was the development of test methods and standards to identify and remediate asphalt mixtures that are prone to moisture induced damage (e.g., American Association of State Highway and Transportation Officials [AASHTO] T 283) (Terrel and Al-Swailmi 1994). For a detailed review of the tests, refer to Airey and Choi (2002) and Solaimanian et al. (2003). These tests were also used to evaluate the effect of antistripping agents and active fillers such as hydrated lime on the moisture sensitivity of asphalt mixtures in the laboratory and in the field (Hudson et al. 1990; Solaimanian et al. 1993; Tunnicliff and Root 1984). The tests were simple to conduct and widely accepted by various state and federal transportation agencies, but their drawbacks include the empirical nature of the procedures, the dependence of the results on the moisture conditioning methodology, and, in several cases, poor correlation with field performance. This prompted further research in two areas: 1) the understanding of the fundamental phenomena that cause moisture damage, and 2) improvement of the test methods and procedures to characterize the moisture sensitivity of asphalt mixtures.

During the last decade, thermodynamic theories, fracture mechanics, continuum damage mechanics, and other analytical methodologies have been used to analyze the effect of moisture in asphalt mixtures. Some research areas that focus on understanding the fundamental phenomena that cause moisture damage include analysis of the contribution of air void distribution and connectivity (Masad et al. 2007b; Masad et al. 2006b), modes of moisture transport (Arambula et al. 2009a; Chen et al. 2004; Kassem et al. 2006; Kringos et al. 2008b; Krishnan and Rao 2001; Masad et al. 2006a; Masad et al. 2007b), and physical characteristics of the material and aggregate-binder adhesive bond (Bhasin 2006; Bhasin et al. 2006a; Bhasin et al. 2006b; Copeland et al. 2007; Copeland 2007; Hefer et al. 2005; Kringos et al. 2008b; Little and Jones 2003; Song et al. 2005). A more recent approach involves the mathematical modeling of fundamental processes that occur during moisture damage (Graham 2009; Kringos et al. 2008a; Kringos et al. 2007; Kringos et al. 2008c).

In addition to the research on the evaluation of phenomena that cause moisture damage, the reevaluation of the most commonly used tests to assess it (Birgisson et al. 2005; Kringos et al. 2009; McCann et al. 2005), the design and implementation of new experiment and procedures

that provide better correlation with field performance (Airey and Choi 2002; Bagampadde et al. 2004; Collop et al. 2004; Kvasnak and Williams 2007; Mallick et al. 2005; Solaimanian et al. 2003), and further assessments of the effects of antistripping agents in the susceptibility of the mixtures to damage (Aksoy et al. 2005; Atud et al. 2007; Chen et al. 2006; Jahromi 2009; Wasiuddin et al. 2007) continue to be important areas of study.

Definition of Moisture Damage

A generalized definition of the term *damage* is the degree of loss of functionality of a system. Within this context, *moisture damage* in asphalt mixtures is broadly defined as the degradation of mechanical properties of the material due to the presence of moisture in a liquid or vapor state. Perhaps the most comprehensive definition of moisture damage in the literature is provided by Kiggundu and Roberts (1988) as "the progressive functional deterioration of a pavement mixture by loss of the adhesive bond between the asphalt cement and the aggregate surface and/or loss of the cohesive resistance within the asphalt cement principally from the action of water." Adhesive and cohesive failures are the last step in a process that starts with different modes of moisture transport and results in the generation of moisture damage, as will be discussed in the following sections.

Moisture Damage Mechanisms

A mechanism is a process that leads to changes in the internal or external conditions of a system producing a new "state" or condition. When the final state of the system represents a reduction in its original integrity, the process is considered a damage mechanism. A *moisture damage mechanism* consists of two steps: 1) a moisture transport process, and 2) a response of the system. The former refers to processes by which moisture in either a liquid or vapor state infiltrates the asphalt mixture as well as the asphalt binder or mastic (i.e., composite comprised of asphalt binder and the fine portion of the aggregates) and reaches the asphalt binder-aggregate interface. The latter refers to the changes generated at the interior of the mixture that lead to a loss in the load carrying capacity of the material.

Materials and system attributes (physical, chemical, and geometrical) control the modes of moisture transport into the bulk of the mixture and the response of the system. Table 2.1 presents the two components of moisture damage mechanisms in asphalt mixtures and some of

the system attributes that control these two components. Specific mechanisms are not presented in this table.

Table 2.1. Components of moisture damage mechanisms

Changes in internal or external conditions	System attributes		Response of the system
	Mixture and pavement related	Moisture states	
Moisture transport	Surface energy of the materials	Unsaturated flow	Detachment/debonding
	Chemical properties of materials (e.g. pH conditions)	or	Displacement
	Aggregate shape, texture, and angularity	Saturated flow	Dispersion
	Air void percent, size, and connectivity/permeability	and/or	Film rupture/ microcracks
	Others (construction issues and environmental factors)	Diffusion	Desorption
			Spontaneous emulsification

Table 2.2 presents the description of the terms reported in the fourth column of Table 2.1. All combinations among columns in Table 2.1 may not be physically or chemically possible. The precise moisture damage mechanism in any given asphalt mixture will be determined by the various physical and physico-chemical properties of the mixture and can be expressed as a combination of one or more of the elements described in this table. The following sections explore these components in more detail.

Figure 2.1 illustrates an aggregate coated with asphalt mastic that is subjected to two possible moisture damage mechanisms. In this example, the high percentage of air voids with low connectivity allows development of high pore pressures in the saturated flow condition and can cause mechanical damage due to film rupture or formation of microcracks. Simultaneously, moisture can also diffuse through the mastic and displace the asphalt binder from the aggregate surface owing to their poor interfacial adhesive bond strength.

Table 2.2. Description of the responses of the system presented in Table 2.1

Responses of the system	Description	Nature of the process
Detachment/ debonding	Separation of an asphalt film from an aggregate surface by a thin film of water without an obvious break in the binder layer (Little and Jones 2003)	Chemical, thermodynamic
Displacement	Loss of material from the aggregate surface through a break in the asphalt film and/or possible separation of the aggregate/mastic interface (Little and Jones 2003)	Mechanical
Dispersion of the mastic	Weakening of the cohesion in the asphalt binder or mastic due to long-term diffusion periods and loss of material due to the presence of flow (Kringos et al. 2008c)	Chemical, thermodynamic
Film rupture/ microcracks	Ruptures in the mastic or aggregates. The effect of microcracks is a general deterioration of the structural integrity of material and the generation of new paths for moisture transport.	Mechanical, thermodynamic
Desorption o the mastic	Washing away of the outer layers of mastics due to the presence of flow (Kringos et al. 2008c)	Mechanical after other processes
Spontaneous emulsification	Inverted emulsion of water droplets in binders (Little and Jones 2003)	Chemical

Finally, it is important to stress that environmental conditions also affect moisture damage mechanisms. For example, high relative humidity, intense rainfall periods, severe freeze-thaw cycles, and other extreme environmental conditions will increase the rate and amount of moisture that can reach the material, consequently increasing the damage potential. Other in-service conditions, such as aging and the dynamic loading produced by traffic, have also been considered important contributors to moisture damage. Lu and Harvey (2006) analyzed more than 63 cores of pavements in California in order to determine the parameters that influence moisture damage the most. The study showed that air void content, pavement structure, rainfall, and pavement age have the highest influence on moisture damage, while repeated loading and cumulative truck traffic have a marginal effect.
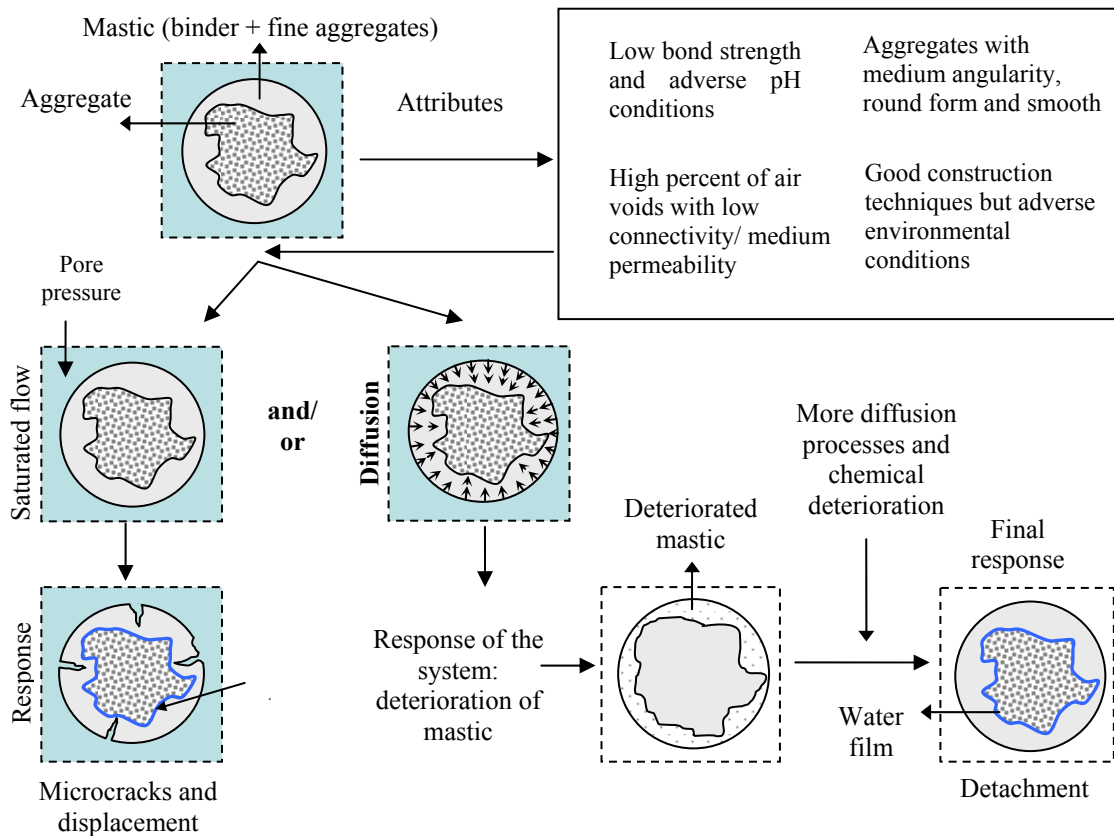
Figure 2.1. Two possible moisture damage mechanisms under the same attributes: a) pore pressure generates microcracks and displacement, and b) diffusion causes detachment

Void Structure in Asphalt Mixtures and its Relationship to Moisture Damage

Moisture transport in a porous medium, such as that of asphalt mixtures, is influenced by the void structure. Therefore, in order to identify the modes of moisture transport and their relationship to moisture damage, it is important to characterize the void structure in these materials. Some transportation agencies attempt to control moisture damage by limiting the percent of air voids, which will in turn limit the access of water to the bulk of the asphalt mixture. For example, the Ministry of Transportation of Ontario specifies that air voids in surface asphalt courses must be as low as possible in order to control moisture damage (Mohamed et al. 1993). Nevertheless, even with a low percentage of air voids, there is evidence of damage produced by infiltration of water (Mohamed et al. 1993), which proves that total air

void content does not provide a comprehensive measure of the rate of moisture transport in asphalt mixtures (Arambula et al. 2007; Masad et al. 2007b). Recent technological advances have made it possible to fully characterize the void structure in asphalt mixtures in terms of size, distribution, connectivity, and tortuosity of the flow path.

The size and distribution of air voids in asphalt mixtures depend mainly on the aggregate properties, mix design, and compaction processes (Brown et al. 2004; Masad et al. 2009). Chen et al. (2004) classified air voids in asphalt mixtures into three categories: effective, semi-effective, and impermeable (Figure 2.2). However, the identification of these different types of air voids in laboratory or field samples is difficult because of the complex internal structure of the material and the limited ability to explore its interior composition. There are various alternatives to determine the void structure of porous specimens. Some common techniques are based on two-dimensional images of the cross sections of the material acquired by Scanning Electron Microscopy (SEM), spectroscopic imaging techniques (to determine the chemical composition), and Atomic Force Microscopy (AFM) (Kosek et al. 2005). Techniques for three-dimensional characterization of porous media include Nuclear Magnetic Resonance (NMR) imaging (Barrie 2000), Transmission Electron Microscopy (TEM) visualization, and X-ray Computed Tomography (CT) reconstruction.

Effective	Semi-Effective	Impermeable

mastic →

voids →

Top-down Connections	Not fully connected through the material	No connections with the borders, isolated
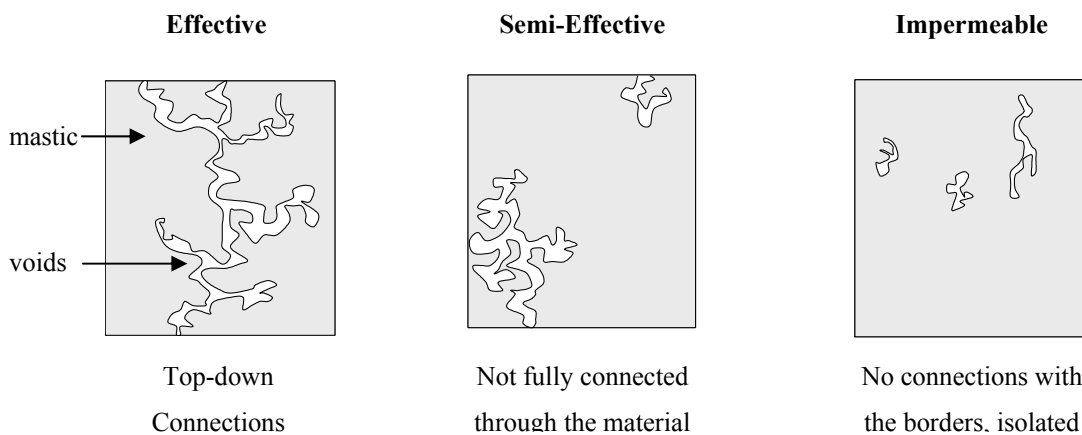
Figure 2.2. Classification of voids in asphalt mixtures; adapted from Chen et al. (2004)

X-ray CT is a non-invasive technique that has gained wide acceptance in the past few years. This technique has been successfully used to characterize the microstructure of porous materials such as solid foam textiles, pharmaceutical granules, biological materials (Kosek et al. 2005), and asphalt mixtures (Arambula et al. 2009b; Arambula et al. 2007; Masad 2004; Masad et al. 2007b; Masad et al. 2006b; Song et al. 2005; Wang et al. 2003). Figure 2.3 illustrates typical cross sections of two different types of asphalt mixtures obtained by this technique. Detailed information about this method can be found in other publications (Masad 2004; Otani and Obara 2004).
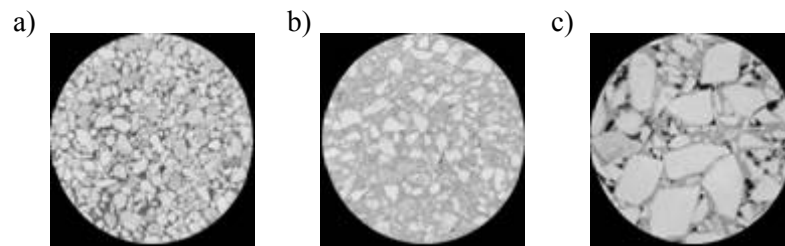
Figure 2.3. Images of cross sections of hot asphalt mixtures: a) and b) dense graded asphalt mixtures, and c) stone matrix asphalt (SMA)

Image analysis can be used to determine the void structure of the material. This non-destructive procedure has three main advantages: 1) it allows probabilistic determination of the air voids by measuring the size of individual voids, 2) it allows the determination of potential paths for moisture transport by identifying interconnected air voids between different sections, and 3) it can be used to compute the tortuosity of the air void paths (i.e., the ratio of the true length of a path to the length of the straight line between its ends).

Al-Omari and Masad (2004) used this technique to determine permeability in asphalt mixtures, which is an important mode of moisture transport. He characterized the air void structure and determined the tortuosity of 14 samples with different total air void contents (10 of them containing limestone and 4 of them gravel). The results from his investigation demonstrated that tortuosities were in a range of 3.16 to 4.94, meaning that, on average, the real length of a path in the specimens was more than 3 times the distance between the extreme points. Figure 2.4 presents the results obtained by Masad et al. (2006b) for air void distribution of

granite and limestone dense mixtures. In this study, the authors analyzed the effect of air void distribution on moisture damage for different types of mixtures. Moisture damage was quantified as the ratio between fatigue life of a moisture conditioned (N_{fc}) specimen (i.e., the specimen after an accelerated process that generates moisture damage) and fatigue life of a dry (N_{fu}) specimen using the Superpave indirect tensile test (IDT).
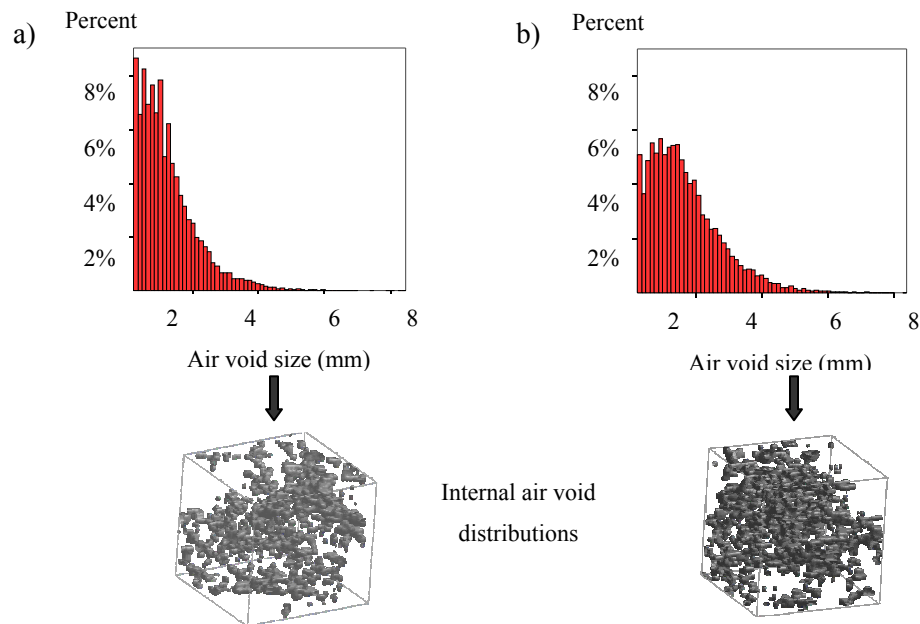
Figure 2.4. Air void distribution and visualization for mixes: a) dense mixture with limestone and b) dense mixture with granite; adapted from Masad et al. (2006b)

Figure 2.5 presents the relationship between air void distribution and moisture damage for granite specimens. These results suggest that there is an average size of air void, referred to as the *pessimum* air void size, for which the moisture sensitivity of the mixture is maximum. The existence of the *pessimum* range was explained by the fact that for small air void sizes the infiltration of water in the mix is low, for large air void sizes the water reaches the material but it is easily drained out, and for the *pessimum* air void size (between 1.2 mm and 1.4 mm for granite and 0.8 mm and 1.0 mm for limestone, Masad et al. 2006b) the water is trapped in the material generating propitious conditions for moisture damage.
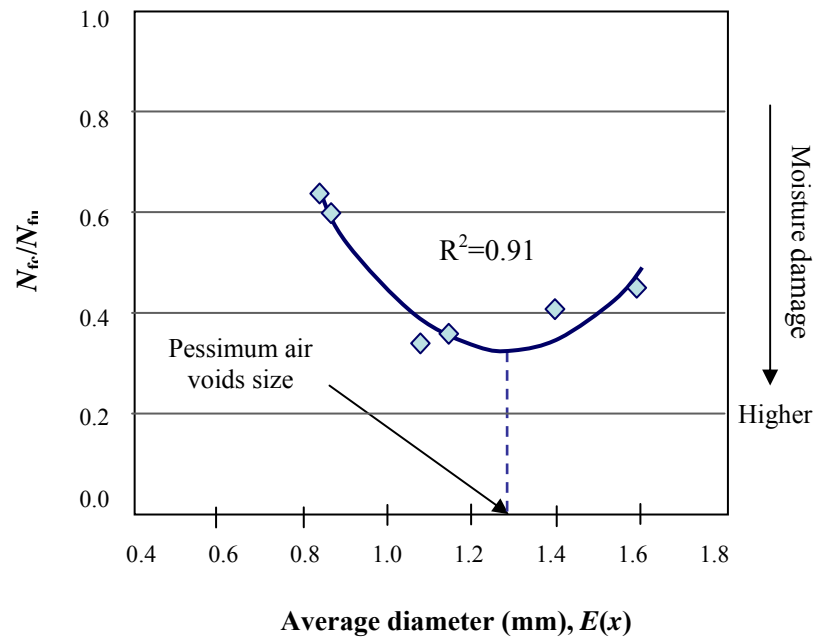
Figure 2.5. Moisture damage expressed as N_f ratio versus average air void diameter for a dense granite mixture; adapted from Masad et al. (2006b)

The concept of *pessimum air voids* was first introduced by Terrel and Al-Swailmi (1993), when they demonstrated that there is a specific total percent of air voids for which the potential of moisture sensitivity in a mixture is maximum (i.e., pessimum air void content). Further, most of the regular dense graded asphalt mixtures are designed with an air void content in the range of 5 to 10 %, which is the most likely range for the pessimum air voids (D'Angelo and Anderson 2003).

Arambula et al. (2007) also demonstrated the importance of characterizing the internal air void structure of asphalt mixtures in order to evaluate moisture damage. They used X-ray CT and image analysis techniques to demonstrate that asphalt mixtures designed with the same asphalt binder and the same target air void content (6 to 7 %) had significant differences in their air void size distribution and connectivity. This information was used to quantify moisture damage using a fracture mechanics based model. The results showed that the samples had different levels of moisture damage susceptibility depending on the air void structure.

It is also important to mention that factors related to construction such as mixture production, placement, and compaction also affect the void structure of asphalt mixtures in the field. For example, Mohamed et al. (1993) found that common compaction techniques in asphalt layers generate cracks, commonly known as *checks*. These cracks are typically 1 to 4 inches in length and are 1 to 3 inches apart. Checks are normally not visible and are generated during the first or second pass of conventional steel-wheel rollers. The authors stressed that the formation and propagation of these cracks promote water transport in locations that were expected to be isolated. Furthermore, they proposed a new compaction technique that reduces the formation of cracks, preventing the general deterioration of the material due to moisture and oxidation (checks are also a route access for air).

Chen et al. (2004) also analyzed the effect of crack width on moisture damage. They found that crack growth and higher air void content had a similar influence on the moisture resistance of asphalt mixtures. This is not surprising because cracks act as *links* between air voids, generating new connected paths. More recently, Masad et al. (2009) evaluated the influence of compaction techniques on the uniformity of the air void phase of asphalt courses. The research methodology consisted of applying the X-ray CT technique to characterize the internal void structure of field cores that were extracted from pavements compacted using diverse patterns. The results showed that internal void distributions within the asphalt layer are highly influenced by the compaction pattern used, and that the efficiency of the compaction process in reducing the air voids within the mixture at a specific location is a function of the relative distance of that location with respect to the roller compactor width.

Studies related to this topic have also been carried out to analyze the effect of lift thickness and other construction characteristics in the void structure of asphalt courses (Brown et al. 2004; Cooley Jr. et al. 2002; Mohamed et al. 1993; St.Martin et al. 2003).

Modes of Moisture Transport

Most of the research pertaining to moisture damage assumes the presence of water in the material. Therefore, the modes by which moisture reaches the mixture have usually been overlooked. The three main modes of moisture transport are: 1) infiltration of surface water, 2) capillary rise of subsurface water, and 3) permeation or diffusion of water vapor (Masad et al. 2007b). Infiltration of water from the surface is the main source of moisture in the pavement and is directly related to rainfall, drainage conditions, and material properties. However, field reports

of pavements with severe moisture damage from regions with low levels of annual rainfall, such as Arizona and New Mexico (Hicks et al. 2003), suggest that permeation of vapor and capillary rise of subsurface water can be equally important modes of moisture transport.

This section describes the main modes of moisture transport in asphalt mixtures:

1) water permeability,
2) water capillary rise, and
3) vapor diffusion.

Permeability

Permeability is defined as the ability of a material, in this case an asphalt mixture, to transmit fluids (Bowles 1984). Research pertaining to the characterization and computation of permeability in asphalt mixtures ranges from development of analytical solutions and models of water transport to experimental field work (Al-Omari et al. 2002; Cooley Jr. et al. 2002; Huang et al. 1999; Masad et al. 2007a; Masad et al. 2004; Mohammad et al. 2003). Table 2.3 presents typical ranges of permeability for three common types of asphalt mixtures (Chen et al. 2004).

Table 2.3. Classification of voids in terms of permeability (k) for asphalt mixtures; after Chen et al. (2004)

k (cm/s)	Permeable condition	Void	Mixture
10^{-4} or lower	Impervious	Impermeable	Dense
10^{-4}-10^{-2}	Poor drainage	Semi-effective	Stone mastic asphalt
10^{-2} or higher	Good drainage	Effective	Porous asphalt

The air void system of a porous medium significantly affects its permeability. Unfortunately, this relationship is neither simple nor evident. Over the past several years a maximum of 8% in-place air void content for dense graded mixtures was considered an acceptable limit to control permeability, but recent studies have shown that this value cannot be generalized for all mixtures (Cooley Jr. et al. 2002).

As discussed in the previous section, there are significant differences in air void size distribution and connectivity in mixtures with the same air void percent.

Table 2.4 presents some correlations that have been established between permeability and air voids, showing that this relationship is exponential in all cases.

Table 2.4. Correlations between permeability and air voids

Mixture	Correlation [1]	Range of x in %	R^2 value	Comments	Authors
Dense graded	$Ln\,(k) = 0.432\,x - 13.386$	2-8	0.85	k in cm/s laboratory permeability	Chen et al. (2004)
Stone mastic asphalt	$Ln\,(k) = 0.459\,x - 9.821$	4-9	0.93		
Porous asphalt	$Ln\,(k) = 0.209\,x - 7.017$	12-20	0.90		
Coarse graded, 9.5 mm NMAS[2]	$k = 0.0054\,x_{ip}^{4.9098}$	---	0.6925	k in 10^{-5} m/s field permeability	Cooley Jr. et al. (2002)
Coarse graded, 12.5 mm NMAS	$k = 0.0047\,x_{ip}^{4.8672}$	---	0.6423		
Coarse graded, 19 mm NMAS	$k = 0.0054\,x_{ip}^{4.9098}$	---	0.6925		
Coarse graded, 25 m NMAS	$k = 0.6739\,x_{ip}^{3.7721}$	---	0.4964		
Florida limestone (dense graded)	$k = 28.83\,PSP^{0.89}$	---	0.68	k in 10^{-5} m/s laboratory permeability	Masad et al. (2006a)
Georgia granite (dense graded)	$k = 4.35\,PSP^{1.181}$	---	0.79		

(1) k = permeability, x = total air void content, x_{ip} = in-place air void content, PSP = pore size parameter of the mix (product of the total air void content by the expected value of the air void diameter square).

(2) Nominal maximum aggregate size.

Masad et al. (2004) developed an empirical equation to determine the permeability of asphalt mixtures based on the Kozeny-Carman equation in saturated porous media. Permeability of the mixture, k (in 10^{-5} cm/s), is expressed as a function of the total air void content in the mix (n) and the aggregate specific surface area in 1/mm (S_{agg}) as follows:

$$k = \frac{n^m \gamma}{c S_{agg}^t \mu},$$

(2.1)

where γ is the unit weight of the fluid and μ is the viscosity of the fluid. The aggregate specific surface area was determined based on the gradation and density of aggregates. The parameters c and t were found to have values close to 1 and 5, respectively, independent of the type of mixture or the methodology used to measure permeability. The authors used permeability values measured on field and laboratory mixtures to calibrate the equation (i.e., the parameter m).

Masad et al. (2006a) improved this equation to account for the effect of asphalt content and saturation level as follows:

$$k = \frac{\overline{C} n^3}{(1-n)^2} \left[D_s \left(1 + \frac{G_{sb}(P_b - P_{ba}(1-P_b))}{G_b(1-P_b)} \right)^{\frac{1}{3}} \right]^2 \frac{\gamma}{\mu},$$

(2.2)

where G_b is the binder specific gravity, P_{ba} is the percent of absorbed binder by weight of aggregate, P_b is the percent of asphalt content by total weight of the mix, G_{sb} is the bulk specific gravity of the aggregate, $\overline{C}$ is a factor that takes air void shape and saturation level into account, D_s is the average diameter of particles, n is the percent of air voids, γ is the unit weight of the fluid, and μ is fluid viscosity. The authors found that air void content (n) is the parameter that has the most influence on permeability, followed by the average aggregate size (D_s).

As can be seen from the previous discussion, permeability is normally calculated as a function of the average percent of air voids. However, if information regarding air void size distribution is available (as discussed previously), it is possible to derive a probabilistic calculation of permeability. Masad et al. (2006b) used a model to correlate permeability and air void distribution—initially developed for soils (Garcia-Bengochea 1978)—in asphalt mixtures using the following expression:

$$k = C_s n \int_{x_{min}}^{x_{max}} x_i^2 f(x_i) dx,$$

(2.3)

where k is permeability, C_s is a shape factor, n is the percent of air voids or porosity, and $f(x_i)$ is the probability density function of air void distribution. The study by Masad et al. (2006b) showed how a comprehensive characterization of the void structure can be translated into a more realistic calculation of permeability.

Besides the void structure in asphalt mixtures, construction factors such as lift thickness, compaction effort, and density homogeneity also determine the effective permeability value in the field. Mohammad et al. (2003) and St. Martin et al.(2003) explored the effect of lift thickness on the permeability of mixtures with a fixed amount of air void content. They established that there is an inverse relationship between these two parameters. For a mixture with 7.0 % air void content, a reduction of 50 % in the permeability level was reported (from $35*10^{-5}$ cm/s to $18*10^{-5}$ cm/s) when the lift thickness changed from 20 to 80 mm (St.Martin et al. 2003). Based on their experimental results, Cooley Jr. et al. (2002) found the following relationship between field permeability (k), air void content (a), NMAS, and lift thickness (h):

$$k_{field} = -5.335 + 4.61\ln(a) + 0.138 NMAS - 0.024h,$$
(2.4)

Cooley Jr. et al. (2002) stress the fact that although some agencies require maximum values of allowable permeability in order to control the performance of the mixtures in service, there is no clear equivalence between field and laboratory measurements of permeability. Therefore, the data obtained from the laboratory must not be directly used as the actual permeability of the material in the field.

Capillary Rise

Capillary rise is defined as the rise in a liquid above the level of zero pressure due to a total upward force produced by the attraction of the liquid molecules to a solid surface (Bowles 1984). In asphalt pavements, capillary rise allows subsurface water to be transported into the bulk through the "capillaries" formed by the interconnected voids. The final height of the column of water above the saturation surface, h, as well as the rate of rise, depend on: 1) the geometrical characteristics of the capillaries (the capillaries are normally assumed to be cylindrical and characterized by their radius, r), 2) the surface tension of water (Ts), 3) the density of the water

(ρ), and 4) the contact angle between the liquid and solid (α). The general equation describing capillary rise in porous media is found by the equilibrium of forces acting on the system:

$$2\pi r T_s \cos\alpha = \pi r^2 h g \rho,$$
(2.5)

where g is the acceleration due to gravity.

The rate of water rise is governed by the following equation (Washburn 1921):

$$\frac{dl}{dt} = \frac{\left[P_A + g\rho h + \frac{2\gamma_{LV}}{r}\cos\alpha\right]\left(r^2 + 4\varepsilon r\right)}{8\eta l},$$
(2.6)

where P_A is the atmospheric pressure, ε is the coefficient of slip, η is the viscosity of the liquid, and l is the total length of the column of liquid in the capillary.

Although capillary rise is an important mode of moisture transport, there is little work pertaining to its quantification and analysis in asphalt mixtures. In general, capillary rise is not expected to take place when water is in contact with neat binder due to the hydrophobic nature of the binder. However, capillary rise does occur in asphalt mixtures because water comes into contact with the mastic and not directly with the neat binder. Masad et al. (2007b) quantified the capillary rise in asphalt mixtures and estimated the effective contact angle between water and mastic using laboratory experiments. Void distributions and connectivities of the dry mixture were determined using X-ray CT and image analysis techniques. The same procedure was used to determine the presence of water within the voids of the specimen after placing them in a shallow distilled water bath of 10 mm for 7, 13, 25, and 29 days (Figure 2.6). In each case, the voids filled with water were identified, and the height of the water column in the air void path was recorded.

Figure 2.7 presents the results for specimens corresponding to two dense asphalt mixtures with different gradations (*A* and *B*) and different trimmed and cored methodologies (*B*1 and *B*2). The fact that capillary rise occurs in asphalt mixtures is demonstrated as shown in this figure. For all mixtures, the effective contact angle was in a range of 59.2 to 71.2º. Faster capillary rise was observed in the specimens with a high voids filled with water content, which also corresponded to the specimens with the lowest contact angles. The results were only

presented for voids that were equal or larger than the image resolution of the equipment. However, it is expected that a greater height of rise took place in smaller voids that were not detected in the images and in the aggregate-binder interfaces.

a)   b)
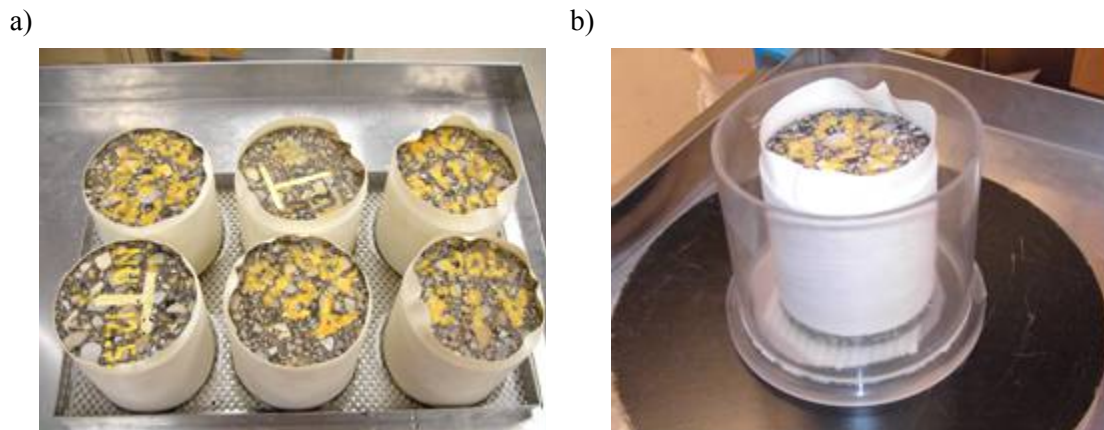
Figure 2.6. Experiment setup: a) specimens sitting in a 10 mm distilled water bath and (b) specimen in the scanning container for X-ray CT; after Masad et al. (2007b)
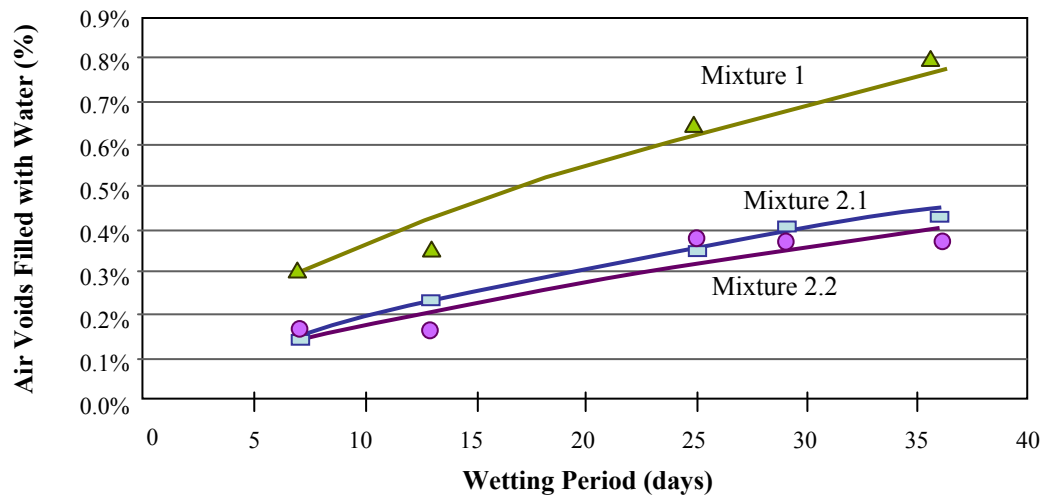
Figure 2.7. Percentage of voids filled with water during time due to capillary rise for three dense mixtures; 1 and 2 represent two different types of gradation; adapted from Masad et al. (2007b)

Vapor Diffusion

The amount of water vapor and the rate at which it accumulates in an asphalt mixture depend on three primary factors: 1) relative humidity, 2) diffusion coefficients, and 3) storage rate and storage capacity (also called water holding potential). Relative humidity depends on environmental conditions, whereas diffusion coefficients and storage capacity are material properties. The storage rate and storage capacity depend on the chemical and thermodynamic properties of the material.

   Sasaki et al. (2006) analyzed vapor mass transfer and water storage mechanisms in asphalt mixtures that generate moisture damage. They simulated environmental conditions for a 24-hour period using a moisture permeation test. Cores from two Japanese national roads (one of them affected by moisture damage) were tested by reproducing the original environmental field conditions (Figure 2.8).
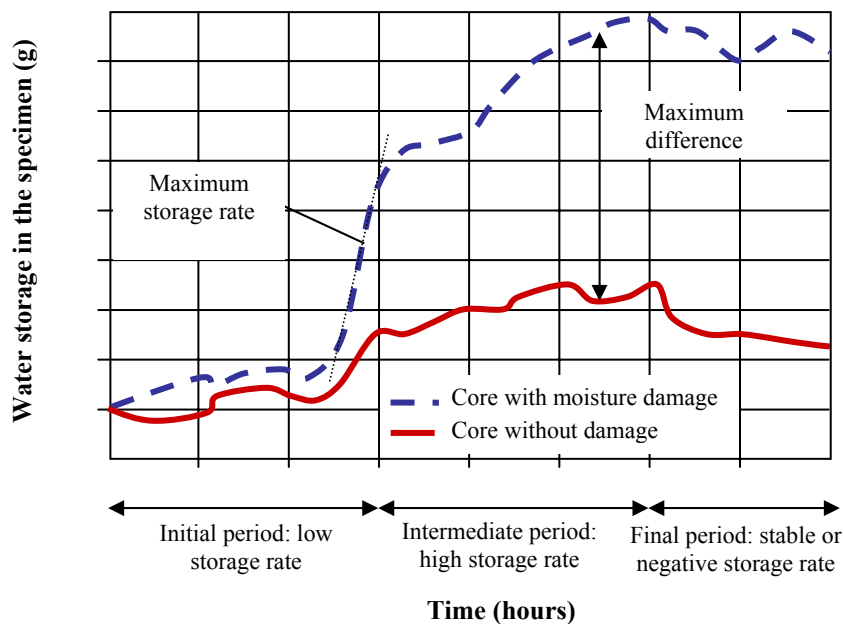
Figure 2.8. Water storage in a 24-hour period using a new moisture permeation machine; adapted from Sasaki et al. (2006)

Their work demonstrated that in a 24-hour period, the core from the stripped pavement absorbed and stored more than 15 g of water as compared to 5 g absorbed from the undamaged cores. They attributed the presence of excess water in the damaged specimen to the presence of more connected water paths relative to the undamaged specimen. Their results support the idea that there is a relationship between vapor transport, storage capacity, and moisture damage.

Kassem et al. (2006) and Kassem (2009) also studied moisture diffusion in asphalt mixtures by measuring suction (i.e., the free energy state of water) using thermocouple psychrometers. They quantified suction by measuring the relative humidity in the air phase of the asphalt mixture. For detailed information regarding the experiment and results, readers are referred to Kassem (2005). The study demonstrated a good correlation between suction and air void size distribution in asphalt mixtures. Furthermore, the authors reported that low suction values were related to high relative humidity gradients in voids and presented higher levels of moisture damage. However, a parabolic relationship between suction and moisture damage was found for limestone mixtures, which suggests that for certain mixtures there is a suction value for which moisture damage can be minimized (i.e., optimum suction value).

Kassem et al. (2006) also determined the diffusion coefficients of three different mastics (*A*, *B*, and *C*) corresponding to mixtures with known qualitative field performance. The diffusion coefficient was measured as the rate of change of suction with time using the wetting (soaking) test with thermocouple psychrometers. They also measured the time for total suction to drop from the oven dry condition to within the range of measurement of the psychrometer, and demonstrated a correlation between this parameter and moisture damage observed in the field (Table 2.5). Since the moisture sensitivity of mixtures is related to the rate of moisture diffusion, mastics that required a short time to reach the measurement range of the psychrometer are considered to be more susceptible to moisture damage (i.e., mastic *C* in Table 2.5).

Table 2.5. Diffusion coefficient *D* and time to reach psychrometer's range for sand asphalt mixtures; after Kassem et al. (2006)

Mix	Reported field performance	Range of α, cm^2/s	Average value of α, cm^2/s	Standard deviation, cm^2/s	Time to reach psychrometer's range, hours
A	Good	$1.28*10^{-7}$-$7.72*10^{-8}$	$1.01*10^{-7}$	$1.869*10^{-8}$	177.7
B	Fair to poor	$1.30*10^{-7}$-$6.43*10^{-8}$	$1.00*10^{-7}$	$2.946*10^{-8}$	137.8
C	Poor	$3.58*10^{-7}$-$1.28*10^{-7}$	$2.29*10^{-7}$	$1.188*10^{-7}$	43.1

Cheng (2002) and Cheng et al. (2002) demonstrated the differences in rates of moisture diffusion and water holding capacity of different asphalt binders using gravimetric measurements under controlled relative humidity conditions. The study showed that the amount of water vapor absorbed by the asphalt binder was significant and also presented the hypothesis that mixtures that contain binders with high water holding potential were more prone to moisture damage.

Kringos et al. (2008c) also identified moisture diffusion as one of the most important causes of degradation of the aggregate-asphalt binder adhesive bonds. The authors have conducted experimental and numerical work on the effects of moisture diffusion on the degradation of adhesive bonds (Kringos et al. 2008b; Kringos et al. 2008c). As part of the experimental work, the authors used a gravimetric technique to quantify moisture diffusion coefficients of mastics of different nature (Kringos et al. 2008b).

More recently, Arambula et al. (2009a) proposed a simple and efficient methodology to quantify water vapor diffusion coefficients of road materials. The technique uses periodic measurements of the weight of cylindrical material-plastic container specimens that are subjected to a controlled temperature and relative humidity environment to compute the water vapor diffusivity of the material. The proposed methodology is similar to the technique specified by the ASTM E96 water method (ASTM 2007). In a different study, Arambula et al.(2009b) used images of the microstructures of dense-graded asphalt mixtures obtained from X-ray CT in three-dimensional (3-D finite element and finite difference element models to estimate the *effective* moisture diffusion coefficients of an asphalt mixture based on the moisture diffusion coefficients of its individual phases (i.e., aggregates, air and mastic). The results from the numerical simulations were compared against experimental data obtained from the same specimens (Kassem et al. 2009), showing that the effective diffusion coefficient obtained using the finite difference method provided closer agreement with the experimental data.

Figure 2.9 illustrates an example set of parameters related to vapor diffusion and its effect on asphalt mixtures. In this illustration, the external condition (e.g., high relative humidity gradients), and the material properties (e.g., high diffusion coefficients, high storage capacity, and high air void connectivity) are shown to favor the diffusion process.
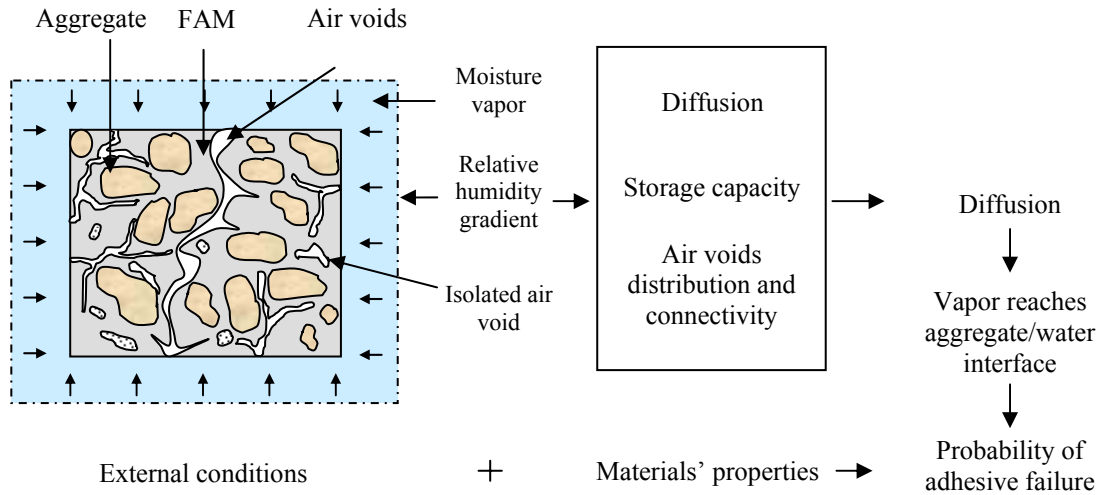
Figure 2.9. Parameters involved in vapor diffusion process and its effect on asphalt mixtures

Aggregate-Binder Interface Characteristics

As explained earlier, moisture in asphalt mixtures promotes the generation of cracks in the material. Crack growth in asphalt mixtures can occur either within the binder or at the binder-aggregate interface. The former is referred to as cohesive cracking (or failure), and the latter is referred to as adhesive cracking. Typically, adhesive failure will occur if the asphalt binder film is very thin, and cohesive failure will occur if it is very thick (Marek and Herrin 1958; Masad et al. 2010). Compared to cohesive bonds, adhesive bonds are considered to play a more important role in moisture damage manifested as stripping of the binder from the aggregate.

Hefer et al. (2005) described the three types of interaction forces responsible for adhesion between the asphalt binder and aggregate. The first type corresponds to electrostatic interactions between ions and refers to forces between two separated charges, resulting from Coulomb's inverse-square law (i.e., Coulomb forces). The second type corresponds to electrodynamic interactions through Van der Waals forces. In this case, the forces result in bonds that are weaker in comparison to ionic bonds and include different types of interactions depending on the molecular electric dipole conditions at the interface of the two materials. The third type corresponds to interactions through electron pair sharing (i.e., covalent bond). In this case, the bonds result from the union of two components when sharing an electron pair; the

electron pair can be donated by the two components or by one of them. The electrostatic and electrodynamic interactions are regarded as *physico-chemical bonds,* and the interactions in the last group are regarded as *chemical bonds*.

Experimental techniques can quantify the susceptibility of adhesive bonds between asphalt binder and aggregates to moisture damage. Huang et al. (2002) presented a comprehensive evaluation of several methods to analyze the aggregate-binder interface system. The authors analyzed the validity, limitations, and potential of five techniques using eight binders (Strategic Highway Research Program [SHRP] core asphalts) and some commonly used aggregates. The techniques evaluated included a sliding plate rheometer (developed by the Western Research Institute, WRI), Differential Scanning Calorimetry (DSC), AFM, liquid chromatography, centrifugation, and infrared (IR) spectroscopy. The authors found that all techniques are rapid procedures that provide valuable information about interactions occurring at the interface of the asphalt binder with the aggregate (also recognized as a thin-film phenomenon). These techniques are supported by theories that explain adhesive bond mechanisms that have been classified as (Hefer et al. 2005; Hicks 1991; Kanitpong and Bahia 2003; Little and Jones 2003):

- weak boundary layers,
- electrostatic forces,
- chemical bonding,
- mechanical bonding, and
- adhesion due to surface free energy.

Weak Boundary Layers

This theory states that adhesive failure may occur due to the presence of an interface region of low cohesive strength (Packham 1992). An example of a weak boundary layer in asphalt mixtures is the aggregate-binder bond that results when aggregates that contain dust on their surface are mixed with binders. The degree of acidity (pH) of the water determines the degree of dissolution. For example, pH values lower than 6 are favorable for the dissolution of surface layers of carbonates, while pH values higher than 8 are favorable for the dissolution of surface layers of silica minerals (Jamieson et al. 1995).

Electrostatic Forces

The electrostatic theory attributes the adhesive strength between two materials to the Coulombic forces of attraction at the surface of the materials (Allan 1992). Interactions between solid surfaces and liquid media containing dissolved ions, such as water, are particularly important to explain moisture damage in asphalt mixtures (Labib 1992; Yoon and Tarrar 1988). When a solid surface with an active charge is exposed to water, two charged *layers* are formed: 1) the *stern* layer and 2) the *mobile* or *diffuse* layer. The former is comprised of one or more layers of ions of opposite charge that bind to the surface in order to neutralize charges. The latter results from the thermal motion of the ions beyond the stern layer (Hefer et al. 2005).

The zeta potential, also known as the electrokinetic potential, is a measure of the electric potential at the shear plane between these two charged layers and has been used to analyze debonding of asphalt binder from the aggregate in the presence of moisture (Labib 1992). The pH value and, consequently, the magnitude and polarity of the zeta potential at the aggregate-binder interface are determined by the environment and by the surface composition of the aggregates (Hefer et al. 2005). Depending on the pH value, the zeta potential of the asphalt binder and aggregate may have the same polarity, which will result in a net repulsion between these two materials, causing them to debond in the presence of water. Figure 2.10 illustrates the zeta potential of different asphalt binders and granite aggregates at different pH values (Labib 1992).
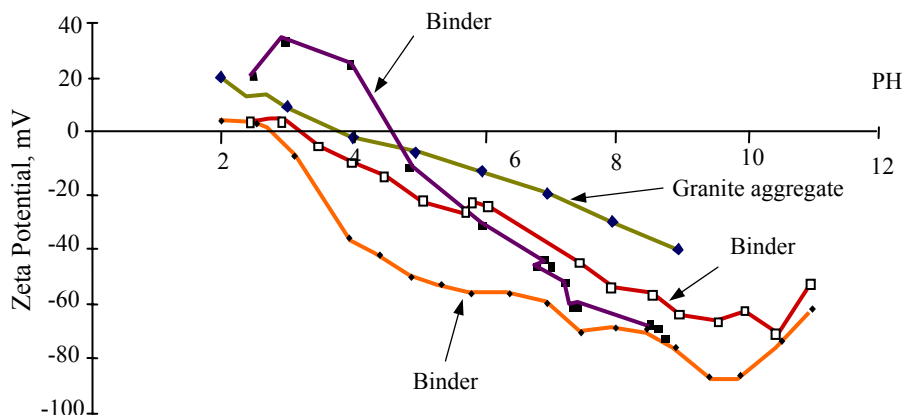
Figure 2.10. Zeta potential of different asphalt binders and limestone aggregate at different pH values; adapted from Labib (1992)

Chemical Bonding

Research on adhesion due to chemical bonding is important in explaining the moisture damage mechanisms in some aggregate-binder systems (Bagampadde et al. 2005; Bagampadde et al. 2006; Curtis et al. 1993; Hefer et al. 2005; Huang et al. 2002; Huang and Robertson 2004; Little and Jones 2003; Petersen and Plancher 1998; Petersen et al. 1982; Plancher et al. 1977). Chemical bonding theory suggests that the adhesive bond between the asphalt binder and aggregate results from a chemical reaction between these two materials. Bonding between two materials due to their surface free energy or electrostatic interactions is also based on the chemical nature of these materials. However, an important distinction between these mechanisms and adhesion due to chemical bonding is that the latter is caused by the formation of a new material because of the reaction between active functional groups from the binder and the aggregate at their interface. Hefer et al. (2005) explain how different chemically active sites on the surface of the mineral aggregate react with various functional groups from the asphalt binder to create interfacial adhesion between these two materials. Therefore, it is imperative to characterize the chemically active sites on mineral surfaces and functional groups in asphalt binders in order to analyze the nature and durability of chemical interactions between these two materials. For asphalt binders the characterization should include the original as well as the oxidative aged asphalt binder (Huang et al. 2002; Huang and Robertson 2004; Negulescu et al. 2006).

In general, aggregates with high carbonate content (also called *basic aggregates*) are easier to coat with binder than aggregates with high silica content (also called *acid aggregates*). This is due to the fact that siliceous aggregates contain high concentrations of hydroxyl groups with greater affinity for carboxylic acid and water. The carboxylic acid components that are present in the binder are adsorbed by the surface of these aggregates, generating a binder-aggregate bond. However, the bonds with the carboxylic acids are also prone to displacement in the presence of water (Huang et al. 2002; Petersen and Plancher 1998; Petersen et al. 1982). The affinity of binder-aggregate combinations in terms of their resistance to moisture damage can be evaluated by identifying the various functional groups within the asphalt binder that are more prone to be adsorbed by the aggregate surface and their tendency to be displaced by water from the aggregate surface. Hefer et al. (2005) summarized the results of three research studies that quantified the relative affinity of aggregate surfaces to functional groups from asphalt binder and water (Table 2.6). It is noted that in most cases functional groups from the asphalt binder that are

strongly adsorbed on the aggregate surface are also more prone to be displaced by water. This suggests that displacement of bitumen by water at the interface region is a chemically favorable phenomenon.

Table 2.6. Results for most strongly adsorbed functional groups for aggregate surfaces and in the presence of water; after Hefer et al. (2005)

Level of adsorption	Most strongly adsorbed functional groups (decreasing order)		
	Plancher et al. (1977)	Peterson et al. (1982)	Curtis et al. (1993)
High	Carboxylic acids	Carboxilic acids	Carboxilic acids
↑	Anhydrides	Anhydrides	Sulfoxides
	2-quinolones	Phenolic	Pyrridine types
	Sulfoxides	2-quinolones	Phenolic
	Pyridine types	Sulfoxides	Pyrrolic
	Ketones	Ketones	Ketones
		Pyrridine types	
Low		Pyrrolic	
Level of adsorption in the presence of water	Functional groups most susceptible to adsorption for water displacement (decreasing order)		
High	Carboxylic acids	Anhydrides	Sulfoxides
↑	Anhydrides	2-quinolones types	Carboxilic acids
	Sulfoxides	Carboxilic acids	Pyrrolic
	Pyridine types	Pyrridine types	Ketones
	2-quinolones	Sulfoxides	Pyrridine types
	Ketones	Ketones	Phenolic
		Phenolic	
Low		Pyrrolic	

Chemical and mineral composition of the aggregate also determine the quality and the durability of the adhesive bond with the asphalt binder. Bagampadde et al. (2005) investigated the moisture susceptibility of asphalt mixtures that were prepared using 11 aggregates from different sources and one binder. The aggregates and binder were characterized based on their mineralogy and chemical composition. The moisture sensitivity of the compacted specimen was

quantified as the ratio between the tensile strength and dynamic modulus measured in the wet condition (i.e., damaged after a water conditioning process) and dry condition (i.e., undamaged) following the AASHTO T 283 methodology. Ratios less than 70 % were associated with lower resistance to moisture damage. Based on a statistical analysis, this study reported that mixtures with aggregates containing alkali metal elements (e.g., sodium and potassium) or aggregates with high contents of quartz and alkali feldspars were more prone to moisture damage. On the contrary, mixtures with aggregates containing calcium, magnesium, and iron were found to be moisture resistant. No correlation with moisture damage was established with aggregates containing alumina. However, since these findings were based on mixtures with a single binder, the results could not be generalized. More recently, Bagampadde et al. (2006) explored the role of asphalt chemistry on moisture damage. They followed a similar methodology as described previously, but with different types of aggregates and four types of asphalt binders. It was observed that characteristics of asphalt binders such as acid number, penetration grade, and molecular size distribution are not statistically significant factors in determining the resistance of mixtures to moisture damage. The authors also reported that the variability in moisture susceptibility is mainly attributed to aggregates rather than to binders. Similar results were also found by Airey et al. (2007) after analyzing the effect of certain properties of binders and aggregates in 14 different mixtures in the promotion of moisture damage using the saturation ageing tensile stiffness (SATS) test developed at the Nottingham Transportation Engineering Centre (NTEC).

Adhesion due to chemical bonding is also useful in explaining the action of additives such as hydrated lime and anti-strip agents in improving the moisture resistance of asphalt mixtures (Bagampadde et al. 2005). Little and Petersen (2005) studied the changes in the rheological properties as well as the physical and chemical interactions that explain the differences in the mechanical response of mastics when hydrated lime is included as a filler. The authors reported that hydrated lime chemically reacts with the carboxylic acids and 2-quinolone types present in asphalt binder, allowing functional groups that are more resistant to water displacement to adsorb and form bonds at the aggregate surface. They also demonstrated an increase in the ability of the asphalt binder to dissipate stresses as well as the fatigue damage resistance of the mixture.

Mechanical Bonding

This theory assumes that the asphalt binder is forced into the irregularities of the aggregate surface, producing a mechanical interlock. The characterization of the physical properties of aggregates, as well as its role in mechanical adhesion and resistance to moisture damage, has been widely analyzed. For example, aggregates with rough surface texture and a high amount of surface pores are more resistant to moisture damage (D'Angelo and Anderson 2003). In terms of angularity, aggregates with high angularity have been normally considered beneficial in producing a better mechanical interlock (Stuart 1990). Analytical approaches have also been developed to characterize adhesive bond from a mechanical framework. An anisotropic viscoplastic model developed by Masad et al. (2005) was used to measure the contribution of the fine and coarse fraction of aggregates to the adhesive bond strength. They used data from compressive triaxial tests at three different confining pressures and five strain rates. The results suggest that at low induced shear strains the resistance of the material is dominated by the fine fraction, while at high shear strains the coarse aggregate controls the resistance and ultimately determines the adhesive strength at the aggregate-binder interface.

Adhesion Due to Surface Free Energy

Physico-chemical adhesion between two materials is a thermodynamic phenomenon that depends on the surface free energy of the materials. Surface free energy (γ in ergs/cm^2) is defined as the amount of external work done on a material to create a new unit surface area in vacuum. The total surface energy of a material γ^{total} can be obtained using Good-Van Oss-Chaudhury theory (VanOss et al. 1988) as:

$$\gamma^{total} = \gamma^{LW} + 2\sqrt{\gamma^+ \gamma^-} \, , \tag{2.7}$$

where γ^{LW} is the Lifshitz van der Waals component (non-polar), γ^+ is the Lewis acid component, and γ^- is the Lewis basic component. The second term of Equation 2.7 is commonly expressed as the acid-base component (γ^{AB}). The work of adhesion between two materials is the amount of work or energy required to separate the materials from their interface to create a new unit of area of each material in vacuum. Work of adhesion can be computed from the surface free energy components of the two materials as follows:

$$W_{AS} = \gamma_A + \gamma_S - \gamma_{AS} = 2\sqrt{\gamma_A^{LW}\gamma_S^{LW}} + 2\sqrt{\gamma_A^+\gamma_S^-} + 2\sqrt{\gamma_A^-\gamma_S^+} \,, \qquad (2.8)$$

where γ_{AS} represents the interfacial energy between the phases *A* (asphalt) and *S* (aggregate). The interaction of the base component of the aggregate with the acid component of asphalt binder contributes the most to the total bond strength at the aggregate-binder interface (Bhasin et al. 2006b). A higher magnitude of work of adhesion indicates higher resistance of the interface to an adhesive failure.

Moisture damage susceptibility can be quantified on the basis of the adhesive bond energy between the asphalt binder and the aggregate and the change in free energy when water displaces asphalt binder from the aggregate surface. The work required for water to displace a unit of the interface and create a new unit of water-asphalt interface and water-aggregate interface is expressed by:

$$W_{WAS} = \gamma_{AW} + \gamma_{SW} - \gamma_{AS} \,, \qquad (2.9)$$

where the subscripts *W*, *A,* and *S* correspond to water, asphalt, and aggregate phases, respectively. W_{WAS} values are typically negative, indicating that the debonding process is thermodynamically favorable. A large magnitude of W_{WAS} implies a higher reduction in the free energy released, which is associated with greater potential for water to displace the binder from the aggregate (Bhasin et al. 2006b). An interesting interpretation of W_{WAS} is given by Bhasin et al.(2006b): "…the negative value of work required to cause debonding, W_{WAS}, can also be interpreted as the work done "by" the system favoring debonding, and therefore in the presence of water, less external work is required to cause the same amount of damage."

In summary, moisture damage in asphalt mixtures is a thermodynamically favorable process. High values of adhesive bond in dry conditions, W_{AS}, (Equation 2.8) and low values of the reduction of free energy in the system, W_{WAS}, (Equation 2.9) are the two desirable conditions for a mixture to prevent moisture damage.

The interfacial energy theory provides a well grounded moisture damage interpretation. It allows, for example, the determination of compatible combinations of aggregates and binders (Bhasin 2006; Bhasin and Little 2007; Bhasin et al. 2006b). Thermodynamic theory also

provides fundamental parameters by which to explain moisture damage in fracture mechanics based models; such as will be described in the following sections (Arambula et al. 2007; Caro et al. 2008b; Lytton et al. 2005; Masad et al. 2006c; Zollinger 2005). Currently, ongoing research is exploring and validating other procedures by which to measure adhesive bonds including thermodynamic conditions and chemical reactions between the components (e.g., microcalorimeter).

Characterization of Moisture Damage

The characterization of moisture damage is essential to quantify the loss of functionality of asphalt mixtures because it permits the determination of thresholds that can be used in the form of specifications to separate acceptable from unacceptable materials or mixtures. Although the problem of moisture susceptibility has been widely studied, its complexity has made it difficult to find a unique test or analytical method to comprehensively quantify damage and accurately predict the material performance in the field (Birgisson et al. 2005; Solaimanian et al. 2003).

The first attempts to quantify moisture damage in asphalt mixtures can be dated back to the late 1960s. The first methods used visual inspection to determine the percentage of aggregate surface that lost asphalt binder coating due to the action of water in a mixture. Subsequently, empirical tests to assess moisture damage in loose or compacted samples using a quantifiable performance parameter were developed. For more information on this classification, refer to the review papers by Airey and Choi (2002) and Solaimanian et al.(2003). These tests are normally simple and easy to conduct, but they do not provide information regarding the causes of damage, making it difficult to propose effective remediation actions for poorly performing mixtures. In addition, the results from the majority of these tests do not correlate well with field performance. In order to overcome these difficulties, new analytically based approaches have been developed during the last five years to characterize moisture damage (Arambula et al. 2007; Bhasin et al. 2006b; Birgisson et al. 2003; Birgisson et al. 2004; Caro et al. 2008b; Kringos et al. 2007; Kringos et al. 2008c; Masad et al. 2006c; Song et al. 2005). These new methodologies consider multiple material properties and are based on thermodynamics, fracture mechanics, continuum damage mechanics, and/or micromechanics.

Test methods to assess moisture damage are usually classified based on the following factors (Airey and Choi 2002; Kiggundu and Roberts 1988; Solaimanian et al. 2003):

- state of mixture (loose versus compacted mixtures);

- mode of loading (static versus dynamic);

- methodology used to induce moisture damage (i.e., moisture conditioning process); and

- scale of performance measurement (macro- versus microscale).

A new classification of test methods used to assess moisture damage is herein proposed (Figure 2.11). This classification is based on the generic nature of each test method, which is also indicative of some of the inherent advantages and disadvantages that are common among test methods in each class. Figure 2.11 presents the three parts of the classification approach. The following sections describe the tests associated with each part of the approach.
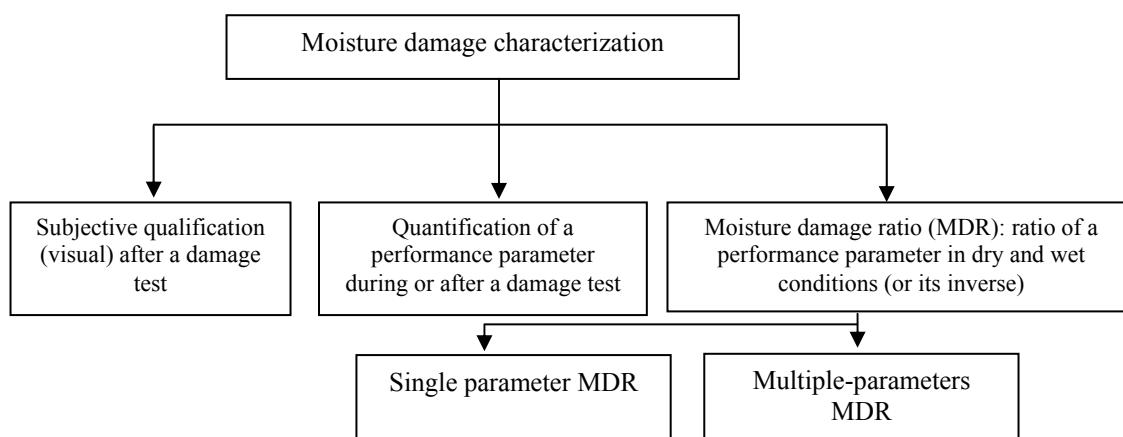
Figure 2.11. Classification of moisture damage assessment

Subjective Qualification

This group includes tests that are typically based on visual or qualitative assessment of moisture damage. The assessment does not identify or explain the fundamental causes of damage. Table 2.7 presents some of the tests in this part. For detailed information refer to Airey and Choi (2002) and Solaimanian et al.(2003).

Table 2.7. Tests in which the assessment of damage is done by visual inspection

Test	Reference	Assessment of damage
Rolling Bottle Method	CEN prEN 12697-11	Visual estimation of the amount of binder retained in the mixture.
Ancona Stripping Test	Bocci and Colagrande (1993)	Visual estimation of the total percent of material stripped.
Boiling Water Test	American Society for Testing and Materials, ASTM D 3625	Visual estimation of the amount of binder loss. Retained coating between 85-90% is considered acceptable.
Film Stripping	California Test 302-1999	Visual estimation of the total percent of material stripped.
Static Immersion Test	American Association of State Highway and Transportation Officials AASHTO T182 ASTM D 1664	Visual estimation of total area of the coated aggregate as above or below 95% (discontinued by ASTM).
Ultrasonic Method	Vuorinen and Valtonen (1999)	Visual estimation of material stripped. It can also include the assessment of the weight of material released from the aggregate (a quantitative assessment of damage derived from this test is included in Table 2.8).
Chemical Immersion Test	Kennedy et al. (1983)	Concentration of sodium carbonate required to produce stripping (identified visually). This value is considered a measure of adhesiveness.

Quantification Using a Performance Index

An improvement over the visual qualitative method to assess moisture damage is the use of a performance parameter derived from a mechanical or chemical test that is linked to moisture damage. The performance parameter is unique to each test method. The test method may be conducted on loose or compacted mixtures with or without loading. Table 2.8 presents test methods that fall into this category, along with a brief description.

Table 2.8. Methods used to quantify moisture damage as the final value of a performance parameter

Test	Reference	Performance index (damage parameter)
First proposal of Ultrasonic Method	Vuorinen and Valtonen (1999)	Loss of weight of a polished stone test specimen of 2 cm by 8 cm coated with 2 g of asphalt binder after the application of ultrasound under water.
Ultrasonic Accelerated Moisture Conditioning Procedure (UAMC)	McCann and Sebaaly (2001) McCann et al. (2005)	Percentage loss in weight of original sample after subjecting it to an ultrasonic bath. The lost material corresponds to small particles of aggregate that are dislodged from larger aggregates when ultrasonic energy is applied. Recently, the authors proposed the use of the rate at which the small particles are released as the asphalt recedes along the surface of the aggregate as a *performance index* that characterizes damage.
Net Adsorption Test (NAT)	SHRP Designation M-001, Curtis et al. (1993)	Net adsorption is defined as the amount of asphalt binder that remains on the aggregate after aqueous desorption. The value is measured based on the amount of binder that is adsorbed onto the aggregate surface from a toluene solution and the amount of binder that is desorbed (i.e., removed) by the addition of water to the mixture. More details in Airey and Choi (2002).
Modified Net Adsorption Test	Walsh et al. (1996)	Same principle as NAT but with modifications in the preparation of the aggregates.
Pneumatic Pull-Off	Youtcheff and Aurilio (1997)	Adhesive bond of asphalt binders (based on the burst pressure required to debond the binder from a stone) as a function of time while exposed to water (tensile and bonding strength in different moisture conditions) (Solaimanian et al. 2003).
Texas Freeze-Thaw Pedestal Method	Kennedy and Anagnos (1984)	Thermal cycles required for causing crack initiation in an asphalt mixture.
Boiling Water Stripping Test	Belgium Road Research Center (BRRC) Procedure ME 65-91	Stripping rate calculated from a calibration curve of acid consumption against percent of uncoated material. The curve is obtained from mixtures with coated and uncoated aggregates in different ratios that are subjected to chemical attacks.
Hamburg Wheel-Tracking Test	Texas Department of Transportation TxDOT standard Tex-242-F, 2004	The test uses wheel tracking to simulate traffic conditions on compacted specimens that are immersed in water. Stripping is identified with the presence of a sudden inflection point in the plastic deformation during the application of cyclic load.

Table 2.8. (Continued)

Test	Reference	Performance index (damage parameter)
Moisture Vapor Susceptibility (MVS)	California Test 307, 1999	Stabilometer value at which the effect of moisture on mixtures is imminent. The stabilometer value is calculated following the test CT 366.
Methylene Blue Test	Ohio Department of Transportation (supplement 1052)	The test identifies the concentration of plastic fines (including clay and organic material) in the mix that can promote emulsification of asphalt in the presence of water More details in Kandhal et al. (1998).

From Table 2.8, the Net Adsorption Test, the Modified Net Adsorption Test, the Boiling Water Stripping Test, the Pneumatic Pull-Off, and the surface energy tests involve the analysis of the chemical compatibility between aggregates and binder or the assessment of the quality of the adhesive bond of the system.

Ratio of a Parameter Derived from Tests on Dry and Moisture Conditioned Specimens

A widely used approach for quantifying moisture damage is the ratio of a parameter (or parameters) derived by testing dry or control specimens to the same parameter(s) derived by testing moisture conditioned specimens. The goal of the moisture conditioning process is to simulate the detrimental effects of moisture on the material during a short time period. Moisture conditioning in these tests can be considered an accelerated damage process (Birgisson et al. 2005; Kiggundu and Roberts 1988). This ratio of parameters affected by moisture conditioning to the control state is referred to Moisture Damage Ratio (*MDR*):

$$MDR = \frac{f(P_1^w; P_2^w; P_3^w; .....; P_n^w)}{f(P_1^d; P_2^d; P_3^d; .....; P_n^d)}, \qquad (2.10)$$

where $P_1^d; P_2^d; P_3^d; .....; P_n^d$ are *n* material properties that are measured in dry condition and $P_1^w; P_2^w; P_3^w; .....; P_n^w$ are the same *n* properties measured after a moisture conditioning process. The function *f* is used to derive the parameters of interest from the material properties and can be based on analytical models or empirical relationships. Occasionally, *MDR* is calculated as the inverse of Equation 2.10 (i.e., dry over wet parameters). In this classification, both cases will be

referred to as *MDR*. With few exceptions (Bhasin et al. 2007; Bhasin et al. 2006b; Masad et al. 2006c), *MDR* corresponds to the net retained value of a parameter based on one or several properties of the material after subjecting it to a moisture conditioning process.

Besides being a quantitative measure of moisture damage, *MDR* can be also used to: 1) evaluate the influence of different factors on moisture damage (e.g., effect of air voids or addition of antistripping agents), and 2) select mixtures based on an acceptable level of damage (i.e., threshold *MDR* value). A threshold or acceptable *MDR* value is usually determined by a comparison between *MDR* values obtained in the laboratory and observed moisture damage in the field for several mixtures.

Numerous test configurations that yield an *MDR* value have been developed in the past few years. The *MDR* can be further divided into the following two groups according to the number of properties included in the function *f* (Equation 2.10):

- *MDR* derived simply as the ratio of a single material property, or *single-parameter MDR*; and

- *MDR* derived as the ratio of a combination of multiple material properties, or *multiple-parameter MDR*. Analytical models are used to derive the function of the multiple material properties are discussed below.

Single-Parameter MDR

Assessment of moisture damage based on single-parameter *MDR* is achieved by conducting commonly used mechanical tests (e.g., tensile strength, fatigue, dynamic modulus, creep compliance, etc.). Typical examples of parameters used to determine *MDR* are stiffness, strength, resilient modulus, and number of cycles to failure. Although single-parameter *MDR* captures the deterioration of an asphalt mixture property due to moisture conditioning on a macroscale level, it does not normally provide explanations for the causes for such deterioration. Also, it does not account for the interaction among the different chemical and physical properties influenced by moisture damage. Table 2.9 enumerates some of the test methods within this category.

Table 2.9. Tests and methods that use a single-parameter performance function in *MDR* evaluation

Test/work	Standard/reference	Material property used in the single-index performance function for *MDR*	Comments
Lottman	NCHRP 246, Lottman (1982)	Indirect tensile strength and stiffness	
Modified Lottman	AASHTO T283	Indirect tensile strength and stiffness	Commonly known as tensile strength ratio (TSR).
Tunnicliff and Root Procedure	ASTM D 4867	Indirect tensile strength	Commonly known as tensile strength ratio.
Duriez Test	NFP 98-251-1	Unconfined compression strength	
Marshall Stability Test	AASHTO T245	Marshall stability	
Immersion Compression Test	AASHTO T165, ASTM D 1075	Compressive strength (wet over dry values)	The MDR in this case is referred to as the Index of Retained Strength (IRS).
Bitutest Protocol	Scholz (1995)	Indirect stiffness modulus using the Nottingham Asphalt Tester	
Environmental Conditioning System (ECS) with Dynamic Modulus	Al-Swalimi and Terrel (1992); NCHRP 9-19, 9-29, and 1-37	Dynamic modulus using ECS (Solaimanian et al. 2006; Solaimanian et al. 2003)	
Environmental Conditioning System with Flow Number		Flow number using ECS (Solaimanian et al. 2006; Solaimanian et al. 2003)	
Environmental Conditioning System with Flow Time		Flow time using ECS (Solaimanian et al. 2006; Solaimanian et al. 2003)	
Flexural Fatigue Beams Test with Moisture Conditioning	Shatnawi et al. (1995)	Fatigue life following AASHTO TP-8	
Disk-Shape Compact Tension Fracture Test (DCT)	Apeagyei et al. (2006)	Fracture energy (G_f)	
		Fracture strength (S_f)	

Table 2.9. (Continued)

Test/work	Standard/reference	Material property used in the single-index performance function for *MDR*	Comments
Dynamic Material Analyzer (DMA) on fine aggregate) mixtures[1] for analyzing moisture damage of mixtures	Song et al.(2005), Masad et al. (2006c)	Fatigue life, N_f (number of cycles to failure under strain control conditions)	Conducted on fine aggregate matrices (FAM) using torsion strain controlled. There is not a threshold value that separates good and poor performance of mixtures.
		Reduction in the dynamic modulus at fatigue life $(G^{*'}/G')$	Small values are desirable.
Static Creep Test	Abo-Qudais and Al-Shweily (2007)	Accumulated microstrain	Comparison of accumulated microstrain after 60 minutes of loading
Pull-Off test	Copeland et al. (2007)	Tensile strength of the binder-rock interface	
Saturation Ageing Tensile Stiffness (SATS)	Collop et al.(2004), Airey et al. (2007)	Tensile stiffness modulus	Calculated at 20ºC using the Nottingham Asphalt Tester (NAT)
Surface energy measurements (Wilhelmey Plate and Universal Sorption Machine)	Bhasin et al.(2007; Bhasin et al. 2006a) Masad et al. (2006c), Little and Bhasin (2007)	Adhesive bond between aggregates and asphalt binders (ΔG_{AS}) and the potential of water to debond the asphalt (ΔG_{WAS})	High values of ΔG_{AS} and low values of ΔG_{WAS} are desirable.

(1) a fine aggregate matrix (FAM) represent the fine matrix of asphalt mixtures. They are composed of asphalt binder and the fine portion of the aggregates (passing the sieve 1.18 mm).

Note that the procedures described by Bhasin et al. (2006a, 2007), Masad et al. (2006c), and Little and Bhasin (2007) employ thermodynamic material properties instead of mechanical properties to explain the loss of adhesion between aggregate and binder in the presence of water. The authors used the surface free energy of aggregates and asphalt binders to quantify moisture damage. For details of procedures to obtain surface free energy of asphalts and aggregates refer to Bhasin (2006). As explained before, surface free energy can be used to calculate the adhesive bond (work of adhesion) between aggregate and binder in a dry state (ΔG_{AS}) as well as the

potential for water to displace the asphalt binder from the aggregate surface (ΔG_{WAS}). In order to analyze the combined effect of these two parameters on moisture damage, Bhasin et al. (2006b) proposed the use of an *MDR* to quantify the moisture damage potential of a material combination:

$$MDR_1 = \left| \frac{\Delta G_{AS}}{\Delta G_{WAS}} \right|,$$

(2.11)

A higher magnitude of adhesion between the asphalt binder and aggregate and a smaller magnitude of the thermodynamic potential for water to cause stripping represents less moisture sensitivity. Therefore, higher values of MDR1 are desirable to control moisture damage. MDR1 does not fit the generic definition of an MDR despite the apparent use of the material property in dry condition in the numerator and the material property in wet condition in the denominator. This is because ΔG_{AS} is a measure of the resistance of the asphalt binder-aggregate interface to resist debonding and ΔG_{WAS} is the thermodynamic potential that drives moisture damage. These two properties are combined as a ratio merely to derive a single dimensionless number to assess moisture damage.

Figure 2.12 illustrates the comparison of the MDR values for 13 mixtures with known field performance in terms of moisture damage. The separation between poor performing mixtures and good performing mixtures using the indicator MDR1 is evident from this figure. More recently, three other similar parameters based on surface free energy of the aggregate and asphalt binder and specific surface area of aggregate were proposed to quantify the resistance of materials to moisture damage (Bhasin et al. 2007; Little and Bhasin 2007). These parameters offer refinements to Equation 2.11, which account for properties such as surface roughness of aggregates and wetability of asphalt binder.

Song et al. (2005) and Masad et al. (2006c) related the *MDR* based on the reduction of the shear modulus measured using DMA, $G^{*'}/G'$ in Table 2.9, to thermodynamic and microstructural material properties as follows (Lytton et al. 2005):

$$\left. \frac{G'}{G} \right|_{cohesive} = \left[1 - 2\pi \bar{\xi} \frac{\bar{r}}{\bar{t}} \left(1 - \frac{G_f \Delta G_f^c}{\pi \tau^2 \bar{r}} \right) \right],$$

(2.12)
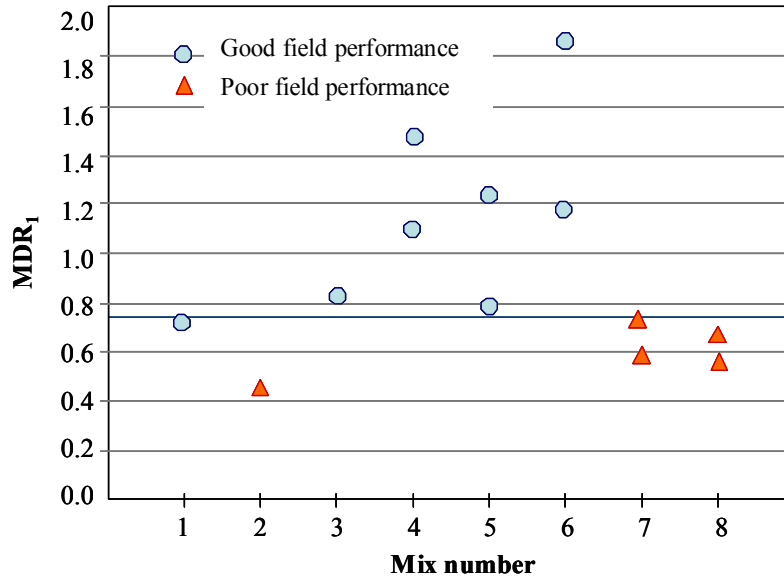
Figure 2.12. Mixture performance and total energy ratio; after Bhasin et al. (2006b)

$$\left.\frac{G'}{G}\right|_{adhesive} = \left[1 - \pi\bar{\xi}\frac{\bar{r}}{\bar{t}}\left[\left(1 - \frac{G_f}{G_s}\right) - \frac{4G_f\Delta G_{AS}}{\pi\,\tau^2\bar{r}}\right]\right], \qquad (2.13)$$

where $\bar{t}$ is the average asphalt film thickness, A is the cross-sectional area of the material, $\bar{r}$ is the average air void radius, G_f is the binder undamaged modulus, G_s is the aggregate undamaged modulus, τ is the applied shear stress, $\Delta G_f{}^c$ is the cohesive bond energy, ΔG_{AS} is the adhesive bond energy, and ξ is a damage parameter defined as the ratio between the area of cracks and voids and the total area of a cross section of the specimen. Equations 2.12 and 2.13 correspond to a strain controlled case, but similar equations can be obtained for a stress controlled condition. Figure 2.13 presents the ratio of (G'/G) in dry and wet conditions for the adhesive and cohesive failure conditions according to Equations 2.12 and 2.13. The figure was constructed based on the data presented by Song et al. (2005).

Although the modified Lottman test (AASHTO T 283) is the most popular test in this category, there is little consensus regarding the most reliable procedure to evaluate moisture damage. Solaimanian et al.(2006), Kiggundu and Roberts (1988), Birgisson et al.(2005), Lu and

Harvey (2006), and Kringos et al. (2009), among others, have pointed out the deficiencies of AASHTO T283 and other tests in terms of their ability to accurately predict the field performance of asphalt mixtures. Kiggundu and Roberts (1988) evaluated the effectiveness of some of the popular tests based on the ability of the test methods to predict field performance. They compiled information from studies involving mixtures designed with materials from 13 different U.S. states, diverse sources of asphalts, and several modifiers and additives. Table 2.10 presents a summary of their findings. As can be seen the highest success rate in predicting moisture damage was 76 %.
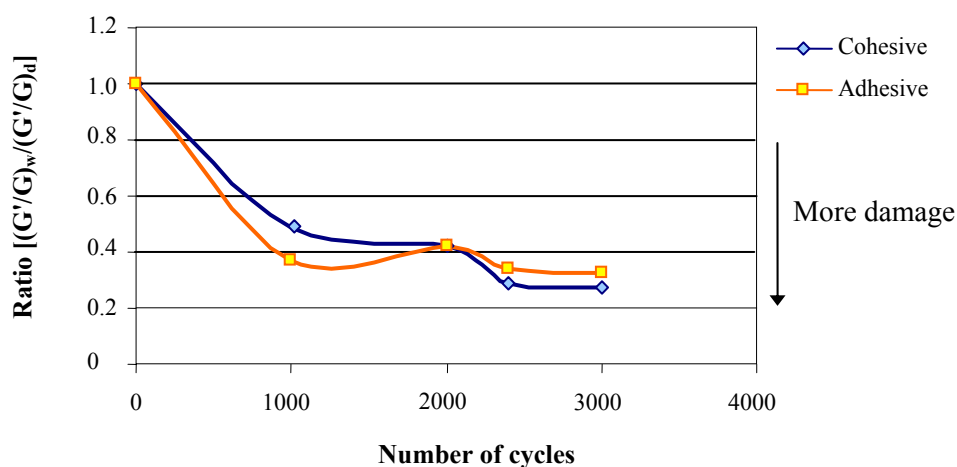
Figure 2.13. Ratio between the normalized (G'/G) in wet and dry conditions for a) cohesive and b) adhesive fracture in dry and wet conditions (based on data from Song et al. 2005)

Solaimanian et al. (1993) evaluated long term stripping performance of 46 different test sections on nine different roads for a period of six years and found no clear relationship between laboratory results and field performance. More recently, Solaimanian et al. (2006) evaluated eight mixtures with three popular tests, including ASSHTO T 283, and found that when using this test, the performance estimation was *good* when the reported field performance was *poor* in two of the mixtures, and one mixture was ranked *poor* although it had a *good* performance. In other words, the AASHTO T283 test had a 63 % success rate of performance prediction, which is similar to the result of Kiggundu and Roberts (1988).

Table 2.10. Success ratings for three tests based on the ratio of a simple index; after Kiggundu and Roberts (1988)

Test method	Minimum requirement	% success
Lottman (NCHRP 246, Lottman 1982)	TSR = 70%	67
	TSR = 80%	76
Tunnicliff-Root (ASTM D 4867)	TSR = 70%	60
	TSR = 80%	67
	TSR = 70-80%	67
Immersion Compression	Strength ratio = 75%	47

These results support the idea that it is extremely difficult to find a single parameter that can be used to successfully characterize and predict moisture damage. The main reason for the need to use multiple parameters to characterize moisture damage is that a single material property cannot simultaneously account for the physical, mechanical, and chemical changes that occur in the materials during the development of moisture damage.

Under these circumstances, it is not sufficient to monitor moisture damage using a single-parameter *MDR* (Birgisson et al. 2003; Birgisson et al. 2004; Masad et al. 2006c). As a result, during the last five years, the effort to develop a multiple-parameter *MDR* derived from analytical methods has gained momentum. Multiple-parameter *MDR* is discussed in the following section.

Multiple-Parameter MDR

The multiple-parameter *MDR* utilizes an analytically-based function to quantify damage by combining more than one material property and considering both dry and wet states. This approach allows a more comprehensive evaluation of moisture damage based on several physical, chemical, and/or mechanical properties. This section presents several examples of the development of multiple-parameter *MDR*.

Birgisson et al. (2003) used the fatigue model for asphalt mixtures proposed by Zhang et al. (2001) to define a performance function as the number of cycles (*N*) required to generate a crack of 1 inch (25.4 mm) under cyclic loading conditions using the SuperPave Indirect Tensile Test (IDT). The model monitors the accumulated creep strain energy of the material (Zhang et al. 2001). Crack growth occurs when the accumulated dissipated creep strain energy (DCSE) (in kJ/m^3) equals the threshold DCSE that defines failure. The model updates the average tensile

stress and repeats the analysis after each crack growth increment until 1-inch crack length is reached. The following equation is used to calculate the DCSE per cycle:

$$DCSE/cycle = \frac{1}{20}\sigma_{AVE}^2 D_1 m(100)^{(m-1)},$$
(2.14)

where σ_{AVE} is average stress in the zone of interest, and D_1 and m are parameters obtained from creep tests. The moisture damage quantified using this approach may be represented in terms of an *MDR* as:

$$MDR_2 = \frac{N_{conditioned}}{N_{unconditioned}} = \frac{f(\sigma_{AVEw}, D_{1w}, m_w)}{f(\sigma_{AVEd}, D_{1d}, m_d)},$$
(2.15)

where σ_{AVE}, D_1 and m are the same parameters as described for Equation 2.14 but measured in dry (subscript *d*) and wet (subscript *w*) conditions. The use of multiple material properties (D_1, m) to determine $N_{conditioned}$ or $N_{unconditioned}$ is evident from the aforementioned discussion. For more details refer to Zhang et al. (2001) and Birgisson et al. (2003).

Birgisson et al. (2004) used the concept of energy ratio (*ER*) introduced by Jailardo (2003) as an *MDR* to quantify moisture damage in asphalt mixtures. *ER* is a measure of the fracture resistance of mixtures and is defined as:

$$ER = \frac{a \times DCSE}{m^{2.98} D_1},$$
(2.16)

where DCSE, *m*, and D_1 have the same meaning as in Equation 2.15, and *a* is defined as:

$$a = 0.0299\sigma^{-3.1}(6.36 - S_t) + 2.46 \times 10^8,$$
(2.17)

where σ is the tensile stress of the asphalt layer (psi), and S_t the tensile strength of the material (MPa). The term $m^{2.98} D_1$ in Equation 2.16 corresponds to the minimum dissipated creep strain energy required for the material to have an acceptable cracking performance. The multiple-parameter *MDR* presented by the authors can be expressed as:

$$MDR_3 = \frac{ER_w}{ER_d} = \frac{f(\sigma_w, S_{t_w}, D_{t_w}, m_w, DCSE_w)}{f(\sigma_d, S_{t_d}, D_{t_d}, m_d, DCSE_d)} = \frac{a_w}{a_d} \frac{D_{1_d}}{D_{1_w}} \frac{DCSE_w}{DCSE_d} \frac{m_d^{2.98}}{m_w^{2.98}}, \quad (2.18)$$

Birgisson et al. (2004) demonstrated that this methodology can be used to: 1) evaluate the loss of resistance to fracture in asphalt mixtures due to moisture damage and 2) identify the effect of antistrip agents on moisture resistance of asphalt mixtures (Figure 2.14).
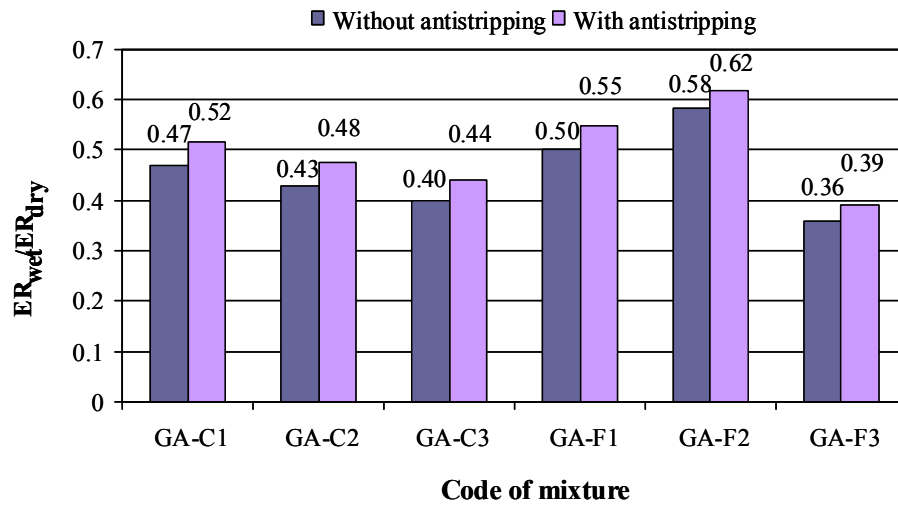
Figure 2.14. Ratio between energy ratio in dry and moisture conditioning states for granite mixtures with and without a liquid antistripping agent; adapted from Birgisson et al. (2004)

Song et al. (2005) used a continuum mechanistic model to analyze moisture damage in asphalt mastic. This approach was initially developed to characterize fatigue damage in asphalt mixtures and was further adapted to analyze fatigue damage in asphalt mastic and fine aggregate matrices (FAM) subjected to dynamic shear strain conditions. FAM refers to an asphalt mixture that is composed by asphalt binder and the fine portion of the aggregates (typically passing the sieve 1.18 mm). In the model, the total damage at the end of a certain number of load cycles (i) is quantified with the damage parameter S:

$$S(i) \cong \sum_{i=1}^{N} \left[\frac{1}{2} (\gamma_{N,i}^R)^2 (C_{i-1} - C_i) \right]^{\alpha/(1+\alpha)} (t_i - t_{i-1})^{1/(1+\alpha)}, \quad (2.19)$$

where C_i is the pseudostiffness, N is the number of cycles applied to the material, $\gamma^R_{N,i}$ is the

reference shear strain at the time i and at the Nth cycle, t_i is the corresponding time, and α is a

material constant. The *MDR* used by these authors is:

$$MDR_4 = \frac{S_w}{S_d} = \frac{f(S_{i_w}, N, \gamma^R_{N,i_w}, t_{i_w}, \alpha_w)}{f(S_{i_d}, N, \gamma^R_{N,i_d}, t_{i_d}, \alpha_d)}, \qquad (2.20)$$

The results showed that MDR_4 was able to accurately represent damage observed in

asphalt mastic specimens. The model was validated using X-ray CT measurements of damage

determined from the ratio of the area of cracks and voids to the total cross-sectional area of dry

and wet specimens.

Masad et al. (2006c) used a crack growth model based on fracture and micromechanics

to analyze the susceptibility of FAM to moisture. DMA tests were conducted to determine the

linear viscoelastic properties and the fatigue life of FAM. In addition, Arambula et al. (2007)

used a comparable model to analyze the effect of air void distributions in asphalt mixtures. In

this case, the parameters for the model were determined by conducting relaxation modulus,

tensile strength, and repeated uniaxial tensile tests on the whole mixtures. The mechanical

models applied in these studies are based on the approach developed by Lytton et al. (1993)

using a fracture law similar to Paris' fracture law to determine the equivalent crack radius (R_c)

expressed as a function of the number of loading cycles and other material properties. The

equivalent crack radius is considered a damage parameter that represents the potential crack

growth in the material. In terms of an *MDR* the expression is:

$$MDR_5 = \frac{R_{c_w}(N)}{R_{c_d}(N)} = \frac{f(N, E_{r_w}, E_{1_w}, \Delta G_{f_w}, n_w, b_w)}{f(N, E_{r_d}, E_{1_d}, \Delta G_{f_d}, n_d, b_d)}, \qquad (2.21)$$

where R_c is the equivalent crack radius that represents the state when multiple cracks are present,

E_1 is the initial relaxation modulus, ΔG_f is the adhesive bond energy between the asphalt binder

and the aggregate, E_R is the reference modulus, b represents the linear relationship that exists

between the normalized pseudostrain energy and the natural logarithm of the load cycles, $b = \partial W_R / \partial \ln(N)$, and n is a material constant used in Paris' fracture law (Schapery 1984). The

expression for the equivalent crack radius used by Masad et al. (2006c) is given by:

$$R_c = r\left(\sigma_t^{\,2}\right)^{\frac{2n+1}{n}} = (2n+1)^{\frac{1+n}{2n+1}}\left(\frac{bE_R}{4\pi E_1 \Delta G_f}\right)^{\frac{n}{2n+1}}\left(N^{\frac{1}{1+n}} - 1^{\frac{1}{1+n}}\right)^{\frac{1+n}{2n+1}}, \qquad (2.22)$$

Figure 2.15 presents results for $R_c(N)$ calculations for mixtures in both dry and wet states obtained for FAM samples representing four different mixtures (Masad et al. 2006c). Two of these four mixtures were reported to have good resistance to moisture damage in the field (3 and 4), and the other two were reported to have poor resistance to moisture damage in the field (7 and 8). This work demonstrates a strong correlation between MDR_5 calculated for FAM and the field performance of the complete or whole mixture.
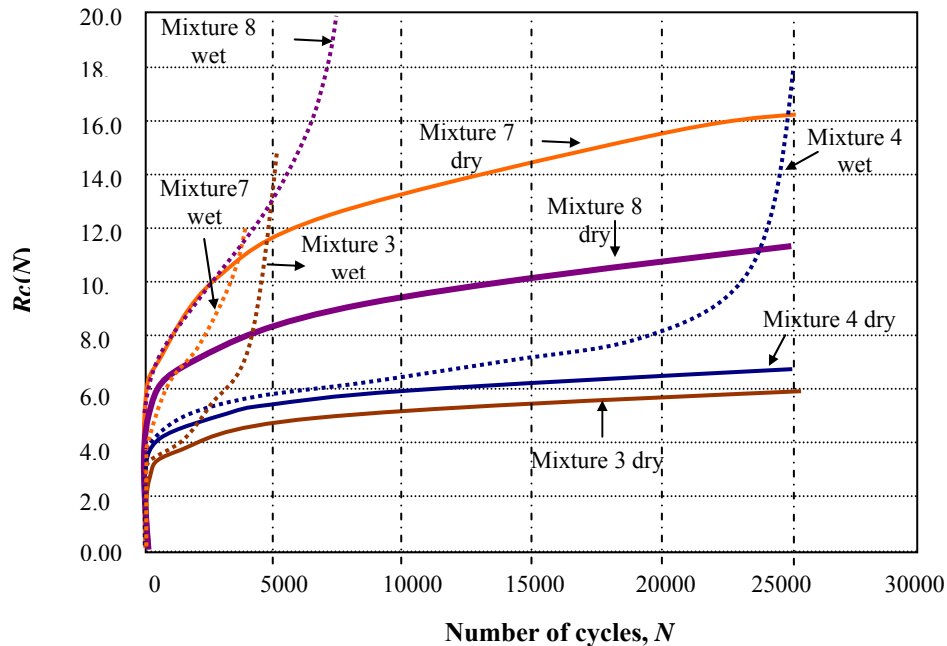
Figure 2.15. Average $R_c(N)$ as a function of N. It is known that samples 3 and 4 presented good performance in the field and samples 7 and 8 poor performance; based on data from Masad et al. (2006c)

In another study, Arambula et al. (2007) used a slight modification of MDR_5 by including tensile strength of the material to compare moisture damage in different mixtures prepared with different air void distributions in the mixtures as shown in Figure 2.16. The first

two figures present the total air void and the average air void size of four different mixtures prepared at the same target of total air void content (6-7 %) with respect to depth. Figure 2.16.c presents the value of MDR_5 at 1,000 loading cycles (Equation 2.21).
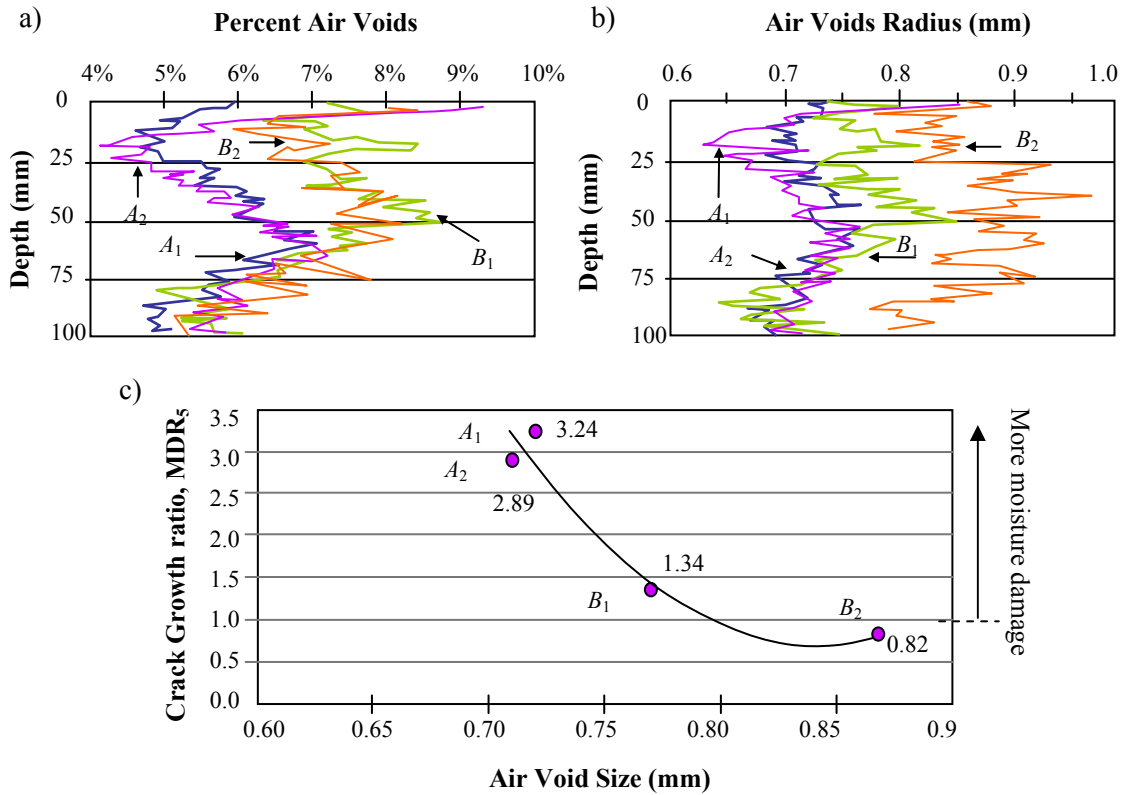
Figure 2.16. a) percent of air voids versus depth of specimens, b) air void size versus depth of specimens, and c) moisture damage for dense asphalt mixtures with gradation A (specimens A_1 and A_2) and gradation B (specimens B_1 and B_2): adapted from Arambula et al. (2007)

Caro et al. (2008b) incorporated a new dimension in the analysis of moisture damage by applying probability theory to the results of a similar fracture mechanics model. The fracture crack growth index used in this study is given by (Masad et al. 2007c):

$$\Delta R(N) = \left[(2n+1)^{n+1} \left(\frac{E_R\, b}{4\, \pi\, E_1\, \Delta G_f} \right)^n N \right]^{\frac{1}{2n+1}} , \tag{2.23}$$

Parameters in Equation 2.23 correspond to those used in Equation 2.22. Shear fatigue tests and relaxation modulus tests conducted in FAM using the DMA, in combination with surface energy measurements were used to computed $\Delta R(N)$. The *MDR* in this case is expressed by:

$$MDR_6 = \frac{\Delta R_w(N)}{\Delta R_d(N)} = \frac{f(N, E_{r_w}, E_{1_w}, \Delta G_{f_w}, n_w, b_w)}{f(N, E_{r_d}, E_{1_d}, \Delta G_{f_d}, n_d, b_d)}, \qquad (2.24)$$

The advantage of incorporating probability theory in the analysis is that it can be used to account for the variability observed in experimental fatigue data and for the inherent uncertainty in the damage process. Therefore, instead of calculating an average *MDR* at a fixed number of loading cycles (N), it is possible to calculate, for example, the probability that the crack growth index in wet conditions is equal or higher than the index in dry conditions (i.e. $p(\Delta R_w \geq \Delta R_d)$ or $p(MDR_6 \geq 1)$), as a function of N. It is expected that the probability of moisture damage increases with the number of load cycles.

Figure 2.17 presents the results for three FAM comprised of the same asphalt binder (PG82-10) and the following aggregates: 1) granite; 2) granite with a 2% substitution of hydrated lime; and 3) limestone. Three important conclusions can be extracted from this figure: 1) the mixture containing only granite aggregate is the most prone to developing moisture damage, 2) the mixture containing hydrated lime as a partial replacement of the granite filler has the lowest chances of developing moisture damage, and 3) although the probability of developing moisture damage increases with the number of loading applications for all mixtures, the rate of increment changes according to the type of material.

Table 2.11 presents a summary of the works and parameters described previously that classify as multiple-parameter *MDR*.
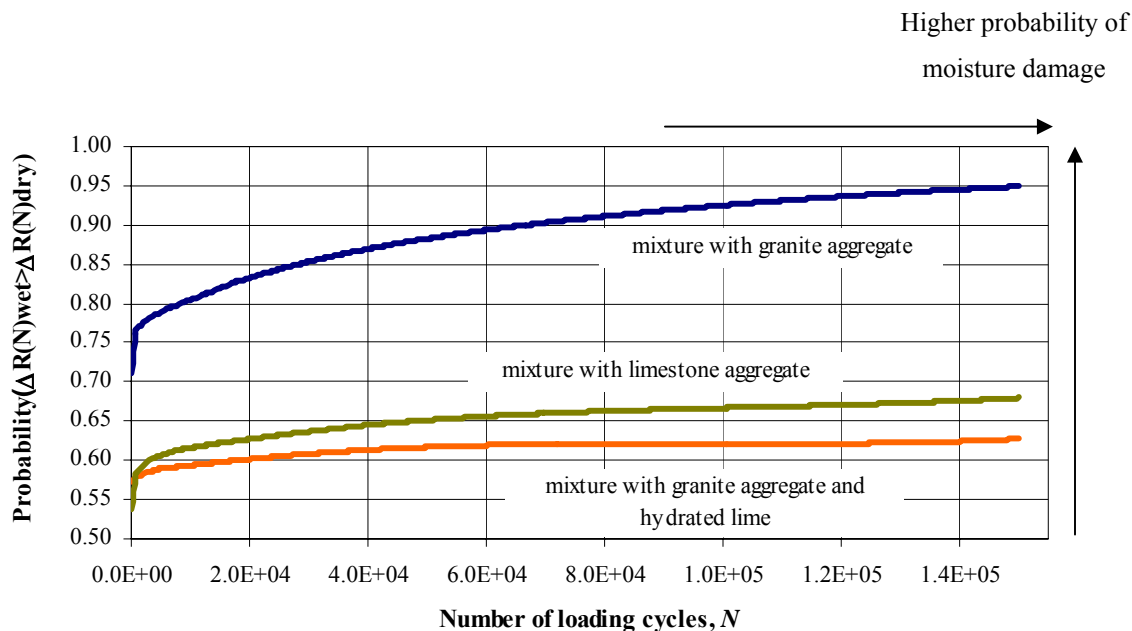
Figure 2.1. Probability that $\Delta R_{wet} \geq \Delta R_{dry}$ as a function of load applications (N) for three FAMs; adapted from Caro et al. (2008b)

Table 2.11. Examples of moisture damage quantification using multiple-parameter *MDR*

Reference	MDR	Function for MDR	Tests required	Indexes for the performance function
Birgisson et al. (2003)	MDR$_2$ (Equation 2.15)	N_f number of cycles for the crack to grow 1 inch long under cyclic loading in Superpave IDT	Tensile strength, resilient modulus, and creep compliance tests	Creep strain energy per cycle, creep strain energy limit (to produce failure), creep properties, tensile strength
Birgisson et al. (2004)	MDR$_3$ (Equation 2.18)	*ER*	Strength tests, resilient modulus, and creep compliance tests (SuperPave IDT)	Tensile strength, resilient modulus, fracture energy limit to failure, dissipated creep strain energy limit, and creep properties
Song et al. (2005)	MDR$_4$ (Equation 2.20)	Ratio between the apparent and the initial shear modulus	Shear oscillation test in DMA	Viscoelastic properties, change in pseudostiffness, reference shear strain at each cycle

Table 2.11. (Continued)

Reference	MDR	Function for MDR	Tests required	Indexes for the performance function
Zollinger (2005), Masad et al. (2006c) and Caro et al. (2008b)	MDR_5 and MDR_6 (Equation 2.21 and 2.24)	Crack growth index (R or ΔR Equations 2.21 and 2.24)	Shear oscillation and relaxation modulus in DMA; USD and WP on aggregates and binder, respectively.	Viscoelastic properties (m and E_1), reference modulus, change of pseudostrain energy with respect to load cycles, and adhesive bond energy (from the surface energy of aggregates and binders)
Arambula et al. (2007)	MDR_5 (Equation 2.24)	Crack growth model, R, in Equation 2.24 and the same model but including the material tensile strength	Relaxation modulus, tensile strength, repeated uniaxial tensile in mixtures; USD and WP on aggregates and binder, respectively	Viscoelastic properties (m and E_1), reference modulus, change of pseudostrain energy with respect to load cycles, adhesive bond energy at the aggregate-binder interface, and tensile strength

Mathematical Modeling

Mathematical modeling is essential for characterizing moisture damage because it can be used to evaluate the actual contribution of various material and mixture properties to damage (Kringos and Scarpas 2005; Kringos et al. 2008c; Little 2005; Selvadurai 2005). For instance, by having a numerical model of fluid flow within asphalt mixtures, it is possible to account for the anisotropic and heterogeneity of the internal structure of the material. Therefore, it is possible to develop realistic simulations of the material distresses due to the presence of moisture.

Al-Omari and Masad (2004), Masad et al., Kutay et al. (2007a; 2007b) developed numerical models to simulate fluid flow in three-dimensional (3-D) microstructures of porous materials. The model by Al-Omari and Masad (2004) and Masad et al. (2007a) uses finite difference techniques to solve the governing fluid flow equations for steady incompressible flow within the actual boundary conditions of the 3-D air void structure. This structure is captured using X-ray CT and reconstructed using image analysis techniques. Kutay et al. (2007a; 2007b) used the Lattice Boltzmann (LB) approach to determine the fluid flow field within the microstructure. These models provide the flow speed and pressure at all points within the void structure, which are important inputs for numerical simulations of moisture damage at the microstructural level.

Masad et al. (2007a) and Kutay et al. (2007a; 2007b) estimated horizontal and vertical permeabilities in different types of asphalt mixtures. The results showed that horizontal permeability was about two orders of magnitude higher than the vertical permeability. Permeability anisotropy was attributed mainly to the non-uniform air void distributions more than to the orientation and shape of such voids. Regions with a low air void concentration were found to act as "bottlenecks" to vertical flow. On the contrary, horizontal flow appears to be significant in regions with a high percent of connected air voids.

Analysis of flow fields showed significant changes in pore pressures and velocities along the depth of the specimen due to the heterogeneity of the void structure. Constricted zones (located at the regions of minimum effective porosities) were observed to have the largest pore pressures and velocities. Figure 2.18 presents the velocity distribution into the void structure of a stone matrix asphalt (SMA) and Figure 2.19 presents the non-uniform flow fields at different depths within an asphalt mix specimen and the corresponding air voids at these depths.
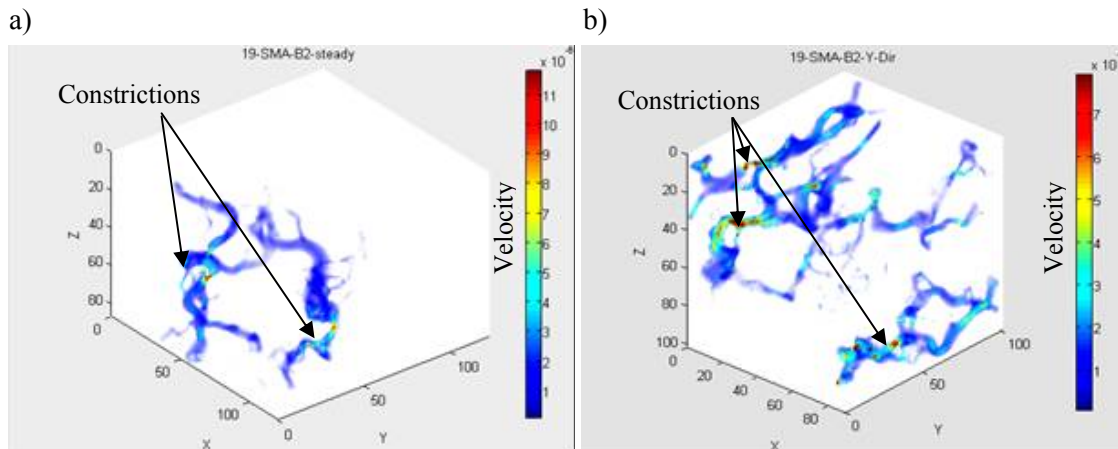
Figure 2.18. Velocity distribution within the pore structure of SMA specimen in steady-state flow conditions (a) in z-direction and (b) in y-direction; adapted from Kutay et al. (2007b)
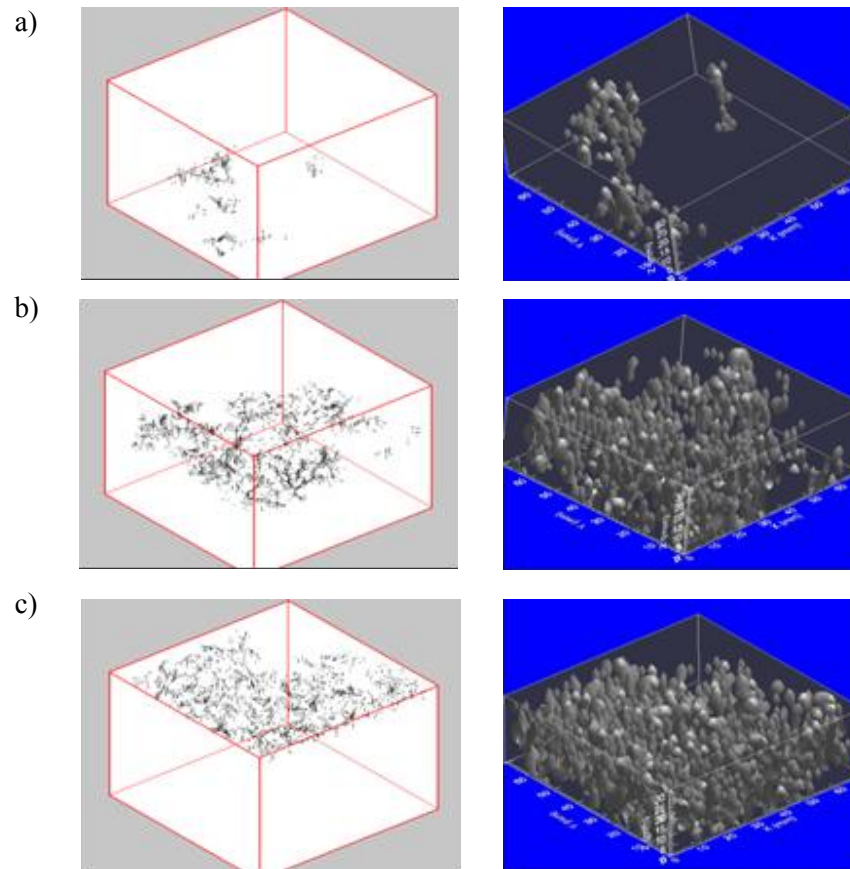
Figure 2.19. Flow patterns (left) and the corresponding air void structures (right) for the (a) top, (b) middle, and (c) bottom parts of an asphalt mix specimen; from Masad et al. (2007a)

The Mechanics of Structural Systems Group at Delft University of Technology in the Netherlands developed a numerical model devoted exclusively to analyzing moisture damage in asphalt mixtures (Kringos et al. 2008a; Kringos et al. 2007; Kringos et al. 2008c). The group developed and used a finite element routine called RoAM (Raveling of Asphalt Mixes), which is a part of the CAPA-3D finite element software, to model:

- dispersion of the mastic due to vapor diffusion,
- desorption of the outer layers of the mastic surrounding the aggregates due to pumping action,
- deterioration of the aggregate-mastic interface due to moisture diffusion and mechanical load, and

- damage of the mastic film, due to the combined action of moisture and mechanical damage.

The model couples physical and mechanical mechanisms by integrating the combined effects of water flow, vapor diffusion into the mastic, mastic dispersion and erosion, adhesive deterioration of the aggregate-mastic system, and mechanical loads. For detail information of the mathematical formulation and numerical implementation, refer to (Kringos et al. 2008c).

In order to facilitate the validation of the model by comparing its results with closed form solutions, the authors have used a simplified version of an asphalt mixture (round aggregates coated by a mastic layer of constant thickness). The model proved to provide accurate results and, therefore, it might be used to simulate the processes under more complex geometry. Figure 2.20 illustrates some results obtained from the model. Simulations of the percent of loss of mastic due to desorption and dispersion in the presence of convective flow (Figure 2.20.a) show that erosion occurs from the outer to the inner layers, as expected, and that the process is a function of the diffusion coefficient of the mastic. Figure 2.20.b illustrates the percent of water content that can be expected at three locations on the aggregate-mastic interface with time due to diffusion. The figure demonstrates the influence of proximity to the source of water on the time required for saturation (node *A* versus node *C*).

More recently, the Materials Group at Texas A&M University worked on implementing moisture damage considerations to a non-linear viscoelasto-viscoplastic model using a continuum damage approach. The model, which uses Schapery's single-integral nonlinear viscoelastic theory coupled with a Perzyna viscoplasticity approach for the undamaged constitutive model (Huang 2008), is able to introduce the effects of moisture and mechanical loading on the cohesive and adhesive degradation of asphalt mixtures. One improvement of this work with respect to previous studies is that the model accounts for the irreversibility process of moisture damage (i.e., if the mixture dries after moisture exposure only part of the damage caused in the material is reversed) and describes damage processes as a function of the moisture history, and not only the current moisture state. Details about the constitutive model can be found in Huang (2008) and details on the addition of damage parameters to the model can be found in Graham (2009).
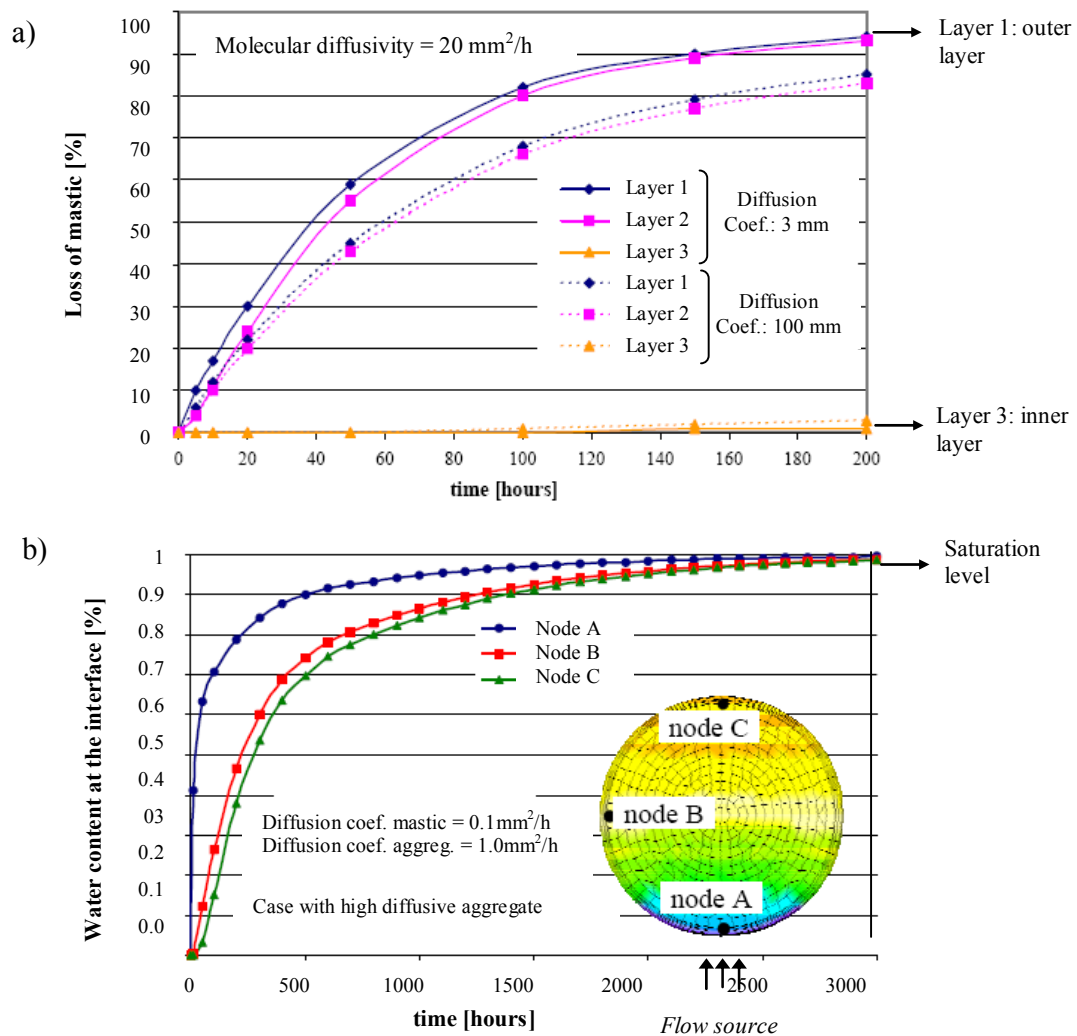
Figure 2.20. Results of a) loss of mastic due to advective flow (desorption and dispersion); adapted from Kringos and Scarpas (2005), b) water content at the aggregate-binder interface versus time; adapted from Kringos and Scarpas (2006)

Summary and Conclusions

The following are the main points discussed in this chapter:

- Moisture damage is defined as the degradation of the mechanical properties of asphalt mixtures due to the presence of moisture (i.e., liquid or vapor). The phenomenon involves thermodynamic, chemical, physical, and mechanical

components that need to be considered when modeling and characterizing asphalt mixtures and pavements.

- The main components of moisture damage mechanisms are identified as: 1) changes in the internal or external conditions due to moisture transport mechanisms and 2) the response of the system as loss of capacity due to the deterioration of cohesive or adhesive bonds. The performance of the system is determined by its attributes (i.e., fundamental properties, void structure, aggregate shape characteristics, etc.) and by the changes in the moisture state (e.g., saturated flow, unsaturated flow, and diffusion).

- Quantification of total air void content cannot fully describe the air void structure of asphalt mixtures. Currently, tools are available by which to identify air void sizes, connectivity, and tortuosity. These parameters provide a better understanding of the modes of moisture transport and their relationship to moisture damage.

- Five different theories that explain the adhesive bond between aggregate and binder were presented: 1) weak boundary layers, 2) electrostatic forces, 3) chemical bonding, 4) mechanical bonding, and 5) adhesion due to surface energy. These theories are fundamental to understand the phenomena occurring at the aggregate-binder interface when moisture is presented and describing moisture damage at the microstructural level.

- Current approaches to characterizing moisture damage in asphalt mixture range from qualitative visual assessment of binder stripped from the aggregates to comprehensive quantitative parameters based on principles of continuum and fracture mechanics. There is a lack of consensus in selecting the best methodology to evaluate moisture resistance of asphalt mixtures despite the availability of a wide variety of approaches.

- Current mathematical models to simulate fluid flow and moisture damage in asphalt mixtures have provided important information to better understand moisture damage mechanisms. The technology available to characterize the internal structure of asphalt concrete materials and to compute complex numerical models makes it possible to consider mathematical modeling as an important field for advancement in this area.

- A new classification of the test methods used to characterize moisture damage was proposed. The common advantages and disadvantages for each class of test methods were discussed in detail. Evidence from the literature suggests that the use of multiple material properties provides a more comprehensive and relatively robust method to quantify moisture damage in asphalt mixtures.

CHAPTER III

FORMULATION OF A COUPLED MICROMECHANICAL MODEL OF MOISTURE DAMAGE IN ASPHALT MIXTURES*

As demonstrated in Chapter I, the understanding of the various mechanisms that lead to moisture damage at the microscale has increased during the last decade. Consequently, new experiments and analytical models have been proposed to characterize moisture damage associated with one or more of these mechanisms. In this context, micromechanical modeling of moisture damage in asphalt mixtures becomes an efficient tool to understand the dynamics of the interaction of different damage mechanisms and to provide guidance for the development of continuum damage models.

This chapter introduces a micromechanical model for moisture-induced damage in asphalt mixtures. The model was developed to couple the effects of moisture diffusion with the mechanical response of the mixture in order to quantify the level of damage within the material. Thus, the mechanical response of the mixtures was made dependent on the amount of moisture content within the material in two different ways: 1) by reducing the viscoelastic asphalt matrix (or fine aggregate matrix, FAM) resistance to damage, and 2) by affecting the mechanical properties of the adhesive bonds at the aggregate-asphalt matrix interfaces. The former represents cohesive deterioration processes within the mixture while the latter simulates adhesive deterioration at the interfaces of the coarse aggregates and the asphalt matrix.

Damage caused by the combined action of moisture and mechanical loading is evaluated based on the location and time for crack initiation and propagation at the aggregate-asphalt matrix interfaces, and on the level of strains and stresses within the bulk of the asphalt matrix. The model was tested using a simplified microstructure of an asphalt mixture. The results show that the micromechanical model can be used to attain a better understanding of the moisture damage mechanisms in asphalt mixtures. In addition, the results also demonstrated that the model can be efficiently used to conduct parametric analysis of the effect of different physical

---

* Most of this chapter is preprinted from the paper: "A Coupled Micromechanical Model of Moisture-Induced Damage in Asphalt Mixtures" by Silvia Caro, Eyad Masad, Amit Bhasin and Dallas Little with permission granted by the Journal of Materials in Civil Engineering (ASCE). The paper is currently in press.

and mechanical material properties on the initiation and evolution of damage (Chapters IV and V).

The first part of this chapter discusses the damage mechanisms that were considered in the model. Next, the modeling methodology and numerical implementation of the model are described. Finally, the last section explains how the model is used to study damage in a two-dimensional micromechanical representation of an asphalt mixture subjected to moisture diffusion and mechanical loading.

Objectives

The objectives of this chapter are:

- identify the requirements for a micromechanical model of moisture-induced damage,
- identify the deterioration mechanisms that should be included in the model,
- formulate the mechanisms to couple the effects of moisture on the mechanical performance of asphalt mixtures, and
- formulate the approach to numerically implement the model.

Components of the Micromechanical Model

Even though there has been significant experimental and analytical research on moisture-induced damage in the last two decades, there are still important gaps related to the development of models and determination of parameters for these models that can be used for predicting the influence of various material properties on moisture-induced damage (Chapter II). Recent modeling efforts based on continuum damage mechanics theory incorporate diverse deterioration processes in asphalt mixtures (Chehab et al. 2007; Kutay et al. 2008) in the absence of moisture. As described in Chapter II, Kringos et al. (2008a; Kringos et al. 2007) and Graham (2009) developed finite element models based on continuum damage mechanics for moisture-induced damage that account for several of the physical and mechanical deterioration mechanisms associated with this phenomenon. These mechanisms include softening of the viscoelastic matrix or binder within the asphalt mixture due to moisture diffusion, and degradation of the adhesive bonds between aggregates and asphalt matrix. Little work has been conducted in micromechanical computational modeling of moisture damage in asphalt mixtures.

Micromechanical modeling has the advantage of establishing a direct link between properties of the materials that constitute asphalt mixtures, design of the asphalt mixture, and performance.

A micromechanical numerical model to characterize microstructural damage in asphalt mixtures due to moisture should consider the following:

- geometry of the microstructure,
- moisture transport mechanisms,
- external loading,
- mechanical properties of materials as a function of moisture concentration,
- theoretical damage models (e.g., fracture mechanics and thermodynamics principles), and
- damage parameters to describe the local and overall degradation of the system through time.

The model proposed in this dissertation integrates these components and implements the solution in finite element software. The most important characteristic of the model is the coupling between moisture transport and the mechanical properties of the materials. In this model, moisture transport is considered to be due to water vapor diffusion. As demonstrated by Lytton et al. (1990), environmental conditions in the field generate relative humidity gradients at the interior of the asphalt pavement layers. These gradients result in the diffusion of moisture through the asphalt mixture. In the case of asphalt mixtures, moisture gradients at the interior of the material exist between the voids of the mixture and the aggregate-asphalt matrix interface, and they initiate moisture diffusion processes through the asphalt matrix film (Arambula et al. 2009a). The asphalt matrix of an asphalt mixture is defined as the viscoelastic composite comprised of the fine portion of the aggregates, the asphalt binder, and the air voids, and, as mentioned in the previous chapter, it is usually referred to as Fine Aggregate Matrix (FAM). Moisture diffusion is an essential component for developing moisture-induced damage because: 1) it modifies the material properties of the asphalt binder or FAM films; and 2) it is the main driving source of moisture that reaches the aggregate-binder interface, which ultimately undermines the quality of the adhesive bond between the two materials.

Moisture degradation of the bulk—normally referred to as cohesive deterioration—can include creep, swelling, post-cure effects, cracking, plasticization by water, and hydrolysis, among others (Zewi et al. 1984). In this model, the effect of moisture on the FAM is restricted to

the degradation of its viscoelastic material properties: no fracture processes within the material are represented.

The proposed model gives special attention to the deterioration processes occurring at the aggregate-FAM interface, an area where little work has been conducted. The displacement of the asphalt binder or FAM film by water from the aggregate surface is a thermodynamically favorable process. This is because of the preference of the aggregate surface to be covered by water instead of asphalt binder, as was explained in Chapter II. This preference makes adhesive failure the predominant mode of fracture when moisture is present at the aggregate-FAM interface. The deterioration of the adhesive bond consists of the breakage of secondary bonds (i.e., Lewis Acid-Base and van der Waals bonds) due to the presence of water at the interface (Hefer et al. 2005). The Appendix of this dissertation summarizes some of the works that have been conducted in fields other than pavements engineering to characterize fracture properties of adhesive-substrate interfaces and the effect of moisture on such systems. Those works partially guided the approaches selected to model the effects of moisture on the adhesive bonds between aggregates and FAM.

Some of the currently available micromechanical techniques to simulate progressive failure within composite materials include the virtual internal bond (VIB) model, the porosity-based Gurson model, the virtual crack closure technique (VCCT), and the cohesive zone model (CZM). Among these, numerical implementation of CZM is considered as one of the simplest and more efficient approaches to numerically simulate crack initiation and propagation within a material (cohesive failure), or between two materials bonded together (adhesive failure) (Hua et al. 2006). For this reason, the current model simulates crack-nucleation, initiation, and propagation at the aggregate-FAM interface by using fracture mechanics principles through the implementation of the CZM technique.

CZM is a computational micromechanics methodology used to model the fracture process as a gradual separation that takes place across a surface. This technique is based on the concepts introduced by Barenblatt (Barenblatt 1959) for brittle materials and by Dugdale (1960) for ductile materials, who suggested the inclusion of a small zone in front of the crack tip—named the *cohesive zone*—that could resist traction separation (Figure 3.1). This zone, usually represented by a *nominal zero-thickness* layer, does not symbolize any physical material element; instead, it represents the cohesive (or adhesive) forces that are needed for separation of bulk materials (Ortiz and Pandolfi 1999). The main advantage for including a traction-resistant

zone in front of the crack tip is that it overcomes the numerical inaccuracies that arise at this zone when applying classical linear elastic fracture mechanics theory.
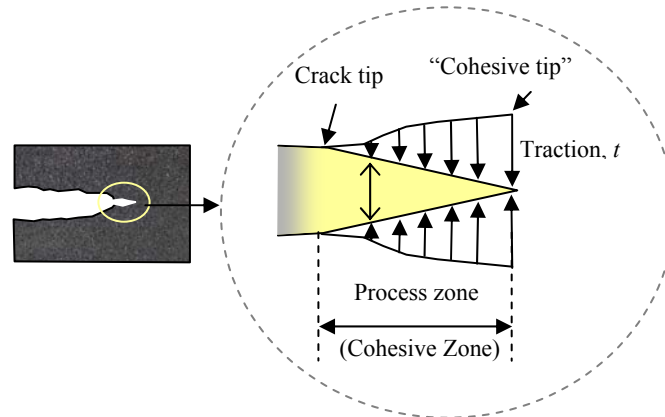
Figure 3.1. Representation of a cohesive zone to simulate a fracture process

The most important component of a CZM is the traction-separation law since it determines the relationship between the traction applied to a cohesive element (σ in Figure 3.2) and the relative displacement between its opposite surfaces (δ in Figure 3.2).
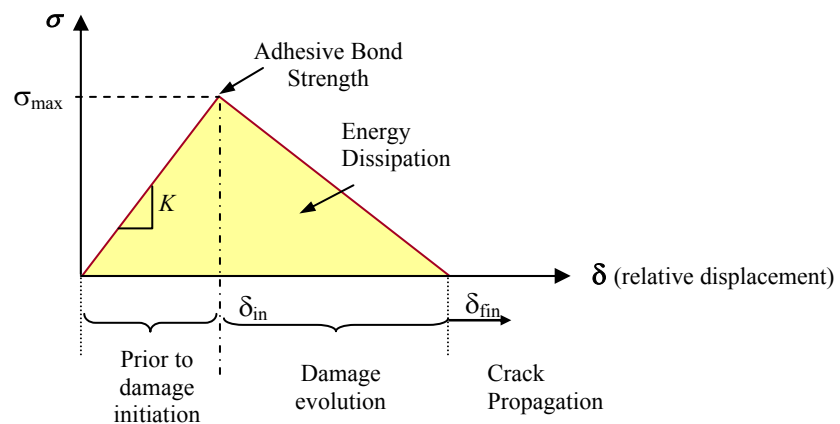
Figure 3.2. Components of a bilinear traction-separation law

As observed in Figure 3.2, the traction-separation law has four main components: 1) the mechanical response of the elements before reaching a damage initiation criterion (from δ_0 to δ_{in} in Figure 3.2), 2) a damage initiation criterion (from δ_{in} to σ_{max}), 3) a damage evolution or propagation criterion (from δ_{in} to δ_{fin}), and 4) a final damage condition (δ_{fin}). Once the damage initiation criterion is reached, the fracture energy of the element is released. A crack initiates when the ultimate damage criterion, which is associated with δ_{fin}, is achieved. The mechanical loading that this element was previously able to resist is then transmitted to the surrounding elements, promoting propagation of the crack through the interface. The fracture toughness of the material, G^c, is usually quantified as the area under the traction-displacement curve. However, important considerations regarding the existence of recoverable energy during the separation process are required when defining this quantity.

A literature review of the application of cohesive zones reveals that the shape of the traction-separation curve has received less attention when compared to the parameters defining the initiation of damage (i.e., σ_{max} and δ_{in} in Figure 3.2) and the final damage condition (i.e., zero traction resistance and δ_{fin} in Figure 3.2). However, recent studies (Alfano 2006; Chandra et al. 2002; Volokh 2004) have shown that it has important consequences in the execution of the fracture process. Figure 3.3 illustrates some of the most commonly used traction-separation laws and Figure 3.4 presents the relationship between the evolution of the fracture process and the traction-separation law (Camanho 2005).
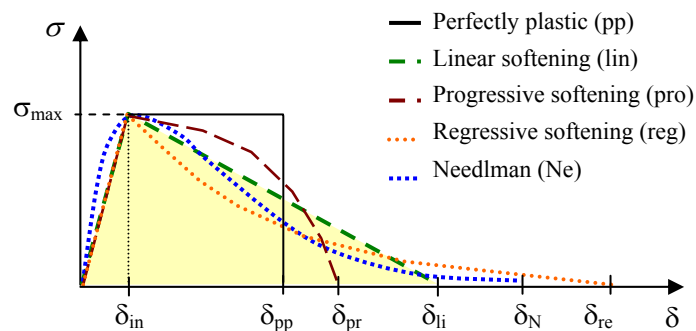
Figure 3.3. Typical traction-separation laws for cohesive zone models; modified after Camanho 2005
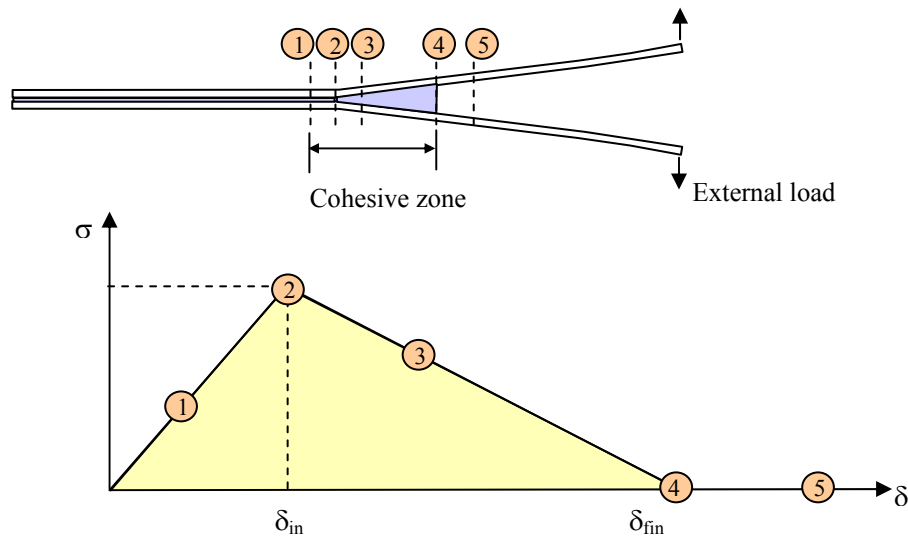
Figure 3.4. Relationship between the traction-separation law and the fracture process; modified after Camanho 2005

Under mixed-mode fracture conditions, three distinct separation laws are required—one for every mode—as well as special criteria defining overall damage initiation and evolution processes. Since this work uses the CZM technique to simulate adhesive fracture, the interfaces of aggregate-FAM systems will be referred to as *adhesive zones*, and the elements in these zones will be named *adhesive elements*.

The CZM technique has been successfully used to model standard delamination tests of structural adhesive joints (Camanho and Davila 2002; Camanho et al. 2003; Ferracin et al. 2003; Ortiz and Pandolfi 1999). Furthermore, this technique has also been used to model the effects of humid environments on the same delamination processes (Hua et al. 2006; Liljedahl et al. 2006; Loh et al. 2003). Details of these works can be found in the Appendix. In the context of asphalt mixtures, CZM has been applied to simulate fracture processes in asphalt mixtures at the macroscale level (Jeng and Perng 1991; Soares et al. 2003) and at the microscale level (Kim et al. 2005; Kim et al. 2008). However, to the best knowledge of the author, the model presented in this chapter uses, for the first time, CZM to simulate the effect of moisture on the adhesive fracture processes in asphalt mixtures.

In summary, the proposed micromechanical model simulates moisture damage initiation and evolution in two different ways: 1) by making the linear viscoelastic material properties of

the asphalt matrix dependent on the amount of moisture, and 2) by reducing the resistance of the interface between the coarse aggregates and the asphalt matrix as a function of the moisture content. The former deals with cohesive deterioration processes in the asphalt matrix and the latter describes the moisture-induced deterioration of the aggregate-FAM adhesive bond. Figure 3.5 summarizes the moisture-damage evolution processes considered by the model. It is noteworthy that, as shown in this figure, the sole presence of moisture degrades the asphalt mixture, even in the absence of mechanical loading. However, such degradation is manifested only when mechanical loading is applied to the system. Table 3.1 describes the components and the corresponding capabilities of the micromechanical model.
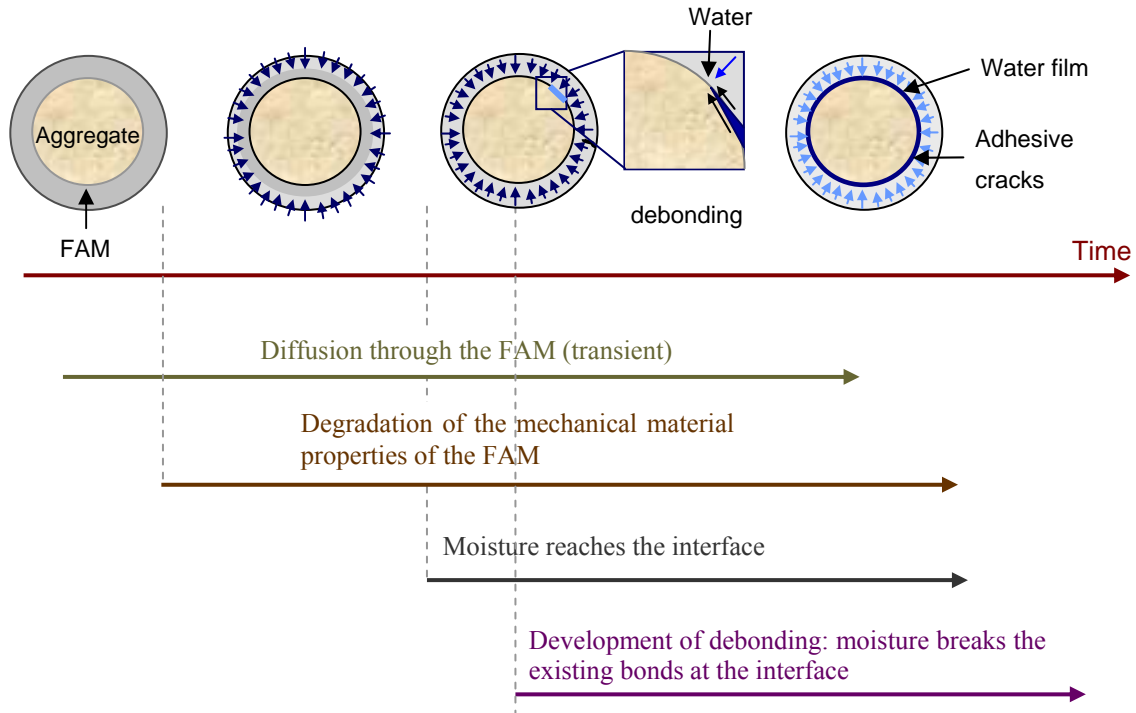
Figure 3.5. Illustration of moisture damage in an aggregate-FAM system due to diffusion of vapor water

Table 3.1. Components of the numerical model

Component	Proposed model
Geometry	Complex geometries can be considered.
Moisture transport mechanisms	Moisture diffusion through FAM-aggregates systems. Water infiltration and capillary rise are not considered in the model.
External loading	Any type of external load can be simulated.
Moisture-dependent material properties	Linear viscoelastic material properties of the FAM are moisture dependent. The mechanical response of the aggregate-FAM interface is moisture dependent.
Fracture mechanics and thermodynamics principles	The cohesive zone modeling technique is used to represent the aggregate-FAM interface (*adhesive zones*). Crack nucleation, initiation and propagation due to the combined effect of moisture and mechanical loading are a natural result of the model.
Damage parameters	The viscoelastic response of the asphalt matrix (FAM) is monitored through time. Location of crack nucleation, time to crack initiation and crack growth rate are monitored at the aggregate-FAM interfaces.

Modeling Methodology

The micromechanical model was developed using a sequentially coupled moisture diffusion-mechanical response scheme in the finite element software Abaqus® (ABAQUS 2007). This modeling technique consists of four stages, as illustrated in Figure 3.6. The first stage includes the general definition of the problem (i.e., geometry, material properties, etc.). The second and third stages constitute the core of the modeling methodology. During the second stage, moisture diffusion profiles under the absence of load are generated within the system. During the third stage, mechanical loading is applied and the moisture profiles generated in the previous stage are used as prescribed conditions of the simulation. In this approach, mechanical loading is applied at the same time that moisture diffuses into the system. It should be noted that the main assumption behind the sequentially coupled methodology is that the mechanical response of the system is dependent on the moisture diffusion processes, but that moisture diffusion is independent of the state of the stresses within the system. This assumption is reasonable since the duration for which traffic loads act at any given point is commonly a small fraction of the typical duration of time over which the relative humidity gradient persists.
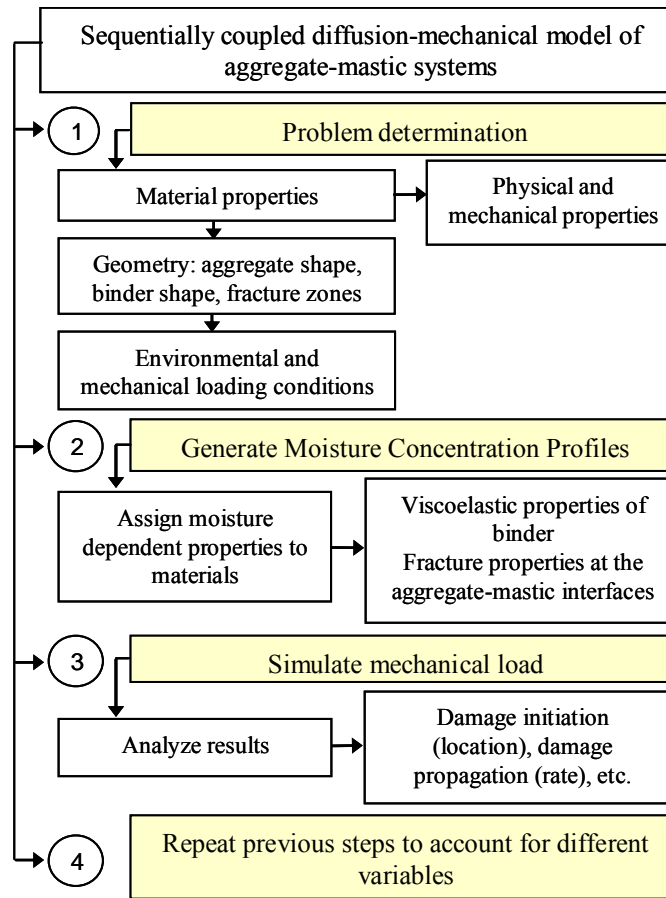
Figure 3.6. Sequentially coupled moisture diffusion-mechanical damage model of asphalt mixtures

Moisture diffusion within the microstructure of the asphalt mixture is assumed to follow Fick's second law, i.e.,

$$\frac{\partial \phi}{\partial t} = D\nabla^2 \phi,$$
(3.1)

where ϕ is the moisture concentration, D is the moisture diffusion coefficient, and ∇ is the vector differential operator.

Moisture content at each node is computed following an implicit scheme (Abaqus®/Standard) where the aggregates and the FAM are modeled using 3-nodes first order

mass diffusion elements (type DC2D4 in Abaqus®), and the interfaces are modeled using 4-nodes linear mass diffusion elements (type DC2D3).

The mechanical simulation is solved using an implicit scheme (Abaqus®/Standard) in which the asphalt matrix is modeled as linear viscoelastic and the aggregates are modeled as linear elastic materials. A bilinear traction-separation law dictates the mechanical response of the interfacial adhesive zones. In other words, prior to damage initiation (before σ_{max} and δ_{in} in Figure 3.2) the mechanical response of the adhesive elements was assumed linear elastic, followed by a linear softening of the elastic stiffness of the elements during the evolution of the damage (after δ_{in} in Figure 3.2). Aggregates and FAM are discretized using first order triangular elements (elements type CPE3 in Abaqus®). The interfaces are composed of adhesive zones using zero-thickness adhesive elements (elements type COH2D4 in Abaqus®).

Coupled Micromechanical Model of Moisture Damage

A two-dimensional micromechanical model of an asphalt specimen composed of two real-shaped coarse aggregates embedded in continuous FAM was developed, implemented, and analyzed following the methodology described in Figure 3.6.

Geometry

The shape and size of the aggregates were obtained from a real image of a 4-inch cylindrical specimen of a hot mix asphalt (HMA) mixture (Figure 3.7). Details of the characteristics of the asphalt mixture can be found in Reyes et al. (2008). Figure 3.7 also presents the geometry of the sample and the idealized model. Since the main objective of the simulation is to present the coupling capabilities of the model to account for damage processes, only two coarse particles were included. Aggregates with radii smaller than 2.5 mm were assumed, for simplicity, to be part of the asphalt matrix.

The implementation of a realistic microstructure geometry in the finite element model requires special attention. Adhesive zones are incorporated in the model as layers of square elements with 0.05 mm in length between the FAM and aggregate phases. Consequently, the finite element mesh within the adhesive zones has to be defined according to a special orientation definition that should be in agreement with the different modes of failure (modes I, II and III). In order to do so, the special *sweep* technique available in Abaqus® is required when

meshing the adhesive zones. This technique uses a pre-defined stack direction to associate normal and tangential local orientations to each element. Figure 3.8 illustrates an example of the finite element mesh of the adhesives zones and their corresponding stack (i.e., normal) direction.

(a)   (b)
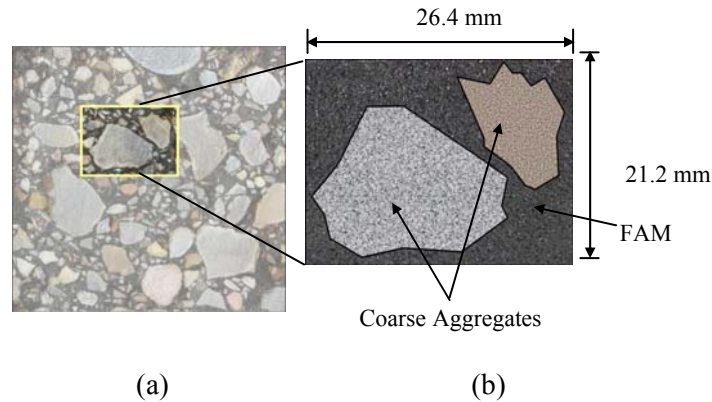
Figure 3.7. Illustration of the generation of the geometry of a micromechanical model from an asphalt mixture, (a) asphalt mixture section, and (b) asphalt mixture model used in simulations
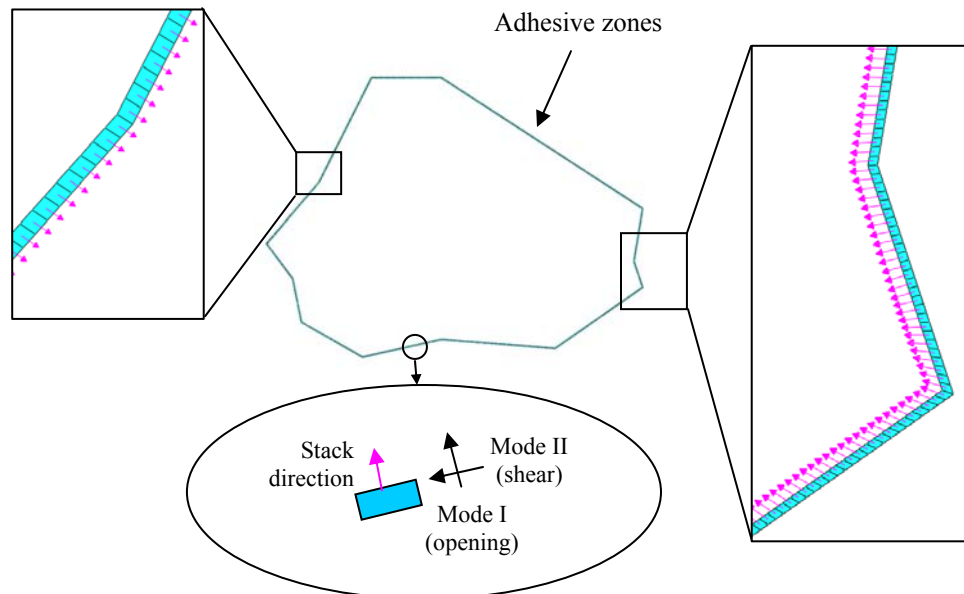
Figure 3.8. Detail of the finite element mesh of the adhesive zones corresponding to one coarse aggregate and the stack orientation associated to each element

Chapters IV and V of this dissertation deal with applications of the model to more complex microstructures. The implementation of more realistic geometry imposes a challenge in terms of the numerical implementation of the adhesive zones. This is because the addition of more aggregate particles is accompanied by the adhesion of more adhesive zones. The adhesive zones need to perfectly fit their surrounding materials (i.e., the external surfaces of the aggregates and the FAM). Besides, the definition of the stack direction for these new adhesive elements (Figure 3.8) usually requires dividing the adhesive zones associated with each aggregate into several regions, which is a complex and time-consuming process. Furthermore, appropriate interaction properties among the FAM, the adhesive zone, and the aggregate surfaces are needed to guarantee continuity of the mass transport and mechanical processes. Interaction properties are particularly important when considering that the resistance of the adhesive zones is considerably smaller than the one of the surrounding materials (especially when compared to the coarse aggregates). Consequently, under compressive loading conditions, the high levels of deformation of the adhesive zones can produce interpenetration between the FAM and the aggregate meshes. Mesh interpenetration between coarse aggregates and the bulk matrix can also occur when the adhesive elements disappear due to the initiation or propagation of adhesive cracking. In order to avoid such instabilities, a surface-based interaction consisting of small-sliding hard-contact properties (ABAQUS 2007) were assigned to the surfaces of aggregates and FAM. Thus, in the case that these two surfaces make contact, their meshes will be restrained from any possible interpenetration.

Material Models and Properties

Physical Material Properties

Table 3.2 lists the moisture diffusion coefficients for the aggregate phase—that was assumed to be limestone—and the FAM. These values were selected within the range of reported values for rocks and FAMs (Arambula et al. 2009a; Dobchuk et al. 2004; Kassem et al. 2006; Kringos et al. 2008b).

Table 3.2. Physical material properties

	Aggregate	Matrix	Interface
Moisture diffusion coefficients (mm^2/s)	$2.44*10^{-4}$	$D_1 = 2.78*10^{-5}$ $D_2 = 5.56*10^{-6}$	Same as the matrix

Mechanical Models and Material Properties

As mentioned previously, the mechanical response of the aggregates was assumed to be linear elastic and the response of the FAM was assumed as linear viscoelastic. The elastic modulus of the aggregates was assumed to be independent of the moisture content within the material. The viscoelastic material properties of the FAM correspond to the values reported by Kim et al. (2005). These data were originally obtained from relaxation tests by means of a dynamic shear rheometer (DSR) at three different temperatures and fitted to a reduced master curve at 25°C reference temperature. Afterwards, the data were converted to uniaxial relaxation modulus in the time domain using linear viscoelastic theory and fitted to a Prony series. The Prony series representation for the viscoelastic response of the FAM, i.e., the relaxation modulus as a function of time (t), is:

$$E(t) = E_{\infty} + \sum E_i \exp\left(-tE_i/\eta_i\right), \tag{3.2}$$

where the parameters E_i and η_i are the Prony series parameters, listed in Table 3.3 and E_{∞} is equal to $1.22*10^2$ Pa. The relaxation modulus of the viscoelastic bulk was assumed to decrease as a function of moisture concentration from its original value in the absence of water to 85% of this value under saturated conditions. A sensitivity analysis was conducted to determine the influence of using different models (e.g., linear, exponential, potential) to represent the softening of the viscoelastic properties on the overall fracture response of the micromechanical model. The reduction of the stresses within the FAM as a function of time and moisture content, and the location and rate of adhesive fracture, showed that there was no significant difference among these models. Therefore, a linear softening decay of the relaxation modulus as a function of moisture was selected for the cohesive degradation model. This assumption is in good agreement with works conducted on polymers (Aiello et al. 2006).

Table 3.3. Prony series parameters characterizing the linear viscoelastic response of the bulk (after Kim et al. 2005). Units of E_i: Pa, units of η_i: Pa.s (i from 0 to 9)

E_1	$7.32*10^7$	η_1	$1.15*10^5$
E_2	$2.55*10^7$	η_2	$4.18*10^5$
E_3	$1.08*10^7$	η_3	$1.08*10^5$
E_4	$2.08*10^6$	η_4	$1.53*10^5$
E_5	$3.32*10^5$	η_5	$2.25*10^5$
E_6	$5.34*10^4$	η_6	$3.51*10^5$
E_7	$8.44*10^3$	η_7	$5.43*10^5$
E_8	$1.33*10^3$	η_8	$8.66*10^5$
E_9	$2.52*10^2$	η_9	$2.04*10^5$

A bilinear traction-separation law, like the one represented in Figure 3.2, was assumed to dictate the mechanical response of the adhesive elements. Before damage initiates the relationship between nominal stresses, σ, and nominal strains (i.e., relative displacement between the opposite faces of the element divided by the thickness of the adhesive layer), ε, is given by:

$$
\begin{pmatrix} \sigma_s \\ \sigma_n \\ \sigma_t \end{pmatrix} = \begin{bmatrix} K_{nn} & 0 & 0 \\ 0 & K_{ss} & 0 \\ 0 & 0 & K_{tt} \end{bmatrix} \begin{pmatrix} \varepsilon_s \\ \varepsilon_t \\ \varepsilon_n \end{pmatrix},
\tag{3.3}
$$

where subscripts n, s, and t represent the normal and two shear directions, and K_{nn}, K_{ss} and K_{tt} are the components of the elastic matrix. For the two-dimensional microstructure model considered, the elastic relationship only includes the normal and first shear components (i.e., n and s). The elastic modulus of these elements was considered the same in all directions and was calculated as an average of the relaxation modulus of the viscoelastic FAM during the total time of the mechanical simulation. Under this condition, it is valid to assume that the stiffness of the adhesive elements before damage initiation is comparable, on average, to that of the viscoelastic matrix. In other words, the adhesive elements are considered part of the asphalt matrix prior to the initiation of interfacial damage.

The criterion for damage initiation defining the bond strength of the adhesive zones was taken to be the quadratic nominal strain condition, and it was set to be independent of the moisture concentration at the interface:

$$\left(\frac{\langle\varepsilon_n\rangle}{\varepsilon_n^0}\right)^2 + \left(\frac{\varepsilon_s}{\varepsilon_s^0}\right)^2 = 1, \tag{3.4}$$

where ε_n and ε_s represent the current level of normal and shear nominal strains in the adhesive element, and ε_n^0 and ε_s^0 the peak values of the nominal strain for the purely normal or shear direction. The brackets in the first term represent the Macaulay condition that indicates that no damage is produced under pure compressive deformations. Once damage initiates the adhesive fracture energy starts being released.

Mixed-mode conditions define the response of the adhesive elements during the evolution of damage. In this analysis, the critical energy released rate in mode I, G_n^C, and in mode II, G_s^C, were assumed to be equal. The degradation of the stiffness of the adhesive elements after damage initiation follows an exponential curve according to the Benzeggagh-Kenane (BK) damage evolution criterion (Benzeggagh and Kenane 1996):

$$G_n^C + \left(G_s^C - G_n^C\right)\left\{\frac{G_s}{G_T}\right\}^{\eta} = G^C, \tag{3.5}$$

where the total released energy, G_T, is equal to the addition of the energy released in the normal and shear directions: $G_T = G_n + G_s$, and η is a material property. Based on the assumption of anisotropy in the critical energy released rate of the interfaces, Equation 3.5 implies that the critical energy released rate of the mixed-mode condition is equal to the energy released rate in each direction, independent of the parameter η. Although this assumption is not a realistic representation of the true material behavior, it is a simplification that permits the efficient inclusion of fracture material properties of the interfaces as the first step towards the development of a more general model. As the mechanical response of the adhesive elements before damage initiation was considered comparable to that of the FAM, the area below the

traction-separation law before damage initiation is assumed to be stored energy. Therefore, the fracture toughness of the material was computed as the area under the curve in the damage evolution region.

As mentioned previously, the release of energy generates a reduction or degradation of the elastic stiffness of the elements (i.e., stiffness softening). This reduction is a function of a scalar factor S, a damage variable that goes from 0, before damage initiation, to 1 when total damage has occurred (i.e., crack initiation). For a linear softening process, the damage variable S is defined by the expression:

$$S = \frac{\delta_{fin}^m \left(\delta_{max}^m - \delta_{in}^m \right)}{\delta_{max}^m \left(\delta_{fin}^m - \delta_{in}^m \right)},$$ (3.6)

where δ^m is the effective displacement of the element (Camanho and Davila 2002) defined as: $\delta^m = (\delta_n^2 + \delta_s^2)^{1/2}$. The subscripts *in* and *fin* refer to the values of the effective displacement at damage initiation and at complete failure, respectively. The subscript *max* refers to the maximum value attained by the effective displacement during the loading history. During the softening of the elastic stiffness, the nominal stresses are computed as:

$$\sigma_n = \begin{cases} (1-S)\overline{\sigma}_n & for \ \overline{\sigma}_n \geq 0 \\ \overline{\sigma}_n & for \ \overline{\sigma}_n \leq 0 \end{cases},$$ (3.7)
$$\sigma_s = (1-S)\overline{\sigma}_s$$

where $\overline{\sigma}_n$ and $\overline{\sigma}_s$ correspond to the stresses if no damage occurs, i.e., Equation 3.3.

The degradation of the stiffness of the adhesive zones (Equation 3.6 and 3.7) is usually associated with numerical stability problems in the implicit finite element solution. Therefore, the selection of the adhesive zones' thickness, the properties of the adhesive zones, the time step increments, and the use of other advanced computational techniques such as viscous regularization (ABAQUS 2007) should be carefully considered in order to achieve numerical convergence. In this model, a small factor of $1*10^{-5}$ viscous regularization for the constitutive equations was used to promote stability. Viscous regularization causes the elastic stiffness matrix of the adhesive element to be positive for small intervals of time. Therefore, the nominal stresses are permitted to be outside the limits imposed by the traction-separation law for a small fraction

of time, which in turn offers stability to the numerical solution. When the viscous regularization parameter is small compared to the characteristic interval time (which in this case is equal to 0.05 s), the quality of the results are not compromised because the numerical solution tends to converge to the solution of the inviscid case (i.e., when no artificial viscous effects are introduced).

Once an adhesive element looses all its traction capabilities (i.e., S reaches a value of 1, the stiffness of the element is 0 and the effective relative displacement equals δ^m_{fin}) the element is deleted. The deletion of the element represents the initiation of an adhesive crack.

Since the stiffness of the adhesive element decreases as a function of the moisture concentration at the interface, the adhesive bond strength and the fracture energy of the interface also decrease with time. These two conditions are in good agreement with many reported observations from experimental works conducted on metal-polymer adhesive joint specimens subjected to hostile moist environments (Kook and Dauskardt 2002; Lane et al. 2004; Mostovoy and Ripling 1969). Table 3.4 summarizes the mechanical responses of the components of the model microstructure.

Table 3.4. Mechanical material properties

	Aggregate	Matrix	Interface
Mechanical properties	$E = 5*10^4$ MPa $\nu = 0.35$	Prony series for shear relaxation modulus $[G(t)]$ obtained from Kim et al. (2005), Table 3.3.	$E_{normal} = E_{shear} = 45$ MPa Failure criteria (n=normal, s=shear): $$\left(\frac{\varepsilon_n}{\varepsilon^n_{max}}\right)^2 + \left(\frac{\varepsilon_s}{\varepsilon^s_{max}}\right)^2 = 1$$ Maximum displacement at failure: $$\delta^s_{max} = \delta^n_{max} = 0.05 \text{ mm}$$ Critical Energy Released rate, G^C (mixed mode) in dry condition: $G^C_n = G^C_s = 1.687*10^{-2}$ N/mm.

Table 3.4. (Continued)

	Aggregate	Matrix	Interface
Moisture dependency of mechanical properties	No moisture dependency	$G(t)$ decreases exponentially from its original value in dry condition to 85% of the original value under saturated conditions.	Normal and shear moduli (E_{normal}, E_{shear}) decrease exponentially from 150 MPa in dry condition to 0 MPa in saturated condition. The failure criterion does not change with moisture content.

Generation of Moisture Diffusion Profiles

The asphalt mixture microstructure was subjected to different moisture diffusion processes in order to generate diverse moisture concentration profiles. These moisture profiles were used afterwards during the mechanical simulation, and their effect on the initiation and evolution of damage was evaluated. Two different values for the moisture diffusivity of the adhesive bulk or FAM were considered in this study (i.e., D_1 and D_2), while the same mechanical properties were used for all simulations (Table 3.2 to Table 3.4). In each case, moisture was allowed to diffuse into the system for 30 days, and the moisture profiles after 10, 20, and 30 days were saved and used to study the mechanical performance of the system (Figure 3.9).
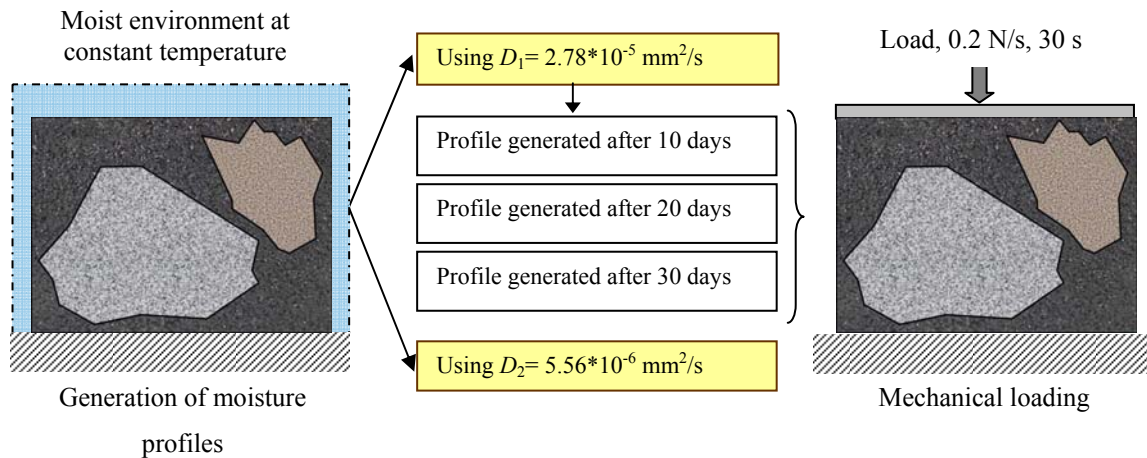
Figure 3.9. Illustration of the simulation methodology

The boundary conditions to model the moisture diffusion consisted of a constant normalized moisture concentration value of 1.0 at the top and two side edges of the model. The normalized moisture concentration was defined as the moisture concentration of the material divided by the maximum moisture content that the FAM can absorb. A normalized moisture concentration value of 0 represents dry conditions and a value of 1.0 represents moisture saturation of the FAM bulk. Figure 3.10 presents the six moisture diffusion profiles (two diffusion coefficients and three time durations of diffusion). As would be expected, the moisture profiles generated with the larger value of moisture diffusivity of the FAM (i.e., D_1) presented higher moisture concentration values at all times. Therefore, the moisture profile obtained after 30 days of moisture diffusion in the sample containing the highest FAM diffusion coefficient (i.e., D_1) is expected to show the poorest performance under mechanical loading.
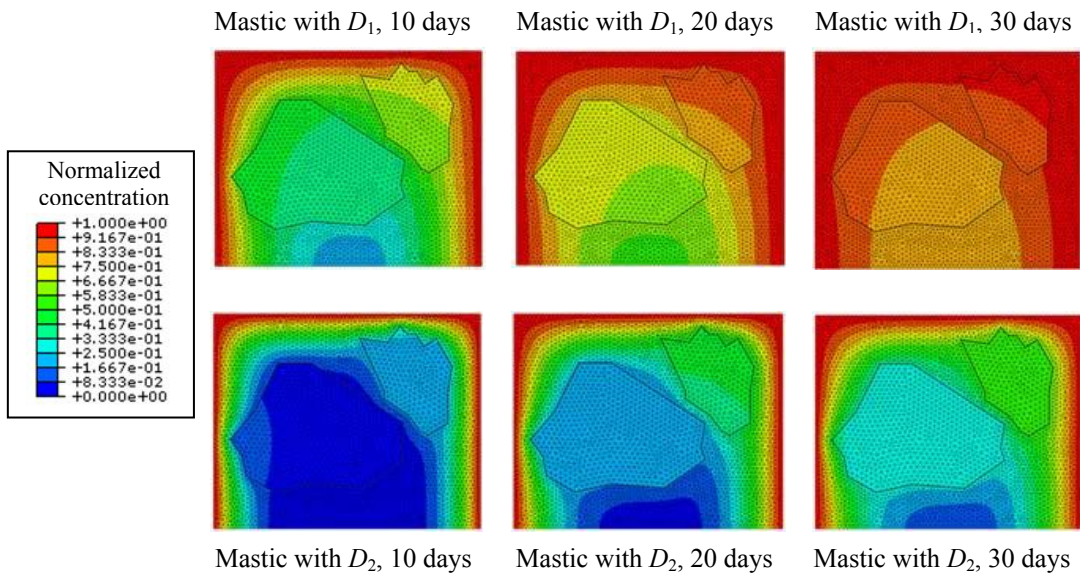
Figure 3.10. Normalized moisture concentration profiles (D_1= 2.78*10^{-5} mm^2/s, D_2 = 5.56*10^{-6} mm^2/s)

Coupling between Moisture Diffusion and Mechanical Loading

The aggregates-FAM model was subjected to a quasi-static compressive load applied at a rate of 0.2 N/s during a total period of 30 s (Figure 3.9). The loading was initially applied to the dry sample and, afterward, the mechanical simulation was conducted using each of the moisture profiles shown in Figure 3.10. Figure 3.11 presents the final state of the system at the end of the mechanical experiment for the dry case and for the moisture-conditioned cases.

Response in dry condition (deformed and original shapes)	FAM with D_1, 10 days	FAM with D_1, 20 days	FAM with D_1, 30 days
	FAM with D_2, 10 days	FAM with D_2, 20 days	FAM with D_2, 30 days
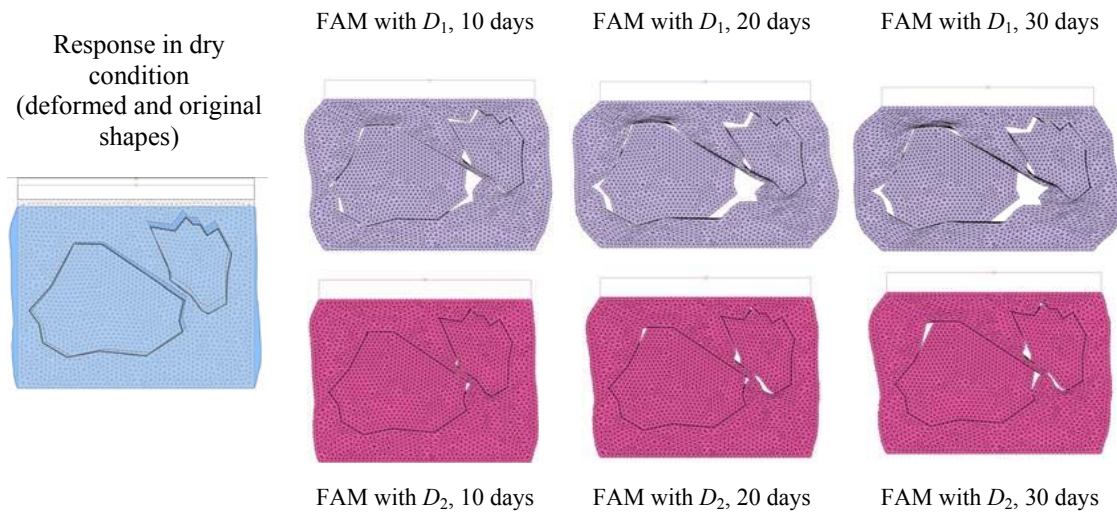
Figure 3.11. Final state of the model after the application of 0.2N/s (30 s) to specimens subjected to different moisture conditioning periods ($D_1 = 2.78*10^{-5}$ mm^2/s, $D_2 = 5.56*10^{-6}$ mm^2/s)

In general, the results obtained in this analysis show that moisture diffusion strongly determines the level and rate of damage in asphalt mixtures, and that the diffusivity and viscoelastic properties of the FAM play an important role in the degradation of the system. Since the mechanical properties of the materials in dry condition are the same for all simulations, it can be concluded that the differences in the mechanical performance are exclusively due to the coupling between the amount and location of moisture within the material. These results suggest, for example, that the moisture-induced damage in two different asphalt mixtures containing the

same materials but different total air void contents can be significantly different, since the air void structure of a mixture influences the moisture diffusivity of the FAM.

Figure 3.12 illustrates the reduction of the quality of the aggregate-FAM interfaces. This figure depicts the principal stress vs. relative displacement (i.e., effective normal opening between the two opposite surfaces of an adhesive element) for an element at the interface (for FAM diffusivity D_1) and shows that the model integrates correctly the expected effects of moisture on the bond strength and on the dissipated energy required to initiate the fracture process.
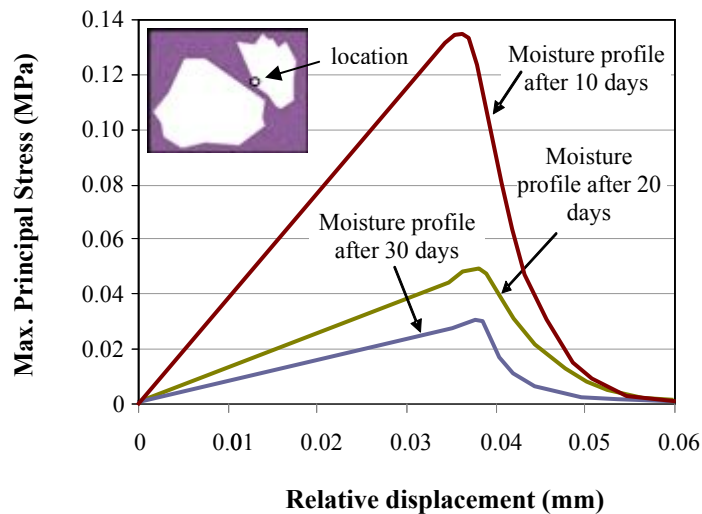
Figure 3.12. Maximum principal stress vs. relative displacement for an element at the aggregate-FAM interface

The results from the simulations also show a relationship between the amount of moisture content in the material and the time required for crack initiation at the aggregate-FAM interface. Figure 3.13 presents such a relationship for a particular zone in one of the aggregate-FAM interfaces. It shows that the time for crack initiation in the model containing the lower moisture concentration profile was 48 % less than the model with the highest moisture concentration values. Furthermore, the results demonstrate that the failure pattern at the interfaces between aggregates and FAM is dependent on the moisture diffusivity of the FAM and on the amount of diffused moisture present within the microstructure (Figure 3.14).
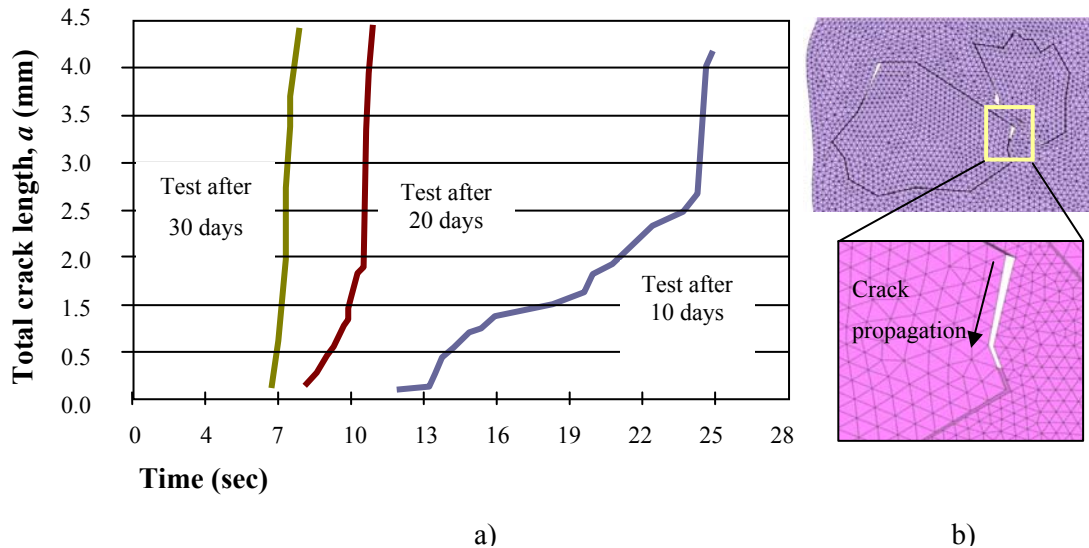
Figure 3.13. Crack length vs. time (a) for the interface zone shown in (b). The three curves correspond to the mechanical tests conducted on specimens that were moisture conditioned for 10, 20, and 30 days
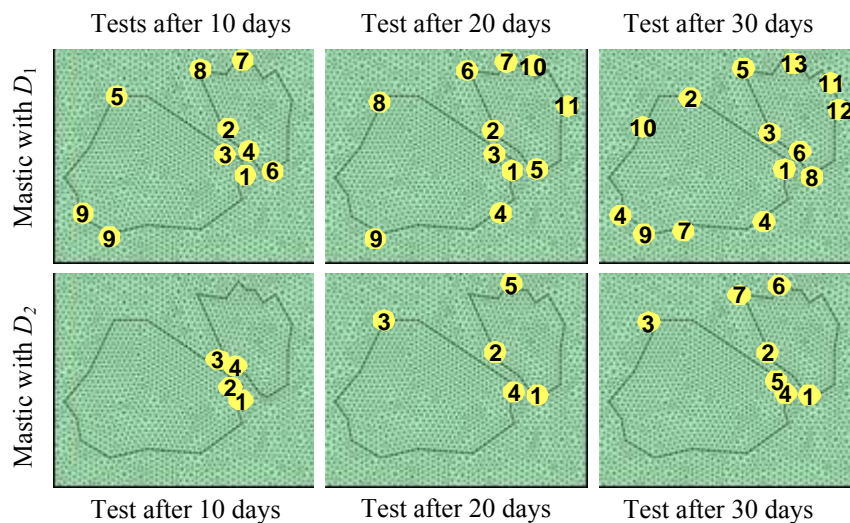
Figure 3.14. Location of crack nucleation (numbers indicate the order of crack appearance; equal numbers at different locations symbolize simultaneous crack initiation). The results correspond to the mechanical test conducted on specimens that were moisture conditioned for 10 days (left), 20 days (center) and 30 days (right). $D_1 = 2.78*10^{-5}$ mm^2/s, $D_2 = 5.56*10^{-6}$ mm^2/s

The effect of moisture on the mechanical response of the FAM is illustrated by examining the change of the maximum principal strain with time (Figure 3.15). The results in the figure prove that the model successfully introduces the deterioration of the viscoelastic properties as a function of moisture concentration. Figure 3.15 also demonstrates that the viscoelastic bulk is able to capture the effects of crack initiation and propagation occurring at the interfaces (i.e., the FAM relaxes when adhesive fracture occurs).
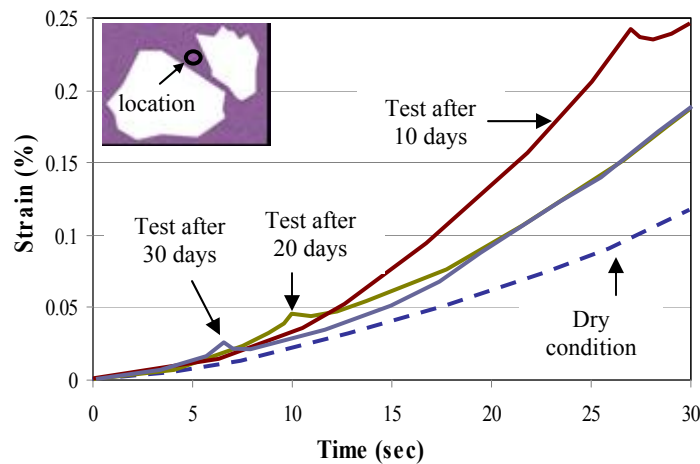
Figure 3.15. Maximum principal strain vs. time for an element at the viscoelastic bulk. The curves correspond to the results of the mechanical tests conducted on a dry and on specimens that were moisture-conditioned for 10, 20, and 30 days

Finally, the overall reduction of the structural capability of the microstructure due to the presence of diffused moisture is evidenced by the time required for crack initiation at the interfaces and by the level of stresses within the FAM before crack initiation. The time required for crack initiation in the aggregate-FAM interfaces was 29.66 s for the dry sample, 16.18 s for the sample containing FAM with a moisture diffusivity value of D_2, and 12.1 s for the sample containing a matrix with a moisture diffusivity value of D_1.

Figure 3.16 presents the state of maximum principal stresses within the microstructure at the time of the appearance of the first crack. For the dry condition, the stresses are considerably higher, suggesting that the failure in the microstructure could occur within the FAM (cohesively) before the appearance of any crack at the interfaces. For the cases where moisture is added, the

level of stress within the bulk is smaller (less than 0.8 MPa in all cases). This result implies that the failure will be predominantely adhesive, as has been shown in the previous figures. It should be noted, however, that the actual type of failure can only be determined by comparing the stress levels in the FAM and at the interfaces with experimental data collected for cohesive and adhesive strengths from different aggregate-FAM systems.
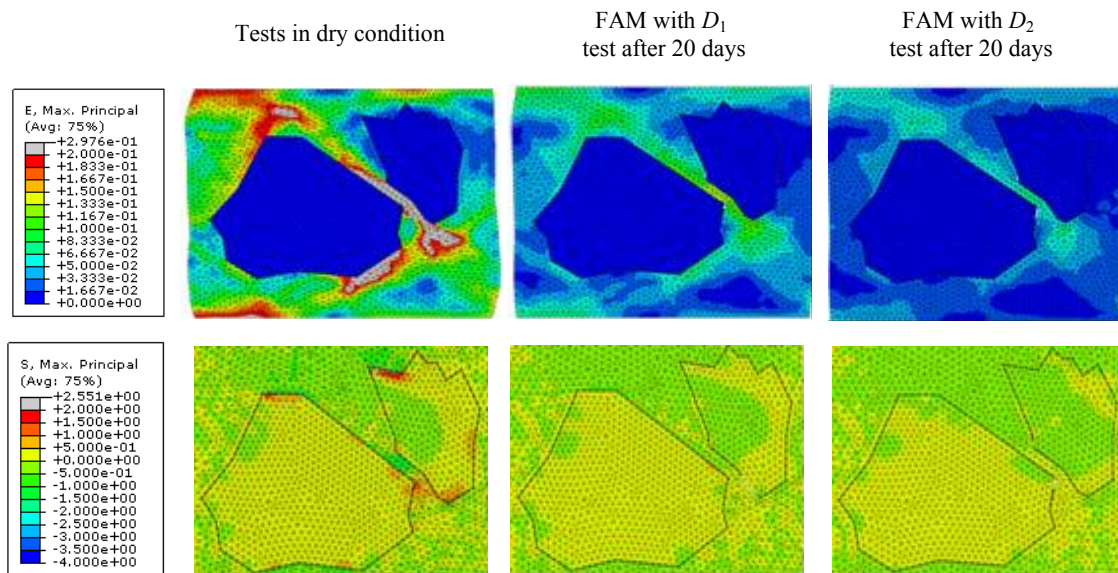
Figure 3.16. Maximum principal stress and strain profiles at crack initiation for a sample in dry state (left), and for samples conditioned for 20 days with a FAM moisture diffusion coefficient of D_1 (center) and D_2 (right)

Summary and Conclusions

This chapter presents the development and implementation of a micromechanical model that couples the effect of moisture diffusion and mechanical loading on the degradation of asphalt mixtures. The model was implemented using the sequentially coupled capabilities of the finite element software Abaqus®. The model is capable of: 1) simulating cohesive degradation of the FAM through the moisture dependency of its linear viscoelastic material properties, and 2)

simulating adhesive deterioration and fracture of aggregate-FAM interfaces using a CZM formulation.

In order to illustrate the potential of the modeling methodology, a two-dimensional microstructure model containing two real shape aggregates was constructed and analyzed. The effect of moisture diffusion on the viscoelastic response of the FAM and crack initiation and propagation at the aggregate-FAM interfaces were studied. It was concluded that the model appropriately couples the moisture dependency of the mechanical properties of the bulk and the fracture properties of the adhesive interface. As a consequence of the coupling conditions, samples with more moisture content are associated with larger deformations, more and longer cracks at the interfaces, and lower carrying-loading capacity of the viscoelastic FAM. Furthermore, an analysis of the level of stresses within the bulk suggests that the fracture locus of the system can change from cohesive—when no water is present—to adhesive—when moisture has enough time to diffuse into the mixture and reach the interface. It was also observed that the viscoelastic FAM is able to capture the debonding processes occurring at the aggregate-FAM interfaces, and that the amount and distribution of moisture content in the system modifies the location, time and rate of crack initiation and propagation along the interfaces.

The model presented in this study can be used to analyze the role of the different geometrical, physical, and mechanical parameters involved in the moisture damage phenomenon. For example, it can be used to study the degradation of asphalt mixtures containing the same design formula (i.e., same gradation and volumetric characteristics) but different combinations of aggregates and asphalt binders (i.e., systems with different bond strength properties). In addition, the model can be used to study the evolution of damage in the asphalt course of a real pavement in which environmental conditions—especially relative humidity—and traffic loading change through time.

Finally, it is important to emphasize that there is a need to conduct experimental measurements in order to determine material properties and parameters needed for proper calibration of the micromechanical model presented in this chapter. Ongoing research is currently being carried out at the Materials Group at Texas A&M University to achieve this objective.

CHAPTER IV
MICROMECHANICAL MODELING OF THE INFLUENCE OF MATERIAL PROPERTIES ON MOISTURE-INDUCED DAMAGE OF ASPHALT MIXTURES

This chapter presents a study of the effects of mechanical and physical material properties and loading conditions on the response of asphalt mixtures subjected to moisture diffusion processes. The analysis was conducted by applying the finite element micromechanical model described in Chapter III that couples the effects of moisture transport and mechanical loading on the mechanical performance of asphalt mixtures. The maximum total force of resistance offered by the asphalt mixture microstructure model for a displacement-controlled load in both the presence and absence of moisture was used as an indicator of its susceptibility to moisture damage.

The information obtained from this sensitivity study provides valuable data on the relative importance of the parameters involved in the initiation and evolution of moisture-induced damage within the microstructure of asphalt mixtures. This information can also be used to guide the development of continuum models in terms of identifying the significant mechanisms and material properties that should be accounted for in order to characterize moisture-induced damage.

The first part of this chapter describes the coupled micromechanical model for moisture-induced damage in asphalt mixtures. The description includes the generation of the microstructure geometry used in the finite element model of the asphalt mixture composite, the material constitutive relationships and properties, and the modeling methodology. The second part presents a parametric analysis of the influence of material properties and loading on moisture-induced damage. To conclude, the last part summarizes and discusses the main findings obtained from this analysis.

Objectives

The objectives of this chapter are:

- apply the micromechanical model of moisture-induced damage introduced in Chapter III to study the effects of different material properties on the sensitivity of asphalt mixtures to moisture damage,

- recognize the role of the moisture diffusion coefficients of the aggregates and the fine aggregate matrix (FAM) on the mechanical performance of asphalt mixtures subjected to moisture diffusion ,

- recognize the role of the adhesive bond properties between the aggregates and the FAM on the initiation of moisture-related damage processes, and

- identify the role of the viscoelastic properties of the bulk matrix (FAM) on the initiation of moisture-related processes.

Parameters of the Coupled Micromechanical Model

In this analysis, asphalt mixtures are modeled as a two-phase composite material containing aggregates and FAM. Although the FAM is itself a composite, at the length scale of interest it can be treated as a homogeneous phase within the asphalt mixture, similar to the assumption made in Chapter III. The micromechanical model also includes the adhesive zones between the aggregates and the FAM as a third independent component, but their material properties are dependent on the physical and mechanical properties of these two materials. The following sections describe the generation of the microstructure model, the materials' constitutive relationships and properties characterizing the three components of the microstructure, and the modeling methodology used for the sensitivity analysis.

Generation of the Microstructure Model

The microstructure model corresponding to the 26.4 mm by 21.2 mm rectangle captured on an asphalt mixture specimen and used in the previous chapter was also used in this study. However, a total of 33 coarse aggregates of different sizes were included in the microstructure. The aggregates were assumed to be embedded in the continuum viscoelastic matrix (FAM). All aggregates finer than 1.18 mm in diameter (i.e., passing sieve #16) were treated as a part of the FAM phase. A 0.4 mm by 0.4 mm grid was used to extract the global coordinates of the vertices characterizing each aggregate. These vertex data were subsequently used to generate the aggregates and the FAM geometry for the finite element model. The geometry of all aggregate

corners with internal angles smaller than 30° were slightly rounded in order to prevent numerical instability issues due to the presence of geometrically distorted elements. During the implementation of the microstructure geometry in finite elements, a thin layer of 0.02 or 0.03 mm thickness was introduced between the aggregates and the FAM to represent the adhesive zones connecting these materials. Figure 4.1 shows the geometry of the asphalt mixture microstructure and the mesh used in the simulations. The average characteristic length of the elements was 0.4 mm for the aggregates, 0.3 mm for the FAM matrix, and 0.1 mm for the interfaces.
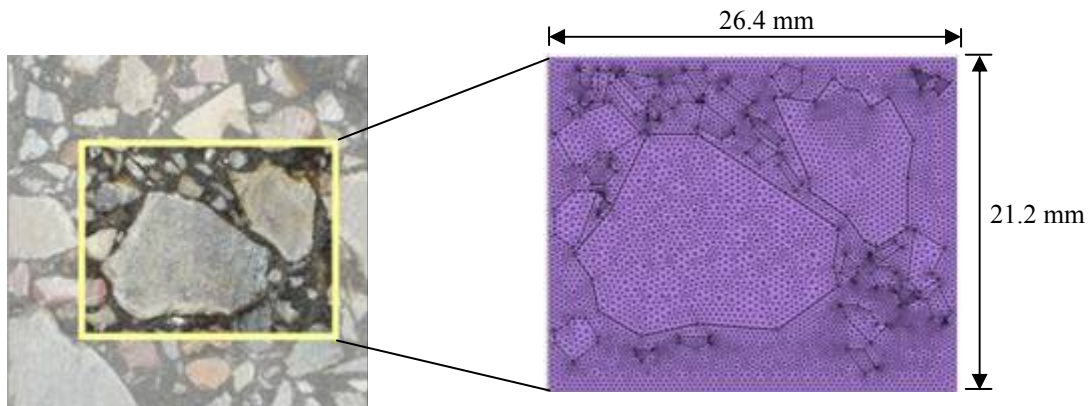
Figure 4.1. Section of the asphalt mixture and its finite element implementation as the microstructure geometry

Material Properties and Models

Mechanical properties representing two types of aggregates and three types of FAM were used in this study. The aggregate or FAM phases were allowed to have different moisture diffusion coefficients. The material properties of aggregates, FAMs, and adhesive zones, as well as the damage models used to describe the moisture-induced deterioration in these materials, are described below.

Moisture Diffusion Coefficients of Aggregates and Matrix

The moisture diffusion coefficients for the aggregates and FAMs were selected based on reported data for rocks and FAMs (Arambula et al. 2009a; Dobchuk et al. 2004; Kassem et al. 2006; Kringos et al. 2008b). Two different diffusion coefficients for the aggregates (D_{AgA} and D_{AgB}) and for the FAM (D_{FAM-A} and D_{FAM-B}) were considered. These diffusion coefficients were assigned to FAM and aggregates irrespective of the mechanical properties of these materials, as shown in Table 4.1. The moisture diffusion coefficients of the adhesive zones were the same as those of the FAM.

Table 4.1. Moisture diffusion coefficients for aggregates and FAM (in mm^2/s)

Aggregates (type 1 or 2)		FAM (type 1, 2 or 3)	
D_{AgA}	D_{AgB}	D_{FAM-A}	D_{FAM-B}
$2.44*10^{-4}$	$1.39*10^{-6}$	$2.78*10^{-5}$	$5.56*10^{-6}$

Mechanical Properties of Aggregates and Matrix

Aggregates were modeled as a linear elastic material while the FAM was modeled as a linear viscoelastic material. The elastic modulus of both aggregates was taken to be $E_{Aggregate}= E_A= 5*104$-MPa, with a Poisson's ratio, ν_A, of 0.4. These properties were assumed to be moisture independent. As explained later, the difference in the mechanical response between the two types of aggregates is determined by the adhesive bond properties that they develop with the asphalt matrix.

In order to analyze the effect of the viscoelastic properties of the first type of FAM (named FAM type 1) correspond to those reported by Kim et al. (2005) and used in the previous chapter. Recalling, these data were collected from relaxation tests on a FAM material at three different temperatures using a dynamic shear rheometer (DSR) and fitted to a Prony series after being converted to the time domain.

In order to analyze the effect of the viscoelastic properties of the bulk matrix in dry condition on moisture induced damage, two hypothetical FAM (types 2 and 3) were generated based on the data published by Kim et al. (2005). FAM type 2 has the same instantaneous and

infinite modulus as Type 1 (G_0 and G_∞ or E_0 and E_∞) but its relaxation time is approximately 50 times longer. FAM types 2 and 3 have the same relaxation time, but the instantaneous modulus of FAM type 3 is 1.8 times than that of FAM types 1 and 2. The Poisson's ratio was 0.4 for the three FAM materials and they were assumed to be time-independent. Table 4.2 summarizes the Prony series parameters for the three viscoelastic matrixes in terms of the shear modulus. Figure 4.2 presents the corresponding shear relaxation modulus vs. time curves that result from using those parameters in Equation 4.1. The instantaneous modulus, G_0, is equal to $4*10^7$ Pa for FAM types 1 and 2, and $7.2*10^7$ Pa for FAM type 3.

$$G(t) = G_0 - \sum_{i=1}^{n} G_i \left[1 - \exp(-t/\tau_i)\right], \text{ and } G_\infty = G_0 - \sum_{i=1}^{n} G_i, \quad (4.1)$$

Table 4.2. Linear viscoelastic properties for the three FAMs under dry condition in terms of a shear relaxation Prony series (Equation 4.1)

	G_i (Pa)		τ_i (1/s)		
i	Types 1 and 2	Type 3	Type 1	Type 2	Type 3
1	$2.61 * 10^7$	$4.70 * 10^7$	$1.57 * 10^{-3}$	$7.86 * 10^{-2}$	$4.37 * 10^{-2}$
2	$9.11 * 10^6$	$1.64 * 10^7$	$1.64 * 10^{-2}$	$8.19 * 10^{-1}$	$4.55 * 10^{-1}$
3	$3.87 * 10^6$	$6.97 * 10^6$	$9.95 * 10^{-2}$	$4.97 * 10^0$	$2.76 * 10^0$
4	$7.42 * 10^5$	$1.34 * 10^6$	$7.36 * 10^{-1}$	$3.68 * 10^1$	$2.04 * 10^1$
5	$1.19 * 10^5$	$2.13 * 10^5$	$6.77 * 10^0$	$3.39 * 10^2$	$1.88 * 10^2$
6	$1.91 * 10^4$	$3.43 * 10^4$	$6.58 * 10^1$	$3.29 * 10^3$	$1.83 * 10^3$
7	$3.01 * 10^3$	$5.43 * 10^3$	$6.43 * 10^2$	$3.22 * 10^4$	$1.79 * 10^4$
8	$4.75 * 10^2$	$8.55 * 10^2$	$6.51 * 10^3$	$3.26 * 10^5$	$1.81 * 10^5$
9	$9.00 * 10^1$	$1.62 * 10^2$	$8.10 * 10^4$	$4.05 * 10^6$	$2.25 * 10^6$

The influence of moisture on FAM properties was accounted for by allowing the relaxation modulus of the bulk matrix to decrease linearly as a function of moisture concentration. This is the same assumption used in the modeling example of Chapter III, and it is based on reported and assumed effects of moisture on the instantaneous relaxation modulus of certain polymer composites (Aiello et al. 2006; Joshi 2008). At any time t, the relaxation

modulus of the FAM changes from its original value calculated using the parameters in Table 4.2—in the absence of water—to 85% of such a value when the material is fully saturated.
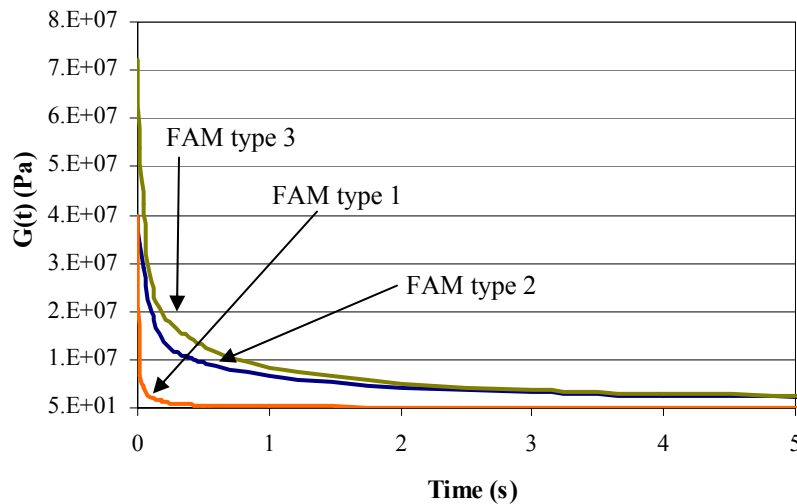
Figure 4.2. Relaxation modulus of the three types of FAM

Properties of Adhesive Zones

The adhesive zones were constructed using the nominal zero-thickness built-in cohesive elements available in Abaqus® (ABAQUS 2007). In this analysis, the linear softening of the elastic stiffness used in the bilinear traction-separation law in Chapter III was replaced by an exponential softening behavior (Figure 4.3), which is believed to provide a better representation of a typical adhesive damage deterioration process. The properties of the adhesive (aggregate-FAM) bonds are functions of the individual physical, chemical, and mechanical properties of the aggregate and FAM materials present at the interface (Hefer et al. 2005). Therefore, as shown in Figure 4.3, parameters of the traction-separation law were assigned such that the mechanical response of an interface—as well as its bond strength and fracture toughness—is unique for each combination of materials.

a)   b)
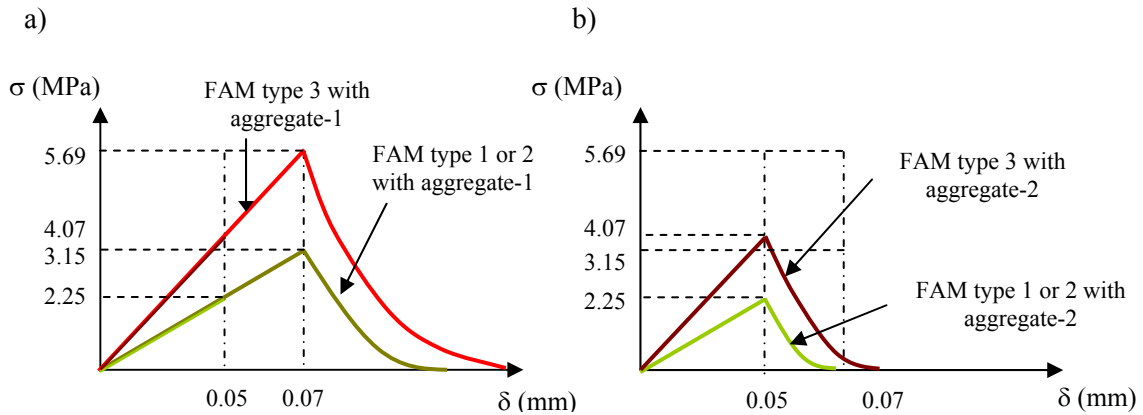
Figure 4.3. Traction-separation laws (opening and shear modes) in dry condition for different combinations of FAM and (a) aggregate-1, and (b) aggregate-2 (σ and δ are the nominal stress and displacement, respectively)

The linear elastic properties of the adhesive zones prior to damage were defined as the average relaxation modulus of the FAM calculated over time. This assumption is used to make the response of the adhesive elements comparable to that of the FAM prior to damage initiation. Hence, elastic stiffness of the interface with FAM type 3 is higher than that with FAM types 1 and 2 (Figure 4.3).

The adhesive zone damage initiation criterion used for this study was the quadratic nominal strain condition (Equation 3.4 in Chapter III). The peak nominal strain values at damage initiation (ε_n^0 and ε_s^0 in Equation 3.4) were made dependent on the aggregate type. The maximum allowable nominal displacement at damage initiation was defined as 0.07 mm (δ_{A1}) for the mixtures containing aggregate-1 (Figure 4.3.a) and 0.05 mm (δ_{A2}) for the mixtures containing aggregate-2 (Figure 4.3.b). As a consequence, mixtures containing aggregate-1 are associated with stronger adhesive bonds than mixtures comprising aggregate-2.

Once damage initiates (when condition δ_{A1} or δ_{A2} is satisfied in Equation 3.4), adhesive fracture at the interface occurs under mixed-mode conditions. The Benzeggagh-Kenane criterion (1996) was used in this analysis to describe the critical fracture energy condition (Equation 3.5). Based on preliminary experimental work on fracture properties of asphalt binder on metal substrates under mode I of failure, it was decided to compute the critical energy released rate for

crack initiation in the pure shear and normal modes (i.e., G^C_I and G^C_{II}) as 10% of the area under the traction-separation curve before damage initiation (Masad et al. 2010).

After damage initiates and the energy is released, the elastic stiffness matrix of the system is reduced by a factor of (1- S), where S is the damage scalar variable described in Chapter III. Recalling, S takes a value of 0 before damage initiation and increases up to 1 when total damage is reached (i.e., crack initiation). In this study, S is computed following an exponential approach as:

$$S = \int_{\delta_m^0}^{\delta_m^f} \frac{\sigma_{n,s}}{G^C - G_0} d\delta , \qquad (4.2)$$

where $\sigma_{n,s}$ is the effective normal or shear stress acting in the adhesive element, δ is the nominal displacement, and G_0 is the cumulative elastic energy in the element when the damage initiation criterion (Equation 3.4) is reached.

A decreasing exponential relationship between the elastic modulus prior to damage initiation and the amount of moisture content at the interface was defined for the adhesive zones. This moisture-dependent relationship results in the strength and fracture toughness of the adhesive bond to be maximum in dry conditions and zero when the interface is fully saturated. In other words, the bond between the aggregates and the bulk matrix is deteriorated, and ultimately broken, by the presence of moisture (even if no load is present). The damage initiation criterion with moisture was kept similar to that used in dry condition for all simulations.

Coupling between Moisture Diffusion and Mechanical Loading

The microstructure model was subjected to two cycles of a mechanical load under different moisture conditions. Moisture was first allowed to diffuse into the samples for 10 days after which a 40-s monotonic load and unload was applied. Moisture continued to diffuse during the mechanical loading and for the following five days. At the end of the 15th day, a second mechanical load—identical to the first one—was applied. Figure 4.4 summarizes the method of subjecting the model to moisture diffusion and mechanical loading. Note that the response of the mixture during the second mechanical loading application will be affected not only by the presence of more diffused moisture within the microstructure but also by the degradation that took place in the material during the first loading application.
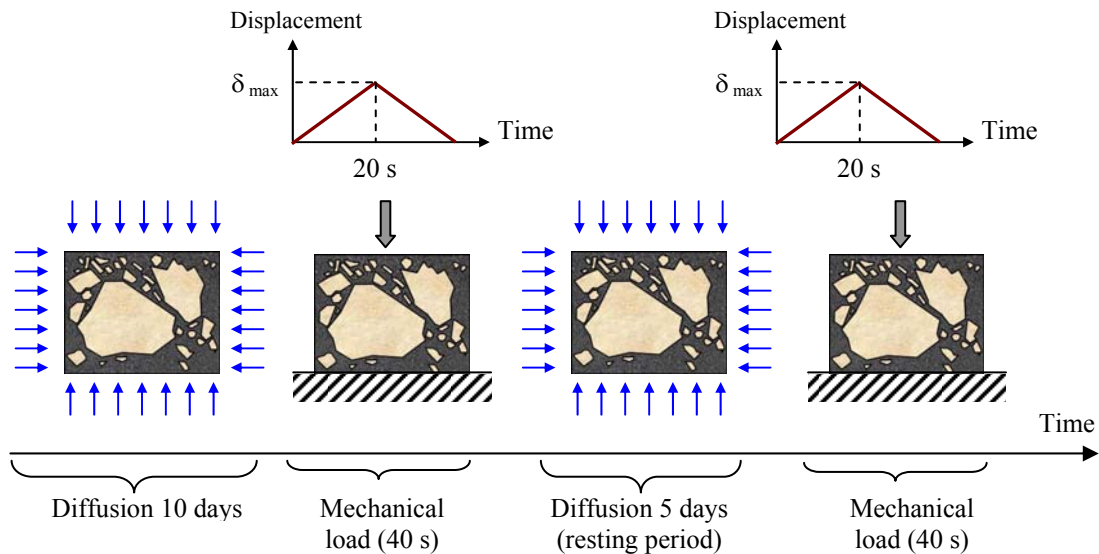
Figure 4.4. Moisture diffusion and mechanical loading applied to the asphalt mixture microstructure
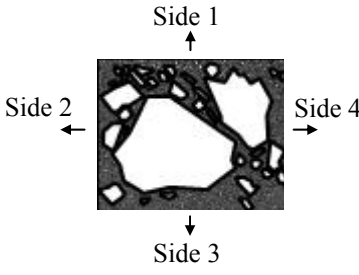
As explained in Chapter III, the two-step sequentially coupled methodology in Abaqus® is used to model the coupling (interrelated effects) between moisture diffusion and mechanical loading. During the finite element simulation of moisture diffusion only, the materials were modeled as first order finite elements with 3-node for the aggregates and the FAM (type DC2D4 in Abaqus®), and 4-node for the interfaces (type DC2D3 in Abaqus®). The finite element simulations during the application of mechanical loading were conducted by using 3-node first order mechanical-based elements (CPE3 in Abaqus®) to represent aggregates and FAM, while the interfaces were modeled using rectangular zero-thickness first order cohesive elements (type COH2D4 in Abaqus®). A small factor of $1*10^{-5}$ viscous regularization was assigned to the adhesive elements in order to promote numerical stability (refer to Chapter III for more details on this topic).

Moisture Diffusion Model and Boundary Conditions

Moisture diffusion was modeled using Fick's second law. At any time, moisture gradients continuously vary within an asphalt mixture layer due to variations in the natural external conditions. In order to simulate the effect of such different boundary conditions, the same asphalt

mixture model was subjected to five different moisture gradients. Each gradient can be thought of as representing a different spatial location within the same asphalt mixture layer. Table 4.3 presents the five different moisture gradients that were used to generate moisture diffusion profiles within the microstructure. The moisture diffusion boundary conditions were used to create a relative humidity gradient that drives moisture diffusion through the FAM for the whole duration of the simulation. The normalized moisture concentration used for the boundary conditions corresponds to the moisture content of the material divided by the saturation moisture content of the FAM.

Table 4.3. Boundary conditions for different moisture gradients applied to the same asphalt mixture

	Boundary Conditions (normalized moisture concentration)			
Moisture gradient	Side 1	Side 2	Side 3	Side 4
A	1.0	None	None	None
B	1.0	None	1.0	None
C	1.0	None	0.4	None
D	1.0	From 0 (top) to 0.4 (bottom)	0.4	From 0 (top) to 0.4 (bottom)
E	1.0	1.0	None	1.0

Parametric Analysis of Moisture-Induced Damage

The roles of the different physical and mechanical properties of aggregates, FAM and aggregate-FAM interfaces were studied by evaluating the response of the asphalt composite with different material properties subjected to the coupled environmental and loading conditions illustrated in Figure 4.4. The significance of external loading conditions was also explored by subjecting the model to five different magnitudes and loading rates.

Material Combinations

The effect of different combinations of aggregates and FAM on the generation of damage was studied by creating 24 different cases. These cases comprise all possible combinations of two aggregates, three types of FAM, two different FAM-aggregate interface properties, and two different moisture diffusion coefficients. As an example, Table 4.4 presents the material properties of the eight possible mixtures that can be constructed using FAM type 1. Note that the properties of the interface fully depend on the aggregate-FAM combination used for the mixture (Figure 4.3). Similar combinations were produced using FAM types 2 and 3. In order to isolate the effect of loading rate and external environmental conditions, all combinations were subjected to the same displacement rate (0.035 mm/s) and moisture boundary conditions (moisture gradient *D* in Table 4.3).

Table 4.4. Possible mixture combinations containing FAM type 1

	FAM		Aggregate		Interfaces	
Mixture	Physical	Mechanical	Physical	Mechanical	Physical	Mechanical
1	$D_{\text{FAM-A}}$	Type 1	D_{AgA}	Aggregate-1	$E_{\text{Type1}}^{(1)}$	δ_{A1}=0.07 mm
2	$D_{\text{FAM-A}}$	Type 1	D_{AgB}	Aggregate-1	E_{Type1}	δ_{A1}=0.07 mm
3	$D_{\text{FAM-A}}$	Type 1	D_{AgA}	Aggregate-2	E_{Type1}	δ_{A2}=0.05 mm
4	$D_{\text{FAM-A}}$	Type 1	D_{AgB}	Aggregate-2	E_{Type1}	δ_{A2}=0.05 mm
5	$D_{\text{FAM-B}}$	Type 1	D_{AgA}	Aggregate-1	E_{Type1}	δ_{A1}=0.07 mm
6	$D_{\text{FAM-B}}$	Type 1	D_{AgB}	Aggregate-1	E_{Type1}	δ_{A1}=0.07 mm
7	$D_{\text{FAM-B}}$	Type 1	D_{AgA}	Aggregate-2	E_{Type1}	δ_{A2}=0.05 mm
8	$D_{\text{FAM-B}}$	Type 1	D_{AgB}	Aggregate-2	E_{Type1}	δ_{A2}=0.05 mm

(1) E_{Type1} represents the elastic modulus defining the response of the adhesive elements before damage initiation. This value depends on the type of FAM material that is being used. For mixtures containing FAM type 2 or 3, E_{Type2} or E_{Type3} are used. $E_{\text{Type1}} = E_{\text{Type2}} = 45.0$ Pa, and $E_{\text{Type3}} = 81.3 *10^7$ Pa.

Loading Rates

Asphalt mixtures are viscoelastic materials and, as such, their mechanical response is a function of the rate of load application. The effect of displacement rates on the development of moisture-

assisted damage was explored by applying five different displacements rates, 1.00, 0.075, 0.05, 0.035, and 0.025 mm/s, to the mixture composed of aggregate-1 and FAM type 1 with moisture diffusion coefficients of D_{AgA} and D_{FAM-A}, respectively. These mixtures were subjected to the boundary conditions specified for moisture gradient A in Table 4.3 .

Results and Discussion

Figure 4.5 presents the change of the moisture profile and the mechanical deformation and adhesive fracture of two mixtures containing aggregate-1 with D_{AgA} and FAM type 1 with D_{FAM-A} (part a) or D_{FAM-B} (part b) for the boundary conditions corresponding to a moisture gradient D (Table 4.3). The moisture profiles presented in this figure represent the four stages of the modeling sequence (Figure 4.4); that is, the two diffusion periods (10 and 15 days) and the two mechanical loading applications.
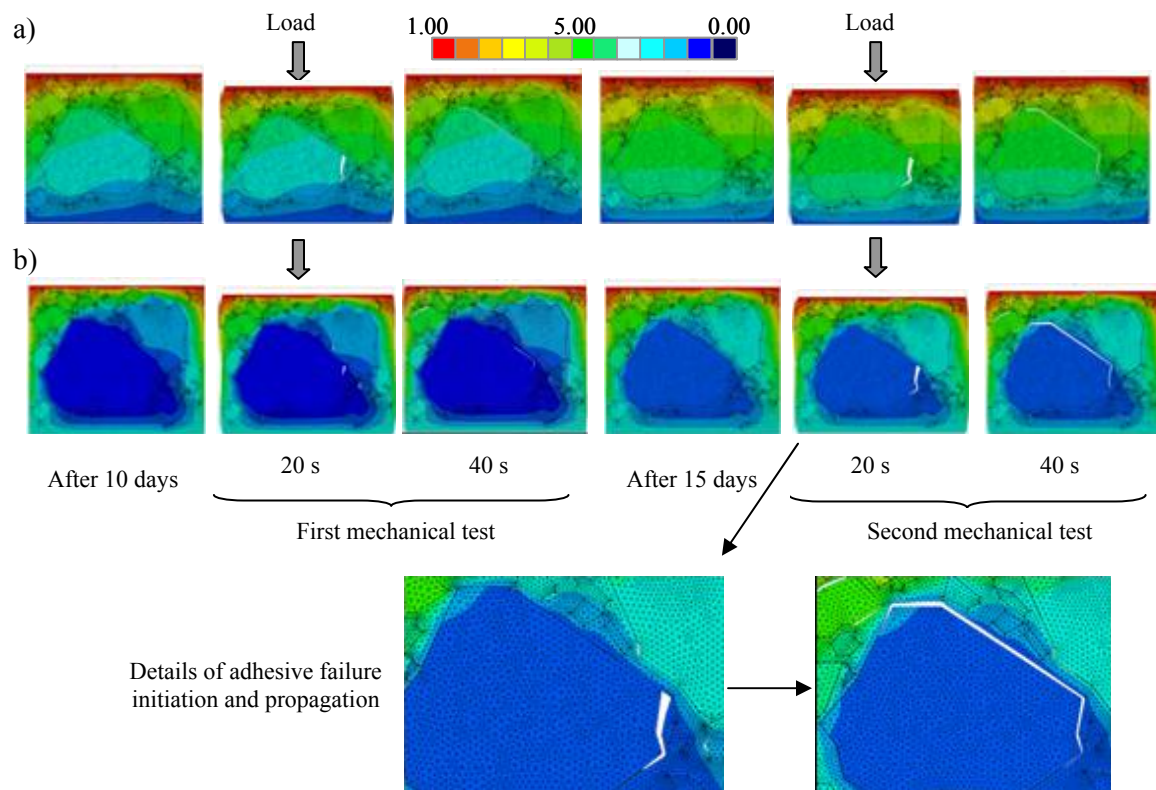
Figure 4.5. Normalized moisture content profiles through time within a sample containing FAM type 1 and aggregate-1 with moisture coefficients of (a) D_{FAM-A} and D_{AgA} (b) D_{FAM-B} and D_{AgA}

Figure 4.6. depicts the increase in moisture content for a specific node within the FAM for different material combinations. The effect of the moisture diffusion coefficients—especially that of the FAM—is clearly exemplified in both figures. It is observed that at a fixed time, samples containing bulk matrices and aggregates with larger diffusion coefficients (D_{FAM-A} and D_{AgA}) will consistently hold more moisture and, as a result, their mechanical properties will decrease more and faster during the mechanical tests. In fact, the model containing FAM type 1 (with D_{FAM-A}) and aggregate-2 (with D_{AgA}) is expected to be the most prone to damage, as it does not only produce the most aggressive moisture profiles, but, based on its mechanical properties (Table 4.4), it also contains the materials with the lowest structural capacity.
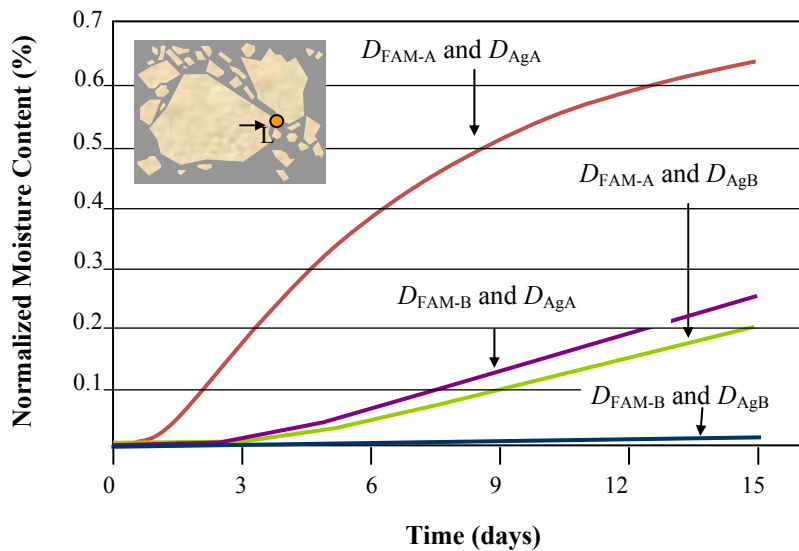
Figure 4.6. Moisture content at a point of the FAM during the 15 days of the simulation for samples with different physical material properties combinations subjected to moisture gradient D (Table 4.3)

Due to the effect of moisture on the mechanical material properties of the FAM and the FAM-aggregate interfaces, a mixture with poor resistance to moisture-induced damage will require less force to reach the constant applied displacement as compared to a mixture with high resistance to moisture-induced damage. In other words, larger values of the maximum total force

experienced by the mixture composite during the mechanical load application are associated with materials with higher stiffness. For a given mixture, the percentage reduction of the maximum force resisted by moisture-conditioned specimens with respect to that in dry condition can be considered as a measurement of the deleterious effect of moisture on the structural capacity of the mixture. Therefore, this parameter was selected to evaluate susceptibility of the mixtures to experience moisture-induced damage as a function of its material properties.

Table 4.5 and Table 4.6 present the maximum force resisted by the samples containing the 24 material combinations selected during the first and second mechanical applications. The table also contains the percent of reduction of the maximum total force sustained by the mixtures in the absence of moisture with respect to the cases where moisture has diffused.

Table 4.5. Maximum total force resisted by mixtures containing aggregate-1 during the two mechanical load cycles and reduction in the maximum total force from the dry to the moisture-conditioned cases (force in N)

	Aggregate-1								
	First mechanical load application								
	Dry	$D_{\text{FAM-A}}$ and D_{AgA}		$D_{\text{FAM-A}}$ and D_{AgB}		$D_{\text{FAM-B}}$ and D_{AgA}		$D_{\text{FAM-B}}$ and D_{AgB}	
FAM	Max. Force	Max. Force	% red.[1]	Max. Force	% red.	Max. Force	% red.	Max. Force	% red.
Type 1	7.70	3.46	55	4.92	36	5.53	28	6.42	17
Type 2	49.11	17.89	64	31.08	37	37.34	24	44.24	10
Type 3	67.85	24.35	64	46.51	31	51.75	24	60.66	11
	Second mechanical load application								
		$D_{\text{FAM-A}}$ and D_{AgA}		$D_{\text{FAM-A}}$ and D_{AgB}		$D_{\text{FAM-B}}$ and D_{AgA}		$D_{\text{FAM-B}}$ and D_{AgB}	
FAM		Max. Force	% red.[1]	Max. Force	% red.	Max. Force	% red.	Max. Force	% red.
Type 1		3.00	61	4.49	42	5.00	35	6.07	21
Type 2		17.33	65	19.49	60	29.02	41	41.54	15
Type 3		21.92	68	33.60	50	44.80	34	58.19	14

(1) % red. is the reduction in the maximum total force resisted by the moisture-conditioned mixtures with respect to that resisted by the same mixture but in dry conditions.

Table 4.6. Maximum total force resisted by mixtures containing aggregate-2 during the two mechanical load cycles and reduction in the maximum total force from the dry to the moisture-conditioned cases (force in N)

FAM	**Aggregate-2**								
	First mechanical load application								
	Dry	$D_{\text{FAM-A}}$ and D_{AgA}		$D_{\text{FAM-A}}$ and D_{AgB}		$D_{\text{FAM-B}}$ and D_{AgA}		$D_{\text{FAM-B}}$ and D_{AgB}	
	Max. Force	Max. Force	% red.[1]	Max. Force	% red.	Max. Force	% red.	Max. Force	% red.
Type 1	7.65	3.04	60	4.73	38	5.35	30	6.385	17
Type 2	46.12	17.52	62	24.09	48	34.65	25	37.786	18
Type 3	62.88	22.22	65	36.53	42	45.76	27	55.452	12
	Second mechanical load application								
		$D_{\text{FAM-A}}$ and D_{AgA}		$D_{\text{FAM-A}}$ and D_{AgB}		$D_{\text{FAM-B}}$ and D_{AgA}		$D_{\text{FAM-B}}$ and D_{AgB}	
FAM		Max. Force	% red.[1]	Max. Force	% red.	Max. Force	% red.	Max. Force	% red.
Type 1		2.26	70	4.20	45	4.51	41	5.92	23
Type 2		16.97	63	18.62	60	25.76	44	24.41	47
Type 3		21.45	66	23.68	62	31.46	50	48.36	23

(1) % red. is the reduction in the maximum total force resisted by the moisture-conditioned mixtures with respect to that resisted by the same mixture but in dry conditions.

Data in Table 4.5 and Table 4.6 were extracted from the mechanical responses (i.e., force vs. time curves) of the mixtures for the two load applications. Figure 4.7 presents some of these responses for a mixture containing FAM type 2 and different aggregates with different combinations of moisture diffusion coefficients (Table 4.1). Several observations can be extracted in terms of the structural quality of the mixtures—in both dry and moist environments—and in relation to the role of the physical and mechanical properties of the individual materials and loading conditions in the susceptibility of the mixtures to undergo damage. These observations are summarized in the following sections.
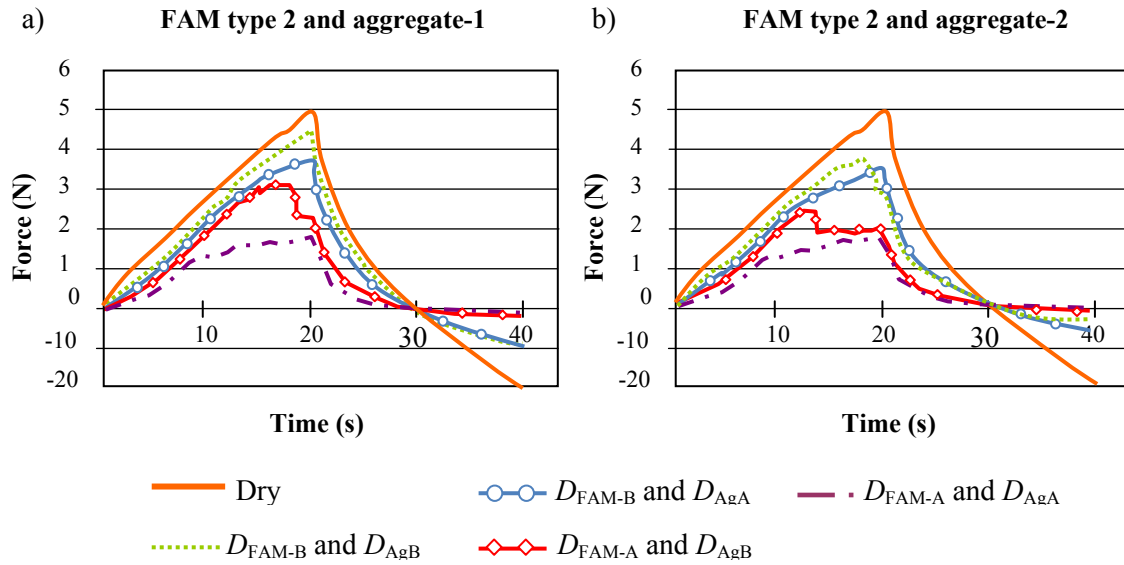
Figure 4.7. Force vs. time curves from a mixture comprised of FAM type 2 and (a) aggregate-1 and (b) aggregate 2, for the four possible moisture profiles generated using an external moisture gradient type D (Table 4.3)

Role of Mechanical Material Properties in Dry Condition

As shown in Table 4.5 and 4.6, the data from response of the samples in dry condition shows that the mixtures containing FAM type 3 and either of the two aggregates had a better mechanical response than the mixtures containing FAM type 1. This is expected because the later has 1.8 times smaller instantaneous modulus and a relaxation time approximately 50 times shorter than FAM type 3 and it is more susceptible to mechanical damage. The effect of the type of interfacial adhesion between the FAM and aggregate in dry condition is also observed in the performance of the mixtures. As discussed earlier, aggregate-1 was assigned stronger interfacial bonds with the FAMs as compared to aggregate 2. Consequently, the maximum force of resistance was always greater in mixtures containing any type of FAM and aggregate-1 than in mixtures containing the same type of FAM but with aggregate-2 (e.g., 49.1 N for a mixture with FAM type 1 and aggregate-1 compared to 46.1 N for a mixture with FAM type 1 and aggregate-2).

Role of Mechanical Material Properties under Moist Conditions

The overall structural performance of the models undergoing moisture diffusion is fully dependent on the mechanical properties of the individual materials. Similar to what was observed in the dry case, under moist conditions, mixtures containing FAM type 1 always experienced small values of maximum total resisted forces, followed by mixtures with FAM types 2 and 3. The percent of reduction of the total maximum force caused by the presence of moisture (35.1% on average) indicates that all mixtures were highly susceptible to the combined deterioration caused by moisture.

For the case of the aggregates, it was observed that all mixtures containing aggregates associated with more resistant adhesive bonds (i.e., aggregate-1) were less susceptible to moisture-induced damage. The average reduction in maximum force due to moisture in mixtures with aggregate-1 was 33% (Table 4.5) compared to 36% for mixtures containing aggregate-2 (Table 4.6).

Role of Moisture Diffusion Coefficients in the Development of Damage

The data corresponding to the microstructures subjected to moisture diffusion suggest that the diffusion coefficient of the FAM is the most relevant parameter influencing moisture damage. Mixtures containing FAMs with the highest diffusion coefficient (i.e., D_{FAM-A}) presented, with no exception, the highest drop in mechanical responses and the highest susceptibility to moisture damage. In fact, the data show that the reduction of the maximum force of resistance of mixtures containing D_{FAM-A} ($2.78*10^{-5}$ mm^2/s) with respect to the dry cases was between 1.9 and 3.7 times larger than similar reductions on those mixtures containing D_{FMA-B} ($5.56*10^{-6}$ mm^2/s).

Although not as significant as the diffusivity of the FAM, it was found that the moisture diffusion coefficient of the aggregates also plays an important role in the development of damage. The average reduction of the structural resistance due to the presence of water was 44% in mixtures containing aggregates with a moisture diffusion coefficient of D_{AgA} ($2.44*10^{-4}$ mm^2/s) while the same average reduction was 26% in those mixtures containing aggregates with a two orders of magnitude smaller moisture diffusion coefficient (i.e., $D_{AgB} = 1.39*10^{-6}$ mm^2/s).

Effect of Repeated Loading and Rate of Loading

The data show that the maximum total forces experienced by the mixtures during the second loading application were 16% smaller than those corresponding to the first load application. Furthermore, the average reduction of the maximum total force with respect to the dry cases during the second loading cycle was approximately 44%. This value is 30% larger than the reduction observed during the first loading application, and it reflects the degradation that has taken place in the microstructure due to the first mechanical cycle and the development of more aggressive moisture profiles within the materials.

Figure 4.8 presents the overall force vs. displacement and force vs. time response as a function of rate of loading for a mixture comprising aggregate-1 and FAM type 1 with D_{AgA} and D_{FAM-A}, respectively. These results were obtained for the first mechanical application under five different displacement rates (moisture gradient A, Table 4.3).
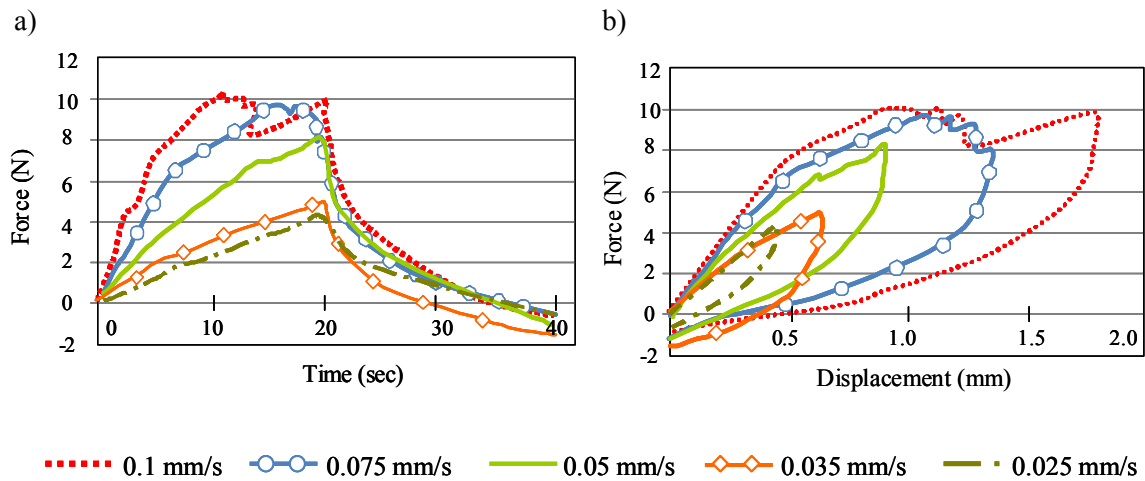
Figure 4.8. (a) Force vs. displacement, and (b) net force vs. displacement for a mixture of aggregate-1 and FAM type 1 subjected to a displacement-controlled test at five different loading rates under a moisture gradient type A (Table 4.3)

As expected for a viscoelastic composite, tests conducted at higher displacement rates produced considerably higher forces. In fact, the overall force resisted by the system during the mechanical simulation and the total dissipated energy by the mixtures (i.e., area within the force

vs. displacement curves in Figure 4.8.b) increased by 3 and 17 times, respectively, when the model was subjected to the 0.1 mm/s rate than when subjected to a 0.025 mm/s rate. The fluctuations observed in the curves in Figure 4.8 for the three larger displacement rates (0.05, 0.075, and 0.1 mm/s) result from the adhesive failure processes taking place within the microstructure. It is important to note that the influence of loading rate on the model is due to the use of a viscoelatic model to represent the FAM. This influence is expected to be even more pronounced if a viscoelastic CZM with time dependency was used instead of the elastic CZM model to represent the aggregate-FAM bond.

Influence of Moisture Gradients

The influence of applying different moisture gradients (Table 4.3) was examined by evaluating the response of one node in the bulk matrix in a mixture composed by FAM type 1 with $D_{\text{FAM-A}}$ and aggregate-1 with D_{AgA}. Figure 4.9 presents the increase in moisture concentration at this node.
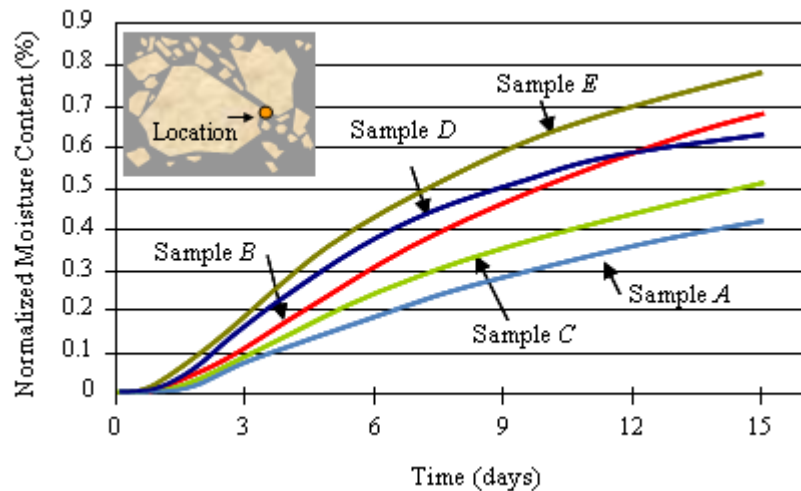
Figure 4.9. Moisture content increment through time in a fixed point of the matrix bulk for samples containing FAM with $D_{\text{FAM-A}}$ and aggregate-1 with D_{AgA}, subjected to different moist environments (Table 4.3)

Based on the data from Figure 4.9—and due to the coupling capabilities of the model— the mechanical properties of cases E and D will decrease rapidly, promoting the development of

damage during a loading application, while the variation in the mechanical properties of the mixture subjected to moisture gradients *A, B*, and *C* will be smaller, preserving the structural resistance of the material.

The percentage reduction in the total maximum force with respect to the dry condition for the five cases herein considered show that, on average, the presence of diffused moisture caused a 50% reduction in the maximum force resisted by the composite (Table 4.7). This reduction is attributed to the combined effect of cohesive weakening of the matrix (which is limited to 15% reduction in the matrix relaxation modulus) and adhesive damage. Since all samples are composed of the same materials, the differences observed in their mechanical responses are exclusively due to the existence of different moisture gradient conditions. In fact, the data in Table 4.7 show that the sole presence of different moisture gradients can decrease the maximum force of resistance of an asphalt mixture model in a range of 19% to 70%.

Table 4.7. Total maximum resisted force and reduction of maximum resisted force with respect to the dry case. Samples with FAM type 1 (with $D_{\text{FAM-A}}$) and aggregate-1 (with D_{AgA})

		Moisture Gradient (Table 4.3)				
	Dry	*A*	*B*	*C*	*D*	*E*
Maximum force response (N)	7.70	4.85	3.53	4.29	3.46	2.94
% reduction with respect to dry		37.1	54.2	44.3	55.0	63.1

Summary and Conclusions

The coupled micromechanical model of moisture-induced damage in asphalt mixtures introduced in Chapter III was used to conduct a parametric study on the effect of material properties on moisture-induced damage. Microstructures containing different physical and mechanical material properties in the two phases (i.e., aggregates and FAM) were subjected to the same environmental and loading conditions. The maximum forces resisted by the microstructure under dry and wet conditions were used to evaluate the influence of those properties on the susceptibility of the mixtures to undergo moisture-related deterioration processes. The effect of moisture gradient and loading rate was also studied using the same evaluation parameters.

The results from the simulations suggest that the physical properties of the materials (i.e., the moisture diffusion coefficients) play a crucial role in the development of damage. It was demonstrated, with no exception, that samples subjected to more aggressive moisture profiles had poorer performance and experienced more damage. A difference of one order of magnitude in the diffusivity of the FAM of the mixture reduced the maximum force experienced by the mixture at a given displacement by up to 3.7 times compared to a similar dry mix. A difference of two orders of magnitude in the diffusivity of the aggregates reduced the maximum force of resistance of the mixtures from 1.2 to almost 2 times in comparison with similar dry mixes. The results also suggest that under the same moisture-gradient and loading rate conditions, the reduction in the mechanical resistance of asphalt mixtures producing stronger adhesive bonds are 14% less than those containing less-resistant adhesive bonds.

CHAPTER V

EFFECT OF THE INTERNAL VOID STRUCTURE ON THE MECHANICAL PERFORMANCE OF ASPHALT MIXTURES SUBJECTED TO MOISTURE DIFFUSION PROCESSES

The internal air void structure of asphalt mixtures plays an important role in influencing the durability of these materials. Voids are recognized as the main access route of air and moisture to permeate to the interior of the mixtures' microstructure. The presence of air within the composite affects the durability of the mixture by promoting oxidation of the asphalt binder. The presence of moisture within the microstructure gradually degrades the structural integrity of the material, as demonstrated in Chapter II of this dissertation.

This chapter focuses on studying the effect of air voids on the mechanical performance of asphalt mixtures that are subjected to the combined action of moisture diffusion and mechanical loading. The analysis was conducted by means of the micromechanical model introduced in Chapter III. Two different approaches were used to treat the air phase of the mixtures within the asphalt microstructure. The first approach relied on explicitly including the air voids as a separate phase of the model. In order to do so, a volumetric distribution of air void sizes measured using X-ray CT in a dense-graded asphalt mixture was used to randomly generate different air void structures. In the second approach, the effect of air void variability and distribution was indirectly included in the model by using a stochastic modeling technique based on random field theory. This theory was used to generate physical and mechanical properties of the bulk asphalt matrix (FAM) that were assumed dependent on probable air void distributions. In both approaches, the total energy dissipated by the microstructure and the stiffness of the mixture that result from simulating moisture diffusion and applying mechanical loading by means of the numerical model developed in Chapter III were used to evaluate their mechanical performance.

Information regarding the mechanical performance of asphalt mixtures containing different air void percentages can be used, among other things, to evaluate the impact of the placement and compaction processes of the mixtures in the field. For example, poor compaction techniques during construction are associated with high spatial air void variability within the asphalt course, which in turn increases the variability of the expected mechanical performance of the material. The methodologies presented in this chapter can help to gain understanding about

the impact of such variability on the durability and expected service life of the pavement. This information could also be used as input in designing inspection and maintenance programs.

This chapter includes two main parts. Each part deals with one of the afore mentioned modeling approaches for accounting for the influence of air void distribution. The characteristics of the geometry of the model, the material properties of the components of the microstructure, the probabilistic and stochastic models used to incorporate the effect of the air voids on the mechanical performance of the mixture, the mechanical modeling methodology, and the results obtained from both approaches are described in the subsequent sections.

Objectives

The objectives of this chapter are:

- study the influence of the air void phase variability and distribution on the mechanical performance of asphalt mixtures subjected to moisture diffusion, and

- analyze the advantages and shortcomings of two different probabilistic-based approaches to include the effects of air voids in the evaluation of the moisture susceptibility of asphalt mixtures.

Role of the Internal Void Structure on Moisture Damage of Asphalt Mixtures

The relationship between the internal air void structure of the mixtures and the different modes of moisture transport has been a topic of great interest when identifying the factors that determine the moisture susceptibility of asphalt mixtures (Caro et al. 2008a). Chapter II of this dissertation explains in detail the relationship among the internal air void structure of asphalt mixtures, the modes of moisture transport, and the susceptibility of this material to moisture damage. A summary of such a relationship is discussed in this chapter for completeness.

Voids have been recognized as the main route of air and moisture access to the microstructure of the mixtures (Brown et al. 2004). While the access of air is directly related to oxidation processes that chemically degrade the integrity of asphalt binder, the ability of moisture to penetrate the microstructure is the indispensable requirement for the initiation of moisture-induced deterioration. Moisture can permeate the internal structure of asphalt mixtures by three different modes: 1) water infiltration, 2) moisture diffusion, and 3) capillary rise (Masad

et al. 2007b). Although the relationship between the total amount of air voids and the different modes of moisture transport is well recognized, the relationship between the internal air void structure of a mixture and its moisture sensitivity is neither simple nor evident. For example, Terrel and Al-Swailmi (1994) suggested that there is not a direct relationship between the amount of air voids within a mixture and moisture damage. The authors presented experimental evidence to indicate that there seems to be a specific value of total air void content that maximizes the susceptibility of a mixture to moisture damage. This value was referred to as the "pessimum" air void content, and the experimental results suggested that it is between 5 and 10 %, which is the typical range of air void content for dense-graded mixtures in the field.

More recently, X-ray CT has been used in combination with image analysis techniques to provide a better characterization of the internal air void structure of asphalt mixtures (Castelblanco 2004; Masad et al. 2007b; Masad et al. 2006b; Masad et al. 2002). Among others, this approach has been applied to determine the probabilistic distribution of air void sizes (Masad et al. 2006b), relate the air void size distribution to the susceptibility of the mixtures to moisture damage (Masad et al. 2006b), and demonstrate the existence of capillary rise as an alternative source of moisture transport within asphalt mixtures (Masad et al. 2007b). In general, these studies have shown that the internal void structure of asphalt mixtures is highly complex and that the classical use of the total air void content might be insufficient to fully characterize it. Information regarding the air void location, size distribution, and connectivity is critical to determine the susceptibility of asphalt mixtures to moisture damage.

Despite the importance of the air void phase in determining the performance of asphalt mixtures, in the majority of the micromechanical modeling works conducted to simulate damage processes in these materials, including moisture damage, the characteristics of the variability and distribution of the air void phase is overlooked. However, a comprehensive characterization of deterioration processes in asphalt mixtures, especially those where the presence of moisture is important, should take into consideration the characteristics of the air void structure.

There exists two common ways of including the air void phase in the numerical modeling of asphalt mixtures at the microscale level: 1) as part of the viscoelastic bulk matrix, FAM, or, 2) as an independent entity (i.e., a separate phase). The first possibility is the easiest and most frequent way of dealing with the air void phase. In this case, the FAM is modeled as a continuum with effective material properties that result from the characteristics of its constitutive components (Caro et al. 2009; Kim et al. 2005). Thus, the air void phase is assumed to be

uniformly distributed within the bulk matrix and the characteristics of the internal air void structure and its variability within the matrix are neglected. The second possibility is the most desirable approach since it is a better representation of an actual mixture.

The first part of this chapter follows the second approach, i.e., a direct addition of the air void phase within the microstructure of the mixture. Sets of air voids with different sizes, each one satisfying a pre-defined total percentage of air voids, were obtained from realizations of a probabilistic distribution of air void sizes obtained by means of X-ray CT in a dense-graded asphalt mixture. The air void phase was assigned its own moisture diffusion coefficient and was treated as a zero-resistance material during the mechanical simulation.

The second part of this chapter introduces a new methodology to include the effect of the air void phase on the micromechanical response of asphalt mixtures. This approach consists of dividing the bulk matrix (FAM) of the microstructure into different sections. Each subsection is treated as a continuum and assigned its own material properties. The effect of the air phase is indirectly accounted for by making the material properties of each section of the FAM a function of probable internal air void structures of the mixture that are obtained by means of a stochastic modeling technique. The main advantage of this approach is that while its numerical implementation is simpler than the explicit inclusion of the voids within the microstructure, it does not ignore the characteristics of the internal air void distribution.

Details about microstructure geometry, material properties, and the application of the modeling approaches are described in the following sections.

Coupled Micromechanical Model

The coupled micromechanical model of moisture-induced damage described in Chapter III was used to conduct the analyses previously described. Recalling, the finite element model couples the effect of diffused moisture on the mechanical response of the asphalt mixtures by: 1) simulating cohesive degradation of the asphalt matrix, and 2) simulating adhesive degradation and fracture of the aggregate-asphalt matrix interfaces (i.e., adhesive zones). Both processes are achieved by making the viscoelastic material properties of the FAM and the mechanical properties of the adhesive bonds dependent on the amount of moisture within the finite elements.

The traction-separation law selected for the adhesive zones is the same as the one used in the parametric analysis of Chapter IV (Figure 5.1). Recalling from Chapter III, σ_n and σ_s in

this Figure 5.1 correspond to the nominal normal and shear stresses, ε_n and ε_s are the nominal normal and shear strains (i.e., relative displacement, δ, divided by the thickness of the adhesive layer), K_{nn} and K_{ss} are the components of the elastic stiffness matrix, and ε^0_n and ε^0_s are the peak values of the nominal strains at which separation processes initiate. Besides, G^C_n and G^C_s correspond to the normal and shear critical energy released rates, G^C represents the overall critical energy released rate of the mixed-mode condition, and the brackets in the first term of the damage initiation criterion symbolize the Macaulay condition (i.e., pure compression conditions do not produce damage). Similar to assumptions made in the previous chapters, the fracture properties of the adhesive zones were supposed to be isotropic (i.e., the traction-separation law was the same for the opening and shear modes). The parameters of the traction-separation law are described later in this chapter.

Linear Elastic: $\begin{pmatrix} \sigma_n \\ \sigma_s \end{pmatrix} = \begin{bmatrix} K_{nn} & 0 \\ 0 & K_{ss} \end{bmatrix} \begin{pmatrix} \varepsilon_n \\ \varepsilon_s \end{pmatrix}$

Damage initiation criterion:

Quadratic nominal strain condition $\left.\right\} \left(\dfrac{\langle \varepsilon_n \rangle}{\varepsilon^0_n} \right)^2 + \left(\dfrac{\varepsilon_s}{\varepsilon^0_s} \right)^2 = 1$

Released energy according to G_c $\qquad G^c = G^C_n = G^C_s$
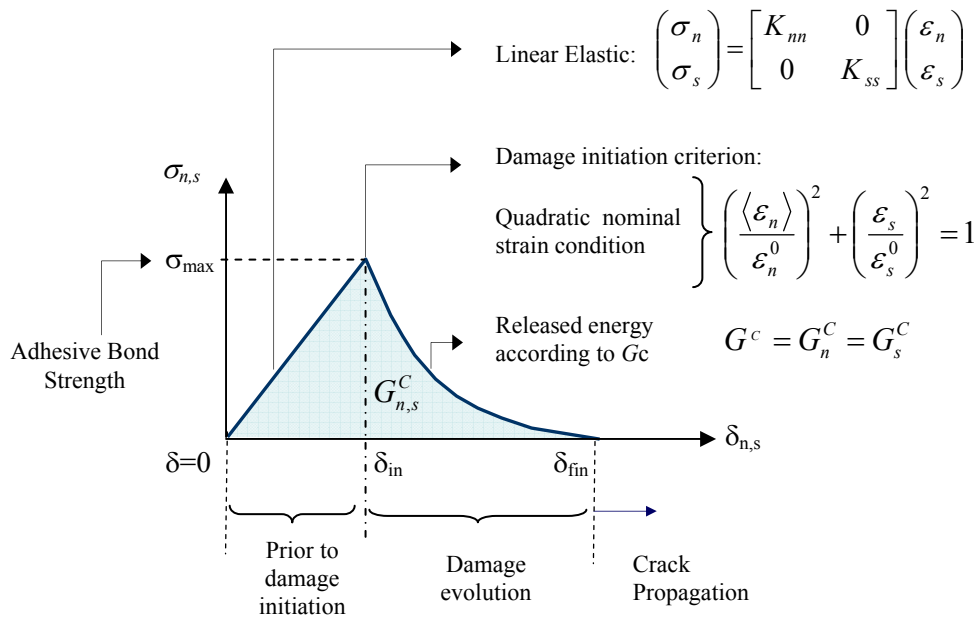
Figure 5.1. Traction-separation law characterizing the mechanical response of the adhesive zones (for modes I and II of failure)

The application of this model to study the role of air voids in the asphalt mixture sensitivity to moisture-induced damage includes three components:

- definition of the geometry of the microstructure model,
- probabilistic generation of the internal air void distribution within the microstructure,
- determination of the material properties of the constitutive phases, and
- determination of the modeling methodology.

The first component includes: 1) the definition of an appropriate size for a two dimensional cross-section of the microstructure of an asphalt mixture, 2) the geometry and location of the aggregates and FAM phases within this cross-section, and 3) addition of the air void structure into the microstructure. The second component includes the physical and mechanical properties of the microstructure components and the designation of their moisture-dependent characteristics. The last component includes the definition of the environmental and mechanical conditions applied to the microstructure model (i.e., magnitudes and boundary conditions), and their finite element implementation. Each of these components is described in the following sections.

Geometry of the Microstructure Model

Determination of a Representative Volume Element (RVE)

A fundamental requirement of micromechanical modeling techniques is to have a microstructure geometry that provides a proper representation of the overall performance of the material. The smallest size of a microscopic sample that properly represents the macroscopic response of a composite is referred to as the Representative Volume Element (RVE).

Several works have been conducted to identify the RVE of asphalt mixtures (Chehab et al. 2000; Kim et al. 2009; Romero and Masad 2001). These studies have concluded that the RVE is highly dependent on the maximum aggregate size present in the mixture. Kim et al. (2009) investigated the appropriate RVE of asphalt mixtures that are not subjected to significant levels of damage and/or deformation. The authors studied the role of different geometrical factors, such as gradation and orientation of aggregate particles, in influencing the RVE. They also compared results from finite element simulations to experimental data in order arrive at the RVEs for different asphalt mixtures. The results from those analyses suggested that a 50 mm by 50 mm

RVE was appropriate to characterize typical dense-graded Superpave mixtures. The authors also emphasized that larger RVEs are required when characterizing the response of mixtures subjected to large deformations or high levels of damage that can promote the generation of diverse heterogeneities.

In Chapters III and IV, microstructures of 26 mm by 22 mm were assumed to be suitable RVE sizes of an asphalt mixture. However, based on the information reported by Kim et al. (2009), it was decided to increase the size of the microstructure sample. Thus, a 50 mm by 50 mm microstructure model was selected for this study.

Characteristics of the Microstructure Model

Figure 5.2 illustrates the geometry of the 50 mm by 50 mm RVE of an asphalt mixture. This RVE corresponds to the cross-section of a Superpave dense-graded asphalt mixture and it contains a total of 241 coarse aggregates (i.e., particles with diameter larger than 0.42 mm) that constitutes 49.4% of the total microstructure. The right-hand side of Figure 5.2 presents a detail of the finite element implementation of the microstructure. Information about the area of each aggregate was used to duplicate the aggregate gradation of the mixture (Figure 5.3).
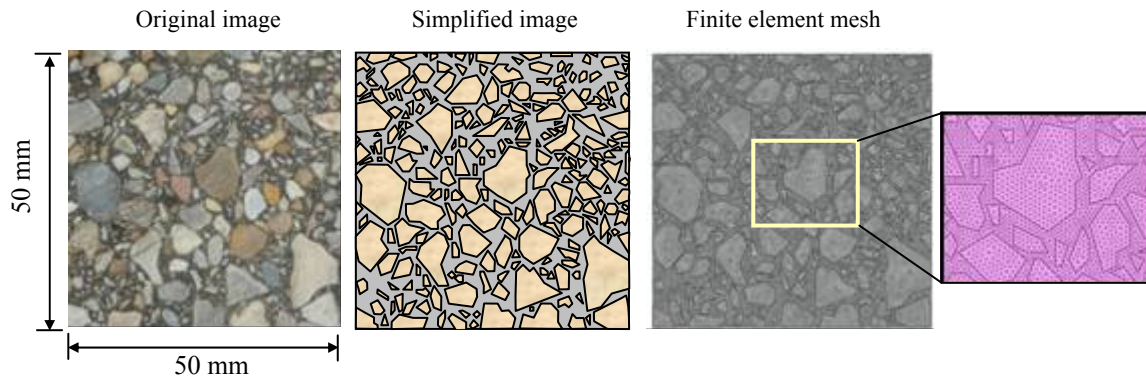
Figure 5.2. Section of the asphalt mixture used for the microstructure model and finite element mesh of the microstructure (no explicit air void phase)

The typical length sizes of the elements were 0.5 mm for the coarse aggregates and 0.3 mm for the FAM. The finite element representation of the aggregate-FAM interfaces consisted

of thin adhesive layers of 0.05 mm thickness that were inserted between the coarse aggregates and the asphalt matrix. These thin layers contain rectangular adhesive elements with a 0.2 mm characteristic length. With the exception of the adhesive elements that were modeled using first order 4-node elements, all the other components of the model were modeled with first order 3-node elements.
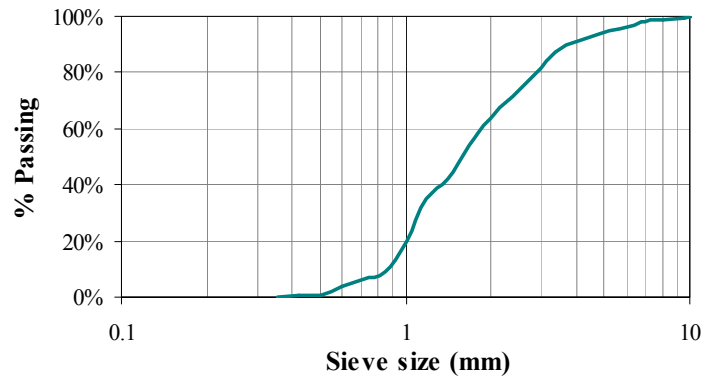
Figure 5.3. Coarse aggregate gradation of the microstructure model

In the first part of this chapter, the asphalt mixture microstructure was modeled as a three-phase material comprised of coarse aggregate, a bulk matrix (FAM), and air voids. In the second part, the microstructure was considered a two-phase material and the air void phase was assumed to be part of the FAM.

First Approach: Explicit Addition of the Air Void Phase in the Microstructure

Probabilistic Generation and Numerical Implementation of the Air Void Phase

Several microstructure models containing different total percent of air voids were randomly generated based on the air void size probability distribution of a dense-graded asphalt mixture. The air void size distribution (Figure 5.4) was obtained after applying image analysis techniques to images captured from a 10 cm diameter cylindrical specimen by means of X-ray CT (Castelblanco 2004). Matlab® was used to determine the probabilistic distribution that better fitted the frequency data provided by Castelblanco (2004). The results showed that a lognormal

distribution with a mean of -0.429 mm and standard deviation of 0.727 mm provides the best fit for the volumetric air void diameter distribution.
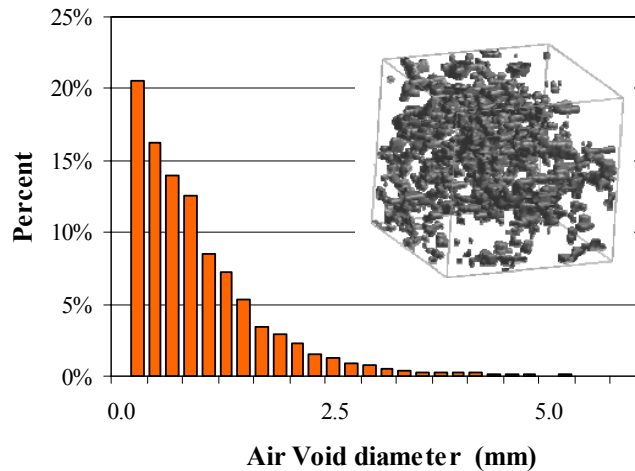
Figure 5.4. Air void size distribution of a dense-graded asphalt mixture; adapted from Castelblanco (2004) and Masad et al.(2006b)

The analysis focuses on the performance of an asphalt mixture when exposed to three different levels of total air void content, i.e., 4%, 7% and 10%, and moisture diffusion. Ten air void sets were randomly generated for the three percentages of air voids. Air voids were all assumed circular, and their radii were obtained from realizations of the lognormal size distribution. The location of the voids within the asphalt mixture microstructure was also randomly selected.

Due to the fact that the total volume of the microstructure model is fixed (Figure 5.2), adding air voids requires the removal of material from one of the two existing phases (i.e., aggregates or FAM). Two extreme cases were considered:

- Case 1: the air voids included in the microstructure replace space that was previously occupied by the FAM.
- Case 2: the air voids included in the microstructure replace space that was previously occupied by the aggregates.

In the first case, the percentage of area and weight of the aggregates remains constant. In other words, the total volume of FAM and air voids in the mixture is kept constant. In the second

case, the total volume of FAM and air voids increases with an increase in the amount of air voids as a result of the reduction of aggregate material. The aggregates that were eliminated in the second case were randomly selected such that the overall gradation of the mixture shown in Figure 5.3 was not altered.

Figure 5.5 illustrates three out of the 10 randomly created microstructure samples at each one of three levels of air void content for Case 1. An average of 128 circular air voids was included in the microstructures holding 4% air voids, 237 in the models having 7% and 344 in the microstructures characterized by 10% air void content.
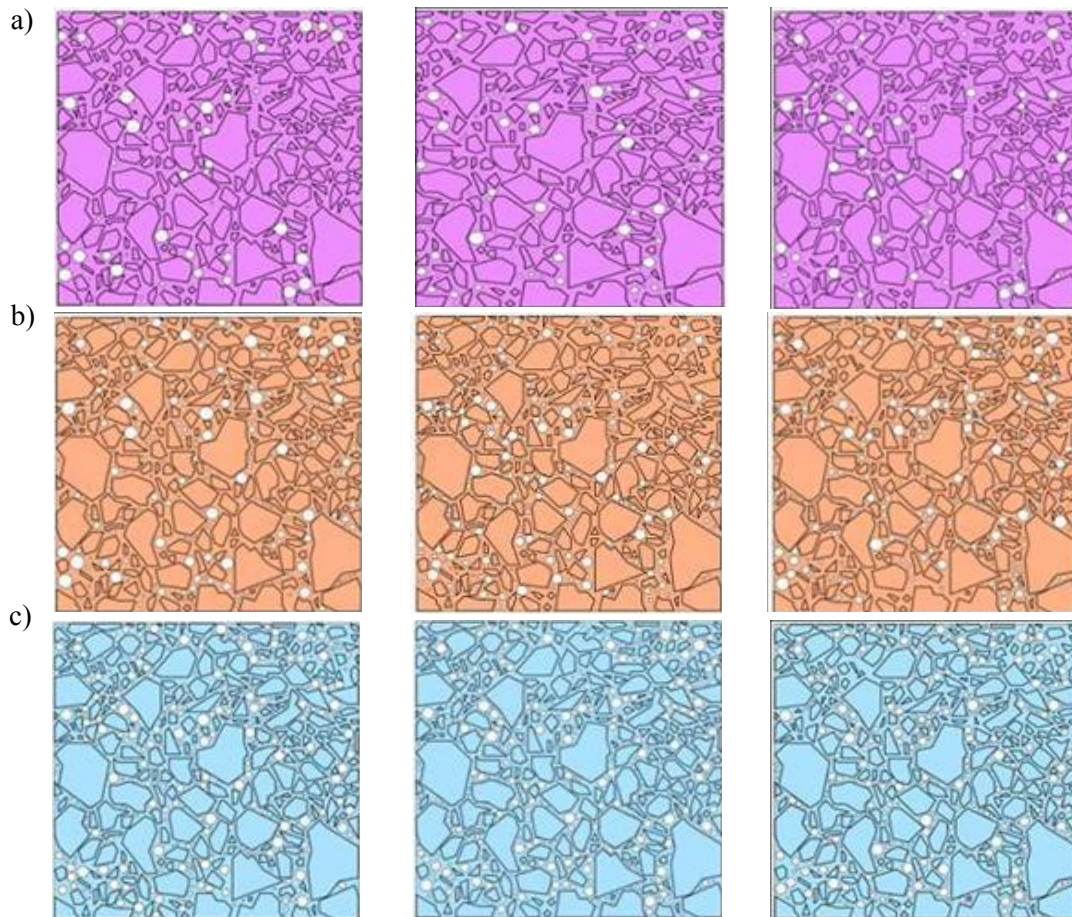
Figure 5.5. Three of the 10 different randomly created air void internal structures for different levels of total air void content in case 1: a) 4%, b) 7% and c) 10%

Figure 5.6 presents the details of five out of the 10 air void structures that were randomly generated for each air void level. In summary, a total of 60 microstructures were generated with the following variables:

- one type of size distribution,
- three different total air void contents (4%, 7%, and 10%),
- two different cases of introducing voids (replacing FAM and replacing aggregates), and
- ten different spatial locations of the voids for each case.
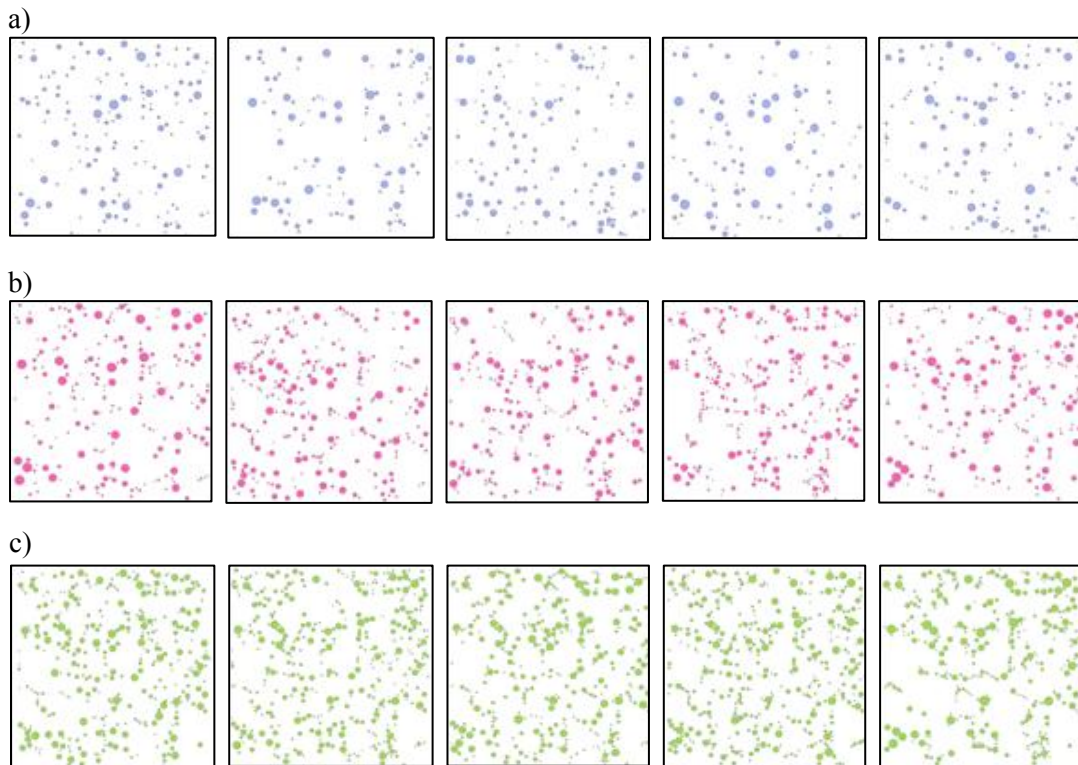
Figure 5.6. Randomly generated void structures at three levels of total air void content
a) 4%, b) 7%, and c) 10%

Material Properties and Models

Table 5.1 lists the diffusion coefficients of the different components of the mixture. The diffusion coefficient of the aggregates corresponds to that of typical limestone rocks (Dobchuk et al. 2004). While the values of the moisture diffusion coefficient for the aggregates and air voids listed in this table were obtained from previously reported data (Dobchuk et al. 2004; Geankoplis 1993), the estimation of the diffusion coefficient of the FAM phase requires special considerations. A review of the literature shows that the diffusion coefficient of FAM changes significantly among different sources (Arambula et al. 2007; Kassem et al. 2006; Kringos et al. 2008b). These differences are mostly due to the lack of a universal definition of FAM. Consequently, the material tested in these works differs in the selected type of fine aggregates, aggregate sizes and proportions, type of asphalt binder, and asphalt binder content. Furthermore, the air void content within these samples is difficult to determine and is usually not reported.

Table 5.1. Moisture diffusion coefficients of the three phases

Moisture Diffusion coefficients (mm^2/s)			
Aggregates[1]	FMA (no voids)	Air Voids	Interfaces
$1.28*10^{-3}$	$1.27*10^{-5}$	26	$1.27*10^{-5}$

(1) Limestone aggregate.

Since the air void phase is herein considered to be independent of the matrix phase, it was necessary to use reported values of diffusion coefficient for a FAM containing a known air void content to estimate the diffusion coefficient of the portion of the matrix that is free of air. In order to do that, the FAM moisture diffusion coefficient reported by Kassem et al. (2006) was selected. The technique used by the authors to prepare the FAM samples was similar to the one utilized by Bhasin et al. (2008), who estimated that the total air void content within the FAM samples was within a range of 12% to 15%. This information was used in a two-dimensional finite element model of transient moisture diffusion in Abaqus®, in which the two phases of the FAM (i.e., air voids and the portion of the FAM free of voids) were separated in the mentioned proportions. The diffusivity of the FAM portion containing no voids was defined as the value that makes the effective diffusivity of the composite to match the diffusion coefficient of the

continuum FAM material reported by Kassem et al., (2006). Thus, while the air phase was assigned the moisture diffusion coefficient of Table 5.1, the moisture diffusion coefficient of the remaining material (i.e., FAM with no voids) was iteratively modified until reaching such criterion.

In terms of the mechanical response of the materials, the aggregates were modeled as a linear elastic material, the FAM was modeled as a linear viscoelastic material, and the air voids were represented as a zero-resistance material. An elastic modulus of $E_{Aggregate}= 5*10^{10}$ Pa, and Poisson's ratio, ν_A, of 0.3 were used for the aggregates. The properties of the aggregates were assumed to be independent of the presence and/or amount of moisture content.

The material properties of the FAM used in this analysis were the same as those used in Chapters III and IV and correspond to the data collected by Kim et al. (2005) on similar materials. In terms of a Prony series, the viscoelastic response of the asphalt matrix is characterized by the parameters listed in Table 3.3, the instantaneous and infinite relaxation modulus are $E_0 = 1.12*10^8$ Pa and $E_\infty= 1.22*10^2$ Pa, respectively, and the Poisson's ratio is $\nu=$ 0.4. Table 5.2 summarizes the material properties of the three phases of the microstructure.

Table 5.2. Original mechanical properties of the microstructure's components

	Aggregates	**FAM**	**Air Voids**
Response	Linear Elastic	Linear Viscoelastic	None
Properties	$E_A=5.0*10^{10}$ Pa $\nu = 0.3$	Prony series reported by Kim et al. (2005) with: $E_0=1.12*10^8$ Pa, $E_\infty= 1.22*10^2$ Pa, and $\nu = 0.4$	Zero resistance material

The influence of moisture on the mechanical response of the FAM was accounted for by linearly reducing the relaxation modulus of this material as the moisture content increased, similar to the approach followed in previous chapters of this dissertation. Thus, the relaxation modulus of the FAM at any time, t, was set to decrease linearly from its original value, in the absence of water, to 90% of that value, when fully saturated. The Poisson's ratio of the FAM was assumed to be time and moisture independent.

The traction-separation law illustrated in Figure 5.1 was used to characterize the mechanical response of the adhesive zones. The peak values of the relative displacement defining the damage initiation criterion were assumed to be the same in the normal and shear modes (δ_{in} in Figure 5.1). These values were estimated as 0.1 mm based on recent experimental work on the adhesive fracture in systems composed by thin asphalt binder layers (i.e., 5 μm) on metal substrate (Masad et al. 2010). The critical energy release rates of the material in each individual mode were estimated based on the same experimental study as 15% of the area within the elastic part of the traction-separation law (Table 5.3) .

The effect of moisture on the mechanical properties of the adhesive zones was accounted for in two different ways: 1) by exponentially reducing the stiffness of the elements prior to damage initiation (*K*, in Figure 5.1), and 2) by linearly reducing the peak values of the nominal strain that defines the damage initiation criterion. The stiffness and peak values of the nominal strain under saturated conditions are 0 and 80% of the original values in dry condition, respectively. These two conditions reflect the moisture dependency of the bond strength and fracture toughness (modes I and II) of the adhesive elements.

Table 5.3. Mechanical response and properties of the adhesive zones

Stage	Response	Properties
Prior to damage initiation	Uncoupled linear elastic	K_{nn} and K_{ss}: components of the elastic matrix $K_{nn} = K_{ss} = 4.48*10^7$ Pa
Damage initiation criterion	Quadratic nominal strain condition	δ^n_{in} and δ^s_{in}: peak values of the relative displacement for the purely normal and shear direction, $\delta^n_{in} = \delta^s_{in} = 0.1$ mm.
Critical fracture energy criterion	Benzeggagh-Kenane criterion	G^C: overall critical energy released rate G^C_n and G^C_s: critical energy released rates for the pure normal and shear modes, $G^c_n = G^c_s = G^c = 4.49*10^{-2}$ N/mm

Modeling Methodology

The asphalt mixture microstructures were subjected to a three-step simulation:

1. A force-controlled loading simulation was first applied in the dry condition. The simulation consisted of loading and unloading the microstructure for a total of 30 s at a monotonic rate of 0.16 N/s (Figure 5.7).

2. Identical undamaged microstructures were subjected to a 10-day moisture diffusion period using the boundary conditions illustrated in Figure 5.7.

3. Finally, the samples were subjected to the same mechanical scheme described in the first step.

The simulation can be thought of as an experimental setup in which different replicates of asphalt mixtures with different air void content levels were subjected to mechanical loading under two different conditions: 1) in a dry state and 2) after a 10-day moisture-conditioning process.
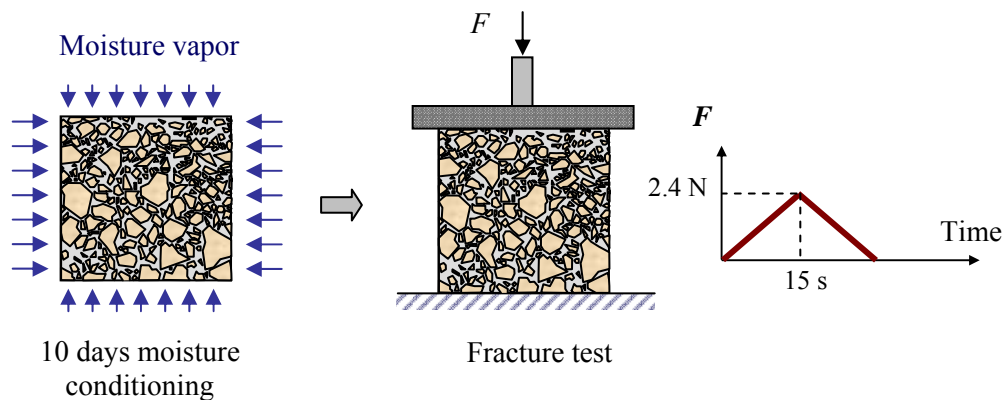
Figure 5.7. Representation of the modeling methodology

The sequential diffusion-mechanical coupling methodology in Abaqus® described in Chapter III was used to couple the effects of diffused moisture with the mechanical performance of the microstructure. Moisture diffusion was modeled using Fick's second law with an implicit numerical scheme. During the moisture diffusion simulation the microstructures were subjected to a fixed boundary condition consisting of a normalized moisture concentration of 1.0 uniformly distributed along their perimeter (Figure 5.7). Diffusion-elements type DC2D4 in Abaqus® were used to model the adhesive zones and elements type DC2D3 in Abaqus® were used for all the other components of the model.

Mechanical loading was modeled using an implicit scheme. The same finite element mesh was used for the diffusion and mechanical loading simulations, although the diffusion-based elements were replaced in the second stage of the simulation by mechanical-based elements (i.e., elements type COH2D4 in Abaqus® for the adhesive zones and elements type CPE3 for all the other components of the model).

Results and Discussion

General Observations

As discussed earlier, the analysis was conducted for two cases of placement of air voids. In the first case, air voids replaced part of the FAM, while in the second case the air voids replaced existing aggregate materials. Mechanical simulations on the 60 different asphalt mixture microstructures generated for both cases (i.e., 10 for each of the three levels of moisture content), were first conducted on samples in dry condition, and later on samples after moisture diffusion (i.e., wet condition). Figure 5.8 presents a typical force-displacement response obtained from one microstructure containing 7% air voids in both dry and wet conditions, as well as the moisture profile within the microstructure after the 10-day period of moisture diffusion.
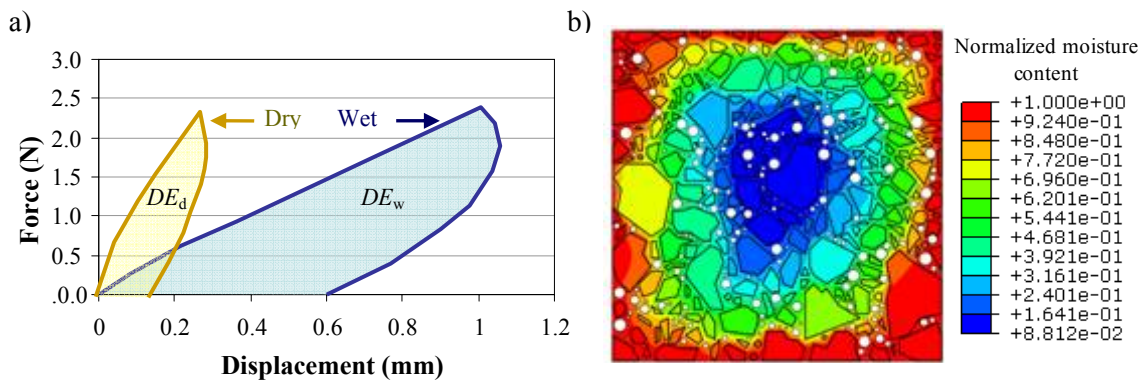
Figure 5.8. a) Mechanical response of a mixture containing 7% total air voids (DE_d = dissipated energy in dry condition, DE_w = dissipated energy in wet condition) and b) moisture profile within the sample

The total dissipated energy (*DE*) of the asphalt mixture during mechanical loading (i.e., area within the force-displacement curves in Figure 5.8) and the stiffness (*K*) of the mixture (i.e., the maximum load divided by the maximum displacement during the loading portion of the test, Figure 5.8) were the parameters selected to study the effect of different air void content on the mechanical performance of the mixtures.

Figure 5.9 presents the values of dissipated energy obtained from the mechanical simulations corresponding to all mixtures (cases 1 and 2 in dry and wet conditions). Four important observations can be extracted from this figure:

- at a fixed value of total air void content, the total energy dissipated by all mixtures in dry condition is always smaller than the total energy dissipated in wet condition;
- the total energy dissipated by the mixtures in wet condition increases with an increase in the total air void content;
- an increase in the amount of air voids results in an increase in the energy dissipated by the mixtures in dry conditions; and
- the total energy dissipated by the mixtures in case 2 (i.e., mixtures rich in FAM) is slightly larger than the total energy dissipated by those values reported for mixtures in case 1.
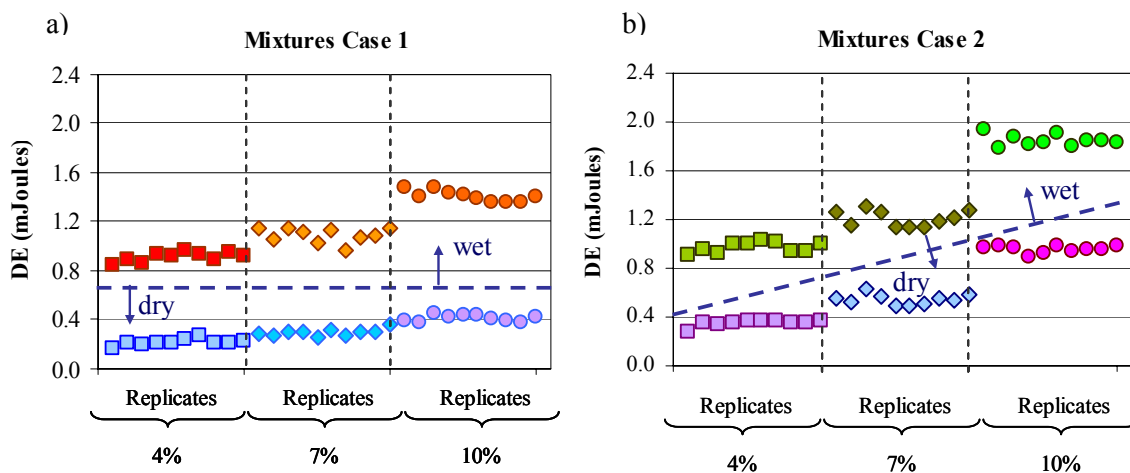
Figure 5.9. Energy dissipated by different replicates of microstructures at four levels of air void content (0%, 4%, 7% and 10%) for asphalt mixtures in a) case 1, and b) case 2

The first observation results from the coupling between moisture and material properties: the presence of moisture reduces the structural capacity of the individual materials causing the moisture-conditioned mixtures to dissipate more energy than their equivalent dry cases. The second observation is impacted by two different factors: 1) an increase in air voids weakens the mechanical resistance of the composite (i.e., there is less total mass to resist force); and 2) the presence of more voids facilitates diffusion of larger amounts of moisture to the inner part of the microstructure, which in turn causes more cohesive and adhesive damage. Finally, the last observation is a direct consequence of the fact that the replacement of aggregate by air voids (case 2) drops the overall resistance of the mixtures in a larger proportion as compared to the case when the total volume of FAM and air voids of the mixture is kept constant (case 1).

Effect of Air Void Content on the Performance of Mixtures Subjected to Moisture Diffusion

The mean values of the evaluation parameters (i.e., total dissipated energy and stiffness of the mixtures) were selected to study the role of air void content on the mechanical response of asphalt mixtures exposed to mechanical loading and moisture diffusion. The 95% confidence intervals of the mean value of these two statistical estimators, as well as their probabilistic distributions, were computed using the *bootstrapping* technique, explained below, at the three different values of total air void content.

Bootstrapping is a re-sampling technique introduced by Efron in 1979 that permits the inference of statistical estimators (Efron 1979). This technique can be applied to produce new samples containing 10 values of dissipated energy and stiffness based on the original set of 10 values that resulted from the numerical simulations. The mean values calculated from these new samples can be used to compute its confidence interval and/or its probabilistic distribution. The bootstrapping technique is based on the assumption that the X values contained in the original sample are independent and identically distributed. Then, values from the original set are randomly extracted one by one until creating a new sample of X values. This process is repeated until Y new samples are produced, each containing X values. For more information on the bootstrapping technique the reader is referred to Davison and Hinkley (2006). The available bootstrapping function in Matlab$^®$ was used to generate 10,000 new samples of dissipated energy and stiffness for each level of air voids. The mean value of these new sets was computed and its 95% confidence interval was determined.

Figure 5.10 illustrates the 95% confidence interval of the mean value of the dissipated energy and the same confidence interval for the stiffness corresponding to samples containing different air void content. It can be observed from this figure that the total dissipated energy rapidly increases with an increase in the total percent of air voids. A third order polynomial can be used to represent the growth of the mean value of the total dissipated energy as a function of the total air void content of the asphalt mixture (Figure 5.10.a) as follows:
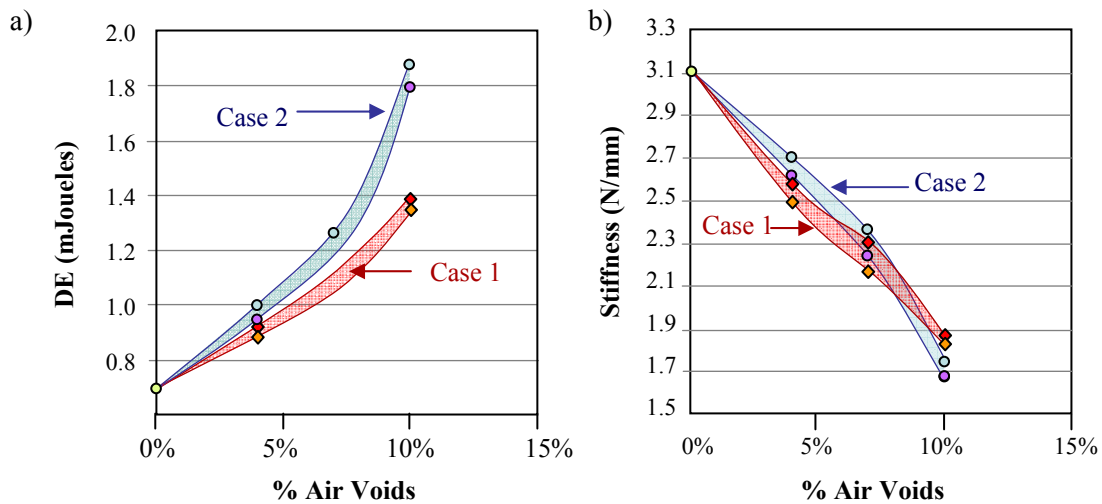
Figure 5.10. 95% confidence interval of a) total dissipated energy, and b) stiffness of asphalt mixtures subjected to the moisture diffusion and mechanical loading processes specified in Figure 5.7

$$\mu_{DE}^{case1} = 2.00*10^3 (AV)^3 - 2.05*10^2 (AV)^2 + 1.21*10^1 AV + 6.87*10^{-1}, \qquad (5.1)$$

$$\mu_{DE}^{case2} = 6.16*10^2 (AV)^3 - 6.53*10^1 (AV)^2 + 7.23 AV + 6.87*10^{-1}, \qquad (5.2)$$

where μ_{DE} is the mean value of the 95% confidence interval of dissipated energy for cases 1 or 2 (in mJoules), and AV is the total percent of air voids within the mixture (in %). Equations 5.1 and 5.2 are only valid for AV in a range from 0 to 10%.

These results show that the difference in the expected value of the total dissipated energy between the mixtures with a constant amount of aggregates (mixtures low in FAM, case 1) and

the mixtures with a variable amount of aggregates (mixtures rich in FAM, case 2) significantly increases with an increase in the air void content. For the 4% and 7% air void content the differences between the confidence intervals of the two cases is less than 9%, while at 10% air void content, the difference in the mean value of the dissipated energy between cases 1 and 2 is more than 33% (Figure 5.10.a). Note that the total energy dissipated for any mixture with the aggregate gradation shown in Figure 5.3 will be in between the bands defined by cases 1 and 2.

The drop of the mean value of the stiffness of the mixtures, K, as a function of the total air void content (Figure 5.10.b) can also be characterized by a third order polynomial:

$$\mu_K^{case1} = -1.00 * 10^3 \left(AV\right)^3 + 1.00 * 10^2 \left(AV\right)^2 - 1.27 * 10^1 \, AV + 3.07 \tag{5.3}$$

$$\mu_K^{case2} = -1.09 * 10^3 \left(AV\right)^3 + 1.75 * 10^2 \left(AV\right)^2 - 1.88 * 10^1 \, AV + 3.07 \tag{5.4}$$

where μ_K is the center value of the 95% confidence interval of the overall stiffness for cases 1 or 2 (in N/mm).

The results in this case show that the moisture and mechanical loading cause a reduction of more than 40% in the stiffness of the mixture when it contains 10% air voids as compared to the case of no voids.

Besides the confidence interval, a hypothesis proof was performed to determine whether the mean values of dissipated energy and stiffness obtained from the re-sampling technique followed a normal distribution. The results confirmed the hypothesis, and Figure 5.11 presents the normal distributions of both parameters for the moisture-conditioned microstructures of case 1. It is interesting to note that the samples containing 7% air voids have the largest dispersion of the data while mixtures with 10% air voids present the minimum data variability. In other words, variability in spatial location of the air voids within the microstructure seems to have a major impact when the mixture contains an intermediate amount of total air voids (i.e., 7%). This information is particularly important when considering that the usual target for air void content of dense-graded mixtures during the compaction process in the field is close to 7%. This result implies that special care is needed during the placement of the mixture in the field to guarantee consistent and homogeneous distributions of air voids. Uniform air void distributions in the asphalt course can contribute to control the variability of the expected mechanical performance

of the mixture. Results for mixtures with variable amount of aggregates (case 2) are qualitatively similar to those presented in Figure 5.11.
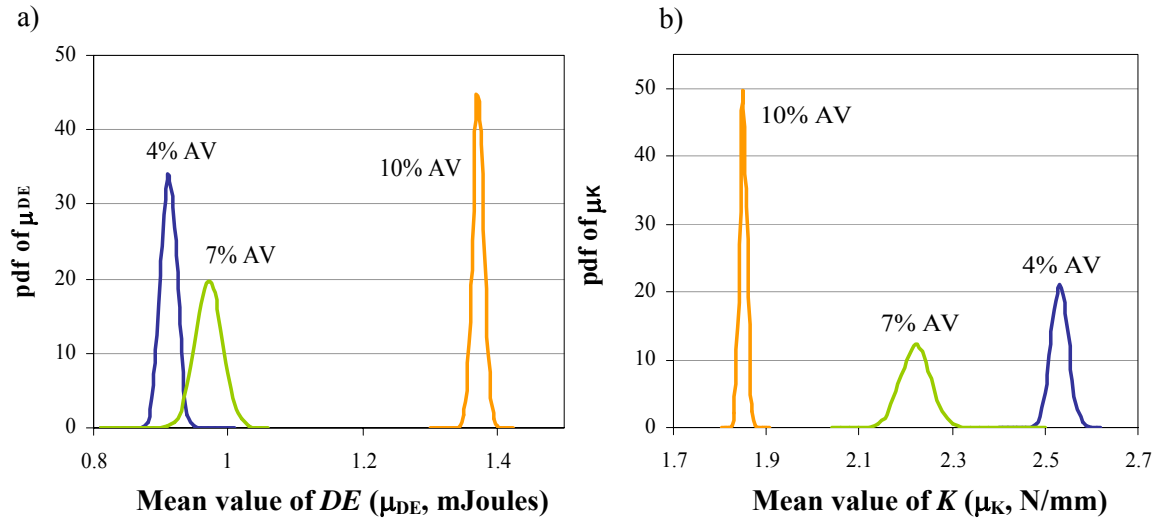
Figure 5.11. Density normal distributions of the mean values of a) the total dissipated energy (μ_{DE}), and b) the overall stiffness (μ_K), for moisture-conditioned mixtures of case 1 with different levels of total air void content (AV)

Differences in the Mechanical Performance of Microstructures in Dry and Moist Environments

The mechanical performance of moisture-conditioned microstructures characterized by different air void contents is affected by two factors: 1) the presence of moisture within the microstructure, and 2) the effect of increasing the amount of air voids on the structural integrity of the mixtures. The former causes a progressive loss of the structural capacity of the mixture by reducing the resistance of the FAM and the aggregate-FAM interfaces as a function of the moisture content. The latter is related to a loss in the overall resistance of the mixture in dry condition due to the replacement of volume of aggregates or FAM by air voids (i.e., a reduction of the bulk specific gravity of the mixture). Therefore, it seems important to study the relationship between the air void content of an asphalt mixture and the individual contributions of these two factors to the overall damage.

Table 5.4 presents the mean value of the ratio of the total dissipated energy and stiffness obtained from the moisture-conditioned mixtures (DE_{wet} and K_{wet}) to those obtained from the dry mixtures (DE_{dry} and K_{dry}) that result from dividing the dry and wet values displayed in Figure 5.12.

Table 5.4. Mean value of the ratio of dissipated energy and stiffness in dry and wet conditions

	Case 1				Case 2		
	Total percent of air voids						
	0%	4%	7%	10%	4%	7%	10%
DE_{wet}/DE_{dry}	5.02	4.37	3.61	3.35	2.83	2.22	1.95
K_{wet}/K_{dry}	0.23	0.25	0.27	0.28	0.35	0.44	0.49
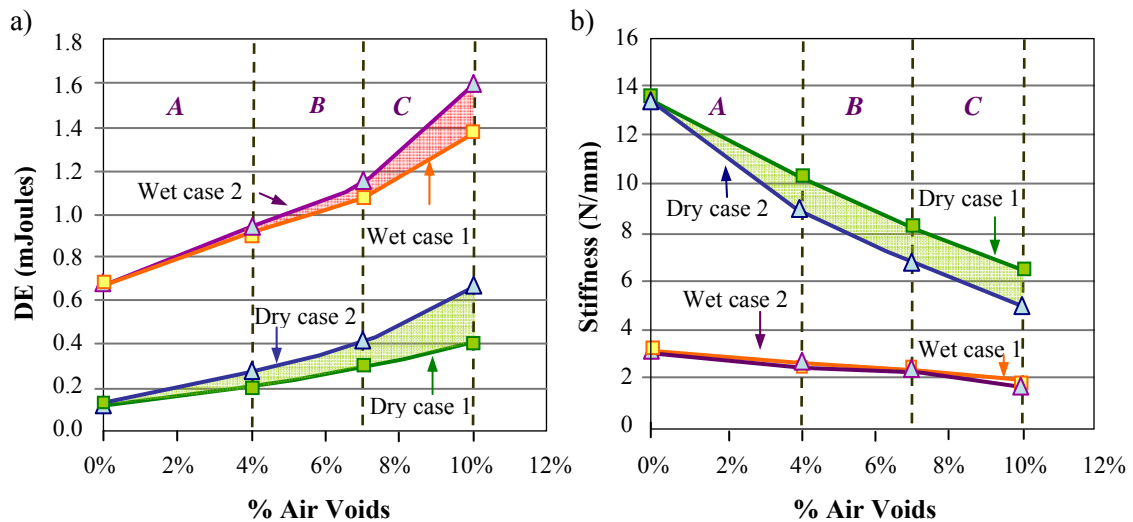
Figure 5.12. Mean values of the 95% confidence intervals of a) dissipated energy and b) stiffness as a function of total air void content of asphalt mixtures subjected to the mechanical loading conditions of Figure 5.7 in both dry and wet conditions

Although the total energy dissipated by the moisture-conditioned mixtures (DE_{wet}) and the total energy dissipated by the dry mixtures (DE_{dry}) increase as a function of the total air void content, data in Table 5.4 show an inverse relationship between the air void content and the ratio

of these two values (DE_{wet}/DE_{dry}). In other words, the data suggest that as the percentage of air voids increases, the contribution of the structural degradation attributable solely to the presence of air voids in the dry microstructure (DE_{dry}) is more pronounced than the degradation exclusively caused by an increase of diffused moisture within the mixture. Similar results are also found when studying the contribution in the reduction of stiffness caused by the presence of air voids (K_{dry}) to the reduction in resistance of the moisture-conditioned microstructures (K_{wet}). It is also interesting to note that although there is a significant difference between the stiffness of the mixtures from case 1 (mixtures low in FAM) and case 2 (mixtures rich in FAM) in dry conditions (upper band in Figure 12.b), that difference becomes insignificant when testing the same mixtures after the moisture-conditioning process (low band in Figure 12.b). That is, the stiffness of the moisture-conditioned mixtures is less sensitive to the volumetric proportions of the aggregates and FAM phases than is the total energy dissipated (Figures 10.b. and 12.b).

The fact that the contribution of the diffused moisture to the overall damage is not as significant as the structural degradation caused by the presence of more air voids can be explained by the internal composition of the asphalt mixtures. For mixtures in case 1, increasing the air void content reduces the FAM fraction and increases the aggregate fraction in the total mix. The properties of FAM and interfaces are influenced by the presence of moisture, whereas the properties of aggregate are not moisture dependent. Therefore, an increase in the aggregate fraction reduces the mixture sensitivity to diffused moisture. For mixtures in case 2, the amount of FAM material remains constant and the aggregate material is substituted by air voids. Dry mixtures with larger amounts of air voids in this case are even weaker than those in case 1, since the high-resistant elastic material of the composite (i.e., aggregates) is being replaced by voids. Although in this case all conditioned mixtures contain a constant amount of the viscoelastic moisture-dependent material, this material has a low value of moisture diffusion coefficient. Therefore, at the end of the moisture diffusion period, mixtures in case 2 contain less moisture than mixtures in case 1. The consequences of these two observations is that, in both cases, the change in the mechanical properties of the materials caused by the presence of moisture is less significant than the structural loss caused by the replacement of aggregate or FAM material by voids.

The change of the total dissipated energy or stiffness with respect to the increase of one unit of air void content (for both dry and moisture-conditioned cases) is also a useful parameter to evaluate the overall damage. This parameter, which is referred to as marginal change, can be

evaluated through the variations in the slope of the curves depicted in Figure 5.12. Data in this figure show that the rate of change of the total dissipated energy (or rate of reduction in stiffness) per unit of percent air voids increases faster in the moisture-conditioned mixtures than in the dry mixtures. This can be verified by comparing the slopes of the dry and wet curves in the three sections of Figure 5.12 (*A*, *B*, and *C*). The slope of the dry curves for the dissipated energy in case 2 (expressed in mJoules / % air voids), for example, increases from $3.4*10^{-2}$ to $4.84*10^{-2}$ when passing from section *A* to section *B*, and from $4.84*10^{-2}$ to $8.29*10^{-2}$ voids when passing from section *B* to section *C*. These values translate into an increase of 41.89% and 71.28% of dissipated energy rate when passing from *A* to *B* and from *B* to *C*, respectively. The calculation of the increase in the slopes for the moisture-conditioned mixtures shows that the rate of the total dissipated energy in the wet cases increases by 10.33% and 114.42% when passing from sections *A* to *B* and from *B* to *C*, respectively. The comparison of these values shows that when the total amount of air voids goes from 7 to 10%, the rate of increase of the total energy dissipated by the moisture-conditioned mixtures is larger than the equivalent rate of increase of the energy dissipated by the dry mixtures. This result suggests that although the rise in air voids is a main cause of the total deterioration observed in the moisture-conditioned mixtures, the addition of more air voids also accelerates the rate of damage that is exclusively due to the moisture-induced cohesive and adhesive deterioration of the mixture.

Second Approach: Indirect Consideration of the Effects of the Air Void Phase by Means of a Stochastic Model

Stochastic Generation of Internal Air Void Distribution

In this second approach, the air void phase was not explicitly included in the model as a separate phase of the microstructure. Instead, existing measured field air void distribution and variability data were used to generate realizations of spatial arrangements at the interior of the mixture's microstructure. In the generation of these spatial arrangements, random field theory was used to treat the air void content as a random vector instead of a constant-deterministic value.

A random field is a generalization of a stochastic process in which a parameter (e.g., material properties in a medium or pixel data from an image) is mapped into a space after taking into consideration its spatial correlation and variability (Fenton and Griffiths 2008). Random field theory has been widely used in geotechnical engineering to model the variability of material

properties in soils; the reader is referred to Kim (2005) and Fenton and Griffiths (2008) for a comprehensive review. The principles of this theory have also been applied to characterize and model physical and mechanical processes in multiphase materials at different length scales (Graham-Brady and Xu 2008; Graham and Deodatis 2001; Torquato 2002) and to conduct complex statistical image analysis, including pattern recognition techniques, with applications in a wide range of areas (Li 2009). In asphalt pavement engineering, the application of this theory has been limited. Some examples include the detection and characterization of surface distresses based on image analysis (Delagnes and Barba 1995), the modeling of the surface roughness of pavements and its effects on stochastic pavement loads (Sun and Kennedy 2002), and the modeling of the variability and distribution of the tire-pavement contact loads (Sun et al. 2006). This probabilistic-based technique, however, has not been used in the past to model the variability and distribution of material properties within an asphalt mixture or to estimate the impact of such variability on the mechanical performance of this material.

Thus, the use of random field theory to generate air void distributions provided a collection of spatially correlated random values of air void content that were mapped into a physical space, i.e., the asphalt mixture. The main advantage of applying random field theory to generate probable air void distributions is that it efficiently captures the complexity associated with this phase by including both its spatial correlation and variability. Details regarding the specific stochastic methodology adopted for this study, including a formal definition of the spatial correlation concept, are presented in the following sections.

The stochastic methodology used to generate diverse air void distributions was designed to reflect the characteristics of a compacted asphalt layer in the field. Although the compaction process aims at a pre-specified target value of air void content (usually 7%), the percent of air voids within the asphalt course is not constant (Brown et al. 2004). The spatial variability of the air voids within the asphaltic layer is mainly determined by the characteristics of the mixture (e.g., physical and volumetric properties, morphological and gradation characteristics of the coarse aggregates, etc.) and by the compaction method (Masad et al. 2009). Therefore, if several field cores are extracted at different locations within the asphalt layer, a variation in air void content is expected. If the compaction process was conducted under strict quality control procedures, the average value of the air void content from the different cores should be close to the target air void content. However, even under these circumstances, the internal distribution of

the air voids within each core could be different due to the inhomogeneous distributions of the mixture components and boundary conditions during compaction.

Based on the previous discussion, the stochastic technique herein used takes into consideration two different types of variability of air voids within asphalt mixtures:

1. The spatial variability of air voids within the asphalt layer (i.e., the difference among the total air void content at different spatial locations at the asphalt layer), and

2. The internal distribution of the air voids within the microstructure of the mixture (i.e., internal spatial air void distribution in a core taken at a particular location).

Figure 5.13 illustrates both the spatial variation in air voids within the asphalt layer and the internal void distribution within each core. Based on the previous considerations, each one of the extracted field cores represented in Figure 5.13 can be thought of as one realization of the air void random field. Therefore, the stochastic technique is capable of producing realistic realizations of the spatial air void distribution within an asphalt layer—each one containing a unique internal void structure—similar to those that would be obtained from randomly selected field cores.
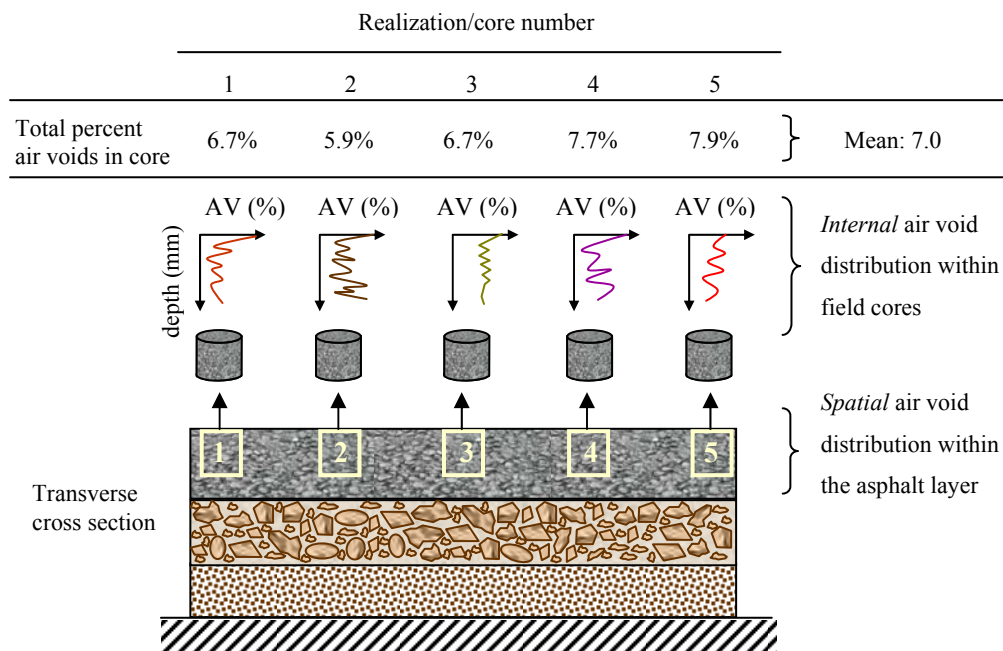
Figure 5.13. Probable realizations of the air void random field in asphalt layers

Covariance Matrix Decomposition Technique

Discrete random field generation methods divide the space of interest into several sections. In this study, the FAM phase of the asphalt mixture was divided into 100 elements (Figure 5.14). A realization of the stochastic process involves assigning a randomly generated value of a parameter P (e.g., hydraulic conductivity, porosity, strength, etc.) to each section. Since each phase of the mixture has higher probability of extending over an area longer than one element, adjacent elements are more likely to have similar values of the parameter P than the values of elements that are further apart. Therefore, the value assigned to a given section should be somehow correlated with the values in neighbor cells. The distance at which this similarity is expected (i.e., the length of influence of the parameter P) is called the autocorrelation distance or autocorrelation length of the random field, L_T. In addition to the correlation length, a random field is also characterized by the mean value of P and a dispersion measure, e.g., standard deviation. These parameters (mean and dispersion measure) are determined experimentally. The average value of P and its variability among different realizations always converge to the mean and standard deviation of the random field.
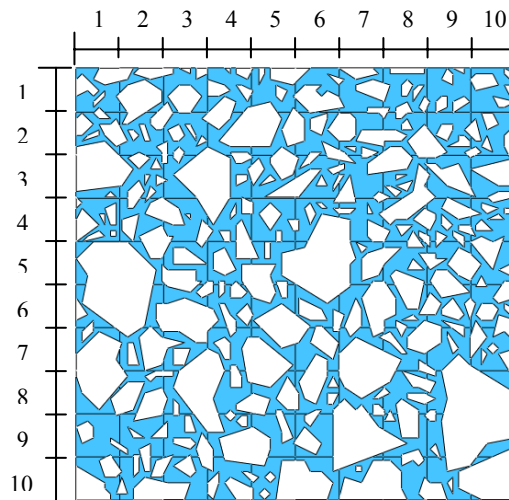
Figure 5.14. 100 divisions of the FAM to which random values of air void content will be assigned

A commonly used random field generation method was proposed by El-Kadi and Williams (2000), who applied a covariance matrix decomposition technique to generate stochastic spatial distributions of the selected parameter P within a fixed space. The covariance decomposition technique is based on two main assumptions: 1) the parameter of interest, P, has a normal or lognormal distribution within the space of interest, and 2) P is characterized by an exponential autocorrelation function. The first assumption defines the process of determining probable values of P for each element of the space, while the second defines how the values of P at different locations are correlated. Both assumptions are supposed to be valid in characterizing the variability and distributions of air voids within the FAM phase of the mixtures.

The value of air voids in each realization is obtained by (El-Kadi and Williams 2000):

$$AV_n = S\varepsilon_n + \mu_n \qquad (5.5)$$

where AV is a [100x1] vector containing the air void content of the 100 elements of the FAM, S is the [100x100] autocorrelation matrix, ε is a [100x1] vector containing standard normally distributed values (i.e., with mean 0 and standard deviation 1), μ is a [100x1] vector containing the mean values of the internal air void distribution within a particular microstructure and the subscript n refers to the results for the n-th realization of the random field. Note that the expected value of Equation 5.5 is, effectively, the mean value of the random field:

$$E[AV_n] = SE[\varepsilon_n] + \mu_n = \mu_n, \qquad (5.6)$$

The autocorrelation matrix, S, can be found from:

$$C = SS^T, \qquad (5.7)$$

where C is the covariance matrix of the field, which has to be positive-definite. The matrix S can be determined from C by using the Cholesky decomposition matrix technique. The Cholesky technique is useful in decomposing a symmetric, non-negative-definitive matrix, like C, into a lower triangular matrix. Details of this methodology can be found elsewhere (Golub and Van Loan 1996).

Although the correlation function depends upon the problem at hand, several common models have been used extensively. Most common models include the polynomial decaying and different exponential correlation functions (Fenton and Griffiths 2008). For the purpose of this dissertation, the following exponential form of the correlation function was selected:

$$C_{i,j} = \sigma\, e^{-\frac{|d_{i,j}|}{L_T}} ,$$

(5.8)

In Equation 5.8 $C_{i,j}$ is the correlation function between the spatial points i and j, σ is the standard deviation of the air voids in the field, $d_{i,j}$ is the distance between points i and j, and L is the autocorrelation distance. For exponential correlation functions, the autocorrelation length, L, is usually defined as the distance where the spatial autocorrelation decays by $1/e$ (i.e., about 37%). Equation 5.8 can be modified to include anisotropy in the correlation of the random field:

$$C_{i,j} = \sigma \exp\left[-\sqrt{\left(\frac{d_{i,j}^x}{L_x}\right)^2 + \left(\frac{d_{i,j}^z}{L_z}\right)^2} \right] ,$$

(5.9)

where L_x and L_z are the autocorrelation distances in the x (i.e., horizontal) and z (vertical) directions, respectively, and $d^x_{i,j}$ and $d^z_{i,j}$ are the horizontal and vertical components of the distance between the points i and j (i.e., rectangular components of $d_{i,j}$). It is noteworthy to observe that large values of the autocorrelation distances (e.g., larger than the size of the space) will produce values of $C_{i,j}$ approximately equal to the standard deviation, which in turn results in a strongly correlated random field.

In summary, the following steps are needed to generate a realization of the air void random field: 1) divide the FAM space into several subdivisions, 2) determine a mean value vector, a standard deviation and the autocorrelation distances of the random field, 4) compute the standard normally distributed vector ε, 3) compute the covariance matrix C (Equation 5.8 or 5.9), 4) apply the Cholesky decomposition technique to determine the matrix S (Equation 5.7), and 5) compute the realization of the air void random field by means of Equation 5.5.

Parameters of the Air Void Random Field

In terms of the actual spatial variability of air void content in the field, most state transportation agencies in the United States have designed quality control methodologies to maintain the maximum allowable standard deviation of the spatial distribution of air voids in the range of 1% to 1.5% (Epps et al. 2002; TxDOT 2004). This variability is verified in the field by experimentally measuring the total air void content of field core specimens obtained at different locations in the asphalt layer. The coefficient of variation (COV) of this property that results from those quality control specifications can then vary in a range of 10 to 20%. Nevertheless, studies conducted in the field to asses the influence of diverse compaction patterns in the pavement have shown that the spatial variability of the air voids in a compacted asphalt layer can reach values of COV nearly 30% (Masad et al. 2009).

In order to analyze the impact of the spatial variability of the air voids on the moisture-related mechanical performance of an asphalt mixture, three different cases were considered. In all cases, it was assumed that the microstructure model belongs to an asphalt course characterized by a mean value of air void content equal to 7%, which is a common target for dense-graded mixtures in the field. The three cases considered coefficients of variation of the air void random field equal to 10%, 20% and 30%. It is expected that the variability of most asphalt layers will be close to the first two cases, while case 3 represents an extreme case of variability. Notice that the three mentioned COVs represent the variability of the air void content of the asphalt mixtures in the field and not the variability of the internal air void distribution within a particular microstructure (i.e., within a field core).

Although the mean value of the air void random field was selected to be 7%, the actual internal air void distribution within a sample of asphalt mixture is not constant. Figure 5 shows the air void distributions within different asphalt field cores that were obtained by means of X-ray CT and image analyses techniques (Masad et al. 1999; Tashman et al. 2001). It can be observed that, in general, the air void content at the surface of the pavement is always larger than that in the middle and bottom sections of the asphaltic layer. This information was used to generate random mean vectors (μ_n in Equation 5.5) that will characterize the internal void distribution within a sample.
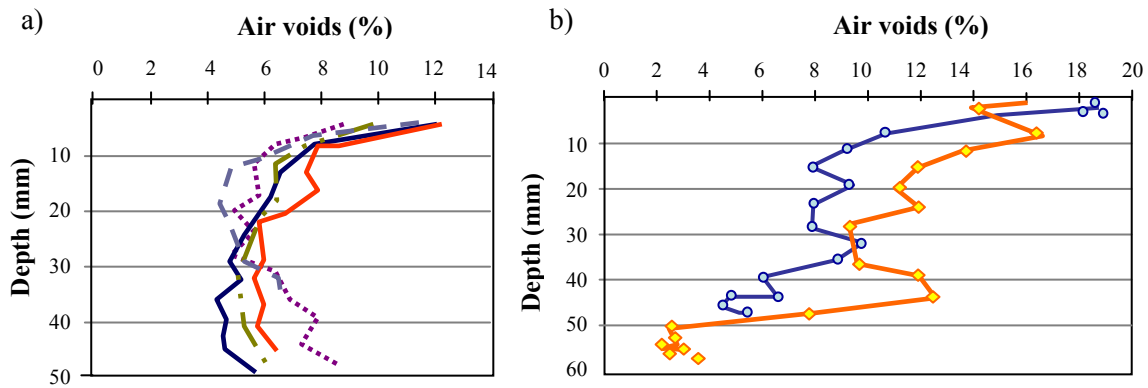
Figure 5.15. Examples of the air void distribution at the interior of different asphalt mixtures in the field. Left, modified after Tashman et al. (2001) and right, modified after Masad et al. (1999)

For simplicity, it was assumed that the distribution of the percentage air voids with respect to depth, $AV(z)$, which defines the mean vector of a realization of the random field (μ_n), follows a parabolic function (i.e., a "C" shape, Figure 5.16):

$$AV(z) = a*(z-25)^2 + AV_{z=25} \,,\tag{5.10}$$

where z represents the depth of a particular location within the microstructure (in mm), and a and $AV_{z=25}$ are the two parameters that define the shape of the vertical air void distribution. Note that $AV_{z=25}$ in Figure 5.16 corresponds to the air void content at 25mm in depth (i.e., at the middle of height of the microstructure and vertex of the parabola).

The vertical air void distribution was generated by randomly selecting the parameter b (Figure 5.16) between 0.25 and 0.7 and by forcing the mean value of the distribution to be 7%. The parameter b symbolizes the ratio between the minimum air void content ($AV_{z=25}$ in Figure 5.16) and the maximum air void content (top and bottom of the sample, $AV_{z=0}$ in Figure 5.16) in the microstructure, as expressed by Equation 5.11. The range of variation of this parameter was obtained based on the shapes of actual air void distributions within diverse field cores as those shown in Figure 5.15. Values of b close to 1.0 are associated with more uniform vertical distributions of voids while values close to 0 are associated with larger dispersion of the internal

void structure. The shape parameters *a* and $AV_{z=25}$ are unique for each value of *b*, and are determined by:
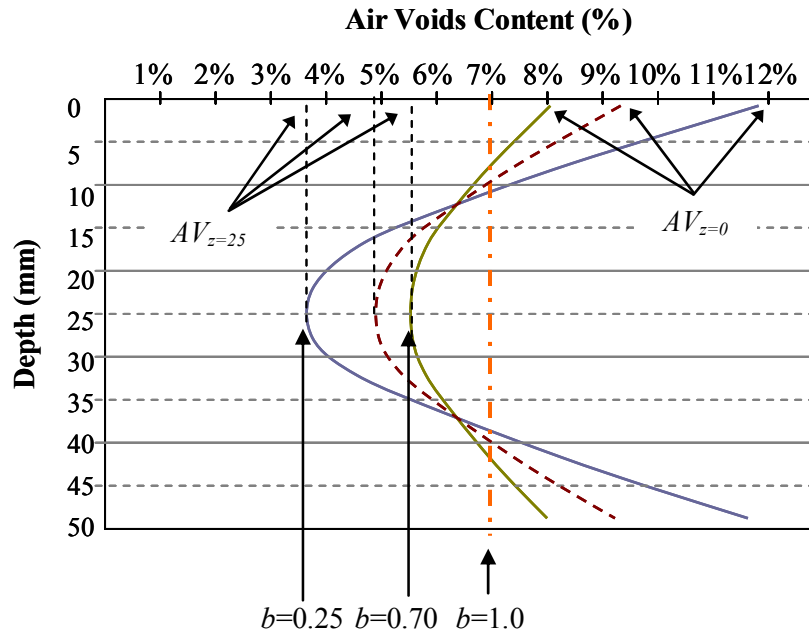
Figure 5.16. Characteristics of the random generation of vertical distributions of air voids. The distribution is used as the mean vector for each realization of the random field

$$b = \frac{AV_{z=25}}{AV_{z=0}} = \frac{AV_{z=25}}{a*25^2 + AV_{z=25}}, \qquad (5.11)$$

It is important to note that although the vector of vertical mean values of voids, $\mathbf{\mu}_n$, was assumed to be parabolic and its mean value was forced to a constant value of 7%, the actual distribution that results from a stochastic realization (Equation 5.5) will not necessarily have this shape or mean value. Finally, the correlation of the air voids within the FAM was assumed to be anisotropic. Based on the compaction techniques used in the field, it is expected that the air void content of elements located at the same depth (i.e., in the same row or layer) will be highly correlated, while larger differences in this value are expected among elements at different vertical locations. Therefore, it was assumed that the horizontal autocorrelation distance of the

air voids within the FAM (L_x in Equation 5.9) was 35 mm, while the vertical autocorrelation distance (L_z in Equation 5.9) was set to 10 mm.

The covariance decomposition technique was implemented in Matlab® and 15 realizations were generated for each of the three cases considered (i.e., air voids with COV of 10%, 20%, and 30%). A typical realization of the air void random field within the FAM is illustrated in Figure 5.17.
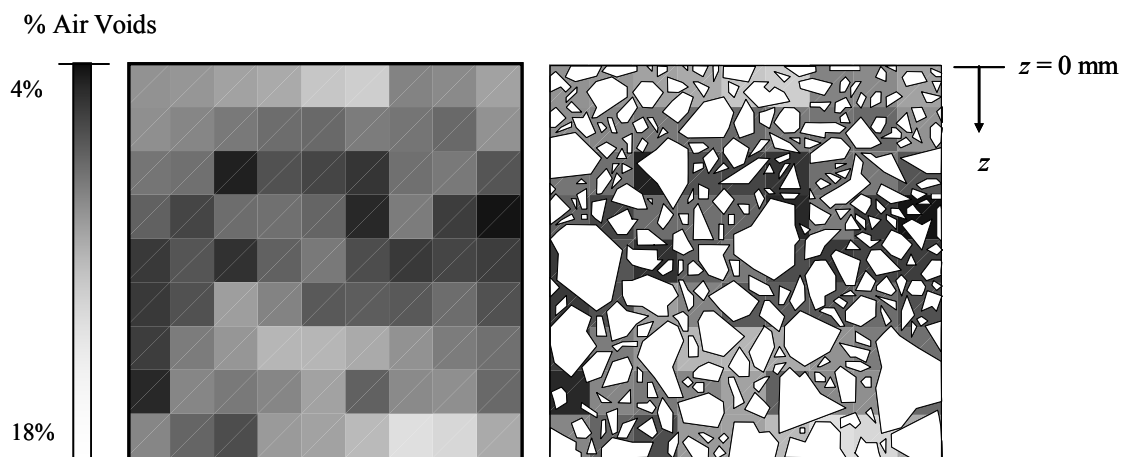
Figure 5.17. Example of the air void content characterizing the 100 divisions of the FAM that resulted from a stochastic realization of the random field

Material Properties and Models

Fine Aggregate Matrix – Moisture Diffusion Coefficient

Moisture diffusion coefficients within the FAM for each realization were determined based on the randomly generated internal air void distribution (Figure 5.17). In order to do so, a relationship characterizing the moisture diffusion coefficient of FAMs as a function of the total percent of air voids is required. Such a relationship can be numerically estimated if the diffusion coefficients of the two phases of the matrix (i.e., air voids and the portion of the FAM that is free of voids) are known. Thus, a two-dimensional finite element model of transient moisture

diffusion in Abaqus® was used to estimate the effective moisture diffusion coefficient of a FAM containing different air void contents (D_{FAM}). The moisture diffusion coefficient of the air phase was adopted from Geankoplis (1993) and the moisture diffusion coefficient of the FAM portion with no voids obtained during the first part of this chapter was used to characterize this phase of the matrix. The results showed the following good fit:

$$D_{FAM} = 3.2 * 10^{-7} \, AV + 1.25 * 10^{-7}, \text{ for } AV \in [0\%, 20\%] \tag{5.10}$$

where the moisture diffusion coefficient has units of mm²/s. This equation was used to transform the air voids in each stochastic realization into random values of the moisture diffusion coefficient of the FAM.

Fine Aggregate Matrix – Mechanical Response

Data collected by Kim et al. (2005) were adopted to characterize the viscoelastic response of a FAM material containing 7% air voids. These data are the same as those used in Chapters III and IV and in the first part of this chapter.

Two different cases were considered for the viscoelastic properties of the FAM:

- Case *A*: the instantaneous relaxation modulus, E_0, is a function of the internal air void distribution of the FAM.
- Case *B*: the viscoelastic material properties are constant within the FAM and are equal to those of a FAM with 7% air voids (Kim et al. 2005).

Note that the only difference between cases *A* and *B* is the assumptions made on the distribution of the mechanical properties of this material. Both cases contain the same FAM moisture diffusion distributions and will produce the same internal moisture profiles within the mixture. However, Case *A* provides a better representation of an actual mixture since, as it was demonstrated in the first part of this chapter, the air void structure highly influences the mechanical resistance of asphalt mixtures.

To the extent of the author's knowledge, there is no published information regarding the relationship between air void content and the viscoelastic response of FAM materials. Consequently, experimental and numerical data regarding the effect of air voids on the resistance of asphalt mixtures (Caro et al. 2010; Epps et al. 2002; Kassem 2009) were used to assume the

shape of the relationship between the initial viscoelastic instantaneous modulus and the percentage air voids for the FAM phase for microstructures in Case *B*:

$$E_0 = -5.0*10^{10} AV^3 + 8.0*10^9 AV^2 - 9.0*10^8 AV + 1.54*10^8 \tag{5.11}$$
$$\text{for } AV \in [4\%, 15\%],$$

where the units of E_0 are Pa. As an example, Figure 5.18 presents the average vertical air voids and instantaneous modulus distributions for the realization illustrated in Figure 5.17.
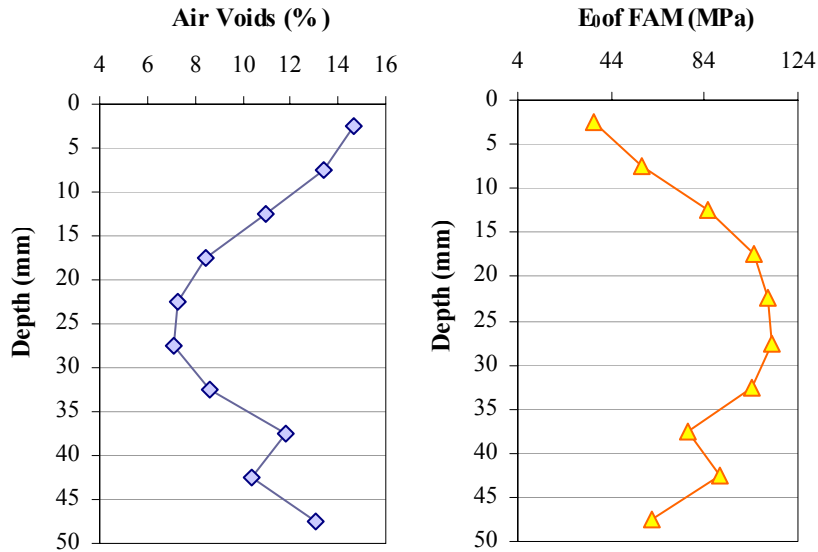
Figure 5.18. Vertical average distribution of the air voids and instantaneous modulus of the FAM for the realization shown in Figure 5.17

The moisture dependency of the mechanical response of the FMA was the same as the one used in the first part of this chapter (i.e., linear reduction of the relaxation modulus as a function of moisture content from 0%—dry condition—to 90% of this value under fully saturated conditions). The Poisson's ratio of the FAM was assumed to be moisture independent.

Coarse Aggregates and Adhesive Zones

The physical and mechanical properties of the coarse aggregates and the adhesive zones in the first part of this chapter were also used in this case. Tables 5.1 and 5.3 summarize the material properties of these components.

Modeling Methodology

The modeling methodology consisted of subjecting the 45 microstructures (i.e., 15 for each case of air void variability) to a 10-day moisture diffusion conditioning process. Afterwards, the microstructures were subjected to a force-controlled test. The mechanical test consisted of loading and unloading the microstructure for a total of 30 s with a monotonic load applied at a rate of 0.28N/s. Figure 5.19 illustrates the process. Notice that the only difference between this methodology and the one used earlier in this chapter (Figure 5.7) is the loading rate used for the mechanical simulation.
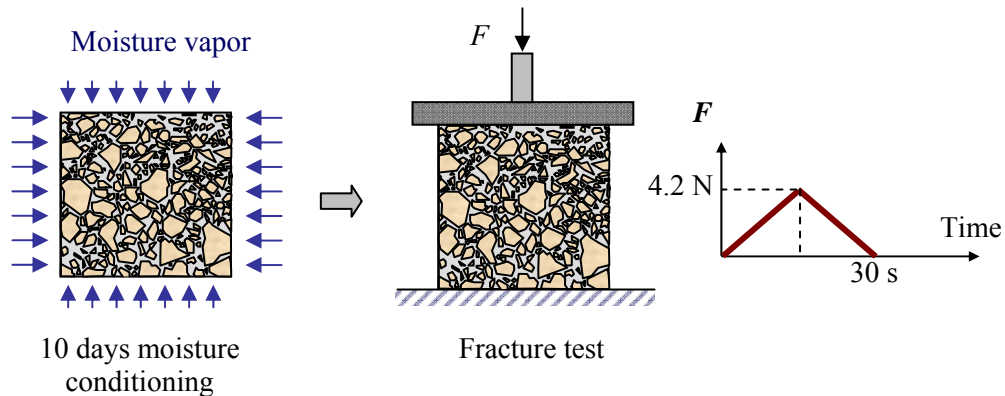
Figure 5.19. Representation of the modeling methodology

The same numerical implementation methodology used in the previous simulations was also used for this analysis (i.e., a two-step sequentially coupled technique). The type of finite elements and their sizes are the same used earlier in this chapter.

Results and Discussion

Total Air Void Content and Distribution within the Microstructures

Figure 5.20 illustrates moisture diffusion profiles within the microstructure on different days. Although the air void phase is not present within the microstructure, as it was in the first approach presented in this chapter, these profiles are strongly affected by the internal distribution of the voids within the materials.

| After 3 days of moisture diffusion | After 6 days of moisture diffusion | After 10 days of moisture diffusion |
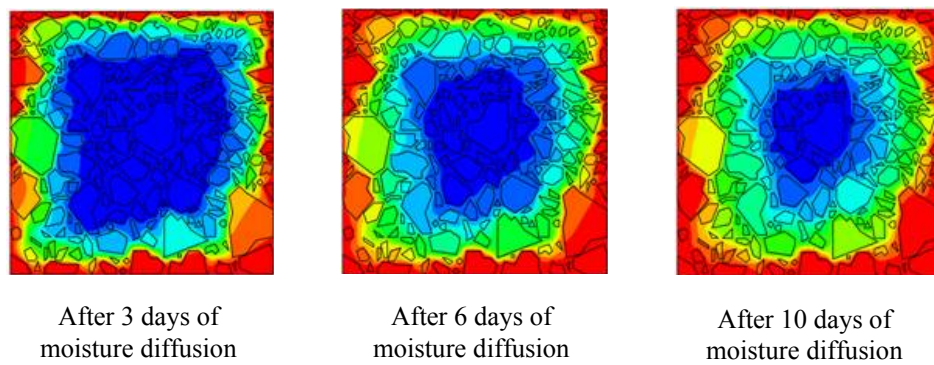
Figure 5.20. Evolution of the moisture diffusion profile through time (third realization of the second case, i.e., air void variability with COV of 20%)

Table 5.5 lists the mean values of the air void content corresponding to the 15 stochastic realizations obtained for each one of the three cases considered (i.e., air voids in the field with COV of 10%, 20% and 30%). An important consequence of the stochastic methodology is that although there is dispersion in the total air void content of the individual realizations, the average air void content among all realizations is very close to the target value of the compacted asphalt layer (i.e., 7%), as can be verified in this table.

Table 5.5. Total air void content for the stochastic generated distributions for asphalt mixtures containing different levels of variability

Air void variability in the field	Total air void content (%) for each stochastic realization (i.e., microstructures)														
	1	**2**	**3**	**4**	**5**	**6**	**7**	**8**	**9**	**10**	**11**	**12**	**13**	**14**	**15**
COV 10%	6.66	7.16	6.28	6.37	7.75	6.87	7.83	6.31	7.12	6.79	6.45	7.55	5.92	7.51	8.41
	Mean value: 7.00% COV: 10.03%														
COV 20%	6.01	6.97	4.77	7.32	7.29	5.94	8.04	7.21	6.10	10.43	8.22	5.45	7.73	7.94	5.26
	Mean value: 6.98% COV: 20.74%														
COV 30%	5.17	8.09	8.50	10.58	8.34	5.42	6.37	6.86	5.40	11.89	4.07	9.26	5.94	8.19	9.30
	Mean value: 7.56% COV: 29.07%														

It should be noted that the mechanical performance of two microstructures containing the same values of total air void content is not necessarily the same. This is due to the fact that the internal distribution of the air voids within the FAM is not identical in any two microstructures. For example, realizations 1 and 9 in the second case of Table 5.5 (i.e., coefficient of variation of air voids in the field equal to 20%) are very close to total air void: 6.01% and 6.1%, respectively; however, the internal distribution of the voids within the bulk matrix is dissimilar, as observed in Figure 5.21. Therefore, some differences can be expected in the mechanical response of both microstructures since they will not produce the same moisture profiles or have the same mechanical resistance.

Mechanical Performance of the Microstructures

Figure 5.22 illustrates a typical force vs. displacement curve that characterizes the mechanical response of one of the microstructures after the mechanical test. Figure 5.23 depicts the moisture profile at the interior of the microstructure after 10 days of moisture diffusion, the maximum deformation state of the sample during the mechanical test, and some details of the adhesive failure occurring at the aggregate-FAM interfaces. The total energy dissipated by the composite, *DE*—defined as the area within the force vs. displacement curve in Figure 5.22—and the stiffness, *K*—defined as maximum applied force divided by maximum displacement in the same

figure—were selected as the two evaluation parameters by which the role of the air void variability in the mechanical performance of the microstructures was studied.
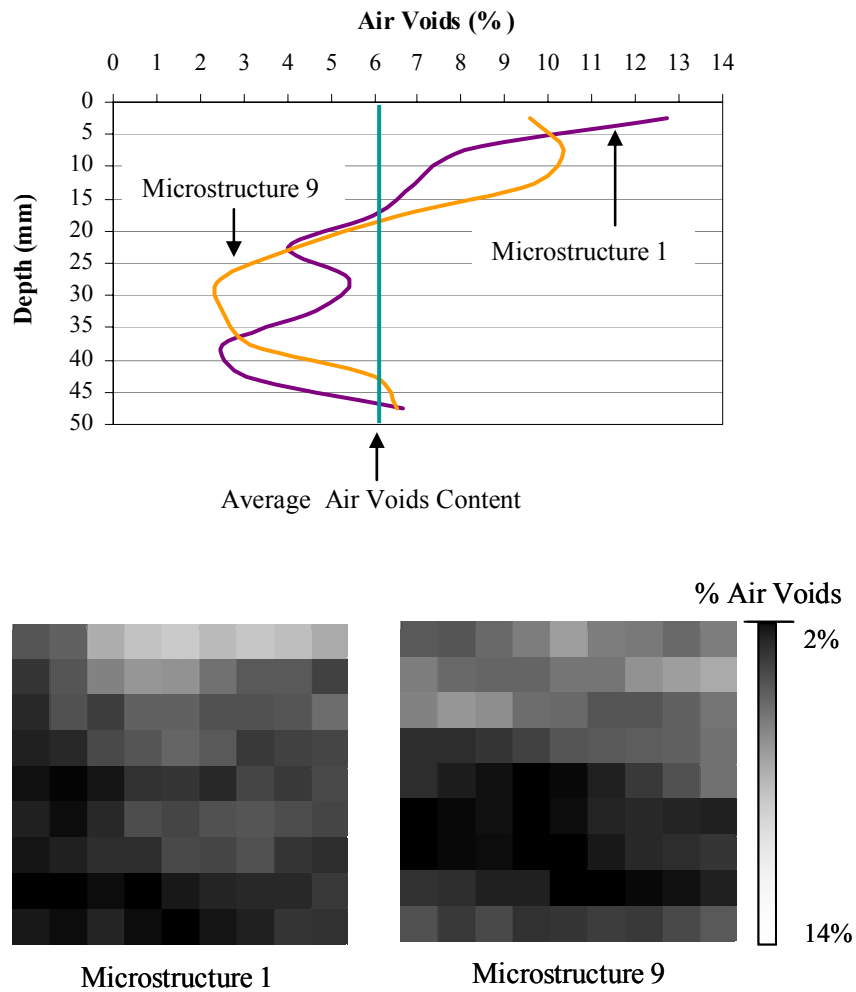
Figure 5.21. Internal air void distributions for two microstructures with similar total air void content (microstructures corresponding to an asphalt mixture with an air void content COV of 20%)
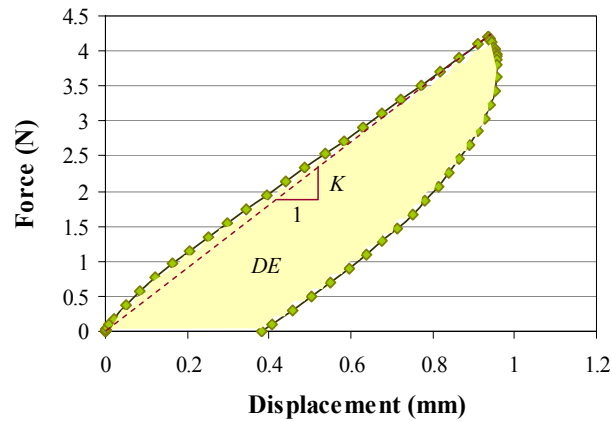
Figure 5.22. Force vs. displacement curve for one microstructure
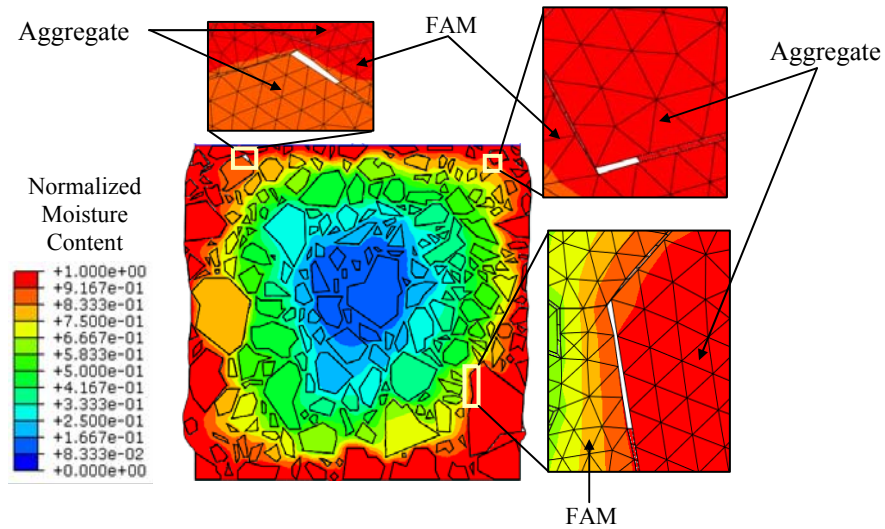
Figure 5.23. Maximum deformation of the microstructure, moisture profile, and adhesive failures

Table 5.6 summarizes the mean value, standard deviation and COV of the total dissipated energy and stiffness corresponding to the 15 realizations in each one of the three spatial air void variability cases. The table includes the results of the cases in which the mechanical properties of the FAM changed within the model according to the corresponding air

void content distributions (Case *A*), as well as the cases in which the viscoelastic properties of the FAM were held constant and equal to the response of a viscoelastic matrix containing 7% air voids (Case *B*).

Table 5.6. Statistical results of the total dissipated energy and overall stiffness for the three cases considered

	Variability in the Air Void Field	Mechanical properties of FAM[1]	Mean	Standard deviation (σ)	COV (%)
Dissipated Energy (*DE*, mJoules)	COV 10%	Case *A*	1.40	$4.04*10^{-2}$	2.9
		Case *B*	1.41	$1.94*10^{-2}$	1.4
	COV 20%	Case *A*	1.40	$7.28*10^{-2}$	5.2
		Case *B*	1.41	$3.17*10^{-2}$	2.3
	COV 30%	Case *A*	1.43	$1.09*10^{-1}$	7.6
		Case *B*	1.43	$4.39*10^{-2}$	3.1
Stiffness (*K*, N/mm)	COV 10%	Case *A*	4.33	$1.31*10^{-1}$	3.0
		Case *B*	4.30	$4.83*10^{-2}$	1.1
	COV 20%	Case *A*	4.35	$2.27*10^{-1}$	5.2
		Case *B*	4.30	$7.61*10^{-2}$	1.8
	COV 30%	Case *A*	4.25	$3.34*10^{-1}$	7.9
		Case *B*	4.31	$1.61*10^{-1}$	3.7

(1) Case *A*: the mechanical properties of the FAM change according the air void distribution within the asphalt matrix. Case *B*: the mechanical properties of the FAM are held constant within this phase.

As expected, an increase in the variability of the air void content within the asphalt mixture increases the variability of *DE* and *K*. Data in Table 5.6 show that the COV of *DE* and *K* in the asphalt mixture is between 25% and 30% of the magnitude of the COV of field air void contents for the microstructures in Case *A*. These variability ranges are in good agreement with those obtained from applying an empirical stiffness performance-model obtained from regression analysis of experimental data (Epps et al. 2002). The application of the regression model by Epps et al. (2002) shows that the COV of the stiffness of an asphalt mixture is 40% of the COV of the field air voids.

Data in Table 5.6 also demonstrate that the variability of the performance parameters (*DE* and *K*) of the microstructures that were assigned constant mechanical properties for the FAM (Case *B*) are always smaller than the variability observed for the same parameters of the microstructures whose FAM mechanical properties were made dependent on the internal air void distributions (Case *A*). The coefficients of variation of *DE* and *K* of the microstructures in Case *B* reflect the dispersion on the mechanical performance of the mixture that is exclusively due to the effect of the air void distribution on the moisture diffusion properties of the FAM. When the effects of the air void distribution on the structural resistance of the mixture are also included (Case A), the variability of the mechanical performance in the mixture rises by a factor of 2.

A careful analysis of the relationship that exists between the air void content of each microstructure and their associated mechanical responses (i.e., *DE* and *K*) for Cases *A* and *B* reveals interesting information. Figure 5.24 illustrates such relationships from where two main observations can be extracted:

1. The relationship between the total air void content of the microstructures and the total energy that the material dissipates during the mechanical test follows a linear relationship. This conclusion is valid for microstructures tested using constant and variable internal viscoelastic material properties of the FAM.

2. A critical air void content exists that changes the relationship between Cases *A* and *B*. Below this threshold value, which is approximately 7.5% (vertical dashed lines in Figure 5.24), the microstructures complying with the conditions of Case *A* demonstrated poorer mechanical responses than those having variable FAM properties. Over this threshold, however, mixtures of Case *A* performed better than those of Case *B*.

The first observation is important because it demonstrates the significance of the air void content in affecting the mechanical performance of asphalt mixtures subjected to moist environments. It is noteworthy that although these relationships provide a broad idea of the expected performance of the mixture, the actual mechanical response also depends on the internal distribution of the air voids and not only on its total percentage of air voids. The second observation is interesting because it suggests that the validity of the assumptions regarding the distribution of the viscoelastic properties within the FAM depends on the amount of air voids present in the mixture.

COV air voids in the field: 10%

COV air voids in the field: 20%

COV air voids in the field: 30%
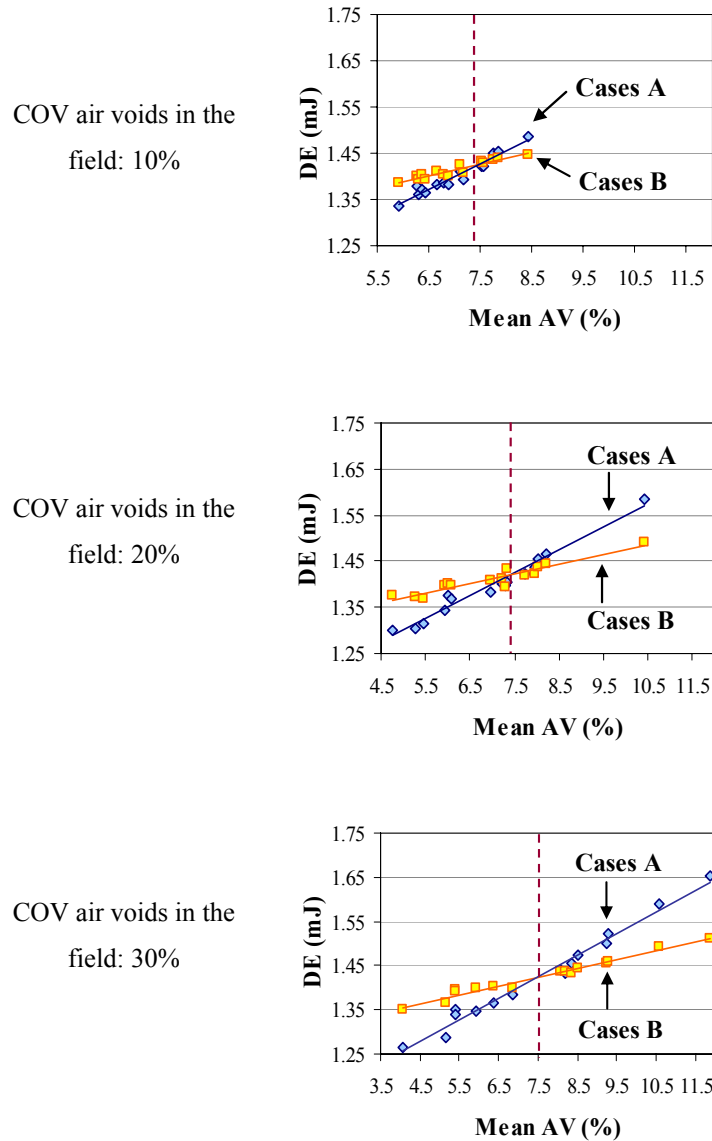
Figure 5.24. Relationship between the average total value of air voids in the microstructure and the dissipated energy

Microstructures in Case *A* are a better representation of a real asphalt mixture. However, its numerical implementation is complex since the geometrical section representing the FAM must be separated into several regions, each one having different moisture-dependent material

properties. Furthermore, it was observed that the adhesive failure at the aggregate-FAM interfaces within microstructures in Case *A* was more severe than that found in Case *B*. The initiation and propagation of adhesive cracks within the model are associated with numerical instability difficulties during the simulation. Therefore, a constant distribution of the mechanical properties of the bulk matrix (Case *B*) is desirable in order to minimize the difficulties associated with the numerical simulations. This assumption seems to be valid when the spatial variability of the field air voids is small (top part of Figure 5.21) and/or when the total air void content is located closer to the mean value of the random field (between 7 and 8%). However, when there is a considerable variability of the air void content in the field (e.g., COV of the air voids in the asphalt layer larger than 20%) and the total air void content of the mixture is greater than 7.5%, this assumption can underestimate the actual structural susceptibility of the mixture to develop damage in the presence of moisture (particularly adhesive damage). Similar results were found for the inverse linear relationship that exists between the total air void content of the microstructures and the mixture's stiffness (*K*).

Finally, the probabilistic distribution characterizing the mechanical response of the microstructures was explored based on the 15 realizations conducted for each of the three spatial field air void variability cases. A best fit analysis of the three sets of data of *DE* and *K* was performed using the *Crystall Ball*® software. The results suggest that the dissipated energy and the stiffness follow a three-parameter Weibull probabilistic distribution:

$$P(k) = \alpha\,\beta^{-1}\left[\frac{(k-c)}{\beta}\right]^{\alpha} - \exp\left\{-\left[\frac{(k-c)}{\beta}\right]\right\}, \qquad (10)$$

where *k* represents either *DE* or *K* and α, β, and *c* are the parameters of the distribution, usually denominated shape, scale, and locator, respectively. Figure 5.25 presents the cumulative probabilistic distribution for *DE* and *K* for the three air void fields considered and for those microstructures with variable FAM viscoelastic properties (Case *A*). The shape of the three cumulative distributions reflects the increase in variability of the air void content within the mixture (Table 5.6). The importance of knowing the probabilistic distribution is that it can be easily used to estimate the expected response of an asphalt mixture when subjected to moisture diffusion and mechanical loading. For example, information from Figure 5.24.b can be used to conclude that the probability that the stiffness of an asphalt mixture is smaller or equal to 4.4

N/mm after being subjected to a 10-day diffusion-conditioning period is between 50 and 60%, independently of the air void variability present in the field.

a)   b)
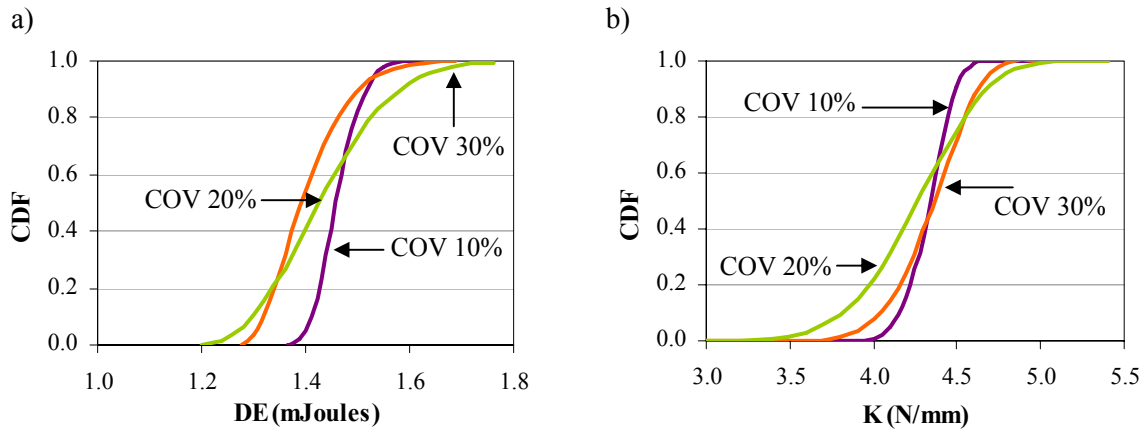
Figure 5.25. Cumulative probabilistic distribution of a) the total dissipated energy and b) stiffness (mixtures in Case *A*); the COV values correspond to the variability of the air void content of the asphalt mixture in the field

Summary and Conclusions

This chapter applied the coupled micromechanical model of moisture-induced damage formulated in Chapter III to study the influence of air voids on the mechanical performance of asphalt mixtures exposed to moisture diffusion processes. The analysis was conducted using two different probabilistic approaches. In the first approach the air void phase was directly included as a separate phase of the microstructure. In the second approach, the properties of the FAM within the microstructure were set to vary according to probable air void distributions.

The importance of the first modeling approach is that it is a realistic representation of an actual asphalt mixture. However, its main shortcoming is the complexity associated with the numerical implementation of the air void phase. The main advantage of the second methodology is that although it does not explicitly include the actual air void structure within the microstructure, it does take into consideration the role of the air void distribution and its variability on the susceptibility of the mixtures to experience moisture-induced damage. Thus, it

constitutes an efficient way of evaluating the effects of compaction processes on the mechanical performance of asphalt courses when compared to the first modeling approach.

The two modeling approaches are useful to understand the impact of amount and spatial variability of the air void phase on the durability and expected service life of asphalt courses. This information can be used as part of the design of inspection and maintenance programs and/or as an input parameter in life-cycle analyses of pavement structures.

Some of the main findings obtained from the results of the first modeling approach are herein summarized:

- The mechanical performance of asphalt mixtures with different percents of air voids in dry and moist conditions showed that an increase in the percent of air voids in the mixture produces: 1) a reduction in the structural integrity of the mixtures (i.e., a reduction in the bulk specific gravity of the mixture), and 2) an increase in the amount of moisture that reaches the interior of the microstructure after the moisture-conditioning period. These two effects increase the total energy dissipated by the moisture-conditioned mixtures and reduce their stiffness.

- The statistical bootstrapping technique was used to compute the 95% confidence interval of the mean value of the dissipated energy and stiffness, and to obtain the probabilistic distribution of these estimators. It was found that the relationship between the amount of air voids and the mean value of the two control parameters can be described by a third order polynomial function and that these estimators follow a normal distribution.

- Different mixtures with an intermediate level of air voids (7%) presented the highest dispersion of the data suggesting that the total content and spatial location of the individual voids has the greatest impact on the overall response of the mixture for this level of air voids.

- A reduction in the structural resistance of the mixtures caused solely by the presence of air voids (in the absence of moisture) was observed to be a major contributor to the overall degradation of the microstructures. However, the data also suggest that the marginal increase of the mechanical degradation per unit of air void content that is exclusively due to the presence of moisture within the mixture grows faster than the increase related to the deterioration caused by the addition of more air voids to the dry microstructure.

Some of the main conclusions obtained from the results of the second modeling approach include:

- Both the variability of the total air void content of an asphalt mixture in the field and the internal distribution of those voids within the microstructure of the mixture play an important role in the mechanical response of the composite.

- The COVs of the energy dissipated by the mixture and its stiffness are 25 to 30% of the magnitude of the COV characterizing the spatial variability of the air void content in the field. For example, if the COV of the air voids in an asphalt layer in the field is 20%, the COVs of the dissipated energy and stiffness of the mixture are expected to be in a range of 5 to 6%. This range was found to be close to reported data on the relationship between the air void variability and the expected mechanical response of the mixtures in the field.

- The use of air void-independent mechanical properties of the FAM is a fair simplification of the problem when the dispersion of the spatial field air voids is low (e.g., COV below 15%) and/or the total air void content of the microstructure is in a range of 7 to 8%.

- Weibull distributions were found to provide a good representation of the mechanical performance of the moisture-conditioned mixtures. This information is useful to conduct probabilistic analysis on the expected response of an asphalt mixture course that is characterized by certain dispersion of the of air void phase.

CHAPTER VI
SUMMARY, CONCLUSIONS, AND FUTURE WORK

General Observations

Moisture damage in asphalt mixtures is defined as the gradual degradation of the mechanical integrity of the material due to the presence of moisture within the microstructure (Chapter II). The importance of characterizing and understanding moisture damage is that this phenomenon is considered a major cause of the deterioration of asphalt mixtures in pavement structures.

Several studies have been conducted during the last decades to identify, characterize, prevent and remediate moisture damage in asphalt pavements. The main approach to the moisture damage problem has focused on the macroscale level, i.e., analyzing and characterizing the effects of moisture on asphalt mixtures as a whole. This tendency, however, has changed during recent years and new works conducted at the microscale level have permitted a better understanding of the kinetics of the phenomenon. In general, current approaches to characterize moisture damage in asphalt mixtures range from qualitative visual assessment of binder detached or stripped form the aggregates to quantitative parameters based on fracture mechanics, thermodynamics and continuum mechanics principles. In the second part of Chapter II, a new classification of the existing methodologies to characterize moisture damage was proposed. It was concluded that approaches that considered more than one parameter or material property to evaluate the susceptibility to damage (i.e., multiple moisture damage ratios approach)—in particular, those with an analytical background—can provided a better characterization of the deterioration processes occurring within the mixture.

Despite the important advancements that have been achieved regarding the moisture-damage phenomenon, there is still many uncertainties associated with the causes and mechanisms of moisture deterioration, and with the individual contribution of each damage mechanism to the overall damage. Therefore, a micromechanical model of moisture damage in asphalt mixtures was developed to gain more understanding of this topic.

The numerical model was applied to analyze the influence of different physical and mechanical material properties and diverse characteristics of the air void structure on the mechanical performance of asphalt mixtures subjected to moisture diffusion processes. This

model can be further used to study the effects of other geometrical, volumetric, physical and/or mechanical characteristics of the mixture on the initiation and evolution of moisture-related degradation processes. Moreover, the model can be used to study the evolution of damage in the asphalt course of a real pavement in which environmental conditions—especially relative humidity—and traffic loading change through time. The following sections present a summary of the main findings obtained in the different study areas of this dissertation.

Formulation of a Micromechanical Model of Moisture-Induced Damage

A micromechanical model of moisture-induced damage was developed and implemented using a sequentially coupled methodology in the finite element package Abaqus®. The model couples the presence of diffused moisture within the microstructure with the mechanical performance of the mixture. The coupling is achieved in two different ways: 1) by degrading the viscoelastic material properties of the asphalt matrix (i.e., cohesive deterioration), and 2) by degrading the mechanical and fracture properties of the aggregate-asphalt matrix adhesive bonds (i.e., adhesive degradation and failure).

In Chapter III, the model was used to simulate damage in a simplified microstructure of an asphalt mixture. The mechanical performance of the microstructure model was evaluated after subjecting it to different moisture diffusion periods and to the same load-controlled mechanical conditions. The results showed that:

- The model successfully integrated the presence of moisture with the reduction of the structural loading capacity of the asphalt matrix and the adhesive bonds.

- Microstructures that were subjected to longer periods of moisture diffusion presented more and longer adhesive cracks and larger levels of deformation within the asphalt matrix.

- The presence of different moisture diffusion profiles within the microstructures significantly impacted the adhesive failure pattern at the interfaces of aggregates and FAM (location and rate of cracks initiation and evolution).

- Adhesive fracture processes at the aggregates-asphalt matrix interfaces were also observed to impact the mechanical response of the surrounding FAM material.

- An evaluation of the level of stresses within the bulk matrix suggested that the fracture locus of the microstructure tends to change from cohesive—in the absence of moisture—to adhesive—under the presence of moisture.

Micromechanical Modeling of the Influence of Material Properties on Moisture-Induced Damage in Asphalt Mixtures

The micromechanical model was used in Chapter IV to study the effect of different material properties on the susceptibility of asphalt mixtures to moisture damage. The modeling methodology consisted of subjecting different asphalt mixtures to the same moisture conditioning and mechanical loading conditions. The mixtures resulted from combining diverse physical and mechanical material properties of two phases of the microstructure model (i.e., bulk asphalt matrix, FAM and coarse aggregates). The modeling technique took into consideration that the properties of the adhesive interfaces (i.e., adhesive zones) are unique for each combination of aggregates and FAM. The mechanical performance of a total of 24 material combinations was analyzed by means of the maximum force that was resisted by the microstructure. The results from the simulations showed the following:

- The moisture diffusion coefficients of the components of the mixture were observed to play a crucial role in the development of damage. Mixtures with larger diffusion coefficients produced more aggressive moisture profiles, which were associated with mixtures that performed poorer and experienced more damage.

- A difference of one order of magnitude in the moisture diffusion coefficient of the FAM reduced the maximum force experienced by the mixture at a given displacement by up to 3.7 times with respect to a similar dry mix.

- A difference of two orders of magnitude in the moisture diffusion coefficient of the aggregates reduced the maximum force of resistance of the mixtures from 1.2 to almost 2 times in comparison with similar dry mixes.

- The properties of the adhesive bonds were also observed to significantly influence the moisture susceptibility of the mixtures. The effect of moisture on mixtures containing less-resistant adhesive bonds was 14% more pronounced than in those mixtures containing strong adhesive bonds.

Effect of the Internal Void Structure on the Mechanical Performance of Asphalt Mixtures Subjected to Moisture Diffusion Processes

Two different probabilistic-based approaches were used in Chapter V to study the influence of the air void variability and distribution on the mechanical performance of asphalt mixtures. In both cases, the micromechanical model introduced in Chapter III was used to simulate moisture diffusion and mechanical loading in a 50 mm by 50 mm microstructure sample that represented the cross-section of a real asphalt mixture. The total dissipated energy by the mixtures and its stiffness were used to evaluate the mechanical performance of the material. These parameters were obtained after subjecting the mixtures to a 10-day moisture diffusion period and a 30-second monotonic force-controlled loading experiment.

The main difference between the two modeling approaches was the methodology used to incorporate the effect of the air void phase within the microstructure of the mixture. In the first approach, the air voids were explicitly included as a separate phase of the microstructure. In this case, a log-normal probabilistic distribution was used to generate different sets of air void sizes that were randomly located within the microstructure. The influence of three main levels of total air void content (4%, 7% and 10%) on the generation of damage was analyzed. In the second approach, the material properties of different subsections of the FAM phase of the microstructure were made dependent on the air void variability and internal distribution within an asphalt mixture layer. In this case, asphalt mixtures containing three different levels of air void variability in the field were considered (i.e., spatial coefficient of variation of the air voids in the field of 10%, 20% and 30%), and a stochastic technique was used to generate probable air void distributions within the FAM.

Some general conclusions obtained from comparing the two modeling approaches include:

- Both methodologies were found to be useful in understanding the impact of the air void phase on the durability and mechanical properties of asphalt layers.
- The first modeling approach is a more realistic representation of an actual asphalt mixture. The main shortcoming of this approach is the complexity associated with its numerical implementation.

- Although the second modeling approach does not includes the actual air void structure within the microstructure, it does account for the presence and internal distribution of the air void phase.

Specific conclusions that resulted from the first modeling approach include:

- An increase in the amount of air voids in the microstructure of asphalt mixtures was observed to have two main impacts: 1) reduction of the structural integrity of the mixtures in dry conditions, and 2) increase of the amount of moisture that can reach the interior of the microstructure. The consequence of these two effects result was an increase of the total energy dissipated by the moisture-conditioned mixture and a reduction of its stiffness.

- The application of the statistical bootstrapping technique lead to the finding that the relationship between the amount of air voids (in a range of 0 and 10%) and the mean value of the two evaluation parameters (i.e., dissipated energy and stiffness) can be represented by a third order polynomial function. Furthermore, the results also showed that the statistical estimators representing the mean value of both parameters follow a normal probabilistic distribution.

- The total amount and spatial distribution of the individual voids at an intermediate level of total air void content (i.e., 7%) were found to have the greatest impact on the overall mechanical response of the asphalt mixture.

- The reduction of the structural resistance of the mixtures that resulted from increasing the total air void content was observed to be a major contributor to the poor mechanical performance reported in the moisture-conditioned microstructures.

The main conclusions obtained from the second modeling approach are:

- The variability (in terms of COV) of the dissipated energy and overall stiffness of the mixture was close to 25 to 30% of the magnitude of the variability of the air void content in the field. These results were found to be in good agreement with reported data on the influence of air void variability on the expected mechanical performance of the mixtures in the field.

- The relationship between the air void content of the microstructures and their mechanical performance followed a linear relationship.

- Weibull distributions were found to provide a good representation of the mechanical performance of moisture-conditioned asphalt mixtures that contain different levels of field air void spatial variability (i.e., COV of 10, 20 and 30%).

Future Research Work

This section provides some future research tasks related to the general phenomenon of moisture damage in asphalt mixtures, and to the specific model developed in this dissertation.

Moisture Damage in Asphalt Mixtures

Future work in the area of moisture-induced damage in asphalt mixtures includes:

- Development of efficient tools to assess compatibility between aggregates and binders in terms of resistance to moisture damage,
- development of new (or improvement of current) procedures to characterize moisture damage in asphalt mixtures. These procedures should include properties of both fine aggregate matrices and whole mixtures,
- validation of laboratory-based accelerated moisture conditioning procedures that are used to simulate moisture damage in field (i.e., moisture conditioning processes),
- development of new probabilistic models, and improvement of existing models, to estimate moisture damage and to make better predictions of the expected performance life of asphalt mixtures in the field,
- completion and/or development of databases with quantitative records of the moisture-related performance of asphalt mixtures in the field. Solaimanian et al. (2003) have pointed out that the "development of better databases for calibration of laboratory results with field data is vital for development of better laboratory tests for moisture sensitivity/stripping and other distress mechanisms,"
- continuation of the development and improvement of mathematical models of moisture-induced damage at the continuum and microscopic levels,
- development of experimental procedures in order to obtain the diffusion coefficients of the constitutive phases of the mixtures,

- development of experimental procedures to obtain the fracture properties of aggregates-asphalt matrix adhesive bonds in the absence and in the presence of moisture, and

- development of experimental procedures to determine the effect of moisture on the viscoelastic material properties of the FAM phase of the mixtures.

The last three tasks are particularly important to improve current research efforts on numerical modeling of moisture damage. Most of these tasks have recently initiated by different research groups (e.g., Texas A&M University, University of Wisconsin-Madison, University of Nebraska, University of Nottingham, Delft University of Technology, among others), and are currently under development.

Micromechanical Model of Moisture-Induced Damage

In terms of the coupled micromechanical model and the modeling methodologies used to study the effect of different characteristics and/or properties of asphalt mixtures on the susceptibility of asphalt mixtures to moisture damage, the following future work can be conducted:

- Calibration of the fracture properties of the adhesive zones of the model by means of experimental results on the effects of moisture on the fracture properties of the adhesive zones and on the viscoelastic properties of the asphalt matrix. Currently, some experimental work in this direction is being carrying out at Texas A&M,

- improvement of the mathematical formulation of the model by explicitly including thermodynamics considerations. In the current model, moisture diffusion is modeled by means of Fick's second law. However, moisture diffusion in asphalt mixtures is driven by the existence of a relative humidity gradient that can be described by a thermodynamic potential (Bhasin 2007; Lytton 2007). Besides, thermodynamic potentials are also present locally at the aggregate-asphalt matrix interfaces, influencing the moisture saturation and delaminating processes in these zones,

- development of new studies to investigate the role of other characteristics and properties of the mixture (e.g., gradation, morphologic characteristics of the aggregate, type of asphalt binder, etc.) on the development of moisture damage,

- development of new studies to investigate the effects of different traction-separation laws of the adhesive zones on the initiation and evolution of adhesive fracture (e.g.,

a linear or non-linear viscoelastic constitutive relationship prior to damage initiation),

- development of new studies to investigate the susceptibility of asphalt mixtures to moisture-damage when subjected to variable and realistic environments and mechanical loading conditions (like those present in the field) and, eventually,

- improvement of the model to also include other modes of moisture transport or different mechanisms of damage within the microstructure (e.g., pore pressure within the air void, liquid water flow, etc.).

REFERENCES

ABAQUS. (2007). *Abaqus user's manual version 6.7*, Hibbit, Karlsson & Sorenson, Inc., Pawtucket, R.I.

Abo-Qudais, S., and Al-Shweily, H. (2007). "Effect of aggregate properties on asphalt mixtures stripping and creep behavior." *Construction and Building Materials*, 21, 1886-1898.

Aiello, M. A., Leone, M., Aniskevich, A. N., and Starkova, O. A. (2006). "Moisture effects on elastic and viscoelastic properties of CFRP rebars and vinylester binder." *Journal of Materials in Civil Engineering (ASCE)*, 18(5), 686-691.

Airey, G. D., and Choi, Y.-K. (2002). "State of the art report on moisture sensitivity test methods for bituminous pavement materials." *Road Materials and Pavement Design*, 3/4, 355-372.

Airey, G. D., Collop, A. C., Zoorob, S. E., and Elliot, R. C. (2007). "Moisture damage assessment of asphalt mixtures using the UK SATS test." *Transportation Research Board 86th Annual Meeting*, Washington, D.C. (in CD-ROM).

Aksoy, A., Samlioglu, K., Tayfur, S., and Ozen, H. (2005). "Effects of various additives on the moisture damage sensitivity of asphalt mixtures." *Construction and Building Materials*, 19, 11-18.

Al-Omari, A., and Masad, E. (2004). "Three dimensional simulation of fluid flow in X-ray CT images of porous media." *International Journal for Numerical and Analytical Methods in Geomechanics*, 28(13), 1327-1360.

Al-Omari, A., Tashman, L., Masad, E., Cooley, A., and Harman, T. (2002). "Proposed methodology for predicting HMA permeability." *Journal of the Association of Asphalt Pavement Technologists (AAPT)*, 71, 30-58.

Al-Swalimi, S., and Terrel, R. L. (1992). "Water sensitivity of asphalt-aggregate mixtures test development." *Rep. No. SHRP-A-403*, Strategic Highway Research Program, Washington D.C.

Alfano, G. (2006). "On the influence of the shape of the interface law on the application of cohesive-zone models." *Composites Science and Technology*, 66, 723-730.

Allan, K. W. (1992). In *Handbook of adhesion: Mechanical theory of adhesion*, edited by D.E. Packham. Longman Group, UK Ltd, London.

Allen, K. W. (1993). "Some reflections on contemporary views of theories of adhesion." *International Journal of Adhesion and Adhesives*, 13(2), 67-72.

Apeagyei, A. K., Buttlar, W. G., and Dempsey, B. J. (2006). "Moisture damage evaluation of asphalt mixtures using AASTO T 283 and DC(T) fracture test." *10th International Conference on Asphalt Pavements*, Quebec, Canada 742-753.

Arambula, E., Caro, S., and Masad, E. (2009a). "Experimental measurements and numerical simulation of water vapour diffusion through asphalt pavement materials." *Journal of Materials in Civil Engineering (ASCE)*, (submitted for evaluation).

Arambula, E., Garboczi, E. J., Masad, E., and Kassem, E. (2009b). "Numerical analysis of moisture vapor diffusion in asphalt mixtures using digital images." *RILEM Materials and Structures Journal*, (in press).

Arambula, E., Masad, E., and Martin, A. E. (2007). "The influence of air void distribution on the moisture susceptibility of asphalt mixes." *Journal of Materials in Civil Engineering (ASCE)*, 19(8), 655-664.

ASTM. (2007). "Standard test method for water vapor transmission of materials." Annual book of ASTM standards, ASTM International, West Conshohocken, PA.

Atud, T. J., Kanitpong, K., and Martono, W. (2007). "Laboratory evaluation of hydrated lime application process in asphalt mixture for moisture damage and rutting resistance." *Transportation Research Board 86th Annual Meeting*, Washington, D.C. (in CD-ROM).

Bagampadde, U., Isacsson, U., and Kiggundu, B. M. (2004). "Classical and contemporary aspects of stripping in bituminous mixes." *Road Materials and Pavement Design*, 5(1), 7-43.

Bagampadde, U., Isacsson, U., and Kiggundu, B. M. (2005). "Influence of aggregate chemical and mineralogical composition on stripping in bituminous mixtures." *International Journal of Pavement Engineering*, 6(4), 229-239.

Bagampadde, U., Isacsson, U., and Kiggundu, B. M. (2006). "Impact of bitumen and aggregate composition on stripping in bituminous mixtures." *Materials and Structures*, 39, 303-315.

Barenblatt, G. I. (1959). "On equilibrium cracks formed in brittle fracture, general concepts and hypotheses." *Journal of Applied Mathematics and Mechanics* 23(3), 622-633.

Barrie, P. J. (2000). "Characterization of porous media using NMR methods." *Annual Reports on NMR Spectroscopy*, 41, 265-316.

Benzeggagh, M. L., and Kenane, M. (1996). "Measurement of mixed-mode delamination fracture toughness of unidirectional glass/epoxy composites with mixed-mode bending apparatus." *Composites Science and Technology*, 56, 439-449.

Bhasin, A. (2006). "Development of methods to quantify bitumen-aggregate adhesion and loss of adhesion due to water." Ph.D. dissertation, Texas A&M University, College Station, Texas.

Bhasin, A. (2007). "Material properties to characterize and model moisture damage in asphalt mixtures." Second International Workshop on Moisture-Induced Damage, College Station, Texas (in CD-ROM).

Bhasin, A., Chowdhury, A., Button, J., and Little, D. N. (2006a). "Evaluation of material property tests to predict moisture susceptibility of HMA." *10th International Conference on Asphalt Pavements*, Quebec, Canada, 701-710.

Bhasin, A., Little, D., Bommavaram, R., and Vasconcelos, K. L. (2008). "A framework to quantify the effect of healing in bituminous materials using material properties." *Road Materials and Pavement Design*, 9, 219-242.

Bhasin, A., and Little, D. N. (2007). "Characterization of aggregate surface energy using the Universal Sorption Device." *Journal of Materials in Civil Engineering (ASCE)*, 19(8), 634-641.

Bhasin, A., Little, D. N., Vasconcelos K.L., and Masad, E. (2007). "Use of surface free energy to identify moisture sensitivity of materials for asphalt mixtures." *Transportation Research Board 86th Annual Meeting*, Washington D.C. (in CD-ROM).

Bhasin, A., Masad, E., Little, D., and Lytton, R. (2006b). "Limits on adhesive bond energy for improved resistance of hot mix asphalt to moisture damage." *Transportation Research Record: Journal of the Transportation Research Board*, 1970 3-13.

Birgisson, B., Roque, R., and Page, G. (2003). "Evaluation of water damage using hot mix asphalt fracture mechanics." *Journal of the Association of Asphalt Paving Technologists (AAPT)*, 73, 424-462.

Birgisson, B., Roque, R., and Page, G. (2004). "The use of a performance-based fracture criterion for the evaluation of moisture susceptibility in hot mix asphalt." *Transportation Research Record: Journal of the Transportation Research Board*, 1891, 51-61.

Birgisson, B., Roque, R., Tia, M., and Masad, E. (2005). "Development and evaluation of test methods to evaluate water damage and effectiveness of antistripping agents." *Rep. No. 4910-4504-722-12*, Florida Department of Transportation and University of Florida at Gainesville.

Blackman, B. R. K., and Kinloch, A. J. (2001). "Fracture tests for structural adhesive joints." In *Fracture Mechanics Testing Methods for Polymers, Adhesives and Composites*, edited by A.Pavan, D.R.Moore and J.G.Williams. Elsevier Science, Amsterdam, 225-270.

Bocci, M., and Colagrande, S. (1993). "The adhesiveness of modified road bitumens." *5th Eurobitume Congress*, Stockholm, Sweden (Paper 1.61).

Bowles, J. E. (1984). *Physical and geotechnical properties of soils*, 2nd Ed., McGraw-Hill, New York.

Brown, E. R., Haini, M. R., Cooley, A., and Hurley, G. (2004). "Relationship of air voids, lift thickness, and permeability in hot mix asphalt pavements." *Rep. No. NCHRP 531*, Transportation Research Board of the National Academies, Washington, D.C.

Camanho, P. P. (2005). "Advances in the simulation of damage and fracture of composite structures." *Proceedings of the X Reunion de Usuarios de Abaqus*, Pamplona, Spain.

Camanho, P. P., and Davila, C. G. (2002). "Mixed-mode decohesion finite elements for the simulation of delamination in composite materials." National Aeronautics and Space Administration (NASA), Langley Research Center, Virginia (USA).

Camanho, P. P., Davila, C. G., and de Moura, M. F. (2003). "Numerical simulation of mixed-mode progressive delamination in composite materials." *Journal of Composite Materials*, 37(16), 1414-1438.

Caro, S., Masad, E., Bhasin, A., and Little, D. (2008a). "Moisture susceptibility of asphalt mixtures, part I: Mechanisms." *International Journal of Engineering Pavements*, 9(2), 81-98.

Caro, S., Masad, E., Bhasin, A., and Little, D. (2009). "A coupled micromechanical model of moisture-induced damage in asphalt mixtures." *Journal of Materials in Civil Engineering (ASCE)*, (in press).

Caro, S., Masad, E., Bhasin, A., Little, D., and Sanchez-Silva, M. (2010). "Probabilistic modeling of the effect of air voids on the mechanical performance of asphalt mixtures subjected to moisture diffusion." *Journal of the Association of Asphalt Paving Technologists (AAPT),* (submitted for evaluation).

Caro, S., Masad, E., Airey, G., Bhasin, A., and Little, D. N. (2008b). "Probabilistic analysis of fracture in asphalt mixtures caused by moisture damage." *Transportation Research Record: Journal of the Transportation Research Board*, 2053, 28-36.

Castelblanco, A. (2004). "Probabilistic analysis of air void structure and its relationship to permeability and moisture damage of hot mix asphalt." M.S. thesis, Texas A&M University, Colllege Station, Texas.

Chandra, N., Li, H., Shet, C., and Ghonem, H. (2002). "Some issues in the application of cohesive zone models for metal–ceramic interfaces." *International Journal of Solids and Structures*, 39, 2827-2855.

Chehab, G. R., O`Quinn, E., and Kim, Y. R. (2000). "Specimen geometry study for direct tension test based on mechanical tests and air void variation in asphalt concrete specimens compacted by Superpave giratory compactor." *Transportation Research Record*, 1723, 125-132.

Chehab, G. R., Seo, Y., and Kim, Y. R. (2007). "Viscoelastoplastic damage characterization of asphalt–aggregate mixtures using digital image correlation." *International Journal of Geomechanics (ASCE)*, 7(2), 111-118.

Chen, C., Tayebali, A. A., and Knappe, D. R. U. (2006). "A procedure to quantify organic antistrip additives in asphalt binders and mixes." *Journal of Testing and Evaluation*, 34(4), 269-274.

Chen, J.-S., Lin, K.-Y., and Young, S.-Y. (2004). "Effects of crack width and permeability on moisture-induced damage of pavements." *Journal of Materials in Civil Engineering (ASCE)*, 16(3), 276-282.

Cheng, D. (2002). "Surface free energy of asphalt-aggregate system and performance analysis of asphalt concrete based on surface energy." Ph.D. dissertation, Texas A&M University, College Station, Texas.

Cheng, D., Little, D. N., Lytton, R. L., and Holste, J. C. (2002). "Use of surface free energy properties of the asphalt-aggregate system to predict moisture damage potential." *Journal of the Association of Asphalt Pavement Technologists (AAPT)*, 71, 59-88.

Collop, A. C., Choi, Y., Airey, G. D., and Elliott, R. C. (2004). "Development of the saturation ageing tensile stiffness (SATS) test." *ICE Journal of Transport*, 157(TR3), 163-171.

Cooley Jr., L. A., Prowell, B. D., and Brown, E. R. (2002). "Issues pertaining to the permeability characteristics of coarse-graded Superpave mixes." *Rep. No. 02-07*, National Center for Asphalt Technology, Auburn University.

Copeland, A. (2005). "Moisture in asphalt pavements in the united states: A financial perspective." *First International Workshop on Moisture Damage* Delft, the Netherlands, (in CD-ROM).

Copeland, A., Youthcheff, J., Kringos, N., and Scarpas, A. (2007). "Measurement of aggregate-mastic bond strength in the presence of moisture: a combined experimental-computational study." *Transportation Research Board 86th Annual Meeting*, Washington, D.C. (in CD-ROM).

Copeland, A. R. (2007). "Influence of moisture on bond strength of asphalt-aggregate systems." Ph.D. dissertation, Vanderbilt University, Nashville, Tennessee.

Curtis, C. W., Ensley, K., and Epps, J. (1993). "Fundamental properties of asphalt-aggregate interactions including adhesion and adsorption." *Rep. No. SHRP-A-341*, Strategic Highway Research Program, Washington, D.C.

D'Angelo, J., and Anderson, R. M. (2003). "Material production, mix design & pavement design effects on moisture damage." *Moisture Sensitivity of Asphalt Pavements: A National Seminar*, San Diego, California, 187-201.

Davison, A. C., and Hinkley, D. (2006). *Bootstrap methods and their applications*, Cambridge University Press, Cambridge, UK.

Delagnes, P., and Barba, D. (1995). "A markov random field for rectilinear structure extraction in pavement distress image analysis." *International Conference on Image Processing*, Washington, D.C.

Dobchuk, B. S., Barbour, S. L., and Zhou, J. (2004). "Prediction of water vapor movement through waste rock." *Journal of Geotechnical and Geoenvironmental Engineering*, 130 (3), 293-302.

Dugdale, D. (1960). "Yielding of steel sheets containing slits." *Journal of Mechanics and Physics of Solids*, 8, 100-104.

Efron, B. (1979). "Boostrap mehods: Another look at the jacknife." *The Annal of Statistics*, 7, 1-26.

El-Kadi, A. I., and Williams, S. A. (2000). "Generating two-dimensional fields of autocorrelated, normally distributed parameters by the matrix decomposition technique." *Ground Water*, 38(4), 523-532.

Emery, J., and Seddik, H. (1997). "Moisture damage of asphalt pavements and antistripping additives: Causes, identification, testing, and mitigation." Transportation Association of Canada, Ottawa, Canada.

Epps, J., Hand, A., Seeds, S., Schulz, T., Alavi, S., Ashmore, C., Monismith, C., Deacon, J. A., Havery, J. T., and Leahy, R. (2002). "Recommended performance-related specification

for hot-mix asphalt construction: Results of the Westrack project." *Rep. No. NCHRP 455*, National Academies Press, Washington D.C.

Fenton, G. A., and Griffiths, D. V. (2008). *Risk assessment in geotechnical engineering*. John Wiley and Sons, New Jersey.

Ferguson, T. P., and Qu, J. (2006). "Predictive model for adhesion loss of molding compounds from exposure to humid environments." *IEEE 2006 Electronic Components and Technology Conference*, 1408-1414.

Fernando, M., Harjoprayitno, W. W., and Kinloch, A. J. (1996). "A fracture mechanics study of the influence of moisture on the fatigue behavior of adhesively bonded aluminum-allow joints." *International Journal of Adhesion and Adhesives*, 16(2), 113-119.

Ferracin, T., Landis, C. M., Delannay, F., and Pardoen, T. (2003). "On the determination of the cohesive zone properties of an adhesive layer from the analysis of the wedge-peel test." *International Journal of Solids and Structures*, 40, 2889-2904.

FHWA. (2006). "Highway statistics 2005." US Department of Transportation, <http://www.fhwa.dot.gov/policy/ohim/hs06/index.htm> (April 14th, 2009).

Field, F., and Phang, W. A. (1967). "Stripping in asphaltic concrete mixes, observations and test procedures." *Canadian Technical Asphalt Association*, 12, 61-68.

Fromm, H. J. (1974). "The mechanisms of asphalt stripping from aggregate surfaces." *Journal of the Association of Asphalt Paving Technologists (AAPT)*, 43, 191-219.

Garcia-Bengochea, I. (1978). "The relation between permeability and pore size distribution of compacted clayey silts." M.S. thesis, Purdue University, West Lafayette, Indiana.

Gdoutos, E. E. (2005). *Fracture mechanics: An introduction*, Springer, The Netherlands.

Geankoplis, C. J. (1993). *Transport processes and unit operations*, PTR Prentice Hall Inc., Englewood Cliffs, New Jersey.

Golub, G. H., and Van Loan, C. F. (1996). *Matrix computations*, 3rd Ed., Baltimore, Maryland.

Graham-Brady, L., and Xu, X. F. (2008). "Stochastic morphological modeling of random multiphase materials." *Journal of Applied Mechanics (ASME)*, 75(6), 174-186.

Graham, L. L., and Deodatis, G. (2001). "Response and eigenvalue analysis of stochastic finite element systems with multiple correlated material and geometric properties." *Probabilistic Engineering Mechanics*, 16(1), 11-29.

Graham, M. A. (2009). "Damaged viscoelastic-viscoplastic model for asphalt mixes." M.S. thesis, Texas A&M University, College Station, Texas.

Hefer, A. W., Little, D. N., and Lytton, R. L. (2005). "A synthesis of theories and mechanisms of bitumen-aggregate adhesion including recent advances in quantifying the effects of water." *Journal of the Association of Asphalt Paving Technologists (AAPT)*, 74, 139-196.

Hicks, R. G. (1991). "Moisture damage in asphalt concrete: Synthesis of highway practice." *Rep. No. NCHRP 175*, National Cooperative Highway Research Program, Washington, D.C.

Hicks, R. G., Santucci, L., and Aschenbrener, T. (2003). "Introduction and seminar objectives." *Moisture Sensitivity of Asphalt Pavements: A National Seminar*, San Diego, California.

Hua, Y., Crocombre, A. D., Wahab, M. A., and Ashcroft, I. A. (2006). "Modelling environmental degradation in EA9321-bonded joints using a progressive damage failure model." *The Journal of Adhesion*, 82, 135-160.

Huang, B., Mohammad, L., Raghavendra, A., and Abadie, C. (1999). "Fundamentals of permeability in asphalt mixtures." *Journal of the Association of Asphalt Paving Technologists (AAPT)*, 68, 479-500.

Huang, C.-W. (2008). "Development and numerical implementation of nonlinear viscoelastic-viscoplastic model for asphalt materials." Ph.D. dissertation, Texas A&M University, College Station, Texas.

Huang, S. C., Branthaver, J. F., and Robertson, R. E. (2002). "Interaction of asphalt films with aggregate surfaces in the presence of water." *Road Materials and Pavement Design*, 3(1), 23-48.

Huang, S. C., and Robertson, R. E. (2004). "Particle size effect of hydrated lime on the long-term aging characteristics of compatible and incompatible asphalts." *3rd Euroasphalt and Eurobitume Congress, Vienna, Austria*, Vienna, Austria, Book 1, 827-834.

Huang, S. C., Robertson, R. E., Branthaver, J. F., and Petersen, J. C. (2005). "Impact of lime modification of asphalt and freeze-thaw cycling on the asphalt-aggregate interaction and moisture resistance to moisture damage." *Journal of Materials in Civil Engineering (ASCE)*, 17(6), 711-718.

Hudson, S. W., Finn, F. N., Treybig, H. J., Epps, J. A., Anderson, V., and Diaz, M. A. (1990). "AC stripping problems and corrective treatments." *Rep. No. FHWA-RD-90-049*, Federal Highway Administration (FHWA), Washington, D.C.

Jahromi, S. G. (2009). "Estimation of resistance to moisture destruction in asphalt mixtures." *Construction and Building Materials*, 23(6), 2324-2331.

Jailardo, A. (2003). "Development of specification criteria to mitigate top-down cracking." M.S. thesis, University of Florida, Gainsville, Florida.

Jamieson, I. L., Moulthrop, J. S., and Jones, D. R. (1995). "Asphalt yearbook: SHRP results on binder-aggregate adhesion and resistance to stripping." Institute of Asphalt Technology, London.

Jeng, Y.-S., and Perng, J.-D. (1991). "Interaction of asphalt films with aggregate surfaces in the presence of water." *Road Materials and Pavement Design*, 3(1), 23-48.

Joshi, N. P. (2008). "Analyses of deformation in viscoelastic sandwich composites subject to moisture diffusion." M.S. thesis, Texas A&M University, College Station, Texas.

Kandhal, P. S., Lynn, C. Y., and Parker, F. (1998). "Test for plastic fines in aggregates related to stripping in asphalt paving mixtures." *Journal of the Association Asphalt Paving Technologists (AAPT)*, 68, 459.

Kanitpong, K., and Bahia, H. U. (2003). "Role of adhesion and thin film thickness of asphalt binders in moisture damage of HMA." *Journal of the Association of Asphalt Paving Technologists (AAPT)*, 72.

Kassem, E. (2005). "Measurements of moisture suction in hot mix asphalt mixes." M.S. thesis, Texas A&M University, College Station, Texas.

Kassem, E. (2009). "Compaction effects on uniformity, moisture diffusion and mechanical properties of asphalt mixtures." Ph.D. dissertation, Texas A&M University, College Station, Texas.

Kassem, E., Masad, E., Bulut, R., and Lytton, R. (2006). "Measurements of moisture suction and diffusion coefficient in hot-mix asphalt and their relationships to moisture damage." *Transportation Research Record: Journal of the Transportation Research Board*, 1970, 45-54.

Kassem, E., Masad, E., Lytton, R., and Bulut, R. (2009). "Measurements of the moisture diffusion coefficient of asphalt mixtures and its relationship to mixture composition." *International Journal of Pavement Engineering* (in press).

Kennedy, T. W., and Anagnos, J. N. (1984). "Modified test procedure for Texas freeze-thaw pedestal test." *Rep. No. 3-0-79-253-7*, Center for Transportation Research (CTR), University of Texas, Austin, Texas.

Kennedy, T. W., Roberts, F., and Lee, K. (1983). "Evaluation of moisture effects on asphalt concrete mixtures." *Transportation Research Record: Journal of the Transportation Research Board*, 911, 134-143.

Kiggundu, B. M., and Roberts, F. L. (1988). "Stripping in HMA mixtures: State-of-the-art and critical review of test methods." *Rep. No. NCAT 88-02*, National Center for Asphalt Technology (NCAT), Auburn, Alabama.

Kim, H. (2005). "Spatial variability of soils: Stiffness and strength." Ph.D. dissertation, Georgia University of Technology, Atlanta, Georgia.

Kim, Y. R., Allen, D. H., and Little, D. N. (2005). "Damage-induced modeling of asphalt mixtures through computational micromechanics and cohesive zone fracture." *Journal of Materials in Civil Engineering (ASCE)*, 17(5), 477-484.

Kim, Y. R., Freitas, F. A. C., and Allen, D. H. (2008). "Experimental characterization of ductile fracture-damage properties of asphalt binders and mastics." *Transportation Research Board 87th Annual Meeting*, Washington D.C.

Kim, Y. R., Sudo-Lutif, J., and Allen, D. H. (2009). "Determination of representative volume elements of asphalt concrete mixtures and their numerical investigation through finite element method." *Transportation Research Board 88th Annual Meeting*, Washington, D.C. (in CD-ROM).

Kinloch, A. J. (1980). "The science of adhesion, part 1: Surface and interfacial aspects." *Journal of Materials Science*, 15, 2141-2166.

Kinloch, A. J., Little, M. S. G., and Watts, J. F. (2000). "The role of the interphase in the environmental failure of adhesive joints." *Acta Materialia*, 48, 4543-4553.

Kook, S., and Dauskardt, R. H. (2002). "Moisture-assisted subcritical debonding of a polymer/metal interface." *Journal of Applied Physics*, 91(3), 1293-1303.

Kosek, J., Stepanek, F., and Marek, M. (2005). "Modeling of transport and transformation processes in porous and multiphase bodies." *Advances in Chemical Engineering*, 30, 137- 203.

Kringos, N., Azari, H., and Scarpas, A. (2009). "Identification of the moisture conditioning related parameters causing variability in the modified Lottman test." *Transportation Research Board 88th Annual Meeting*, Washington, D.C. (in CD-ROM).

Kringos, N., and Scarpas, A. (2005). "Raveling of asphaltic mixes due to water damage: Computational identification of controlling parameters." *Transportation Research Record: Journal of the Transportation Research Board*, 1929, 256-165.

Kringos, N., and Scarpas, A. (2006). "Numerical simulation of the physical processes inducing moisture damage in asphaltic mixtures." *10th International Conference on Asphalt Pavements*, Quebec, Canada, 732-741.

Kringos, N., Scarpas, A., Copeland, A., and Youtcheff, J. (2008a). "Modelling of combined physical-mechanical moisture-induced damage in asphaltic mixes, part 2: Moisture susceptible parameters." *International Journal of Pavement Engineering*, 9(2), 129-151.

Kringos, N., Scarpas, A., and deBondt, A. (2008b). "Determination of moisture susceptibility of mastic-stone bond strength and comparison to thermodynamical properties." *Journal of the Association of Asphalt Paving Technologists (AAPT)*, 77, 475-478.

Kringos, N., Scarpas, A., and Kasbergen, C. (2007). "Three dimensional elasto-visco-plastic finite element model for combined physical-mechanical moisture induced damage in asphaltic mixes." *Journal of the Association of Asphalt Paving Technologists (AAPT)*, 76, 495-524.

Kringos, N., Scarpas, A., Kasbergen, C., and Selvadurai, P. (2008c). "Modelling of combined physical-mechanical moisture-induced damage in asphaltic mixes, part 1: Governing processes and formulations." *International Journal of Pavement Engineering*, 9(2), 115-118.

Krishnan, J. M., and Rao, C. L. (2001). "Permeability and bleeding of asphalt concrete using mixture theory." *International Journal of Engineering Science*, 39(6), 611-627.

Kutay, M. E., Aydilek, A. H., and Masad, E. (2007a). "Computational and experimental evaluation of hydraulic conductivity anisotropy in hot-mix asphalt." *International Journal of Pavement Engineering*, 8(1), 29-43.

Kutay, M. E., Aydilek, A. H., and Masad, E. (2007b). "Estimation of directional permeability of HMA based on numerical simulation of micro-scale water flow." *Transportation Research Record: Journal of the Transportation Research Board*, 2001, 29-36.

Kutay, M. E., Gibson, N., and Youtcheff, J. (2008). "Conventional and viscoelastic continuum damage (VECD) based fatigue analysis of polymer modified asphalt pavements." *Journal of the Association of Asphalt Paving Technologists (AAPT)*, 77, 395-434.

Kvasnak, A. N., and Williams, R. C. (2007). "Evaluation of the interaction effects between asphalt binders and fillers using a moisture susceptibility test." *Journal of the Association of Asphalt Paving Technologists (AAPT)*, 78, 163-199.

Labib, M. E. (1992). "Asphalt-aggregate interactions and mechanisms for water stripping." *American Chemical Society, Division of Fuel Chemistry*, 37, 1472-1481.

Lam, D. C. C., and Wang, J. (2007). "Hygrothermal delaminations in lead-free solder reflow of electronic packages." *The Journal of Electronic Materials*, 36(3), 226-231.

Lam, D. C. C., Yang, F., and Tong, P. (1999). "Chemical kinetic model of interfacial degradation of adhesive joints." *IEEE Transactions of Components and packaging Technology*, 22(2), 215-220.

Lane, M. W., Liu, X. H., and Shaw, T. M. (2004). "Environmental effects on cracking and delamination of dielectric films." *IEEE Transactions on Device and Materials Reliability*, 4(2), 142-147.

Leung, S. Y. Y., Lam, D. C. C., Luo, S., and Wong, C. P. (2004). "The role of water in delamination in electronic packages: Degradation of interfacial adhesion." *Journal of Adhesion Science Technology*, 18(10), 1103-1121.

Li, S. Z. (2009). *Markov random field modeling in image analysis (advancements in image recognition)*, 3rd Ed., Springer, London.

Liljedahl, C. D. M., Crocombe, A. D., Wahab, M. A., and Ashcroft, I. A. (2006). "Modelling the environmental degradation of the interface in adhesively bonded joints using a cohesive zone approach." *The Journal of Adhesion*, 82, 1061-1089.

Little, D., and Petersen, J. C. (2005). "Unique effects of hydrated lime filler on the performance-related properties of asphalt cements: Physical and chemical interactions revisited." *Journal of Materials in Civil Engineering (ASCE)*, 17(2), 207-218.

Little, D. N. (2005). "Bond energy." *International Workshop on Moisture Induced Damage of Asphaltic Mixes*, Delft (in CD-ROM).

Little, D. N., and Bhasin, A. (2007). "Using surface energy measurements to select materials for asphalt pavements." *Rep. No. NCHRP 09-37*, Texas Transportation Institute (TTI), College Station, Texas.

Little, D. N., and Jones, D. R. (2003). "Chemical and mechanical mechanisms of moisture damage in hot mix asphalt pavements." *Moisture Sensitivity of Asphalt Pavements: A National Seminar*, San Diego, California, 37-70.

Liu, M., and Kennedy, T. W. (1991). "Field evaluation of stripping and moisture damage in asphalt pavements treated with lime and antistripping agents." *Rep. No. 3-9-86-441, 441-2F*, University of Texas, Austin, Texas.

Loh, W. K., Crocombe, A. D., Abdel Wahab, M. M., and Ashcroft, I. A. (2003). "Modelling interfacial degradation using interfacial rupture elements." *The Journal of Adhesion*, 79, 1135-1160.

Lottman, R. P. (1978). "Predicting moisture-induced damage to asphaltic concrete." *Rep. No. NCHRP 192*, National Cooperative Highway Research Program, Washington, D.C.

Lottman, R. P. (1982). "Predicting moisture-induced damage to asphaltic concrete: Field evaluation." *Rep. No. NCHRP 246*, National Cooperative Highway Research Program, Washington, D.C.

Lu, Q., and Harvey, J. T. (2006). "Field investigation of factors associated with moisture damage in asphalt pavements." *10th International Conference on Asphalt Pavements*, Quebec, Canada, 691-700.

Lytton, R. L. (2007). "The effect of moisture on field performance of asphalt surfaces." *Second International Workshop on Moisture Induced Damage of Asphalt Mixes*, College Station, Texas (in CD-ROM).

Lytton, R. L., Masad, E. A., Zollinger, C., Bulut, R., and Little, D. (2005). "Measurements of surface energy and its relationship to moisture damage." *Rep. No. 0-4524-2*, Texas Transportation Institute (TTI), College Station, Texas.

Lytton, R. L., Pufhl, D. E., Michalak, C. H., Lian, H. S., and Dempsey, B. J. (1990). "An integrated model of the climatic effects on pavements." *Rep. No. FHWA-RD-90-033*, Federal Highway Administration (FHWA), Washington, DC.

Lytton, R. L., Uzan, J., Fernando, E. G., Roque, R., Hiltmen, D., and Stoffels, S. (1993). "Development and validation of performance prediction models and specifications for asphalt binders and paving mixtures." *Rep. No. SHRP A-357*, Strategic Highway Research Program, Washington, D.C.

Mallick, R. B., Pelland, R., and Hugo, F. (2005). "Use of accelerated loading equipment for determination of long term moisture susceptibility of hot mix asphalt." *Transportation Research Board 85th Annual Meeting*, Washington D.C., (in CD-ROM).

Marek, C. R., and Herrin, M. (1958). "Tensile behavior and failure characteristics of asphalt cements in thin films." *Association of Asphalt Paving Technologists 33rd Annual Meeting (AAPT)*, 386-421.

Masad, E. (2004). "X-ray computed tomography of aggregates and asphalt mixes." *Materials Evaluation*, 62(7), 775-783.

Masad, E., Al-Omari, A., and Chen, H.-C. (2007a). "Computations of permeability tensor coefficients and anisotropy of asphalt concrete based on microstructure simulation of fluid flow." *Computational Materials Science*, 40(4), 449-459.

Masad, E., Al-Omari, A., and Lytton, R. (2006a). "A simple method for predicting laboratory and field permeability of hot mix asphalt." *Transportation Research Board 85th Annual Meeting*, Washington, D.C. (in CD-ROM).

Masad, E., Arambula, E., Ketcham, R. A., Abbas, A. R., and Martin, A. E. (2007b). "Nondestructive measurements of moisture transport in asphalt mixtures." *Journal of the Association of Asphalt Paving Technologists (AAPT)*, 76, 919-952.

Masad, E., Birgisson, B., Al-Omari, A., and Cooley, A. (2004). "Analytical derivation of permeability and numerical simulation of fluid flow in hot-mix asphalt." *Journal of Materials in Civil Engineering (ASCE)*, 16(5), 487-496.

Masad, E., Castelblanco, A., and Birgisson, B. (2006b). "Effects of air void size distribution, pore pressure, and bond energy on moisture damage." *Journal of Testing and Evaluation*, 34(1), 1-9.

Masad, E., Castelo Branco, V. T. F., Dallas N., L., and Lytton, R. L. (2007c). "A unified method for the analysis of controlled-strain and controlled-stress fatigue testing." *International Journal of Pavement Engineering*, 9(4), 233-243.

Masad, E., Howson, J. E., Bhasin, A., Caro, S., and Little, D. (2010). "Relationship of ideal work of fracture to practical work of fracture: Background and experimental results." *Journal of the Association of Asphalt Paving Technologists (AAPT)*, (submitted for evaluation).

Masad, E., Jandhyala, V. K., Dasgupta, N., Somadevan, N., and Shashidhar, N. (2002). "Characterization of air void distribution in asphalt mixes using X-ray computed tomography." *Journal of Materials in Civil Engineering (ASCE)*, 14(2), 122-129.

Masad, E., Kassem, E., and Chowdhury, A. (2009). "Application of imaging technology to improve the laboratory and field compaction of HMA." *Rep. No. FHWA/TX-09/0-5261-1*, Texas Transportation Institute (TTI), College Station, Texas.

Masad, E., Muhunthan, B., Shashidhar, N., and Harman, T. (1999). "Quantifying laboratory compaction effects on the internal structure of asphalt concrete." *Transportation Research Record: Journal of the Transportation Research Board*, 1681, 179-184.

Masad, E., Tashman, L., Little, D., and Zbib, H. (2005). "Viscoplastic modeling of asphalt mixes with the effects of anisotropy, damage and aggregate characteristics." *Mechanics of Materials*, 37, 1242-1256.

Masad, E., Zollinger, C., Bulut, R., Little, D., and Lytton, R. (2006c). "Characterization of HMA moisture damage using surface energy and fracture properties." *Journal of the Association of Asphalt Paving Technologists (AAPT)*, 75, 713-754.

McCann, M., Anderson-Sprecher, R., and Thomas, K. P., Huang, S. (2005). "Comparison of moisture damage in hot mix asphalt using ultrasonic accelerated moisture conditioning and tensile strength test results." *Transportation Research Board 84th Annual Meeting*, Washington, D.C, (in CD-ROM).

McCann, M., and Sebaaly, A. (2001). "Quantitative evaluation of stripping potential in hot mix asphalt using ultrasonic energy for moisture accelerated conditioning." *Transportation Research Record: Journal of the Transportation Research Board*, 1767, 48-59.

Mohamed, E. H. H., Halim, A. O. A. E., and Kennepohl, G. J. (1993). "Assessment of the influence of compaction method on asphalt concrete resistance to moisture damage." *Construction and Building Materials*, 7(3), 149-156.

Mohammad, L. N., Herath, A., and Huang, B. (2003). "Evaluation of permeability of Superpave asphalt mixtures." *Transportation Research Board 82nd Annual Meeting*, Washington, D.C. (in CD-ROM).

Mostovoy, S., and Ripling, E. J. (1969). "Influence of water on stress corrosion cracking of epoxy bonds." *Journal of Applied Polymer Science*, 13, 1083-1111.

Negulescu, I., Louay, M., Daly, W., Abadie, C., Cueto, R., Daranga, C., and Glover, I. (2006). "Chemical and rheological characterization of wet and dry aging of SBS copolymer modified asphalt cements: Laboratory and field evaluation." *Association of Asphalt Paving Technologists 81st Annual Meeting*, Savannah, Georgia (in CD-ROM).

Nicholson, V. (1932). "Adhesion tension in asphalt pavements, its significance and methods applicable in its determination." *Journal of the Association of Asphalt Paving Technologists (AAPT)*, 3, 28-48.

O'Brien, E. P., White, C. C., and Vogt, B. D. (2006). "Content and adhesive fracture energy of polymer coatings on different surfaces." *Advanced Engineering Materials*, 8(1-2), 114-118.

Ortiz, M., and Pandolfi, A. (1999). "A class of cohesive elements for the simulation of three-dimensional crack propagation." *International Journal for Numerical Methods in Engineering*, 44, 1267-1282.

Otani, J., and Obara, Y. (2004). "X-ray CT for geomaterials: Soils, concrete, rocks." *Proceedings of the International Workshop on X-Ray CT for Geomaterials: GEOX2003*, Kimamoto, Japan.

Packham, D. E. (1992). *Handbook of adhesion*, Longman Group, UK Ltd, London.

Petersen, J. C., and Plancher, H. (1998). "Model studies and interpretive review of the competitive adsorption and water displacement of petroleum asphalt chemical functionalities on mineral aggregate surfaces." *Petroleum Science Technology*, 16(1-2), 89-131.

Petersen, J. C., Plancher, H., Ensley, E. K., Venable, R. L., and Miyake, G. (1982). "Chemistry of asphalt aggregate interaction: Relationship with pavement moisture-damage prediction test." *Transportation Research Record: Journal of the Transportation Research Board*, 843, 95-104.

Plancher, H., Dorrence, S. M., and Petersen, J. C. (1977). "Identification of chemical types in asphalts strongly absorbed at the asphalt-aggregate interface and their relative displacement by water." *Journal of the Association of Asphalt Paving Technologists (AAPT)*, 46, 151-175.

Reyes, J., Mahmoud, E., Abdallah, I., Masad, E., Nazarian, S., Langford, R., Tandon, V., and Button, J. (2008). "Quantifying the role of coarse aggregate strength on resistance to load in HMA." *Rep. No. 0-5268-2*, Center of Transportation Infrastructure Systems, Texas Transportation Institute (TTI), El Paso, Texas.

Rippling, E. J. (1971). "Stress corrosion cracking of adhesive joints." *Journal of Adhesion*, 3(2), 145-163.

Ritter, J. E., and Conley, K. (1992). "Moisture-assisted crack propagation at polymer/glass interfaces." *International Journal of Adhesion and Adhesives*, 12(4), 245-250.

Romero, P., and Masad, E. (2001). "Relationship between the representative volume element and mechanical properties of asphalt concrete." *Journal of Materials in Civil Engineering*, 13(1), 77-84.

Ruth, B. E. (1984). "Proceedings of the symposium: Evaluation and prevention of water damage to asphalt pavement materials: A symposium." *ASTM Committee D-4 on Road and Paving Materials*, ASTM Special Technical Publication: Williamsburg.

Sasaki, I., Moriyoshi, A., Hachiya, Y., and Nagaoka, N. (2006). "New test method for moisture permeation in bituminous mixtures." *Journal of the Japan Petroleum Institute*, 49(1), 33-37.

Schapery, R. A. (1984). "Correspondence principles and a generalized J-integral for large deformation and fracture analysis of viscoelastic media." *International Journal of Fracture Mechanics*, 25, 195-223.

Scholz, T. V. (1995). "Durability of bituminous paving mixtures." Ph.D. dissertation, University of Nottingham, Nottingham (UK).

Selvadurai, P. (2005). "Characterization, visualization and simulation of the fundamental processes." First International Workshop on Moisture Damage, Delft (in CD-ROM).

Shatnawi, S. R., Nagarajaiah, M., and Harvey, J. (1995). "Moisture sensitivity evaluation of binder-aggregate mixtures." *Transportation Research Record: Journal of the Transportation Research Board*, 1492, 71-84.

Soares, J. B., de Freitas, F. A. C. M., and Allen, D. H. (2003). "Considering material heterogeneity in crack modeling of asphaltic mixtures." *Transportation Research Record: Journal of the Transportation Research Board*, 1832, 113-120.

Solaimanian, M., Fedor, D., Bonaquist, R., Soltani, A., and Tandon, V. (2006). "Simple performance test for moisture damage prediction in asphalt concrete." *Journal of the Association of Asphalt Pavement Technologists (AAPT)*, 75, 345-380.

Solaimanian, M., Harvey, J., Tahmoressi, M., and Tandon, V. (2003). "Test methods to predict moisture sensitivity of hot mix asphalt pavements." *Moisture Sensitivity of Asphalt Pavements: A National Seminar*, San Diego, California, 77-110.

Solaimanian, M., Kennedy, T. W., and Elmore, W. E. (1993). "Long term evaluation of stripping and moisture damage in asphalt pavements treated with lime and antistripping agents." *Rep. No. CTR 0-1286-1F*, Texas Department of Transportation, Center for Transportation Research, University of Texas, Austin, Texas.

Song, I., Little, D. N., Masad, E., and Lytton, R. L. (2005). "Comprehensive evaluation of damage in asphalt mastics using X-ray CT, continuum mechanics, and micromechanics." *Journal of the Association of Asphalt Paving Technologists (AAPT)*, 74, 885-920.

St.Martin, J., Cooley, L. A., and Hainin, H. R. (2003). "Production/construction issues for moisture sensitivity of hot mix asphalt pavements." *Moisture Sensitivity of Asphalt Pavements: A National Seminar*, San Diego, California, 209-222.

Stuart, K. D. (1990). "Moisture damage in highway mixtures-a state-of-the-art report." *Rep. No. FHWA-RA-90-019*, US Department of Transportation, Washington, D.C.

Sun, L., Kenis, W., and Wang, W. (2006). "Stochastic spatial excitation induced by a distributed contact on homogeneous random fields." *Journal of Engineering Mechanics*, 132(7), 714-722.

Sun, L., and Kennedy, T. W. (2002). "Spectral analysis and parametric study of stochastic pavement loads." *Journal of Engineering Mechanics*, 128(3), 318-327.

Tashman, L., Masad, E., Peterson, B., and Saleh, H. (2001). "Internal structure analysis of asphalt mixes to improve the simulation of Superpave gyratory compaction to field conditions." *Journal of the Association of Asphalt Pavement Technologists (AAPT)*, 70, 605-645.

Taylor, M. A., and Khosla, N. P. (1983). "Stripping of asphalt pavements: State of the art." *Transportation Research Record: Journal of the Transportation Research Board*, 911, 150-158.

Terrel, R. L., and Al-Swailmi, S. (1993). "The role of pessimum voids concept in understanding moisture damage to asphalt concrete mixtures." *Transportation Research Record: Journal of the Transportation Research Board*, 1386, 31-37.

Terrel, R. L., and Al-Swailmi, S. (1994). "Water sensitivity of asphalt-aggregate mixes: Test selection." *Rep. No. SHRP-A-403*, Strategic Highway Research Program, Washington, D.C.

Thelen, E. (1958). "Surface energy and adhesion properties in asphalt-aggregate systems." Highway Research Board, Washington, D.C.

Torquato, S. (2002). *Random heterogeneous materials*, Springer, New York.

Tunnicliff, D. G., and Root, R. E. (1984). "Use of antistripping additives in asphaltic concrete mixtures: Laboratory phase." *Rep. No. NCHRP Report 274*, National Cooperative Highway Research Program, Washington, D.C.

TxDOT. (2004). "Standard specifications for construction and maintenance of highways, streets and bridges." Texas Department of Transportation, Austin, Texas.

VanOss, C. J., Chaudhury, M. K., and Good, R. J. (1988). "Interfacial Lifshitz-van der Waals and polar interactions in macroscopic systems." *Chemical Reviews*, 88(6), 927-941.

Volokh, K. Y. (2004). "Comparison between cohesive zone models." *Communications in Numerical Methods in Engineering*, 20, 845-856.

Vuorinen, M. J., and Valtonen, J. P. (1999). "A new ultrasound method for measuring the resistance to stripping." *Eurobitume Workshop 99: Performance Related Properties for Bituminous Binders*, Luxembourg.

Walsh, G., Jamieson, I., Thorton, J., and O'Mahony, M. (1996). "A modified SHRP net adsorption test." *1st Eurasphalt & Eurobitume Congress*, Strasbourg.

Wang, L. B., Frost, J. D., Voyiadjis, G. Z., and Harman, T. P. (2003). "Quantification of damage parameters using X-ray tomography images." *Mechanics of Materials*, 35(8), 777-790.

Washburn, E. W. (1921). "The dynamics of capillary flow." *The Physical Review*, 17(3), 273-283.

Wasiuddin, N. M., Fogle, C. M., Zaman, M. M., and O'Rear, E. A. (2007). "Effect of antistrip additives on surface free energy characteristics of asphalt binders for moisture-induced damage potential." *Journal of Testing and Evaluation*, 35(1), 1-9.

Weiderhorn, S. M., Fuller, E. R., and Thomson, R. (1980). "Micromechanisms of crack growth in ceramics and glasses in corrosive environments." *Metal Science*, 14, 450-458.

Williams, T., and Miknis, F. (1998). "The effect of antistrip treatments on asphalt-aggregate systems: An environmental scanning electron microscope study." *Journal of Elastomers and Plastics*, 30(4), 282-295.

Yoon, H. H., and Tarrar, A. R. (1988). "Effect of aggregate properties on stripping." *Transportation Research Record: Journal of the Transportation Research Board*, 1171, 37-43.

Youtcheff, J., and Aurilio, V. (1997). "Moisture sensitivity of asphalt binders: Evaluation and modeling of the pneumatic adhesion test results." *Canadian Technical Asphalt Association 42nd Annual Conference*, Ottawa, 180-200.

Zewi, I. G., Flashner, F., Dodiuk, H., and Drori, L. (1984). "Durability of structural adhesive joints." *International Journal of Adhesion and Adhesives*, 4(3), 137-140.

Zhang, Z., Roque, R., Birgisson, B., and Sangpetngam, B. (2001). "Identification and verification of a suitable crack growth law." *Journal of the Association of Asphalt Paving Technologists (AAPT)*, 70, 206-241.

Zollinger, C. J. (2005). "Application of surface energy measurement to evaluate moisture susceptibility of asphalt and aggregates." M.S. thesis, Texas A&M University, College Station, Texas.

APPENDIX

WORKS ON ADHESIVE FRACTURE UNDER MOIST ENVIRONMENTS

The study of adhesive bonding has being a main research topic under the general framework of the science of adhesion (Kinloch 1980). Several theories have been developed to explain the nature of adhesive bonds; e.g., mechanical interlock, adsorption interactions, electrostatic forces and diffusion mechanisms, among others (Allen 1993; Hefer et al. 2005; Kinloch 1980). However, these theories can be highly complex, and sometimes insufficient, when analyzing the corrosive effects caused on the joint under moist environments.

There are two main approaches to analyze the effect of moisture in structural adhesive joints:

1) as a water-assisted deterioration process, and

2) as a stress-enhanced debonding process.

In the first case, water assists the deterioration process but other mechanisms, principally external stresses, are the major contributors to damage. In the second case, hydrolysis and other water-induced processes are the main source of damage, and stresses play a secondary role in the deterioration process. Examples of this second case include degradation of electronic packages under special moisture conditions (Lam and Wang 2007; Lam et al. 1999). Researchers have shown that the former is the predominant mechanism for most currently used structural joints. Therefore, the characterization of the interfacial deterioration is based on the mechanical response of these systems when subjected to different environmental conditions.

Most research dealing with experimental measurements of water-assisted debonding analyze the crack growth of pre-cracked adhesive joints specimens under different loading and moisture conditions (e.g., different relative humidity and/or experiments conducted under water). Examples of such works can be found in Mostovoy and Ripling (1969), Weiderhorn et al., (1980), Ritter and Conley (1992), Fernando et al. (1996), Kinloch et al. (2000), Kook and Dauskardt (2002), Leung et al. (2004), Lane et al. (2004), Liljedahl et al. (2006), O'Brien et al. (2006), Ferguson and Qu (2006), among others. In all cases, principles of linear elastic fracture mechanics are applied to quantify the critical energy released rate (G_C) characterizing the fracture growth process, based on the information of crack growth length, external stresses and geometrical configuration of the specimen (Blackman and Kinloch 2001). Studies conducted using this scheme differ in two main aspects: 1) the external loading conditions used in the test

(i.e., static or dynamic, mode I loading or mixed mode, etc.), and 2) the moisture-conditioning process that is applied to the specimens prior to testing. The main conclusions common to the works conducted under the fracture mechanics framework are:

- There is a threshold value of energy released rate (or stress intensity factor) below which no environmental deterioration is observed (Gdoutos 2005; Lam et al. 1999). This value is usually referred to as G_{TH}. This threshold value decreases when humidity conditions increase. In other words, in the presence of moisture less energy is required to start the cracking process. Figure A.1 shows the decrease in G_{TH} (i.e., intersection of the curves with the horizontal axis) for two different metal-epoxy joints subjected to displacement-controlled conditions in a four-point flexure test (Figure A.1.a) and to static load conditions in a double cantilever beam test (Figure A.1.b),

- severe humidity conditions produce a reduction in the fracture toughness of the adhesive joint. Ripling (1971) was one of the first authors reporting this result when he found that the fracture toughness of an adhesive joint composed by a hardener and a resin was reduced by about 70% with the presence of water under long term static loading conditions. More recently, Ferguson and Qu (2006) successfully developed a model to characterize the observed loss of interfacial fracture toughness in terms of five key parameters related to moisture effects,

- the fracture locus under humid conditions is, in most cases, adhesive (Kinloch 1980). It has been observed that adhesive joints that present adhesive fracture in dry conditions maintain that failure pattern in humid conditions, while adhesive joints with cohesive fracture locus in dry conditions normally switch to an adhesive fracture locus in humid conditions (Ferguson and Qu 2006), and

- fracture toughness is a function of the experiment conditions. In the case of viscoelastic adhesives, loading rate and adhesive thickness highly influenced the fracture toughness results.
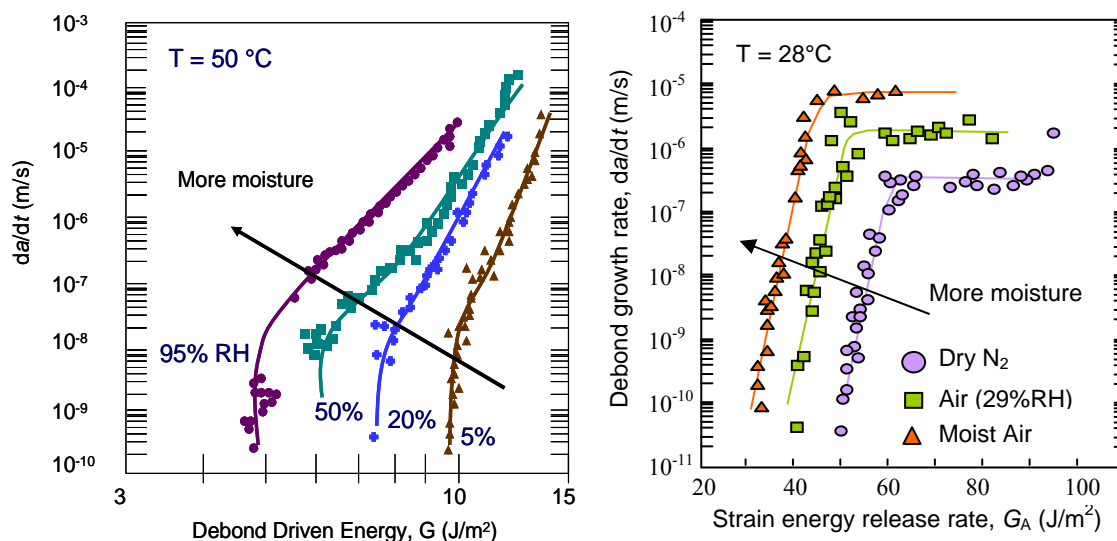
Figure A.1. Results for two metal-copper adhesive joint subjected to mode I test (a) adapted from Lane at al. (2004), and (b) adapted from Kook and Dauskardt (2002)

Although experimental results as those presented in Figure A.1 permit to verify the dependency of adhesive joints to cracking under hostile conditions, they do not provide information about the thermodynamic, chemical or other specific processes occurring in the interface. In fact, few works have been conducted to relate the results obtained from fracture tests of adhesive joints to the thermodynamic or chemical kinetics processes at the interface. Examples of such works include the studies from Kook and Dauskardt (2002) and Leung et al. (2004). Kook and Dauskardt (2002) assumed that the debonding process characterizing the first part of a crack propagation rate vs. fracture energy curve (Figure A.1.b) was proportional to the rate at which water breaks the existing bonds at the interface. Based on a chemical kinetics model, the authors were able to successfully fit the experimental observations (Figure A.1.b). Leung et al. (2004) also developed an analytical model based on chemical kinetics principles and shear fracture test results at different humid and temperature conditions to delineate the material parameters that govern the deterioration process at the interface of a metal-epoxy system. The authors concluded that the effect of temperature in the moisture-degradation of interfacial bonds follows a chemical kinetics model with Arrhenius form. The authors were also able to identify the role of certain chemical agents in the deterioration process, e.g., they concluded that the degradation rate is highly influenced by the hydrogen ion concentration at low acidity and that

the influence of the applied stresses on this rate can be characterized by the activated area coefficient of the activated state divided by the overall bond density.

In terms of modeling, most work has been focused in evaluating the capabilities of different numerical techniques to simulate the delamination process observed in fracture mechanics-based tests. Within these techniques, the cohesive zone model (CZM) has proved to be one of the most successful and efficient tools to accomplish this purpose. Details regarding this numerical technique and references of works conducted in this direction can be found in Chapter III of this dissertation.

VITA

Silvia Caro Spinel was born in Bogotá, Colombia. In September 2000, she received her Magna-Cum-laude B.S. in civil engineering from the Universidad de Los Andes (Bogotá, Colombia). In September 2001, she received her M.S. also in civil engineering (degree with honors), with emphasis in road infrastructure, from the same institution. Her masters' thesis consisted of developing a finite difference model to study the effect of climate effects (i.e., rainfall and temperature regimes) on the mechanical properties of asphalt pavements.

From June 2001 to December 2005, she worked as an associate researcher and lecturer in the Department of Civil and Environmental Engineering at the Universidad de Los Andes.

From January 2006 to December 2009, she attended Texas A&M University to pursue her doctoral degree. She initially received a graduate research assistantship from the Zachry Department of Civil Engineering, and later from the Texas Transportation Institute (TTI). As part of a research collaboration program between the Texas A&M University and the University of Nottingham (UK), she worked on developing a probabilistic-based model on the susceptibility of fine aggregate matrix materials to moisture damage. More recently, she participated in the Asphalt Research Consortium (ARC)—a research program sponsored by the Federal Highway Administration (FHWA) through the Western Research Institute (WRI)—with the objective of formulating a micromechanical model of moisture-induced cohesive and adhesive deterioration in asphalt mixtures.

Her permanent address is:
Departamento de Ingeniería Civil y Ambiental
Universidad de Los Andes
Carrera 1 Este No. 19ª - 40 (Edificio Mario Laserna)
Bogotá, Colombia

Her e-mail address is: scaro@uniandes.edu.co